Systems biology of human metabolism -

Defining the epithelial to mesenchymal transition and the activity of human gluconokinase

Neha Rohatgi

Thesis for the degree of Philosophiae Doctor

Supervised by:

Ottar Rolfsson & Steinn Gudmundsson

Doctoral committee:

Ólafur Eysteinn Sigurjónsson, PhD

Ines Thiele, PhD

Ólafur Þór Magnússon, PhD

December 2016

UNIVERSITY OF ICELAND
SCHOOL OF HEALTH SCIENCES
FACULTY OF MEDICINE

Kerfislíffræði efnaskipta: Að leggja skilning á bandvefslíka umbreytingu og Glúkonókínasa með notkun skorðaðra líkana og skammtastilltri jafnhita-varmamælingu

Neha Rohatgi

Ritgerð til doktorsgráðu

Leiðbeinendur:

Óttar Rolfsson & Steinn Guðmundsson

Doktorsnefnd:

Ólafur Eysteinn Sigurjónsson, PhD

Ines Thiele, PhD

Ólafur Þór Magnússon, PhD

Desember 2016

UNIVERSITY OF ICELAND
SCHOOL OF HEALTH SCIENCES
FACULTY OF MEDICINE

ISBN 978-9935-9319-9-3

Printing by Haskolaprent.

Reykjavik, Iceland 2016

Ágrip

Rannsóknir á efnaskiptum eru nauðsynlegar til að skilja undirliggjandi forsendur sjúkdóma og til að efla lyfjameðferðir þar sem breytingar í efnaskiptaferlum eru miðlægar í mörgum sjúkdómum. Margar aðferðafræðilegar nálganir á borð við lífefnafræði, lífeðlisfræði og kerfislíffræði eru notaðar til greininga efnaskiptaferlum. Þessari ritgerð er skipt í þrjá hluta sem fjalla á ólíkan hátt um efnaskipti í mannafrumum með kerfislíffræðilegum- og lífefnafræðilegum aðferðum.

Fyrsta rannsóknin fjallar um notkun skorðaðra efnaskiptalíkana til rannsókna á breyttum efnaskiptaferlum við bandvefsumbreytingu (epithelial to mesenchymal transition - EMT). EMT er vel þekkt ferli í fósturþroskun þar sem þekjuvefs frumur umbreytast í bandvefslíkar frumur. Brenglun á EMT ferlinu hefur verið tengt myndun meinvarpa í brjóstakrabbameinum. Sérhæfð efnaskiptalíkön byggð á gögnum um genatjáningu og mælingar á upptöku og seytingu næringarefna frá brjóstaþekjufrumulínunni D492 og bandvefslíkri dóttufrumulínu hennar D492M. Með notkun þessara efnaskiptalíkana er mögulegt að spá fyrir um breytingar í innanfrumu efnaskiptaferlum sem verða við bandvefsumbreytingu. Líkönin benda til þess að munur sé í miðlægum kolefnis efnaskiptum ásamt breytilegri nýtingu amínósýra milli frumulínanna tveggja. Greiningu á lífsnauðsynlegum genum fyrir hvora frumulínu „in Silico“ bendir til þess að SLC7A5 undireiningin í LAT1 amínósýruferjunni sé nauðsynlegur fyrir lifun bandvefslíkra frumna en ekki nauðsynlegur fyrir þekjuvefsfrumur. Aðferðafræðin sem notast var við í þessari rannsókn getur nýst við frekari rannsóknir á bandvefsumbreytingu. Gögnin sem kynnt eru í þessari rannsókn má nýta til að spáð fyrir um ný möguleg lyfjamörk til krabbameins meðferða.

Í annari rannsókninni er fjallað um nýlega skilgreint efnaskiptaensím í mönnum, glúkonókínasa. Þrátt fyrir tilvist glúkonats í líkamsvessum og útbreidd a notkun þess í matar- og lyfjaiðnaði, hafa efnaskipti glúkonats í mönnum verið lítt rannsökuð. Efnahvörf sem miða að niðurbroti glúkonats var bætt við efnaskiptalíkan rauðra blóðkorna til þess að meta vægi glúkonats í efnaskiptum manna. Með því að bæta við efnaskiptaferlum fyrir niðurbrot glúkonats komu fram breytingar á NADPH framleiðslu, sem er tengt við stýringu oxunarálags og fitusýruefnaskiptum þeirra. Tölvulíkönin sýna fram á að glúkonókínasa virkni hefur marktæk áhrif á efnaskiptaferla og er vert frekari rannsókna.

Seinasta rannsóknin snýst um að mæla parametra hreyfiorkunnar fyrir glúkónokínasa með skammtastilltri jafnhita-varmamælingu (ITC) ásamt greiningu hvarfgangs. Niðurstöðurnar sýna að hvarfgangurinn myndar þríundarklósamband við ATP sem fyrsta hvarfefni og að glúkonat sýnir hvarfefnahindrun. Þessi rannsókn sýnir að skammtastillt jafnhita-varmamæling getur verið gagnlegt til að ákvarða hvarfgang ensím-hvataðra hvarfa ásamt því að skilgerina parametra hreyfiorkunnar.

Rannsókninar sem notaðar eru í þessari ritgerð renna stoðum undir að hefðbundin lífefnafræði og kerfislíffræði eru samfallandi aðferðir sem leyfa dýpri og öflugri skilning á efnaskiptaferlum.

Lykilorð:

Efnaskifti, Efnaskipta reiknilíkön, bandvefsumbreyting,glúkónat, Efnafræði Ensíma.

Abstract

Studying human metabolism is crucial for the understanding of diseases and improvement of therapy as metabolic alterations are central to a number of human diseases. A variety of experimental disciplines, such as biochemistry, biophysics and systems biology are involved in the elucidation of metabolic pathways. The work presented in this thesis is divided into three main studies, which expand the knowledge of human metabolism using systems biology and biochemical techniques.

In the first study presented in this thesis, constraint-based modeling was used to investigate metabolic changes during epithelial to mesenchymal transition (EMT), which is a developmental process where epithelial cells de-differentiate into mesenchymal-like cells. Dysregulation of EMT has been associated with cancer metastasis. Context-specific genome-scale metabolic models were derived from a generic human metabolic model using transcriptomic and extracellular metabolomics data from isogenic breast epithelial cell lines (D492 and D492M), which allowed *in silico* predictions of the metabolic changes during EMT. The models revealed differences in the central carbon metabolism along with different utilization of amino acids in the two cell lines. *In silico* gene essentiality analysis predicted that components of the SLC7A5 subunit of the large neutral amino acid transporter LAT1 was exclusively essential for mesenchymal cell survival. This study presented a platform for further studies on EMT. Further, the predicted metabolic targets can aid the development of novel cancer therapeutics.

In the second study, the effects of a novel human metabolic enzyme, gluconokinase, was investigated. Despite the presence of gluconate in human bio-fluids and its widespread use in food and pharmaceutical industry, the details of gluconate metabolism in humans is relatively unexplored. Reactions specific for consumption of gluconate were added to a red blood cell metabolic model, in order to evaluate the impact of gluconate on human metabolism. It was found that adding gluconokinase to the model affects NADPH production in red blood cells, which in turn is closely associated with oxidative stress regulation and fatty acid metabolism in the cells. The computational simulations demonstrated that gluconokinase activity has significant effects on the overall metabolism of the cell and is worth investigating further.

In the final study, kinetic parameters of human gluconokinase were determined using isothermal titration calorimetry (ITC) along with the mechanism of the reaction. The results establish that the reaction follows a ternary complex mechanism with ATP being the first binding substrate and

gluconate displaying substrate inhibition. This study demonstrated that ITC could be used as a tool to determine mechanisms of enzyme catalyzed reactions along with kinetic parameters.

The studies presented in this thesis emphasize that traditional biochemical assays and advanced systems biology methods are complementary tools, which allow a more complete understanding of human metabolism.

Keywords:

Metabolism, Constraint-based metabolic modeling, Epithelial to mesenchymal transition (EMT), Gluconate, Isothermal titration calorimetry (ITC)

Acknowledgements

The completion of this PhD, in University of Iceland, would not have been possible without the help of my supervisor, Dr. Ottar Rolfsson. I would like to thank him for all the help and guidance he gave me during the years. Secondly, I would like to thank Dr. Steinn Gudmundsson for being the advisor of my PhD and providing many useful suggestions and motivation through the years. I would like to thank both of them for their patience and support all the while I was learning to write and present scientific text.

I would further like to thank the Stem Cell Research Unit, Læknagarður and Dr. Skarphedinn Halldorsson for fruitful collaboration and helping me in my PhD project.

Many thanks to all the people associated with the Center for Systems Biology who have provided their guidance and friendship. I would also like to thank Arnar Sigurðsson for translating the abstract in Icelandic. Special thanks to Sonal and Kristine for reading and commenting on all my texts.

I thank my family and friends for their constant support and encouragement. I would not have been able to do this without them.

Contents

List of abbreviations

List of all abbreviations used in the thesis.

ATP: Adenosine triphosphate

CBM: Constraint-based modeling

COBRA: Constraint-based reconstruction and analysis

E. coli: Escherichia coli

EMT: Epithelial to mesenchymal transition

EPI model: Epithelial cell metabolic model (D492)

EGF: Epidermal growth factor

FAD: Flavin adenine dinucleotide

FBA: Flux balance analysis

FVA: Flux variability analysis

GEM: Genome-scale metabolic model

GIMME: Gene inactivity moderated by metabolism and expression

GENRE: Genome scale metabolic reconstruction

Glcn: Gluconate

GntK: Gluconokinase

GPR: Gene-Protein-Reaction association

HGF: Hepatocyte growth factor

HMDB: Human metabolome database

HMLE: Human mammary epithelial cells

HMR: Human metabolic reaction

HMS: Hexose monophosphate shunt

INIT: Integrative network inference for tissues

iMAT: Integrative metabolic analysis tool

ITC: Isothermal titration calorimetry

KEGG: Kyoto Encyclopedia of Genes and Genomes

α-KG: Alpha-ketoglutarate

LP: Linear programming

MBA: Model building algorithm

MCF-7: Michigan Cancer Foundation-7

MES model: Mesenchymal cell metabolic model (D492M)

MET: Mesenchymal to epithelial transition

mCADRE: Metabolic context-specificity assessed by deterministic reaction evaluation

NAD+: Nicotinamide adenine dinucleotide oxidized

NADH: Nicotinamide adenine dinucleotide reduced

NADP+: Nicotinamide adenine dinucleotide phosphate oxidized

NADPH: Nicotinamide adenine dinucleotide phosphate reduced

S matrix: Stoichiometric matrix

SNP: Single-nucleotide polymorphism

TCA: Tricarboxylic acid cycle

TGF-b: Transforming growth factor-b

UV: Ultraviolet light

VEGF: Vascular endothelial growth factor

List of figures

List of original papers

This thesis is based on the following original publications, which are referred to in the text by their Roman numerals (I-III):

I. Skarphedinn Halldorsson §, **Neha Rohatgi** §, Manuela Magnusdottir, Kumari Sonal Choudhary, Thorarinn Guðjónsson, Erik Knutsen, Anna Barkovskaya, Bylgja Hilmarsdottir, Maria Perander, Gunhild M. Mælandsmo, Steinn Gudmundsson and Ottar Rolfsson. “Metabolic re-wiring of isogenic breast epithelial cell lines following epithelial to mesenchymal transition.” (Submitted for publication, § indicates equal contribution)

II. **Neha Rohatgi**, Tine Kragh Nielsen, Sara Petersen Bjørn, Ivar Axelsson, Giuseppe Paglia, Bjørn Gunnar Voldborg, Bernhard O. Palsson and Ottar Rolfsson. “Biochemical Characterization of Human Gluconokinase and the Proposed Metabolic Impact of Gluconic Acid as Determined by Constraint Based Metabolic Network Analysis.” *Plos One*. 2014, doi: 10.1371/journal.pone.0098760

III. **Neha Rohatgi**, Steinn Gudmundsson and Ottar Rolfsson. “Kinetic analysis of gluconate phosphorylation by human gluconokinase using isothermal titration calorimetry.” *FEBS Letters*. 2015, doi: 10.1016/j.febslet.2015.10.024

All papers are reprinted by kind permission of the publishers

Other publications:

I. Kumari Sonal Choudhary, **Neha Rohatgi**, Skarphedinn Halldorsson, Eirikur Briem, Thorarinn Gudjonsson, Steinn Gudmundsson and Ottar Rolfsson. “EGFR Signal-Network Reconstruction Demonstrates Metabolic Crosstalk in EMT.” *Plos Computational Biology*, doi:10.1371/journal.pcbi.1004924

II. Neha Rohatgi, Miha Škalič, Steinn Gudmundsson and Óttar Rolfsson. “ITEKA (Isothermal titration calorimetry enzyme kinetic analyzer).” (Manuscript in preparation).

III. Neha Rohatgi, Steinn Gudmundsson and Óttar Rolfsson. “Condition specific model generation toolbox.” (Manuscript in preparation).

Declaration of contribution

Paper I:

Skarphedinn Halldorsson, Neha Rohatgi, Steinn Gudmundsson and Ottar Rolfsson designed the study, collected the data, analyzed the data and wrote the manuscript. Manuela Magnusdottir, Kumari Sonal Choudhary, Thorarinn Guðjónsson, Erik Knutsen, Anna Barkovskaya, Bylgja Hilmarsdottir, Maria Perander and Gunhild M. Mælandsmo contributed to data collection, data analysis and the writing of the manuscript.

Paper II:

Ottar Rolfsson and Neha Rohatgi performed the experiments, analyzed the data and wrote the paper. Tine Kragh Nielsen, Sara Petersen Bjørn, Ivar Axelsson and Giuseppe Paglia performed the experiments and analyzed the data. Ottar Rolfsson and Bernhard O. Palsson conceived and designed the experiments.

Paper III:

Neha Rohatgi designed the study, carried out the experiments, performed the data analysis and wrote the paper, Steinn Gudmundsson performed data analysis and Ottar Rolfsson designed the study, carried out experiments and wrote the paper.

1 Introduction

1.1 Metabolism

Metabolism' is the comprehensive set of processes used by living organisms to obtain and consume the energy required in order to maintain life (DeBerardinis & Thompson, 2012). It is an enormous system with thousands of enzymatic reactions and metabolites arranged in consecutive metabolic pathways. Metabolic reactions are largely categorized into two classes: anabolic reactions which synthesize metabolites that carry out cellular functions and catabolic reactions which degrade metabolites to produce energy (Voet & Voet, 2011). It is a highly dynamic and well regulated process which is constrained by the laws of chemistry and physics. In addition, gene expression profiles contribute to the definition of metabolic phenotypes of a cell which can be adjusted according to environmental or cellular changes. This allows the cell to respond to external and internal perturbations (Palsson, 2006).

1.1.1 Metabolism in diseases

Metabolic perturbations are integral to a myriad of human diseases because metabolism influences and is influenced by almost all cellular processes, such as transcription and translation of genes. The fundamental ideas on metabolism and its byproducts being related to diseases trace back to 2000 years ago when physicians reported that urine of people suffering from a common hereditary disease (diabetes) attracted ants due to high levels of sugar (DeBerardinis & Thompson, 2012). This insight dates before the formal study of metabolism came into place but may be regarded as an early example of linking metabolic intermediate to a disease. A greater appreciation for the relationship between diseases and the precise metabolic events related to these diseases was developed between the 1920s and 1960s when most of the biochemical pathways were described. Metabolic diseases could be linked to diet and lifestyle patterns, e.g., obesity, dyslipidemia or caused by genetic mutations, e.g., albinism, cystinuria (Fernandes et al., 2006). Another genetically defined disease with metabolic perturbations is cancer. The metabolic alterations in cancer promote malignant transformation, initiation and progression of tumors (Hanahan & Weinberg, 2011). Other diseases shown to be associated with changes in core metabolic pathways are diabetes, cardiovascular disorders and arthritis. Close association of common diseases with metabolic alterations is the

reason why studying metabolism has been one of the most fruitful pursuit in disease oriented research for decades (DeBerardinis & Thompson, 2012).

1.1.2 Study of metabolism

Studying metabolic pathways and their role has been prominent in biochemical research for decades. Metabolism can be studied at various levels: (i) the sequence of the reactions in a pathway can be investigated; (ii) the mechanism of each reaction can be studied by isolating the corresponding enzymes; (iii) the mechanisms by which a pathway is regulated can be studied; and (iv) the relation between different metabolic pathways and their output can be studied at the systems scale. A variety of experimental disciplines are involved for the elucidation of a metabolic pathway on all the levels mentioned above. Most of the methods used to understand metabolism involve perturbing the metabolic network and detecting the effects on the metabolic intermediates. Radioactively labeled intermediates and products can be used to define the paths from precursors to the final products. The enzymes that catalyze the chemical reactions in the pathway can be extracted and purified to study their kinetics and responses to inhibitors (Voet & Voet, 2011). These hypothesis-based approaches, where, individual components are isolated and studied as directed by experimentally verifiable hypothesis, were used for most of the biochemical studies in 1900s and have led to a huge biochemical knowledgebase in the form of scientific literature. A different more recent approach called Systems Biology has emerged which aims to study biological processes at cellular/systems level, taking the interactions between the components into account (Voet & Voet, 2011). Systems biology tools rely on high throughput measurement techniques and various publically available databases containing metabolic data collected in decades by biochemists.

1.1.3 Metabolic knowledgebase

Metabolic information, gained from biochemical research and advanced high-throughput measurements, is made available in form of easily accessible databases. MetaCyc is one such database of experimentally validated metabolic pathways which contains more than 12,000 reactions and metabolites (as of November 12, 2015) (Caspi et al., 2016). The Human Metabolome Database (HMDB) is another database containing information about 42,000 metabolites found in the human body (as of April 26, 2016) (Wishart et al., 2013). The Kyoto Encyclopedia of Genes and Genomes (KEGG) database has nearly 10,000 reactions and 15,000 metabolites annotated (as on April 26, 2016) (Kanehisa, 2002). Information in these databases have made the research in systems biology grow rapidly, in recent years.

This thesis was set out to expand the knowledge of human metabolism using different methods ranging from traditional biochemical methods to advanced systems biology tools. The main studies mentioned in this thesis can be divided into two sections; (i) investigation of metabolic changes during a developmental biological event called epithelial to mesenchymal transition (EMT) using systems biology tools and; (ii) investigation of a recently identified human metabolic function (phosphorylation of gluconate by gluconokinase) using constraint-based modeling and characterization of the enzyme using biochemical methods. The following sections will provide an overview of the concepts and methods relevant to this thesis.

1.2 Systems biology

Systems Biology is a field of study that combines mathematical modeling, computational simulation and biological science, with the goal to predict the behavior of the whole biological system on the basis of the different components included (Voet & Voet, 2011). It focuses on the nature of associations between individual components and the functional states of the system that arise from the interactions of all the participating components (Palsson, 2006; Palsson, 2009).

1.2.1 History of systems biology

For most part of its history, biological research has been reductionist in nature, i.e., the system is divided into its component parts to study the individual components. These studies explain the behavior of the system in terms of its component parts by extrapolating the results from the components to the system. But living systems exhibit complex nonlinear characteristics owing to inter-linking of the various processes. Therefore, this approach fails to give satisfactory information about the properties of the system as a whole. With the rapid progress in molecular biology techniques and computational tools in the latter half of the 20^{th} century, an enormous amount of biological data is readily available. This gave biologists an opportunity to use integrative approaches to study metabolism and other biological processes. Thus systems biology was born to achieve greater understanding of complex biological networks at the cellular/systems level (Kitano, 2001). The huge amount of biological data allows the characterization of thousands of biological components simultaneously and can be used to reconstruct biological networks that can be converted into computational models. These computational metabolic models enable the estimation of phenotypic traits of an organism based on its genetic composition and form the basis of systems biology to study metabolism (Thiele & Palsson, 2010).

1.2.2 Modeling formalisms

As systems biology is an interdisciplinary field and cellular networks are highly complex, several different kinds of formalisms are used to create computational models focused on the application of interest (Machado et al., 2011). There are several different types of computational models of biological networks depending on the formalism used and the cellular process under study. For example:

- Boolean networks have been used to model signaling pathways (Gupta et al., 2007)
- Bayesian networks to understand and represent gene regulatory and signaling networks (Grzegorczyk et al., 2008; Sachs et al., 2005)
- Petri nets to infer metabolic, gene regulatory and signaling networks (Chaouiya et al., 2004; Hardy & Robillard, 2008; Koch et al., 2005)
- Ordinary differential equations to model metabolic pathways (Chassagnole et al., 2002)
- Piecewise-linear differential equations to reconstruct gene regulatory networks (Batt et al., 2005)
- Artificial neural networks to analyze gene expression (Vohradsky, 2001)
- Constraint-based modeling for studying metabolic, gene regulatory and signaling networks (Choudhary et al., 2016; Gianchandani et al., 2009; Gopalakrishnan & Maranas, 2015; Heinken et al., 2013; Heinken & Thiele, 2015; Kauffman et al., 2003; Papin & Palsson, 2004; Schilling et al., 2000; Segre et al., 2002; Shlomi et al., 2005; Wang et al., 2009).

Constraint-based modeling formalism was used in this thesis and is explained in detail in the next sections.

1.3 Constraint-based modeling

Constraint-based modeling (CBM) is a widely used formalism for studying cellular metabolism. CBM helps define a set of different phenotypes under relevant constraints. Owing to the simplicity of CBM, genome-scale metabolic models containing thousands of reactions can be routinely generated. It overcomes the limitations in lack of experimental data for parameters required in detailed dynamic modeling. There are numerous environment and genetic constraints under which cells operate and evolve which are discussed in the following section.

1.3.1 Constraints in biology

A cell's fitness is its ability to survive and grow/reproduce while satisfying a variety of constraints that control the range of possible phenotypes. The constraints that limit the functional states of a cellular network can be classified in different ways. The four major categories of constraints are: (i) physicochemical constrains such as the conservation of mass, (ii) spatial and topological constraints that define the structural arrangement of the functions in different cellular compartments, (iii) environmental constraints like temperature, pH and the availability of nutrients, and (iv) regulatory constraints such as evolutionary changes. In CBM, the mathematical formulation of constraints is accomplished using equalities and inequalities. The equations for conservation of mass, osmotic pressure, electro-neutrality and free energy around biochemical loops are defined by equality constraints. In constraint based modeling, conservation of mass is represented by the steady-state. At the steady-state the rate of synthesis of each internal metabolite equals the rate of its depletion, thus there is no net accumulation or degradation of metabolites in the network (Price et al., 2004). The concentrations and/or kinetic constants of proteins are represented by inequalities which allows a range of possible values (Palsson, 2006). Uptake and secretion of metabolites is also defined in the same way.

1.3.2 Constraint-based metabolic models

A genome scale metabolic reconstruction (GENRE) is a set of biochemical reactions occurring in a particular cell, tissue or organism. It also contains information about the interactions between different components of a cell such as genes, proteins and metabolites. A reconstruction can be converted to a computational model by incorporating the necessary information and assumptions. These computational models are called genome-scale metabolic models (GEMs) and are useful for simulation of various biological functions (Becker et al., 2007). The first GEM was generated in 1999, after that many more have followed and the number has been increasing exponentially over the past decade (Palsson, 2009). In 2007 one of the most complete human metabolic network reconstructions, *H. sapiens* Recon 1, was published. Recon 1 was updated and expanded resulting in the more comprehensive Recon 2, which is constantly being updated (Duarte et al., 2007; Thiele et al., 2013). Another high-quality genome-scale metabolic model for the generic human cell (referred as EHMN: Edinburgh Human Metabolic Network) was generated in 2007 by integrating genome annotation and metabolic reaction information from literature and different databases (Ma et al., 2007). Constraint-based metabolic models have been used (i) in metabolic engineering (Gopalakrishnan & Maranas, 2015; Kauffman et al., 2003), (ii) to predict knockout phenotypes (Segre et al., 2002; Shlomi et al.,

2005), (iii) to predict drug targets (Folger et al., 2011), (iv) to fill gaps in metabolic knowledge (Rolfsson et al., 2013; Rolfsson et al., 2011), (v) to study host-pathogen interactions (Heinken et al., 2013; Heinken & Thiele, 2015) and more.

1.3.3 Components of metabolic models

Gene-Protein-Reaction associations

Metabolic models have a hierarchical structure where metabolic reactions are connected to proteins and the genes are associated with the proteins. These Gene-Protein-Reaction (GPR) associations are a unique feature of metabolic network reconstructions. These GPRs are formulated as Boolean rules that considers subunits of a protein complex using “AND” operators and isozymes using “OR” operators. The GPRs are the crucial access points for incorporation of the genetic, transcriptomic or proteomics data into the metabolic networks. Thus, the accuracy of the GPR formulation is important for the contextualization of any metabolic network.

Stoichiometric matrix

Another component of a metabolic model is a stoichiometric matrix, denoted by *S*, which translates all the metabolic information in the model into a computable format. A stoichiometric matrix of size *m x n*, is created from the stoichiometric coefficients of the metabolites present in the reaction network. The *m* rows and *n* columns of the *S* matrix correspond to metabolites and reactions in the network, respectively. A negative integer indicates a metabolite being consumed and a positive integer indicates a metabolite being produced in the reaction. Most of the reactions involve few metabolites, thus most of the entries in individual columns are zero, this makes *S* a sparse matrix (Palsson, 2006).

Constraint based metabolic models operate under steady state assumption, represented mathematically:

$$Sv = 0$$

where *S* is the stoichiometric matrix as described above and *v* is the flux vector, containing all reaction fluxes. A vector *v* satisfying the above equation is said to be a steady-state flux distribution. Flux is the rate of consumption or production of a metabolite in a reaction. The commonly used units for flux are “mM/gDW/h” and “mM/cell”.

Bounds

All the fluxes in the model have upper and lower limits that are known as flux bounds. These bounds are defined by inequality constraints $v_{min} \leq v \leq v_{max}$.

The bounds can be defined based on experimental data for the activity or concentration of proteins or thermodynamics of the reactions that dictates the directionality of reactions. A model with all this information can be interrogated for feasible biological states using various computational methods (Orth et al., 2010).

Objective Function

In typical genome-scale metabolic models the number of reactions is higher than the number of metabolites, this implies that the system of mathematical equations generated from this information will have fewer equations than unknowns. Such a system of equations is referred to as underdetermined and does not have a unique solution. The solution space can be analyzed in order to infer various properties of the metabolic network using tools from linear algebra. The methods used for investigating the solution space and identifying the optimal solutions are described in the following sections.

Figure 1 explains the various components of a metabolic model using an example reaction network.

(a)

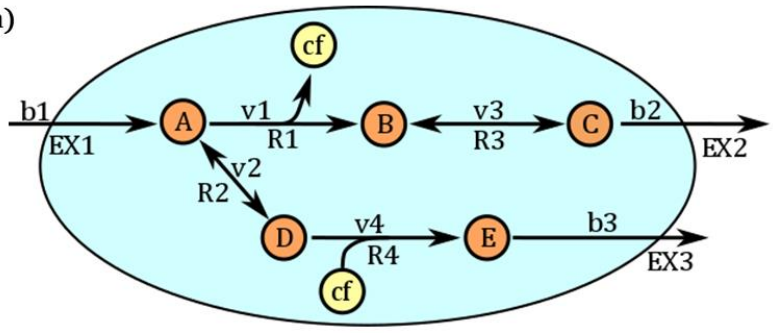

(b) GPR (Reaction, R1): (gene1) or (gene2 and gene3)

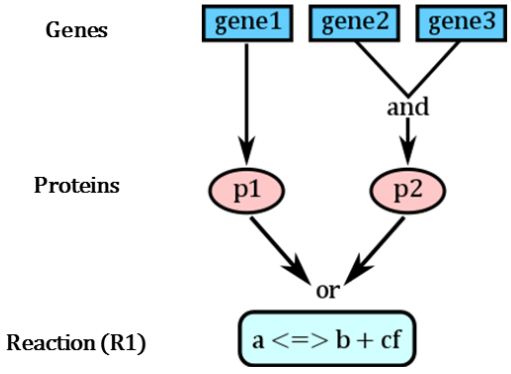

(c)

$$\begin{array}{c} \\ \text{Metabolites} \end{array} \begin{array}{c} \begin{array}{ccccccc} \text{R1} & \text{R2} & \text{R3} & \text{R4} & \text{EX1} & \text{EX2} & \text{EX3} \end{array} \\ \text{Reactions} \\ \begin{array}{c} \text{A} \\ \text{B} \\ \text{C} \\ \text{D} \\ \text{E} \\ \text{cf} \end{array} \begin{bmatrix} -1 & -1 & 0 & 0 & -1 & 0 & 0 \\ 1 & 0 & -1 & 0 & 0 & 0 & 0 \\ 0 & 0 & 1 & 0 & 0 & 1 & 0 \\ 0 & 1 & 0 & -1 & 0 & 0 & 0 \\ 0 & 0 & 0 & 1 & 0 & 0 & 1 \\ 1 & 0 & 0 & -1 & 0 & 0 & 0 \end{bmatrix} \end{array} \cdot \begin{bmatrix} v1 \\ v2 \\ v3 \\ v4 \\ b1 \\ b2 \\ b3 \end{bmatrix} = \begin{bmatrix} d[\text{A}]/dt \\ d[\text{B}]/dt \\ d[\text{C}]/dt \\ d[\text{D}]/dt \\ d[\text{E}]/dt \\ d[\text{cf}]/dt \end{bmatrix}$$

Stoichiometric Matrix *(S)* — Flux Vector *(v)* — Time derivative of metabolite concentration

(d)

Steady state assumption	$\mathbf{Sv = 0}$
Kinetic/Thermodynamic constrains on reaction fluxes	$0 \leq v1 \leq \infty$ $-\infty \leq v2 \leq \infty$ $-\infty \leq v3 \leq \infty$ $0 \leq v4 \leq \infty$ $-1 \leq b1 \leq 0$ $0 \leq b2 \leq 1$ $0 \leq b3 \leq \infty$
Objective	maximize b3

Figure 1. Components of metabolic models:

(a) An example reaction network consisting of six metabolic intermediates (A, B, C, D, E, cf), four metabolic reactions (R1, R2, R3, R4) and three exchange reactions (EX1, EX2, EX3). (b) An example Gene-Protein-Reaction association showing that R1 can be catalyzed by two isozymes (p1 or p2). It also shows that p1 is encoded by gene1 and p2 is a dimeric protein encoded by two genes (gene2 and gene3). (c) The metabolic information in panel a represented as a stoichiometric matrix. (d) The constraints used in a constraint based metabolic model. Adapted and modified from (Carron, 2011; Schellenberger et al., 2011).

1.3.4 Methods for flux analysis

Flux distribution through a metabolic network is the ultimate representation of phenotype of the cell in specific conditions. As discussed above CBM methods use environmental and genetic constraints imposed on a metabolic network to define a solution space, which contains all the feasible functional states of the network (Covert et al., 2004; Schellenberger et al., 2011). Each particular functional state in the solution space corresponds to a possible phenotype of the cell. Large-scale omics data such as transcriptomic, proteomic or metabolomics data can be used to define the constraints and reduce the set of feasible functional states. CBM methods provide a set of solutions that can be used to direct biological hypothesis development (Schellenberger et al., 2011). The constraint based reconstruction and analysis (COBRA) toolbox is an implementation in MATLAB, which provides tools to analyze, interpret and predict the feasible phenotypic states of GEMs (Palsson, 2015). Some of the methods to determine metabolic fluxes relevant to the studies described in this thesis are listed below.

Flux balance analysis

Flux balance analysis (FBA) is a commonly used flux analysis technique for studying metabolic models to predict the flux of metabolites through reactions within a metabolic network under specific constraints (Orth et al., 2010). FBA uses linear programming (LP) to determine a single (non-unique) flux distribution while optimizing for a specific biological objective function, for example, growth, ATP production, etc. (Nikoloski et al., 2008). This can be used in the analysis of specific cell behaviors in steady state conditions.

The following LP is used to perform flux balance analysis

$$\text{Maximize } c^T v$$

$$\text{subject to}$$

$$Sv = 0$$

$$v_{min} \leq v \leq v_{max}$$

The c vector specifies the cellular objective and the v vector is the flux distribution of the network, which indicates the contribution of reaction to the phenotype and is determined by solving the LP. The matrix S is the stoichiometric matrix and the vectors, v_{min} and v_{max} are boundary constraints on the flux vector as described previously (Mahadevan & Schilling, 2003; Orth et al., 2010). FBA has diverse applications in physiological studies, for example: (i) genome-scale synthetic biology (Feist & Palsson, 2008), (ii) gene knockout simulations (Edwards & Palsson, 2000; Folger et al., 2011), (iii) to

predict the yields of cofactors such as ATP or NADH (Varma & Palsson, 1993) and more.

The flux distribution obtained by solving FBA is one of an infinite number of alternative flux solutions possible for the optimal value of objective function. Typically, genome-scale metabolic models are able to achieve alternate, or equivalent, steady-state flux distribution corresponding to the same values of optimal objective function, meaning genome-scale constraint-based metabolic models can achieve same optimal functional state in many different ways (Palsson; Reed & Palsson, 2004). The big grey dots in **Figure 2** represent two alternative optimal solutions. These alternative optimal flux solutions reflect that biological networks can accomplish the same function in various different ways. This issue of alternate solutions is common and worth investigating in order to characterize large-scale metabolic networks.

Flux variability analysis

Flux variability analysis (FVA) determines the range of the allowable fluxes through each reaction while maintaining a defined state of the network, e.g., supporting maximum biomass production (Mahadevan & Schilling, 2003). FVA provides insights into alternate optimal solutions, network flexibility and redundancy (Gudmundsson & Thiele, 2010; Thiele et al., 2010). It also helps in the identification of reactions that are important in the network by identifying reactions that have a narrow range of fluxes through them (Mahadevan & Schilling, 2003) and studying flux distributions under suboptimal growth (Reed & Palsson, 2004).

Sampling of flux solutions

Uniform random sampling of the flux solution space allows the unbiased evaluation of its contents (Palsson, 2006). FBA optimizes a user-specified cellular objective, e.g. growth, while fulfilling certain constraints, resulting in a single flux distribution. FVA gives the range of possible fluxes for each reaction. Whereas, random sampling returns a set of flux distributions from the pool of fluxes that satisfy the constraints. These sampled flux distribution points can then be used to determine the *distribution* of fluxes for each reaction (Schellenberger & Palsson, 2009). This technique allows the evaluation of statistical scores for the significance of flux change between conditions (Bordel et al., 2010). Random sampling of feasible flux solution space can be used to determine correlation between reaction fluxes (Papin et al., 2004).

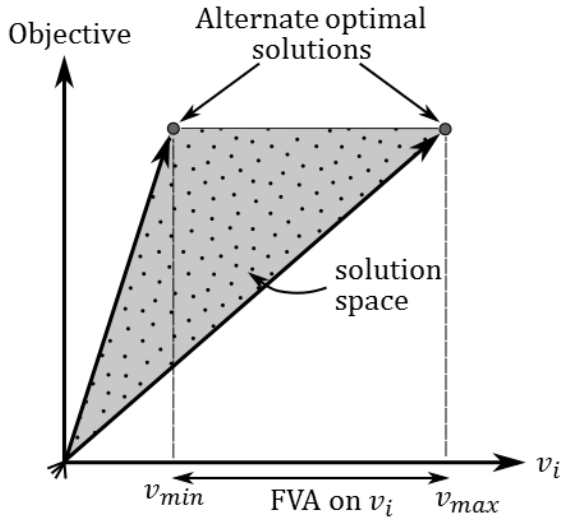

Figure 2. Illustration of different flux analysis methods (FBA, FVA and random sampling):

In the illustration the vertical axis represents the flux through the objective function and horizontal axis represents the flux (v_i) of a reaction *i*. The grey region represents the allowable solution space under specific constraints. The grey big dots represent alternate optimal solutions. FBA determines one of the infinite optimal solutions. FVA gives the allowable range on reaction *i*. The black small dots represent sample points obtained after randomly sampling the solution space. Adapted and modified from (Palsson, 2015).

1.3.5 Types of metabolic models

Metabolic network reconstructions can be divided into two categories; global metabolic models containing metabolic information about the whole organism, e.g. Recon 1, a human metabolic model and context specific metabolic models containing cell/tissue specific information, e.g. iAB-RBC-283, a model for red blood cell metabolism. These models can be generated manually in an iterative process or automatically using computational algorithms.

Global metabolic models

Recon 1 was the first global model of human metabolism, generated using the human genome annotation data and the biochemical knowledgebase accumulated over decades (Duarte et al., 2007). Recon 1 contains 3744 reactions, 2744 metabolites and 1496 genes, and was extensively manually curated using data from the scientific literature. Recon 1 has been used as a platform for studies of various aspects of human metabolism (Bordbar et al.,

2011a; Bordbar et al., 2011b; Folger et al., 2011; Shlomi et al., 2009). Recon 2 is an updated version of Recon 1 and is currently one of the most comprehensive representations of human metabolism publically available. Recon 2 (version Recon 2.04) captures the functions of 1789 unique genes, 2626 unique metabolites and 7440 reactions. These models contain the information for known metabolic reactions in humans irrespective of the tissue, cell or condition; therefore, these are referred to as global or generic metabolic models. The Human Metabolic Reaction (HMR) is another global metabolic model, containing 3765 genes associated with over 8000 reactions and over 3000 unique metabolites in the latest version HMR2 (Mardinoglu et al., 2014).

The utility of global metabolic models has been demonstrated in several studies. Duarte et al. (2007) identified sets of reactions which are causally connected to hemolytic anemia and predicted potential drug targets for hypercholesterolemia (Duarte et al., 2007). Shlomi et al. (2009) predicted metabolic biomarkers in inborn errors of metabolism (Shlomi et al., 2009). Rolfsson et al. (2013) utilized the generic human metabolic model Recon 1 to uncover novel metabolic functions in humans (Rolfsson et al., 2013). The global human metabolic reconstructions have also been used to reconstruct functional metabolic models of specific human cells or tissues; some of these models are explained in the next section. These cell/tissue-specific models (also known as context-specific models) can be used to investigate the metabolic state of the tissue under different physiological conditions using COBRA tools.

Context-specific metabolic models

The global metabolic models capture the whole body metabolism irrespective of the cell, tissue or condition. However, no one cell in the whole body utilizes all the possible pathways at any given time. The active metabolism in a particular cell depends on the context, for example the skeletal muscles and the brain can utilize ketone bodies as an energy source but the liver cannot; cancer cells have highly active glycolysis compared to normal cells. Therefore, in order to examine a specific condition or cell, a context-specific (cell-specific) model is required. Some examples of cell/context-specific models and their applications are described below:

Platelets: Proteomic datasets and the scientific literature were used to define the platelet metabolic network (iAT-PLT-636) based on Recon 1. It is a manually curated, functionally tested, and validated model of platelet metabolism. The model contains 1,008 reactions including enzymes associated with 403 diseases and 231 FDA approved drugs, 739 metabolites and 636 genes. This model was used to evaluate the effects of aspirin

resistance on platelet metabolism using constraint-based modeling techniques. This study demonstrated that in order to synthesize eicosanoids and to combat reactive oxygen species stress, platelets redirect the flux through glycolysis, fatty acid metabolism, and the nucleotide metabolism (Thomas et al., 2014).

Red blood cells: iAB-RBC-283 is a full bottom-up reconstruction of erythrocyte metabolism with extensive manual curation using literature assessment. The reactions inferred from proteomic datasets were cross-referenced with previous experimental studies and metabolomic data. The final model contains 369 reactions including 292 intracellular reactions and 77 transporters, 267 unique metabolites, and 283 genes. The model was utilized to qualitatively detect the *in silico* metabolic signatures for the conditions pertaining to the morbid SNPs from the Online Mendelian Inheritance in Man (OMIM) and FDA-approved drugs from DrugBank (Bordbar et al., 2011b).

Hepatocytes: Reconstruction of the liver metabolism was inferred from Recon 1 and the literature and various datasets including metabolomic, transcriptomic, proteomic, and phenotypic data of the liver. The liver model contains a network of 1827 reactions and 1360 metabolites. The model was used to predict fluxes across a variety of hormonal and dietary conditions. The flux predictions correlate well with measured fluxes and the biomarker predictions were more accurate than for the generic human model (Jerby et al., 2010).

Cardiomyocytes: The first cardiomyocyte metabolic model named CardioNet was derived from Recon 1 based on gene expression information from two different datasets available on gene expression omnibus (Barrett & Edgar, 2006) and evidence for metabolic reactions active in cardiomyocytes. The model comprising of 1793 metabolic reactions was used to demonstrate the effect of changed amount of glucose, lactate, fatty acids and ketone bodies on the processes essential for cardiomyocytes, such as efficiency of the maintenance of ATP, synthesis of cardiolipin, ceramide and other phospholipids (Karlstadt et al., 2012).

Cancer cells: Folger et al. (2011) constructed the first metabolic model of cancer metabolism that captured the key metabolic functions shared across various cancer types (Folger et al., 2011). The cancer metabolic model was derived from the human metabolic model Recon 1 using cancer gene expression data utilizing a variant of the MBA algorithm. The model predicted cytostatic drug targets, some of which were targeted by known, approved or experimental anticancer drugs. The model was also used to compile probable treatments for specific cancers based on cancer type-specific gene

expression and mutations (Folger et al., 2011). Agren et al. (2012) generated genome-scale metabolic models for 16 cancer types and 69 human cell types using the INIT algorithm (Agren et al., 2012). Comparison of the metabolic models of cancer types and healthy cell types helped to reveal cancer-specific metabolic features comprising generic potential drug targets for cancer treatment (Agren et al., 2012).

These examples of context-specific models discussed above demonstrate the importance of generating and investigating cell/condition specific models. The following section describes available algorithms for generating these context-specific models.

1.3.6 Context-specific model generation algorithms

Increasing availability of omics data including quantifications of thousands of cellular components is readily available and the apparent benefits of generating context-specific models have directed the development of methods to integrate this data with metabolic models. Many algorithms have been developed for generating context-specific models from generic metabolic models, for example, GIMME (Becker & Palsson, 2008); MBA (Jerby et al., 2010); iMAT (Zur et al., 2010); mCADRE (Wang et al., 2012); INIT (Agren et al., 2012); FASTCORE (Vlassis et al., 2014).

FASTCORE is an algorithm for generating context-specific metabolic models using generic genome-wide metabolic models. The input for the FASTCORE algorithm is a set of reactions called core reactions that are active in the cell or tissue under study. This set is based on the biological data, such as gene and protein expression data, specific for the cell/tissue under study. The algorithm searches for a consistent subset of the generic model containing all the core reactions and a minimum number of additional reactions. Consistency of a network implies nonzero fluxes. FASTCORE is devoid of free parameters and derives more compact metabolic models in significantly lesser time than its rival method MBA (Vlassis et al., 2014). The main advantage of FASTCORE is that it is fast enough to allow multiple runs. This feature can be very useful in testing the robustness of the model generated by FASTCORE as a function of other parameters such as threshold used in the gene expression data. Different sets of core reactions defined by a range of threshold values can be used to generate models using FASTCORE in a few minutes, whereas most other algorithms would either need extremely long time or would even fail if they require manual work to curate and assemble the model.

In first study described in this thesis, FASTCORE and transcriptomic data were used to derive context-specific metabolic models in order to study epithelial to mesenchymal transition (EMT). This approach assumes that

transcriptomic data can be used to define the presence or absence of flux in reactions. This assumption is supported in multicellular organisms by the complete activation or deactivation of pathways in tissue-specific manner (Machado & Herrgard, 2014).

The following sections give an overview of EMT and associated processes.

1.4 Epithelial to mesenchymal transition

Epithelial to mesenchymal transition (EMT) is a fundamental developmental process where epithelial cells undergo multiple biochemical changes and de-differentiate into mesenchymal-like cells (Kalluri & Weinberg, 2009). EMT is associated with several phenotypic changes such as, loss of cellular polarity, degradation of the basement membrane along with gain of migratory and invasive properties (**Figure 3**) (De Craene & Berx, 2013). These changes are coupled with modifications in genes and proteins of different families such as cadherins, catenins, growth receptors and transcription factors. Decreased expression of epithelial markers such as E-cadherin and increased expression of mesenchymal markers like N-cadherin and vimentin are indicators of EMT (Acloque et al., 2009). EMT is a reversible process, i.e., the epithelially derived mesenchymal cells can return to their original epithelial phenotype and initiate new tissues via mesenchymal to epithelial transition (MET) (Kalluri & Weinberg, 2009). Based on the parent tissue and developmental stage of the organism, EMT has been categorized into three different types; EMT type 1 which is associated with implantation and organ development in the embryo after fertilization; EMT type 2, which is associated with tissue regeneration, wound healing and organ fibrosis; and EMT type 3, which is related to cancer metastasis (Kalluri & Weinberg, 2009; Nantajit et al., 2015).

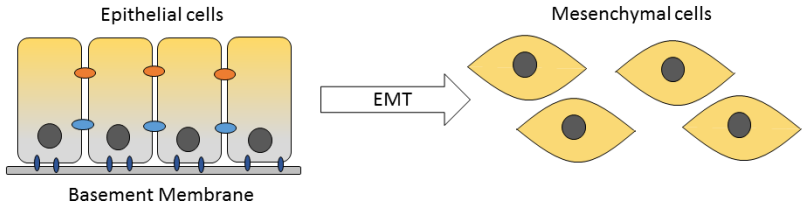

Figure 3. EMT:

The cartoon figure above illustrates epithelial to mesenchymal transition, where membrane bound polar epithelial cells undergo various changes and become motile.

1.4.1 EMT in cancer metastasis

EMT is crucial for embryonic development and tissue repair, whereas its dysregulation can be highly damaging (Acloque et al., 2009). EMT has been associated with cancer progression to distant tissues and formation of secondary tumors (Polyak & Weinberg, 2009). The epithelial cells bound to the basement membrane transform to invasive mesenchymal-like cells which exist essentially without direct cell-cell contact. The ability of the tumor mesenchyme to separate from basement membrane and intravenously migrate to a distant tissue is an important initiating step in tumor metastasis (Acloque et al., 2009). During this migratory process, the mesenchymal cancer cells have enhanced invasiveness and protection from apoptosis and senescence. Upon lodging at the distant site the mesenchymal-like cells undergo MET, potentially due to the absence of EMT-inducing signals from the primary tumor site that stimulated EMT in the first place (Nantajit et al., 2015).

1.4.2 Factors inducing EMT

A number of factors can induce EMT including epidermal growth factor (EGF), transforming growth factor-b (TGF-b), vascular endothelial growth factor (VEGF) and hepatocyte growth factor (HGF) (Garg, 2013; Sigurdsson et al., 2011). The signaling factors affect transcriptional regulators such as Snail, Slug, ZEB1, ZEB2, FOXC2 and Twist, which in turn control the expression of mesenchymal and epithelial markers (Garg, 2013). EMT-inducing factors promote the disorganization of the basal cytoskeleton, loss of polarity of the epithelial cells and the disruption of intercellular adhesion complexes. Thus, the cells gain migratory and invasive properties, which help the cells to leave the parent tissue and begin to migrate individually (Acloque et al., 2009).

1.4.3 EMT metabolism

EMT is a reversible process; therefore, it is likely that EMT is not aided by permanent genetic changes but by transient molecular alterations (Li & Li, 2015). EMT is closely associated with reversible epigenetic regulatory mechanisms that rely on dynamic transcriptional programming changes rather than affecting the genetic sequence (Tam & Weinberg, 2013). DNA methylation and covalent post-transcriptional modifications of histone proteins such as, phosphorylation, acetylation, biotinylation and methylation mediate these modifications of the gene expression. The enzymes responsible for these modifications require metabolic intermediates such as, FAD, acetyl-CoA, α-KG and NAD+, as substrates or cofactors (Kaelin & McKnight, 2013; Lu & Thompson, 2012). Therefore, variation in the levels of metabolic fluxes can affect the activities of chromatin modifying enzymes and

in turn the gene expression (Li & Li, 2015). Recent evidence has confirmed that changes in metabolic enzymes affect epigenetic modifications during EMT. For example, fructose-1,6-bisphosphatase and ATP-citrate lyase have been shown to be associated with EMT in different cancer cells (Dong et al., 2013; Hanai et al., 2012). These results show that metabolism impacts and is impacted by EMT but the studies of the cellular metabolic changes associated with EMT are still scarce (Li & Li, 2015). Although the interest in understanding the metabolism of EMT is increasing in recent years, not many studies have used the systems approach to understand EMT metabolism.

1.4.4 Approaches for studying EMT

EMT has mainly been studied using targeted molecular biology approaches but it is a complex process which affects and is affected by all the processes in the cell, including, metabolism and signaling, therefore systems level understanding of the changes during EMT is important. A few studies using different systems level approaches to understand EMT have been published in past years, for example, Shaul et al. (2014) analyzed the differences in expression of metabolic genes in different cancer cell lines. They demonstrated that carcinomas bearing mesenchymal markers contain a unique set of 44 metabolic genes. They also demonstrated that upregulation of the metabolic enzyme dihydropyrimidine dehydrogenase was necessary for the cells to attain mesenchymal characteristics upon initiation of EMT (Shaul et al., 2014). Thomson et al. (2011) measured variations in epithelial, ‘metastable’ mesenchymal and ‘epigenetically-fixed’ mesenchymal states using correlation of RNA transcript, phosphopeptide, protein and phosphoprotein levels in the cells. They extensively analyzed large-scale data sets in order to gain a better understanding of the differences in various stages of EMT. From their analysis they concluded that there are a number of recurring themes in the transcriptional and protein regulatory changes observed during EMT, these include changes in the cell–cell junctional proteins, pro-invasive and pro-migratory proteins along with changes in the flux through metabolic pathways and secreted cytokines. For instance, they demonstrated a shift from EGFR and IGF1R activated signaling networks to autocrine survival networks during EMT. Their analysis also showed reductions in oxidative and redox stress networks with EMT (Thomson et al., 2011). In another study Kalita et al. (2013) investigated the changes in innate pathways in a primary airway epithelial cell model of EMT using gene expression profiling and deterministic mathematical modeling. Their results demonstrate that the epigenetic changes during EMT cause dynamic state changes of the innate signaling pathway (Kalita et al., 2013). These are a few examples of studies that include large-scale data to understand EMT.

In the first part of this thesis, as mentioned above, biological data from D492, a breast epithelial cell line that can undergo EMT, were used to derive context-specific metabolic models. These models were utilized to simulate and gain a better understanding of metabolic changes during EMT. These metabolic models were used to predict targets to revert mesenchymal phenotype to epithelial. As mentioned in previous sections, metabolic models are tools used to direct biological hypothesis, which have to be tested using classical biochemistry and molecular biology experiments. The hypotheses generated using EMT metabolic models are in the process of being tested but have not been included in this thesis due to time constraint. But the second section of this thesis is based on the testing of hypothesis generated from a previous computational study.

1.5 Gluconate metabolism in humans

In the second part of this thesis, gluconokinase, a human metabolic function recently identified in a gap filling study, was investigated using constraint-based modeling. Additionally, the enzyme was expressed and characterized using various biochemical techniques. The following text gives a background of gluconate, gluconokinase, how gluconokinase was identified and the biochemical techniques used in the characterization of human gluconokinase.

The technique of using a metabolic reconstruction along with reaction databases to pinpoint missing links in metabolic knowledge is called gap-filling. Metabolic reactions in a reconstruction which are not completely connected to the rest of the network can be identified using constraint-based methods. These reactions either utilize metabolites which are not produced in a metabolic model or produce metabolites which are not consumed in the model. Such reactions and metabolites highlight the parts of the metabolic reconstruction which lack information. Metabolic models can therefore be used to identify parts of metabolic networks where knowledge is incomplete. The novel gluconokinase function and a library of chemical reactions were identified using Recon 1, in this manner (Rolfsson et al., 2013; Rolfsson et al., 2011).

Gluconokinase is a metabolic enzyme which catalyzes the phosphorylation of gluconate using ATP to form 6-phosphogluconate (Zhang, Y. et al., 2011), which is an intermediate of the pentose phosphate pathway (hexose monophosphate shunt, HMS) **(Figure 4)**. Gluconate is a compound that is naturally found in fruits, vegetables and dairy products. Due to its refreshing taste, it is also artificially added to processed food and pharmaceuticals (Ramachandran et al., 2006; Singh & Kumar, 2007). Gluconate has been shown to be present in human bio-fluids (Bouatra et al., 2013; Psychogios et al., 2011). Despite the presence of gluconate in human

bio-fluids and its widespread use, the details of gluconate production and consumption in humans were relatively unexplored. Given that gluconate is absorbed, its metabolism is likely to follow the route shown in (**Figure 4B**). Human gluconokinase is likely to play a crucial role in human metabolism by metabolizing gluconate and feeding HMS. It is therefore, worth investigating.

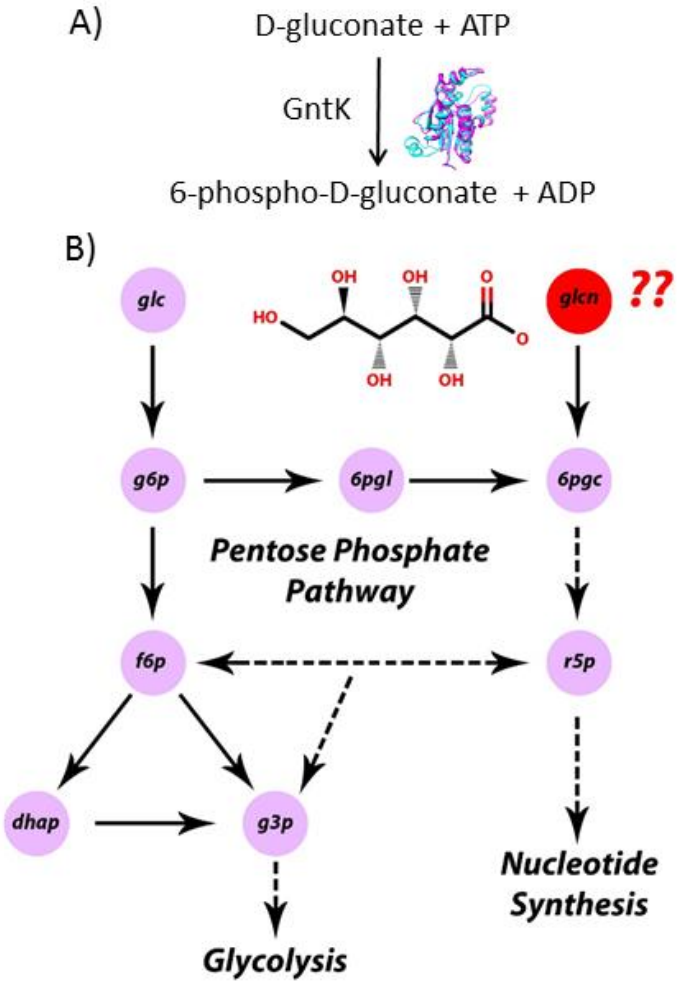

Figure 4. Overview of gluconate metabolism in humans:

Panel A) Chemical reaction showing ATP dependent conversion gluconate to 6-phosphogluconate by gluconokinase (EC 2.7.1.12). Panel B) The product of gluconokinase, 6-phosphogluconate can be degraded through pentose phosphate pathway.

1.6 Enzyme assays

All enzyme assays rely ultimately on determining the catalytic activity of the enzyme, including studies that are not principally kinetic (Cornish-Bowden, 2004). Initial studies investigating rates of enzymatic reactions were first performed in the latter part of 19th century using primitive assays. Methods for enzymes purification and pH control did not exist at that time. Usually the course of the reaction was followed over a period of time by following the change in a measurable property of the reaction, e.g., color. However, modern assays of measuring rate of reaction at varying concentrations of substrates and inhibitors give easily understandable results. These assays can be performed using discontinuous methods, where samples from the reaction mixture are removed at regular intervals and examined to evaluate the progress of the reaction. For example, chromatographic techniques can be used to measure the progress of a reaction by measuring the amount of product formed in the sample removed from the reaction mixture. Continuous enzymatic assays are more convenient because the extent of the reaction is observed continuously with the help of automated recording techniques and no further work is needed. Examples of continuous assays for studying enzyme kinetics are spectrophotometric and calorimetric assays.

1.6.1 Spectrophotometric assays

Spectrophotometric assays follow the course of an enzymatic reaction by measuring a change in the light absorbed by the assay solution. UV light is often used in these assays because NADH and NADPH, which are common coenzymes, absorb UV light, while their oxidized forms NAD^+ and $NADP^+$ do not. For instance, an oxidoreductase that uses NADH could be characterized by measuring the decrease in the light absorbed at 340 nm. Even if an enzyme reaction cannot be followed directly by analyzing a change in the absorbance of light, it may still be possible to follow it indirectly by coupling it to another reaction and using spectrophotometric assay. In coupled assays, two reactions are combined in such a way that the product of one reaction is the substrate of another reaction that can be easily detected using spectrophotometer, which is a standard procedure used in enzyme kinetic assays. For example, in order to study the activity of pyruvate kinase, the production of pyruvate can be coupled to NADPH production, using lactate dehydrogenase, as shown in **Figure 5**. This is a widely used method to study enzyme kinetics (Jones & Hirst, 2013; Rohatgi et al., 2014; Wilkinson et al., 1984).

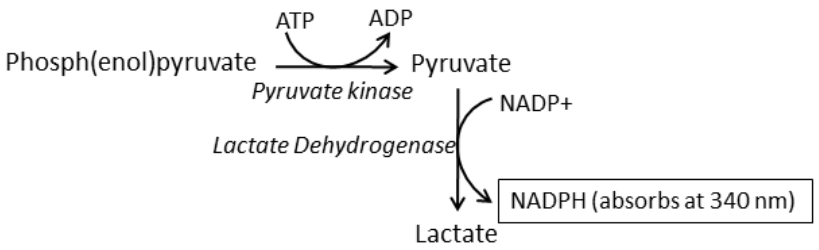

Figure 5. Example coupled assay:

Activity of the enzyme pyruvate kinase can be measured by coupling the production of pyruvate to lactate dehydrogenase. Changes in the concentration of NADPH can be estimated by measuring changes in absorbance at 340 nm using a spectrophotometer.

1.6.2 Isothermal titration calorimetry

All chemical reactions or physical changes are accompanied by a heat change; heat is either taken up from the surroundings (endothermic reactions) or heat is given to the surroundings (exothermic reactions). The rate and amount of heat exchanged with the surroundings is equal to the rate and amount of the reaction that has occurred, respectively. Isothermal titration calorimetry (ITC) is a calorimetric technique that measures the amount of heat changes during a reaction or a process. Thus ITC is a suitable instrument to measure the rate and amount of chemical reactions and physical processes. ITC is a suitable technique for directly determining the energetics of bio-molecular binding processes, such as DNA-protein binding, protein-protein binding, protein-ligand binding, etc. (Freyer & Lewis, 2008)

The working principle of ITC

An ITC instrument operates according to the dynamic power compensation principle, that is, it measures the power required in order to maintain the measurement cell at a constant temperature (isothermal). There are two cells in an ITC instrument, a measurement cell containing the reaction mixture and a reference cell containing the buffer (**Figure 6**). Heat absorbed or released from the chemical reaction is detected and the power applied to the reaction cell is adjusted so that the temperature of the two cells remains constant. Therefore, the raw signal in the ITC is the power applied in order to keep the cell at a constant temperature as a function of time (µcal/sec). The heat change can then be calculated by integrating the power applied by the instrument over the time of the measurement (Freyer & Lewis, 2008).

The heat changes that occur during a reaction can be used to determine the binding stoichiometry (n), binding affinity (K_a) and enthalpy changes (ΔH) of the interaction between the molecules in the solution. From these initial parameters, Gibbs energy changes (ΔG) and entropy changes (ΔS) can be calculated using the following relationship:

$$\Delta G = - RT\ln K_a = \Delta H - T\Delta S$$

where, R is the gas constant and T is the absolute temperature. More details on ITC data analysis are given in Paper III.

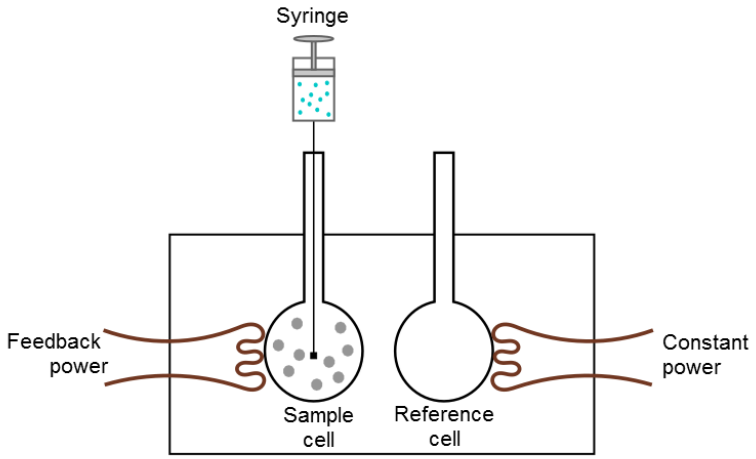

Figure 6. Representation of typical ITC setup:

The sample cell and the reference cell are maintained at a constant temperature. The change in heat required to maintain the temperature of the sample cell is equivalent to the progress of reaction after adding the substrate from the syringe into the sample cell. Adapted and modified from (Zhou et al., 2011).

Applications of ITC

ITC provides label-free, rapid and accurate measurements of the thermodynamics of molecular interactions. It can, therefore, be applied to a diverse range of systems including, protein-ligand, protein-protein and protein-membrane interactions and enzyme kinetics. This makes ITC a widely applicable technique in industries such as the pharmaceutical and food making industries.

Thermodynamic applications: The main application of ITC is to measure the affinities of biomolecules in order to understand the mechanism of interaction. ITC has been used in several studies, to investigate protein-ligand binding. For example, Day et al. (2002) demonstrated the interactions of carbonic

anhydrase II with two variations of a common drug pharmacophore. These two bindings have very similar free energies but the enthalpies differ by a factor of 2.5 (Day et al., 2002). This study also demonstrates how important it is to measure the thermodynamics and the computational predictions of thermodynamic parameters are not always accurate. Another study illustrating the discrepancies between predicted and measured binding energetics was done by Cho et al. (2010) who used ITC, to measure the effects of mutations on binding thermodynamics in a model interacting system. X-ray structural determination was used to study crystal structures of each of the mutant proteins in both the bound and unbound states. This allowed direct comparison of binding energetics and structural changes during binding. Their results suggested that previously reported discrepancies between predictive algorithms for estimating binding energies from structural parameters, and experimentally measured binding energetics may be largely explained by conformational changes in the bound ligands, or transitions from unfolded to folded states during binding (Cho et al., 2010). These studies successfully demonstrate the applicability of ITC in determining the thermodynamics of binding.

Kinetic applications: Apart from thermodynamic studies, ITC is also an adequate method for the characterization of enzyme-catalyzed reactions because it does not need the chromogenic, fluorogenic or radioisotope labeled ligands used in most enzyme assay methods. ITC has been successfully used to nondestructively characterize enzymes with physiologically relevant substrates having spectroscopically opaque solutions. Applicability of ITC was demonstrated by Todd and Gomez in a study characterizing enzymes from all the enzyme commission categories; dihydrofolate reductase, creatine phosphokinase, hexokinase, Heliobacter pylori urease, trypsin, HIV-1 protease, heparinase and pyruvate carboxylate. The study demonstrated that ITC is a universal assay, which can have widespread applications in functional genomics (Todd & Gomez, 2001). In another study Henzler et al. (2008) investigated the activity of β-glucosidase immobilized onto spherical polyelectrolyte brushes (SPBs) using isothermal titration calorimetry (ITC). Their results also reveal that ITC is a more accurate method than UV-Vis spectroscopy for studying the activity of immobilized enzymes (Henzler et al., 2008). These studies demonstrate that ITC is an excellent method for determining kinetic parameters of enzyme-catalyzed reactions.

2 Aims

The general aim of this thesis was to expand the knowledge of human metabolism using systems biology methods and biochemistry techniques. This was achieved in two parts, (i) using CBM to understand metabolic changes associated with EMT and (ii) using CBM and ITC to expand the knowledge of a recently identified enzyme, human gluconokinase. The specific aims of the studies included in this thesis are summarized below:

Paper I:	To generate metabolic models for studying the metabolic changes during epithelial to mesenchymal transition using systems biology tools.
Paper II:	To characterize human gluconokinase (Gnt*K*) and gluconate metabolism using substrate specificity, spectrophotometric assays and metabolic modeling.
Paper III:	To uncover the reaction mechanism of human gluconokinase using isothermal titration calorimetry.

The specific studies presented in this thesis are connected in the context of metabolic model building and analysis. The process of model building can be divided into three major steps: 1) generating a draft model, 2) *in silico* analysis of the model and 3) validation of the results. The validated results can be used for generating research hypothesis, which can direct biological experiments.

In the first study, models were generated and analyzed to study EMT. The validation of all the model predictions is in pipeline for future work.

Gluconokinase was identified as a human metabolic function in a previous gap filling study (Rolfsson et al., 2013; Rolfsson et al., 2011). This hypothesis was tested in the second part of this thesis that includes Paper II and III. This section demonstrates how pre-existing knowledge can be integrated with metabolic models to direct biological research.

Therefore, this thesis demonstrates all the steps of model building and analysis using different biological problems.

3 Summary of main contributions

This chapter reviews the work presented in this thesis, focusing on my contributions to the individual studies. Parts of these discussions refer to the published articles and the manuscript presented in the next chapter.

3.1 Paper I: Metabolic re-wiring of isogenic breast epithelial cell lines following epithelial to mesenchymal transition

This study describes and compares the metabolic phenotypes of isogenic breast epithelial cell lines using systems biology tools. In this project, I generated and analyzed metabolic models to study EMT. Steinn Gudmundsson supervised the model generation and analysis process. Skarphedinn Halldorsson collected and analyzed the cellular data. Ottar Rolfsson supervised the project. Other co-authors contributed to the resources, expression data and metabolomics profiling of the cells.

The two cell lines investigated here are D492, a breast epithelial cell line and D492M, a mesenchymal cell line that originated from D492 co-cultured with endothelial cells (Sigurdsson et al., 2011). The motivation for this work came from the fact that EMT metabolism has mainly been studied using targeted molecular biology approaches, whereas, it is a complex process and systems analysis could provide valuable information about EMT. In past years, a few studies using systems based analysis have successfully presented novel insights into EMT, as discussed in the introduction chapter (section 1.4.4). In this study, we present the first genome-scale metabolic models to simulate metabolic changes during EMT.

Metabolic models of the two cell lines were derived from Recon 2 based on gene expression data and metabolite uptake/secretion profiles. The curated metabolic models of D492 are the first models of EMT metabolism generated to date. The methodology used to generate the models represents a novel approach to constructing context-specific metabolic models. We used a transcriptomic dataset together with metabolic uptake/secretion profiles, descriptive of both cell lines, to generate a basis for model construction (the EMT model). This model was manually curated to check for discrepancies. Then we further constrained the EMT model to generate metabolic models descriptive of D492 and D492M metabolism, called the EPI and MES models respectively. The approach allows direct comparison of metabolic models

and is of value when modeling biological events such as EMT where one phenotype is derived from the other and the transition is reversible.

The metabolic models predicted higher flux through the biomass reaction in EPI model than in MES model indicating faster growth of the epithelial cells. The prediction of higher growth for epithelial cells was in agreement with the experimentally determined growth rates of the cells. The difference in the flux through biomass reaction in the models was due to lower cardiolipin synthase activity in the MES model, suggesting altered mitochondrial metabolism. To test this hypothesis, maximum mitochondrial ATP production was predicted by adding a demand reaction for mitochondrial ATP to the EPI and MES models and performing flux balance analysis. Maximal mitochondrial ATP production in the EPI model was found to be nearly 4 times higher than in the MES model. These predictions were supported by experimental data, which showed that D492 cells have higher spare capacity to perform oxidative phosphorylation than D492M cells.

The differences in the metabolic phenotypes of the models were further studied using random sampling of the flux solution space. Flux distributions of the two models were compared using the two-sample Kolmogorov-Smirnov test. This revealed that the metabolic reactions involved in the N- and O-glycan metabolism carried more flux in the MES model, along with keratan sulfate metabolism. All the reactions in purine synthesis and cysteine metabolism were upregulated in the EPI model. The overall glycolytic flux was higher in EPI model. In the MES model flux towards single carbon metabolism from glycolysis was higher. In the EPI model glutamine was used for purine synthesis, while MES model glutamine was converted to alpha-ketoglutarate which fed into TCA cycle.

We further used the models to identify which reactions were important for converting the epithelial phenotype to a mesenchymal–like phenotype and vice-versa. For this purpose, an optimization algorithm was designed to find reactions crucial for transforming the epithelial phenotype into the mesenchymal-like phenotype and vice-versa. For converting the epithelial phenotype to mesenchymal i.e., EMT, most of the reactions requiring regulation were involved in keratan sulfate degradation. For transforming the mesenchymal phenotype to epithelial i.e., MET, out of the 335 target reactions 288 were extracellular transporters associated with only 5 genes. A large number of target reactions were involved in nucleotide interconversion, glycine, serine, alanine and threonine metabolism and arginine and proline metabolism. We then identified transcription factors (TFs) that have been associated with the genes required for EMT and MET in the D492 models using online databases. The TFs Sp1 and TFIID exhibit binding to genes associated with EMT while C/EBPbeta, Msx-1, N-Myc and HFH-1 were

predicted to bind to genes associated with MET. The results represent hypothesis of transcription factors important for developmental regulation in the D492 cell model.

Gene targets lethal in one of the models but not in the other were predicted using the COBRA toolbox. Gene targets exclusively lethal for the EPI model were fumarase, succinate dehydrogenase (complex II) and ATP synthase. These genes were associated with reactions in the TCA cycle and oxidative phosphorylation while the genes lethal for the MES model were associated with anaplerotic reactions that feed into the TCA cycle. This included reactions involved in acetyl-CoA and fumarate production and SLC7A5 sub-unit of the large neutral amino acid transporter LAT1. These results predict that D492M cells can bypass the electron transport chain by supplying mitochondria with TCA cycle intermediates derived from branched chain or other non-polar amino acids.

To summarize, we constructed context-specific metabolic models for pre- and post- EMT phenotypes. We used these models to elucidate the metabolic changes during EMT.

3.2 Paper II: Biochemical Characterization of Human Gluconokinase and the Proposed Metabolic Impact of Gluconic Acid as Determined by Constraint Based Metabolic Network Analysis

The second paper describes the characterization of isoform I of human gluconokinase (hGntK) expressed in *E. coli* and its effects on human metabolism. The motivation for this work came from the fact that human gluconokinase activity was recently identified in a gap filling study using a generic human metabolic reconstruction (Rolfsson et al., 2013). This posed questions about the role of gluconate in human metabolism as gluconate is widely found in nature. In this project, I used constraint - based metabolic modeling methods to evaluate the impact of gluconate on human metabolism.

Reactions specific for uptake and consumption of gluconate were added to the red blood cell metabolic model (iAB-RBC-283), along with the gluconokinase reaction. 6-phosphogluconate formed by gluconokinase reaction is a pentose phosphate pathway (hexose monophosphate shunt, HMS) intermediate. As expected, adding gluconate phosphorylation reactions to the model resulted in an increase in the flux range of all reactions in the HMS. The NADPH produced in HMS caused higher flux through reactions producing reduced glutathione and reactions associated with fatty acid

metabolism. Glycolysis and HMS are closely interlinked which led to increased flux in glycolysis and ultimately pyruvate and lactate.

The effect of GntK flux on the objective function in the model (ATP dependent Na2+/K+ pump) was investigated using robustness analysis, where FBA was performed at forced and increasing rates from 0 to 20 mmol/gDW/h of gluconate uptake. The maximum objective was obtained at a flux of 0.2 mmol/gDW/h through the gluconokinase reaction. This flux was roughly 18% of the fixed glucose uptake rate (1.12 mmol/gDW/h). From 0.2 to 4.5 mmol/gDW/h the objective plateaued out and then sharply dropped. This was because the metabolites required for gluconate catabolism became limiting. Shadow prices for each metabolite were calculated to investigate which metabolites were limiting. In the absence of gluconate, 89 out of the 267 metabolites in the model affected the flux through the objective while in the presence of gluconate only 10 metabolites had an effect. The metabolites limiting in presence of gluconate were associated with either bicarbonate transport/exchange (such as bicarbonate, chloride, potassium, bilirubin monoglucuronide, bilirubin, biliverdin and carbon monoxide) or glutathione synthesis (such as L-cysteine, γ-L-glutamyl-L-cysteine and glycine). These metabolites were limiting because these were needed to combat the effect of increased levels of NADPH and carbon dioxide generated from gluconate catabolism.

Further investigation into the limiting factors of gluconate metabolism was performed by relaxing the bounds constraining each exchange reaction, followed by flux variability analysis. The reactions affecting the objective in the absence of gluconate were exchanges for glucose, galactose, glucosamine mannose, fructose, inosine and adenosine. However, in the presence of gluconate only one reaction (bicarbonate exchange) had an effect on the objective. This indicated that metabolism of gluconate via the HMS compensates for glucose, galactose, glucosamine mannose, fructose, inosine and adenosine.

The precise cellular role of the enzyme gluconokinase is still unknown, however this study predicts that gluconokinase activity in human metabolism has significant role in the overall metabolism, which is worth investigating further.

3.3 Paper III: Kinetic analysis of gluconate phosphorylation by human gluconokinase using isothermal titration calorimetry

In the final work presented in this thesis the kinetics of phosphorylation of gluconate by hGntK was determined using isothermal titration calorimetry along with the mechanism of the reaction. In this study, I designed, carried out the ITC experiments and analyzed the data. Steinn Gudmundsson contributed to data analysis. Ottar Rolfsson contributed to the design of the study and supervised the project.

The motivation behind this work was that ITC is a powerful technique that can be used to determine kinetic parameters and mechanism of the reaction without the need for coupling the reaction or labeling the substrates, which is required in spectrophotometry.

The determination of reaction enthalpy (ΔH) is a prerequisite for determining kinetic parameters using ITC. Reaction enthalpy is used to relate power, the parameter measured by ITC, to product/substrate concentration allowing the reaction rate to be calculated through change in concentration over time. The heat was determined as a function of time (µcal/s), after multiple injections of gluconate (Glcn) into the calorimeter cell containing the reaction mixture. Each injection resulted in an exothermic reaction and after complete consumption of gluconate, the heat flow returned to the baseline level. The enthalpy change (ΔH) of the reaction calculated at these experimental conditions was -8.02 ± 0.13 kcal/mol at 25 ˚C and -8.22 ± 0.15 kcal/mol at 37 ˚C (physiological temperature).

In order to determine the rate of gluconate phosphorylation by hGntK, a large amount of either substrate (ATP or Glcn) was injected into the reaction mixture containing much lower concentration of the enzyme. This ensures there is no significant reduction in substrate concentration and the reaction progresses at a steady rate. With ATP as varying substrate the rate of the reaction increased as the concentration of ATP increased and then reached a maximum value, resulting in a typical Michaelis-Menten parabolic curve. Whereas, with gluconate as varying substrate, the rate first increased and then decreased with increasing substrate concentration. This reduction in reaction rate was indicative of reaction inhibition due to excess gluconate.

As the reaction was inhibited at higher gluconate concentrations, we used this substrate inhibition to differentiate between a ternary-complex mechanism and a substituted-enzyme mechanism (ping-pong mechanism), without the need to do product inhibition studies (Cornish-Bowden, 2004). Hanes-Woolf plots were plotted and analyzed, where the ratio of substrate concentration to reaction rate [S]/V is plotted against substrate concentration

[S]. The plots for ATP injections at variable gluconate concentration were linear having no common point of intersection, while gluconate injections produced bent curves all intersecting at the horizontal axis. Hanes-Woolf plots for both the substrates together suggest an ordered ternary complex mechanism with ATP binding first and inhibition by gluconate. Gluconate inhibition implies that it binds to ADP-Enzyme complex forming a dead end ADP-Enzyme-Glcn complex and that 6-phosphogluconate is the first product to leave the enzyme. In order to validate our hypothesis regarding the mechanism of the reaction we performed substrate-binding experiments. Employing ITC and microscale thermophoresis, we showed that ATP binds to the free enzyme, whereas gluconate binding is negligible. This confirms that ATP is the first substrate to bind to the enzyme followed by gluconate.

The data was fitted to equations describing either ternary complex and substituted enzyme complex reaction mechanisms. The equation for ternary complex mechanism, with substrate inhibition was the best fit as determined by comparing the residual errors and parameter estimates. The turnover number, k_{cat} decreases with increasing constant gluconate but remains nearly unchanged increasing constant ATP. We also observed that K_{si}, which is a constant that defines the strength of inhibition by Glcn, increases with increasing ATP. Combined, this further supports inhibition by Glcn.

To summarize, in this study we demonstrated that ITC can be used to determine mechanisms of enzyme catalyzed reactions, for which it is currently not commonly applied.

4 Conclusions and future directions

Metabolic alterations are central to a number of human diseases and almost all cellular processes are affected by metabolism. Therefore, increasing the knowledge of metabolic pathways and their functions is essential to improving our understanding of disease and therapy. A variety of experimental disciplines are involved for the elucidation of a metabolic pathway, ranging from classical biochemical enzymatic assays to high-throughput metabolomics analysis. This thesis has expanded the knowledge of human metabolism using a combination of biochemical techniques and systems biology methods. The main conclusions are summarized below along with potential future directions.

Paper I:

In the first study of this PhD project, constraint-based modeling was used to understand the metabolic changes accompanying EMT. Some crucial metabolic changes that occur during EMT were revealed, most notably changes in amino acid influx into TCA cycle. This study provided an approach to predict reactions which can be altered in order to convert one phenotype into another, which was used to predict reactions to revert EMT. Nucleotide interconversion and amino acid metabolism were crucial for the reversion of the mesenchymal phenotype to the epithelial phenotype. The transcription factors associated with these metabolic targets to revert EMT were determined using bioinformatics tools. Some of the predicted transcription factors, for e.g., N-Myc, Pax5 and HFH-1 (or FOXQ1) have been previously associated with EMT and cancer metastasis (Ansieau et al., 2014; Benzina et al., 2013; Fan et al., 2014; Kim et al., 2014; Sahni et al., 2014; Zhang, H. J. et al., 2011). However, there were a few transcription factors, for e.g., Msx-1, which have not been studied in the context of EMT, to the best of our knowledge. These transcription factors will be interesting to follow. Because transcription factors control whole pathways at the same time, these findings could prove to be important in finding ways to manipulate metabolism in order to control EMT.

These detailed insights into the EMT metabolism could not have been drawn from the transcriptomic and/or metabolomic data alone. The hypotheses generated from this study have directed further research into understanding the changes in lipidome during EMT. This has led to overseas collaborations and enabled the lab in acquiring research grants.

The knowledge obtained from the models can be directed towards drug discovery for cancer treatment. To follow up on this study, the targets predicted by the models can be knocked out in the cells to check the accuracy of the predictions. These validated targets could be developed towards preventing EMT during cancer metastasis. These targets and the model generation approach is a promising tool for personalized diagnostics and medicine. Large-scale omics data can be generated for the individual patients, which can be integrated with these models to predict the efficacy of the drugs. This will prove to be very useful in taking individual differences amongst people while administering drugs.

The models were manually curated and validated with experimental cellular data, but there is always scope to further improve the models, for instance, the internal fluxes, which are currently constrained using micro-array data could be better constrained using fluxomic data. Improving the models will help in increasing the accuracy of the models in predicting metabolic differences between the two states, epithelial and mesenchymal. Moreover, more accurate models will predict precise targets. Metabolomic measurements indicating the flow of key metabolites in the central carbon metabolism could be used to improve the model predictions, for example labeled glutamine and glucose could be fed to D492 and D492M cells during growth and their metabolic mass signatures could be traced using mass spectrometry.

Metabolic changes are closely associated with signaling pathways and it has been established that the changes in signaling pathways during EMT are dependent on the cell line used (Choudhary et al., 2016). Therefore, it is important to evaluate the similarities and differences in metabolic changes during EMT across different cell systems. There are many other cell systems used to study EMT, such as HMLE and MCF-7. Metabolic models for these cell systems could be used to investigate the similarities and differences across the different cell lines. This exercise could also be helpful in finding factors which are common for EMT across cell lines.

Paper II:

Phosphorylation of gluconate by gluconokinase was previously identified as a missing link in the knowledge of human metabolism, in a gap-filling study on Recon 1 (Rolfsson et al., 2013). The next step after the identification of the novel gluconokinase function in human metabolism was to characterize the enzyme and assess how it affects the whole cell system. Therefore, in the second study I used computational-metabolic modeling to understand the effect of gluconate metabolism on red blood cell metabolism. This study revealed that gluconate uptake and consumption can have significant effects

on the fatty acid metabolism and oxidative stress of the cell. Additionally, this project demonstrated how metabolic models can be integrated with biological knowledge to develop functional genomic hypotheses.

Although this paper describes the potential effects of gluconokinase on human metabolism, the complete understanding of sub-cellular location and purpose of gluconokinase in the human body is still lacking. This study can be further expanded to understand the reason for gluconokinase activity in human metabolism and its effect on human health. The effects of changing environmental conditions on gluconokinase expression in the cell could also give important insights into the purpose of gluconate phosphorylation in the cell.

Paper III:

Spectrophotometric assays were used in the second study to estimate the kinetic parameters of gluconokinase but the detailed mechanism of reaction and thermodynamics were still lacking. Therefore, in the third study I used ITC to deduce the mechanism of gluconokinase reaction. This study revealed that gluconokinase follows a ternary complex mechanism with ATP binding first, and is inhibited by gluconate. This kind of detail on the mechanism of reaction can be obtained using spectrophotometry, but the method is complex and requires either coupling of enzymes or labeling of the substrate.

ITC experiments provide a rapid method of determining kinetic data. Moreover, ITC is regularly used in the pharmaceutical industry on a large-scale to study the binding of drug targets to proteins. Therefore, in the future this approach can be used to determine the kinetic parameters for a large number of enzymes, which can be further used to generate kinetic models of larger metabolic pathways. Kinetic models can be used to perform time-course simulations, which is not a possibility in steady-state models.

ITC is routinely used to investigate the thermodynamics of binding, whereas, to the best of our knowledge, it has not been used to determine the change in gibb's energy (ΔG) and entropy (ΔS) of enzyme catalyzed reactions. These experiments can be fairly easily used to estimate the thermodynamic parameters of enzymes on a larger scale. These parameters can then be used to constrain the steady-state model for reversibility of reactions. This will make future models more accurate. A follow up study to determine the thermodynamic parameters of gluconate phosphorylation is in progress.

This thesis provides an overview of how different approaches in metabolic modeling and biochemistry can be combined to get an overall detailed understanding of the metabolic system. A metabolic enzyme, previously identified using generic genome-scale metabolic model was investigated using constraint-based modeling methods and a cell-specific metabolic model. The enzyme was further characterized by using isothermal titration calorimetry. These techniques together give a more complete picture, and

are complementary to each other as complete knowledge gained by using them together cannot be obtained by using any one method.

References

Acloque, H., Adams, M. S., Fishwick, K., Bronner-Fraser, M., & Nieto, M. A. (2009). Epithelial-mesenchymal transitions: the importance of changing cell state in development and disease. *Journal of Clinical Investigation, 119*(6), 1438-1449.

Agren, R., Bordel, S., Mardinoglu, A., Pornputtapong, N., Nookaew, I., & Nielsen, J. (2012). Reconstruction of genome-scale active metabolic networks for 69 human cell types and 16 cancer types using INIT. *PLoS Comput Biol, 8*(5), e1002518.

Ansieau, S., Collin, G., & Hill, L. (2014). EMT or EMT-Promoting Transcription Factors, Where to Focus the Light? *Front Oncol, 4*, 353.

Barrett, T., & Edgar, R. (2006). Gene expression omnibus: microarray data storage, submission, retrieval, and analysis. *Methods Enzymol, 411*, 352-369.

Batt, G., Ropers, D., de Jong, H., Geiselmann, J., Mateescu, R., Page, M., & Schneider, D. (2005). Validation of qualitative models of genetic regulatory networks by model checking: analysis of the nutritional stress response in Escherichia coli. *Bioinformatics, 21*, I19-I28.

Becker, S. A., Feist, A. M., Mo, M. L., Hannum, G., Palsson, B. O., & Herrgard, M. J. (2007). Quantitative prediction of cellular metabolism with constraint-based models: the COBRA Toolbox. *Nat Protoc, 2*(3), 727-738.

Becker, S. A., & Palsson, B. O. (2008). Context-specific metabolic networks are consistent with experiments. *PLoS Comput Biol, 4*(5), e1000082.

Benzina, S., O'Brien, P., Guerrette, R., & Robichaud, G. (2013, 15 April 2013). *Breast cancer malignancy is regulated by PAX5 through the disruption of FAK1 signaling.* Paper presented at the AACR 104th Annual Meeting 2013, Washington, DC. Philadelphia (PA).

Bordbar, A., Feist, A. M., Usaite-Black, R., Woodcock, J., Palsson, B. O., & Famili, I. (2011a). A multi-tissue type genome-scale metabolic network for analysis of whole-body systems physiology. *BMC Syst Biol, 5*, 180.

Bordbar, A., Jamshidi, N., & Palsson, B. O. (2011b). iAB-RBC-283: A proteomically derived knowledge-base of erythrocyte metabolism that can be used to simulate its physiological and patho-physiological states. *BMC Syst Biol, 5*, 110.

Bordel, S., Agren, R., & Nielsen, J. (2010). Sampling the solution space in genome-scale metabolic networks reveals transcriptional regulation in key enzymes. *PLoS Comput Biol, 6*(7), e1000859.

Bouatra, S., Aziat, F., Mandal, R., Guo, A. C., Wilson, M. R., Knox, C., Bjorndahl, T. C., Krishnamurthy, R., Saleem, F., Liu, P., Dame, Z. T., Poelzer, J., Huynh,

J., Yallou, F. S., Psychogios, N., Dong, E., Bogumil, R., Roehring, C., & Wishart, D. S. (2013). The Human Urine Metabolome. *PLoS ONE, 8*(9).

Carron, I. (2011). Instances of Null Spaces: Can Compressive Sensing Help Study Non Steady State Metabolic Networks ? : Nuit-Blanche.

Caspi, R., Billington, R., Ferrer, L., Foerster, H., Fulcher, C. A., Keseler, I. M., Kothari, A., Krummenacker, M., Latendresse, M., Mueller, L. A., Ong, Q., Paley, S., Subhraveti, P., Weaver, D. S., & Karp, P. D. (2016). The MetaCyc database of metabolic pathways and enzymes and the BioCyc collection of pathway/genome databases. *Nucleic Acids Research, 44*(D1), D471-D480.

Chaouiya, C., Remy, E., Ruet, P., & Thieffry, D. (2004). Qualitative modelling of genetic networks: From logical regulatory graphs to standard Petri nets. *Applications and Theory of Petri Nets 2004, Proceedings, 3099*, 137-156.

Chassagnole, C., Noisommit-Rizzi, N., Schmid, J. W., Mauch, K., & Reuss, M. (2002). Dynamic modeling of the central carbon metabolism of Escherichia coli. *Biotechnology and Bioengineering, 79*(1), 53-73.

Cho, S., Swaminathan, C. P., Bonsor, D. A., Kerzic, M. C., Guan, R., Yang, J., Kieke, M. C., Andersen, P. S., Kranz, D. M., Mariuzza, R. A., & Sundberg, E. J. (2010). Assessing energetic contributions to binding from a disordered region in a protein-protein interaction. *Biochemistry, 49*(43), 9256-9268.

Choudhary, K. S., Rohatgi, N., Halldorsson, S., Briem, E., Gudjonsson, T., Gudmundsson, S., & Rolfsson, O. (2016). EGFR Signal-Network Reconstruction Demonstrates Metabolic Crosstalk in EMT. *PLoS Comput Biol, 12*(6), e1004924.

Cornish-Bowden, A. (2004). *Fundamentals of enzyme kinetics* (3rd ed.): Portland Press.

Covert, M. W., Knight, E. M., Reed, J. L., Herrgard, M. J., & Palsson, B. O. (2004). Integrating high-throughput and computational data elucidates bacterial networks. *Nature, 429*(6987), 92-96.

Day, Y. S., Baird, C. L., Rich, R. L., & Myszka, D. G. (2002). Direct comparison of binding equilibrium, thermodynamic, and rate constants determined by surface- and solution-based biophysical methods. *Protein Sci, 11*(5), 1017-1025.

De Craene, B., & Berx, G. (2013). Regulatory networks defining EMT during cancer initiation and progression. *Nature Reviews Cancer, 13*(2), 97-110.

DeBerardinis, R. J., & Thompson, C. B. (2012). Cellular Metabolism and Disease: What Do Metabolic Outliers Teach Us? *Cell, 148*(6), 1132-1144.

Dong, C., Yuan, T., Wu, Y., Wang, Y., Fan, T. W., Miriyala, S., Lin, Y., Yao, J., Shi, J., Kang, T., Lorkiewicz, P., St Clair, D., Hung, M. C., Evers, B. M., & Zhou, B. P. (2013). Loss of FBP1 by Snail-mediated repression provides metabolic advantages in basal-like breast cancer. *Cancer Cell, 23*(3), 316-331.

Duarte, N. C., Becker, S. A., Jamshidi, N., Thiele, I., Mo, M. L., Vo, T. D., Srivas, R., & Palsson, B. O. (2007). Global reconstruction of the human metabolic

network based on genomic and bibliomic data. *Proc Natl Acad Sci U S A, 104*(6), 1777-1782.

Edwards, J. S., & Palsson, B. O. (2000). Metabolic flux balance analysis and the in silico analysis of Escherichia coli K-12 gene deletions. *BMC Bioinformatics, 1*, 1.

Fan, D. M., Feng, X. S., Qi, P. W., & Chen, Y. W. (2014). Forkhead factor FOXQ1 promotes TGF-beta 1 expression and induces epithelial-mesenchymal transition. *Molecular and Cellular Biochemistry, 397*(1-2), 179-186.

Feist, A. M., & Palsson, B. O. (2008). The growing scope of applications of genome-scale metabolic reconstructions using Escherichia coli. *Nature Biotechnology, 26*(6), 659-667.

Fernandes, J., Berghe, G., Saudubray, J.-M., Walter, J. H., & SpringerLink (Online service). (2006). *Inborn Metabolic Diseases Diagnosis and Treatment*. from http://dx.doi.org/10.1007/978-3-540-28785-8

Folger, O., Jerby, L., Frezza, C., Gottlieb, E., Ruppin, E., & Shlomi, T. (2011). Predicting selective drug targets in cancer through metabolic networks. *Mol Syst Biol, 7*, 501.

Freyer, M. W., & Lewis, E. A. (2008). Isothermal titration calorimetry: Experimental design, data analysis, and probing Macromolecule/Ligand binding and kinetic interactions. *Biophysical Tools for Biologists: Vol 1 in Vitro Techniques, 84*, 79-113.

Garg, M. (2013). Epithelial-mesenchymal transition - activating transcription factors - multifunctional regulators in cancer. *World J Stem Cells, 5*(4), 188-195.

Gianchandani, E. P., Joyce, A. R., Palsson, B. O., & Papin, J. A. (2009). Functional States of the Genome-Scale Escherichia Coli Transcriptional Regulatory System. *Plos Computational Biology, 5*(6).

Gopalakrishnan, S., & Maranas, C. D. (2015). 13C metabolic flux analysis at a genome-scale. *Metabolic Engineering, 32*, 12-22.

Grzegorczyk, M., Husmeier, D., Edwards, K. D., Ghazal, P., & Millar, A. J. (2008). Modelling non-stationary gene regulatory processes with a non-homogeneous Bayesian network and the allocation sampler. *Bioinformatics, 24*(18), 2071-2078.

Gudmundsson, S., & Thiele, I. (2010). Computationally efficient flux variability analysis. *BMC Bioinformatics, 11*, 489.

Gupta, S., Bisht, S. S., Kukreti, R., Jain, S., & Brahmachari, S. K. (2007). Boolean network analysis of a neurotransmitter signaling pathway. *Journal of Theoretical Biology, 244*(3), 463-469.

Hanahan, D., & Weinberg, R. A. (2011). Hallmarks of cancer: the next generation. *Cell, 144*(5), 646-674.

Hanai, J., Doro, N., Sasaki, A. T., Kobayashi, S., Cantley, L. C., Seth, P., & Sukhatme, V. P. (2012). Inhibition of lung cancer growth: ATP citrate lyase

knockdown and statin treatment leads to dual blockade of mitogen-activated protein kinase (MAPK) and phosphatidylinositol-3-kinase (PI3K)/AKT pathways. *J Cell Physiol, 227*(4), 1709-1720.

Hardy, S., & Robillard, P. N. (2008). Petri net-based method for the analysis of the dynamics of signal propagation in signaling pathways. *Bioinformatics, 24*(2), 209-217.

Heinken, A., Sahoo, S., Fleming, R. M., & Thiele, I. (2013). Systems-level characterization of a host-microbe metabolic symbiosis in the mammalian gut. *Gut Microbes, 4*(1), 28-40.

Heinken, A., & Thiele, I. (2015). Systematic prediction of health-relevant human-microbial co-metabolism through a computational framework. *Gut Microbes, 6*(2), 120-130.

Henzler, K., Haupt, B., & Ballauff, M. (2008). Enzymatic activity of immobilized enzyme determined by isothermal titration calorimetry. *Anal Biochem, 378*(2), 184-189.

Jerby, L., Shlomi, T., & Ruppin, E. (2010). Computational reconstruction of tissue-specific metabolic models: application to human liver metabolism. *Mol Syst Biol, 6*, 401.

Jones, A. J. Y., & Hirst, J. (2013). A spectrophotometric coupled enzyme assay to measure the activity of succinate dehydrogenase. *Analytical Biochemistry, 442*(1), 19-23.

Kaelin, W. G., Jr., & McKnight, S. L. (2013). Influence of metabolism on epigenetics and disease. *Cell, 153*(1), 56-69.

Kalita, M., Tian, B., Gao, B., Choudhary, S., Wood, T. G., Carmical, J. R., Boldogh, I., Mitra, S., Minna, J. D., & Brasier, A. R. (2013). Systems approaches to modeling chronic mucosal inflammation. *Biomed Res Int, 2013*, 505864.

Kalluri, R., & Weinberg, R. A. (2009). The basics of epithelial-mesenchymal transition. *J Clin Invest, 119*(6), 1420-1428.

Kanehisa, M. (2002). The KEGG database. *Novartis Found Symp, 247*, 91-101; discussion 101-103, 119-128, 244-152.

Karlstadt, A., Fliegner, D., Kararigas, G., Ruderisch, H. S., Regitz-Zagrosek, V., & Holzhutter, H. G. (2012). CardioNet: A human metabolic network suited for the study of cardiomyocyte metabolism. *Bmc Systems Biology, 6*.

Kauffman, K. J., Prakash, P., & Edwards, J. S. (2003). Advances in flux balance analysis. *Current Opinion in Biotechnology, 14*(5), 491-496.

Kim, M. J., Lim, J., Yang, Y., Lee, M. S., & Lim, J. S. (2014). N-myc downstream-regulated gene 2 (NDRG2) suppresses the epithelial-mesenchymal transition (EMT) in breast cancer cells via STAT3/Snail signaling. *Cancer Letters, 354*(1), 33-42.

Kitano, H. (2001). *Foundations of systems biology*: MIT Press.

Koch, I., Junker, B. H., & Heiner, M. (2005). Application of Petri net theory for modelling and validation of the sucrose breakdown pathway in the potato tuber. *Bioinformatics, 21*(7), 1219-1226.

Li, L., & Li, W. (2015). Epithelial-mesenchymal transition in human cancer: comprehensive reprogramming of metabolism, epigenetics, and differentiation. *Pharmacol Ther, 150*, 33-46.

Lu, C., & Thompson, C. B. (2012). Metabolic regulation of epigenetics. *Cell Metab, 16*(1), 9-17.

Ma, H. W., Sorokin, A., Mazein, A., Selkov, A., Selkov, E., Demin, O., & Goryanin, I. (2007). The Edinburgh human metabolic network reconstruction and its functional analysis. *Molecular Systems Biology, 3*.

Machado, D., Costa, R. S., Rocha, M., Ferreira, E. C., Tidor, B., & Rocha, I. (2011). Modeling formalisms in Systems Biology. *AMB Express, 1*, 45.

Machado, D., & Herrgard, M. (2014). Systematic evaluation of methods for integration of transcriptomic data into constraint-based models of metabolism. *PLoS Comput Biol, 10*(4), e1003580.

Mahadevan, R., & Schilling, C. H. (2003). The effects of alternate optimal solutions in constraint-based genome-scale metabolic models. *Metab Eng, 5*(4), 264-276.

Mardinoglu, A., Agren, R., Kampf, C., Asplund, A., Uhlen, M., & Nielsen, J. (2014). Genome-scale metabolic modelling of hepatocytes reveals serine deficiency in patients with non-alcoholic fatty liver disease. *Nature Communications, 5*.

Nantajit, D., Lin, D., & Li, J. J. (2015). The network of epithelial-mesenchymal transition: potential new targets for tumor resistance. *J Cancer Res Clin Oncol, 141*(10), 1697-1713.

Nikoloski, Z., Grimbs, S., May, P., & Selbig, J. (2008). Metabolic networks are NP-hard to reconstruct. *J Theor Biol, 254*(4), 807-816.

Orth, J. D., Thiele, I., & Palsson, B. O. (2010). What is flux balance analysis? *Nat Biotechnol, 28*(3), 245-248.

Palsson, B. (2006). *Systems biology : properties of reconstructed networks*: Cambridge University Press.

Palsson, B. (2009). Metabolic systems biology. *Febs Letters, 583*(24), 3900-3904.

Palsson, B. (2015). *Systems biology : constraint-based reconstruction and analysis*: Cambridge University Press.

Papin, J. A., & Palsson, B. O. (2004). The JAK-STAT signaling network in the human B-cell: an extreme signaling pathway analysis. *Biophys J, 87*(1), 37-46.

Papin, J. A., Reed, J. L., & Palsson, B. O. (2004). Hierarchical thinking in network biology: the unbiased modularization of biochemical networks. *Trends Biochem Sci, 29*(12), 641-647.

Polyak, K., & Weinberg, R. A. (2009). Transitions between epithelial and mesenchymal states: acquisition of malignant and stem cell traits. *Nature Reviews Cancer, 9*(4), 265-273.

Price, N. D., Reed, J. L., & Palsson, B. O. (2004). Genome-scale models of microbial cells: Evaluating the consequences of constraints. *Nature Reviews Microbiology, 2*(11), 886-897.

Psychogios, N., Hau, D. D., Peng, J., Guo, A. C., Mandal, R., Bouatra, S., Sinelnikov, I., Krishnamurthy, R., Eisner, R., Gautam, B., Young, N., Xia, J. G., Knox, C., Dong, E., Huang, P., Hollander, Z., Pedersen, T. L., Smith, S. R., Bamforth, F., Greiner, R., McManus, B., Newman, J. W., Goodfriend, T., & Wishart, D. S. (2011). The Human Serum Metabolome. *Plos One, 6*(2).

Ramachandran, S., Fontanille, P., Pandey, A., & Larroche, C. (2006). Gluconic acid: properties, applications and microbial production. *FOOD TECHNOL BIOTECH, 44*(2), 185-195.

Reed, J. L., & Palsson, B. O. (2004). Genome-scale in silico models of E-coli have multiple equivalent phenotypic states: Assessment of correlated reaction subsets that comprise network states. *Genome Research, 14*(9), 1797-1805.

Rohatgi, N., Nielsen, T. K., Bjorn, S. P., Axelsson, I., Paglia, G., Voldborg, B. G., Palsson, B. O., & Rolfsson, O. (2014). Biochemical characterization of human gluconokinase and the proposed metabolic impact of gluconic acid as determined by constraint based metabolic network analysis. *PLoS One, 9*(6), e98760.

Rolfsson, O., Paglia, G., Magnusdottir, M., Palsson, B. O., & Thiele, I. (2013). Inferring the metabolism of human orphan metabolites from their metabolic network context affirms human gluconokinase activity. *Biochemical Journal, 449*, 427-435.

Rolfsson, O., Palsson, B. O., & Thiele, I. (2011). The human metabolic reconstruction Recon 1 directs hypotheses of novel human metabolic functions. *BMC Syst Biol, 5*, 155.

Sachs, K., Perez, O., Pe'er, D., Lauffenburger, D. A., & Nolan, G. P. (2005). Causal protein-signaling networks derived from multiparameter single-cell data. *Science, 308*(5721), 523-529.

Sahni, S., Bae, D. H., Lane, D. J., Kovacevic, Z., Kalinowski, D. S., Jansson, P. J., & Richardson, D. R. (2014). The metastasis suppressor, N-myc downstream-regulated gene 1 (NDRG1), inhibits stress-induced autophagy in cancer cells. *J Biol Chem, 289*(14), 9692-9709.

Schellenberger, J., & Palsson, B. O. (2009). Use of randomized sampling for analysis of metabolic networks. *J Biol Chem, 284*(9), 5457-5461.

Schellenberger, J., Que, R., Fleming, R. M., Thiele, I., Orth, J. D., Feist, A. M., Zielinski, D. C., Bordbar, A., Lewis, N. E., Rahmanian, S., Kang, J., Hyduke, D. R., & Palsson, B. O. (2011). Quantitative prediction of cellular metabolism

with constraint-based models: the COBRA Toolbox v2.0. *Nat Protoc, 6*(9), 1290-1307.

Schilling, C. H., Letscher, D., & Palsson, B. O. (2000). Theory for the systemic definition of metabolic pathways and their use in interpreting metabolic function from? A pathway-oriented perspective. *Journal of Theoretical Biology, 203*(3), 229-248.

Segre, D., Vitkup, D., & Church, G. M. (2002). Analysis of optimality in natural and perturbed metabolic networks. *Proceedings of the National Academy of Sciences of the United States of America, 99*(23), 15112-15117.

Shaul, Y. D., Freinkman, E., Comb, W. C., Cantor, J. R., Tam, W. L., Thiru, P., Kim, D., Kanarek, N., Pacold, M. E., Chen, W. W., Bierie, B., Possemato, R., Reinhardt, F., Weinberg, R. A., Yaffe, M. B., & Sabatini, D. M. (2014). Dihydropyrimidine Accumulation Is Required for the Epithelial-Mesenchymal Transition. *Cell, 158*(5), 1094-1109.

Shlomi, T., Berkman, O., & Ruppin, E. (2005). Regulatory on/off minimization of metabolic flux changes after genetic perturbations. *Proceedings of the National Academy of Sciences of the United States of America, 102*(21), 7695-7700.

Shlomi, T., Cabili, M. N., & Ruppin, E. (2009). Predicting metabolic biomarkers of human inborn errors of metabolism. *Mol Syst Biol, 5*, 263.

Sigurdsson, V., Hilmarsdottir, B., Sigmundsdottir, H., Fridriksdottir, A. J. R., Ringner, M., Villadsen, R., Borg, A., Agnarsson, B. A., Petersen, O. W., Magnusson, M. K., & Gudjonsson, T. (2011). Endothelial Induced EMT in Breast Epithelial Cells with Stem Cell Properties. *Plos One, 6*(9).

Singh, O. V., & Kumar, R. (2007). Biotechnological production of gluconic acid: future implications. *Appl Microbiol Biotechnol, 75*(4), 713-722.

Tam, W. L., & Weinberg, R. A. (2013). The epigenetics of epithelial-mesenchymal plasticity in cancer. *Nat Med, 19*(11), 1438-1449.

Thiele, I., Fleming, R. M. T., Bordbar, A., Schellenberger, J., & Palsson, B. O. (2010). Functional Characterization of Alternate Optimal Solutions of Escherichia coli's Transcriptional and Translational Machinery. *Biophysical Journal, 98*(10), 2072-2081.

Thiele, I., & Palsson, B. O. (2010). A protocol for generating a high-quality genome-scale metabolic reconstruction. *Nat Protoc, 5*(1), 93-121.

Thiele, I., Swainston, N., Fleming, R. M., Hoppe, A., Sahoo, S., Aurich, M. K., Haraldsdottir, H., Mo, M. L., Rolfsson, O., Stobbe, M. D., Thorleifsson, S. G., Agren, R., Bolling, C., Bordel, S., Chavali, A. K., Dobson, P., Dunn, W. B., Endler, L., Hala, D., Hucka, M., Hull, D., Jameson, D., Jamshidi, N., Jonsson, J. J., Juty, N., Keating, S., Nookaew, I., Le Novere, N., Malys, N., Mazein, A., Papin, J. A., Price, N. D., Selkov, E., Sr., Sigurdsson, M. I., Simeonidis, E., Sonnenschein, N., Smallbone, K., Sorokin, A., van Beek, J. H., Weichart, D., Goryanin, I., Nielsen, J., Westerhoff, H. V., Kell, D. B.,

Mendes, P., & Palsson, B. O. (2013). A community-driven global reconstruction of human metabolism. *Nat Biotechnol, 31*(5), 419-425.

Thomas, A., Rahmanian, S., Bordbar, A., Palsson, B. O., & Jamshidi, N. (2014). Network reconstruction of platelet metabolism identifies metabolic signature for aspirin resistance. *Sci Rep, 4*, 3925.

Thomson, S., Petti, F., Sujka-Kwok, I., Mercado, P., Bean, J., Monaghan, M., Seymour, S. L., Argast, G. M., Epstein, D. M., & Haley, J. D. (2011). A systems view of epithelial-mesenchymal transition signaling states. *Clin Exp Metastasis, 28*(2), 137-155.

Todd, M. J., & Gomez, J. (2001). Enzyme kinetics determined using calorimetry: A general assay for enzyme activity? *Analytical Biochemistry, 296*(2), 179-187.

Varma, A., & Palsson, B. O. (1993). Metabolic Capabilities of Escherichia-Coli .2. Optimal-Growth Patterns. *Journal of Theoretical Biology, 165*(4), 503-522.

Vlassis, N., Pacheco, M. P., & Sauter, T. (2014). Fast reconstruction of compact context-specific metabolic network models. *PLoS Comput Biol, 10*(1), e1003424.

Voet, D., & Voet, J. G. (2011). *Biochemistry* (4th ed.): John Wiley & Sons.

Vohradsky, J. (2001). Neural network model of gene expression. *Faseb Journal, 15*(3), 846-854.

Wang, D. Y., Cardelli, L., Phillips, A., Piterman, N., & Fisher, J. (2009). Computational modeling of the EGFR network elucidates control mechanisms regulating signal dynamics. *BMC Syst Biol, 3*, 118.

Wang, Y., Eddy, J. A., & Price, N. D. (2012). Reconstruction of genome-scale metabolic models for 126 human tissues using mCADRE. *BMC Syst Biol, 6*, 153.

Wilkinson, A. P., Rhodes, M. J. C., & Fenwick, G. R. (1984). Determination of Myrosinase (Thioglucoside Glucohydrolase) Activity by a Spectrophotometric Coupled Enzyme Assay. *Analytical Biochemistry, 139*(2), 284-291.

Wishart, D. S., Jewison, T., Guo, A. C., Wilson, M., Knox, C., Liu, Y. F., Djoumbou, Y., Mandal, R., Aziat, F., Dong, E., Bouatra, S., Sinelnikov, I., Arndt, D., Xia, J. G., Liu, P., Yallou, F., Bjorndahl, T., Perez-Pineiro, R., Eisner, R., Allen, F., Neveu, V., Greiner, R., & Scalbert, A. (2013). HMDB 3.0-The Human Metabolome Database in 2013. *Nucleic Acids Research, 41*(D1), D801-D807.

Zhang, H. J., Meng, F. Y., Liu, G., Zhang, B., Zhu, J., Wu, F., Ethier, S. P., Miller, F., & Wu, G. J. (2011). Forkhead Transcription Factor Foxq1 Promotes Epithelial-Mesenchymal Transition and Breast Cancer Metastasis. *Cancer Research, 71*(4), 1292-1301.

Zhang, Y., Zagnitko, O., Rodionova, I., Osterman, A., & Godzik, A. (2011). The FGGY carbohydrate kinase family: insights into the evolution of functional specificities. *PLoS Comput Biol, 7*(12), e1002318.

Zhou, X. D., Kini, R. M., & Sivaraman, J. (2011). Application of isothermal titration calorimetry and column chromatography for identification of biomolecular targets. *Nature Protocols, 6*(2), 158-165.

Zur, H., Ruppin, E., & Shlomi, T. (2010). iMAT: an integrative metabolic analysis tool. *Bioinformatics, 26*(24), 3140-3142.

Papers

Paper I

Metabolic re-wiring of isogenic breast epithelial cell lines following epithelial to mesenchymal transition

Skarphedinn Halldorsson[1,2, §*], Neha Rohatgi[1,2, §], Manuela Magnusdottir[1], Kumari Sonal Choudhary [1,2], Thorarinn Guðjónsson[2,3], Erik Knutsen[5], Anna Barkovskaya[6,7], Bylgja Hilmarsdottir[6], Maria Perander[5], Gunhild M. Mælandsmo[6,8], Steinn Gudmundsson[1,4] and Óttar Rolfsson[1,2].

1Center for Systems Biology, University of Iceland, Reykjavik, Iceland.

2 Biomedical Center, University of Iceland, Reykjavík, Iceland.

3 Department of Anatomy, Faculty of Medicine, Department of Laboratory Hematology, University Hospital, Reykjavik, Iceland.

4 School of Engineering and Natural Sciences, University of Iceland, Reykjavik, Iceland.

5 Department of Medical Biology, UiT – The Arctic University of Norway, Tromsø, Norway.

6 Department of Tumor Biology, Institute for Cancer Research, Norwegian Radium Hospital, Oslo, Norway

7 Department of Circulation and Medical Imaging, Faculty of Medicine, Norwegian University of Science and Technology, Trondheim, Norway.

8 Department of Pharmacy, UiT – The Arctic University of Norway, Tromsø, Norway.

§ Equal contribution *Corresponding author

Abstract

Background: Epithelial to mesenchymal transition (EMT) is a fundamental developmental process with strong implications in tumor progression and metastasis. Although metabolic alterations have been shown to play pivotal roles in cancer development, studies focused on the metabolic re-wiring that takes place during EMT are still limited.

Methods: Here, we performed metabolomics profiling of the breast epithelial cell line D492 and its isogenic EMT derived mesenchymal phenotype, D492M to create genome-scale metabolic models (GEMs) descriptive of metabolism in both cell lines.

Results: Glycolytic flux as well as oxidative phosphorylation was higher in the epithelial phenotype, while the mesenchymal phenotype was more tuned to amino acid anaplerosis and fatty acid oxidation to fuel the TCA cycle. Through comparative bioinformatics analysis, PPAR-γ1, PPAR- γ 2 and AP-1 were found to be the most influential transcription factors associated with the metabolic re-wiring. In silico gene essentiality analysis predicted that the neutral amino acid transporter LAT1 were essential for mesenchymal cell survival, while components of the respiratory chain were crucial for the epithelial phenotype.

Conclusions: The results define different metabolic traits in cells undergoing EMT and suggest metabolic addiction in the mesenchymal phenotype. We present tools to carry out integrated data analysis and generate metabolic models, which aid in identifying critical metabolic nodes that may serve as therapeutic targets aiming to prevent EMT to inhibit metastatic dissemination.

Introduction

Epithelial to mesenchymal transition (EMT) is a process where cells of epithelial origin lose their polarity and cell-cell adhesion and change their phenotype to mesenchymal-like cells. EMT is a fundamental process in embryonic development allowing cells to detach from the newly formed epithelium and migrate to other parts of the developing embryo (Kalluri, 2009; Kalluri & Weinberg, 2009). Once they have reached their destination, these epithelial-derived mesenchymal cells revert to their original phenotype via mesenchymal to epithelial transition (MET) and take part in establishing new tissues and organs.

Many carcinomas are known to revive these mechanisms during cancer invasion and metastasis. EMT shifts the phenotype of the polarized epithelial cell, bound to its neighbors and the extracellular matrix via tight junctions, desmosomes and E-cadherin, to an invasive mesenchymal phenotype that exists largely without direct cell-cell contacts or defined cell polarity. The ability to separate from neighboring cells and penetrate into the surrounding tissues is an important initiating step in tumor metastasis (Acloque, Adams, Fishwick, Bronner-Fraser, & Nieto, 2009). EMT also acts in tumor progression by providing increased resistance to apoptotic agents (Polyak & Weinberg, 2009), and by producing supporting tissues that enhance the malignancy of the central tumor (Petersen et al., 2003). As such, the EMT confers on epithelial cells precisely the set of traits that would empower them to disseminate from primary tumors and seed metastases (Barriere, Fici, Gallerani, Fabbri, & Rigaud, 2015).

Metabolic alterations have been shown to play a role in determining cellular phenotypes. For example, knock-down of fructose-1,6-bisphosphatase has been shown to induce EMT in basal-like breast cancer cells (Dong et al., 2013) while knockdown of ATP citrate lyase has been shown to revert the EMT phenotype in non-small cell lung carcinoma cells (Hanai et al., 2012). Mutations or epigenetic changes that cause accumulation of certain metabolites have also been shown to induce EMT (Shaul et al., 2014). While

these findings show that metabolic alterations are important for induction and maintenance of a mesenchymal phenotype; studies of the global metabolic changes that occur during EMT are still limited.

Genome scale metabolic models (GEMs) provide descriptions of metabolic phenotypes that can be queried computationally through constraint-based modeling (O'Brien, Monk, & Palsson, 2015). The building of GEMs and their application to the analysis of metabolism of diverse biological processes is well established (Palsson, 2015). EMT metabolism has so far mainly been investigated through more targeted cell and molecular biology based approaches. Previous efforts show that systems based analysis may provide important insights into EMT metabolism (Shaul, Freinkman et al. 2014, Yizhak, Le Devedec et al. 2014), in particular constraint based modelling methods (Choudhary et al., 2016).

Here, we describe and compare the metabolic phenotypes of two isogenic breast epithelial cell lines, an epithelial “mother” cell line (D492) and a mesenchymal “daughter” cell line (D492M) that arose through spontaneous EMT in 3D co-culture with endothelial cells (Sigurdsson et al., 2011). Ultra performance liquid chromatography Mass Spectrometry (UPLC-MS) on spent media was used to quantify uptake and secretion of 43 selected metabolites. These data, coupled with microarray and RNA sequencing expression profiles, were used to build GEMs descriptive of metabolism in the two cell lines. We validated the computationally proposed metabolic phenotypes through enzymatic assays of intracellular ATP, NADH, NADPH and glutathione levels together with mitochondrial functionality assays. The GEMs were then used to predict enzymatic reactions and pathways of importance for the metabolic re-programming that occurs during EMT. Some of these reactions, in particular the large neutral amino acid transporter LAT1, appear important for cancer remission following breast cancer treatment. The results represent the construction of the first curated GEMs descriptive of metabolism pre- and post EMT. As such they serve as tools for future investigation of EMT metabolism. Furthermore, the results highlight how GEMs can be applied to the integrated

analysis of polyomics data and propose metabolic biomarkers of importance for EMT and metastasis.

Materials and Methods

Cell culture

D492 and D492M cells were cultured on collagen coated surfaces in H14 medium as previously described (Sigurdsson et al., 2011) at 37°C, 5% CO2. Proliferation and ATP concentration was measured with a CellTiter GloTM assay (Promega). Cell volume was calculated based on diameter measurements obtained from a Countess cell counting instrument (Invitrogen). For UPLC-MS, cells were seeded in triplicates into 24-well plates in 400 µL H14 medium at 15000 cells/cm2. Media was collected from cultures after 24 and 48 hours along with cell-free controls, centrifuged to remove cellular debris and stored at -80°C until further analysis.

Cell profiling

Total RNA sequence profiles were obtained for D492 and D492M as outlined in supplementary methods. Microarray expression profiles of D492 and D492M cells were obtained from (Sigurdsson et al., 2011). Medium metabolites were measured using an established metabolomics pipeline. Both the metabolite isolation procedure and metabolomic pipeline analysis were adapted from Paglia et al. 2014 (Paglia et al., 2014). The methods are explained in supplementary materials and methods. To account for differences in cell weight and growth rate, the measured metabolite concentrations were normalized to cell weight and growth rates as previously described (Jain et al., 2012). Seahorse XFe-96 metabolic extracellular flux analyzer (Seahorse Biosciences) was used to measure the oxygen consumption rate (OCR) and the extracellular acidification rate (ECAR). See supplementary materials and methods for details. Intracellular NAD+/NADH, NADP+/NADPH and GSH/GSSG were assayed with respective GloTM kits from Promega. Additional glucose and lactate measurements were performed in an ABL 90 blood gas analyzer (Radiometer, Brønshøj, Denmark).

Generation of a breast tissue specific metabolic model

RNA-seq data from the D492 and D492M cells were used to create a breast tissue specific model from the human metabolic reconstruction RECON2 (Thiele et al., 2013) as follows. All genes with expression values exceeding a fixed threshold in either the D492 or D492M data sets that were also present in RECON2 were identified. The gene-protein-reaction rules (GPRs) of RECON2 were then used to identify the associated metabolic reactions and the FASTCORE model building algorithm (Vlassis, Pacheco, & Sauter, 2014) used to build a functional metabolic network from the list of reactions. The resulting network, referred to as the EMT model, was manually curated in order to ensure that no major pathways and metabolites were missing. Details of the model construction are provided in supplementary materials and methods.

Construction and analysis of the D492 and D492M GEMs

The EMT model was used to create models of the epithelial D492 cells and mesenchymal D492M cells. Random sampling was first used to estimate flux ranges of all the reactions in the EMT model. While the RNA-seq data had considerably more coverage, it lacked the necessary replicates. Therefore, the microarray expression data was used to constrain the EMT model to simulate the effects of up and downregulated genes on reaction flux. This gave rise to models EPI (epithelial) and MES (mesenchymal) once metabolomics constraints had been applied. The two models generated in this manner therefore had the same stoichiometry but different constraints on reaction fluxes as defined by differential expression of metabolic genes and extracellular metabolomics measurements. Deriving the two models from a common model was done because the D492M cells initially arose from D492 cells and this facilitated both model curation and subsequent model comparisons. See supplementary material and methods for details.

Analysis of the EPI and MES models

We used flux balance analysis (FBA) (Fell & Small, 1986; Savinell & Palsson, 1992) and the generic biomass reaction present in RECON2 to predict the maximum growth rates of the EPI and MES models. Random sampling

(Schellenberger & Palsson, 2009) was used to compare the two. An optimization algorithm was used to identify targets for transforming the epithelial phenotype into the mesenchymal phenotype and vice-versa. The algorithm works by relaxing flux bounds for reactions in one model in order to obtain a flux distribution that is as close as possible to the flux distribution in the other (Choudhary et al., 2016). The genes corresponding to these reactions were identified via the GPRs and the associated transcription factors then located in SABiosciences' proprietary database (http://www.sabiosciences.com/chipqpcrsearch) Gene essentiality analysis was performed on the EPI and MES models by simulating single gene knockouts with FBA.

Results

D492M cells show reduced size and growth rate compared to D492 cells

In order to accurately calculate metabolic uptake and secretion rates morphological parameters including cell size and weight, and proliferation rates were established. In 2D culture, D492 cells display the typical cobblestone morphology of epithelial cells while D492M cells have acquired the spindle-like phenotype of mesenchymal cells, characterized by multiple membrane protrusions (**Figure 1A, top row**). In 3D culture, D492 cells form organized, branching structures while D492M form colonies that have lost polarity and cell-cell contact (**Figure 1A, bottom row**). Growth rate measurements in 2D indicated population doubling times of 25 hours for D492 cells and roughly 32 hours for D492M cells, corresponding to growth rates of 0.028 h^{-1} and 0.022 h^{-1}. We subsequently calculated the volume and measured the dry-weight of D492 and D492M cells. D492 cells are larger than D492M cells with an average volume of 1700 fL compared to 1400 fL of D492M cells. Dry weights were measured at 1 ng and 0.53 ng, respectively (**Figure 1B**). In summary, D492 and D492M are isogenic cell lines with epithelial and mesenchymal phenotypes, respectively. D492M show reduced size, mass and proliferation rate compared to the parental D492 cell line.

A

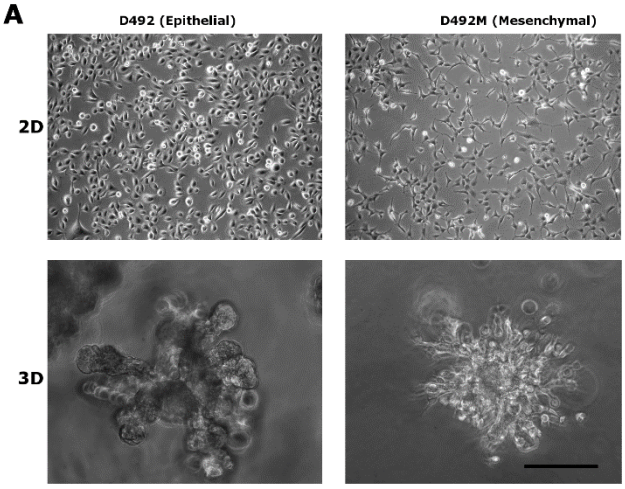

B

	D492 (Epithelial)	**D492M** (Mesenchymal)
Proliferation rate (h^{-1})	0,028	0,022
Dry weight (*ng/cell*)	1	0,53
Volume (*pL/cell*)	1,7	1,4

Figure 1. A) D492 cells (top left) have the typical almond morphology of epithelial cells when grown on culture plastic. When cultured in rBM/matrigel, D492 form branching lobular-like structures reminiscent of terminal duct lobular unit in vivo (bottom left). In contrast, D492M cells form clusters of disorganized mesenchymal like cells (bottom right). When isolated and re-grown on tissue culture plastic, these cells retain a mesenchymal phenotype (top right). Bar = 100 µm. B) Measured growth rates, dry weight and volume of D492 and D492M cells.

Extracellular metabolomics changes are indicative of differences in metabolism in D492 following EMT

In order to distinguish between the metabolic phenotypes associated with D492 and D492M we carried out metabolic analysis of spent media after 48 hours of cell culture. Targeted metabolomic analysis of a total of 43 metabolites in the growth medium afforded quantitative consumption rates of 7 compounds in central carbon metabolism, 23 amino acids or derivatives thereof, 6 nucleotide derivatives, 5 vitamins and 2 choline derivatives. Metabolite uptake rates of D492 epithelial cells were generally higher than that of D492M mesenchymal cells consistent with their increased proliferation rate (**Figure 2).**

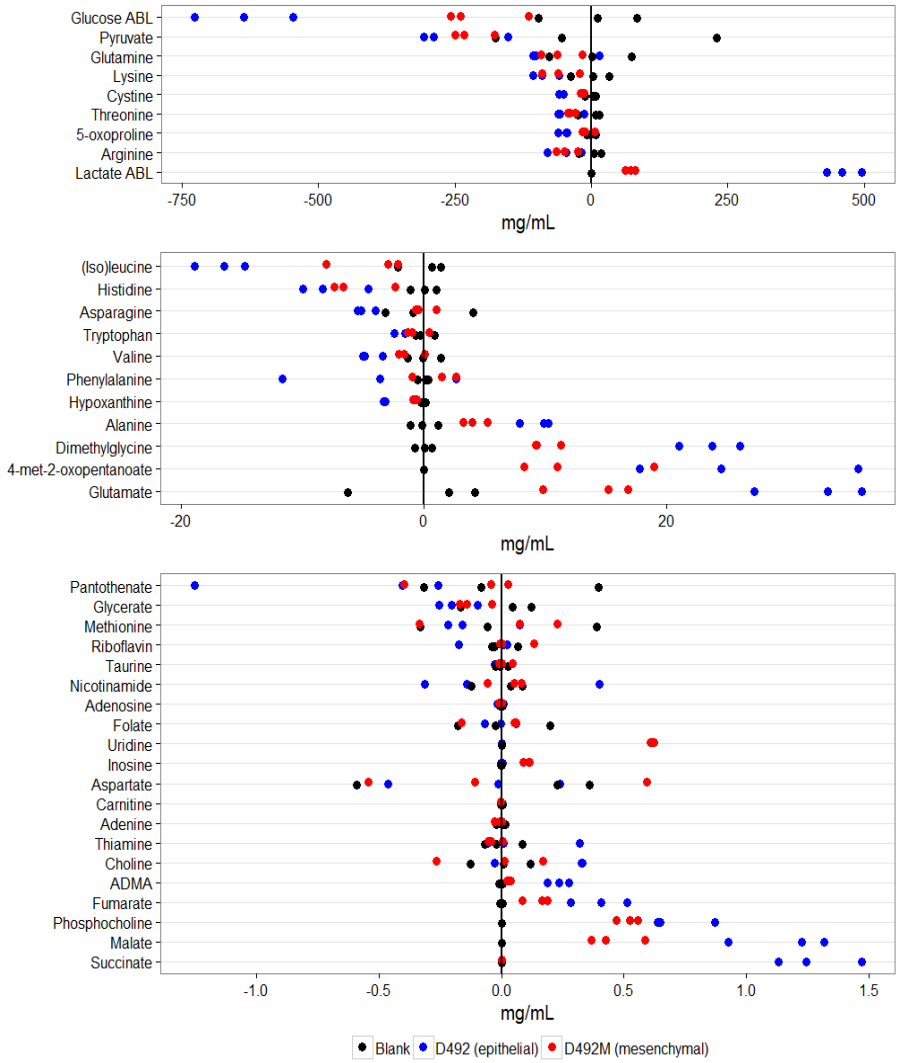

Figure 2. Concentration differences in spent medium from D492 and D492M cells compared to control samples. Blue dots represent medium uptake or secretion in wells containing D492 cells (epithelial), red dots represent medium uptake or secretion by D492M cells (mesenchymal). Black dots represent deviation of individual blank measurements from mean blank (vertical black line). Negative values indicate uptake of metabolite from the medium, positive values indicate secretion into the medium.

During growth the two cell lines consumed and secreted metabolites reflecting their nutritional requirements and active metabolic pathways. D492 cells had increased glucose and lactate, consumption and secretion rates respectively, as compared to D492M cells. The calculated glucose to lactate ratio of D492 was 0.74 but only 0.4 in the D492M cells, suggestive of altered utilization of carbons originating from glucose. Given the number of possible metabolic fates of glucose the results are suggestive of altered glycolysis, one carbon metabolism and/or TCA cycle activity.

Apart from glucose and lactate, the most prominent differences were observed in the amino acids glutamine, threonine, lysine, arginine, cystine, and (iso)-leucine (**SI Figure 1**). While the altered profiles of these amino acids may reflect demand due to protein synthesis, catabolism of amino acids also serves to fuel flux through the TCA cycle. We therefor hypothesized that anaplerosis of amino acids may contribute differently to TCA cycle flux between the two cell lines. To explore this further, we turned to genome scale metabolic modeling.

D492 and D492M metabolism captured in GEMs

In order to obtain a holistic description of D492 and D492M metabolism, we built GEMs of both phenotypes based on the generic human metabolic reconstruction RECON2 (Thiele et al., 2013) using the measured metabolite uptake and secretion rates and transcriptomic data (**Figure 3A**). The number of overlapping genes between the RNA-seq data set and RECON2 was 1284 but 338 additional genes were needed in order to make a functional model representing both cell lines, referred to as the EMT metabolic model (**Figure 3B**). Cell specific models were obtained by mapping microarray expression data to the EMT model. Based on the selected cut-off value, a total of 74 genes were upregulated in the D492 expression data and 65 in the D492M data (**Figure 3B**). After restricting the corresponding fluxes and applying metabolomics constraints, we obtained the functional EPI and MES models. Comparison between RECON2 and the EMT model is provided in **Figure 3C.**

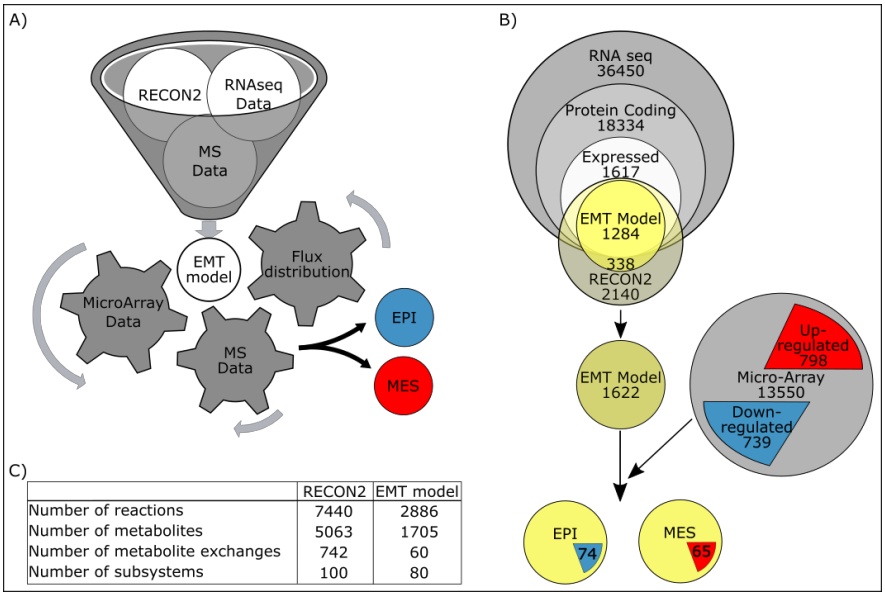

C)

	RECON2	EMT model
Number of reactions	7440	2886
Number of metabolites	5063	1705
Number of metabolite exchanges	742	60
Number of subsystems	100	80

Figure 3. EMT Model reconstruction: **A)** An overview of the model reconstruction. Gene expression data and mass spectrometry data for epithelial (D492) and mesenchymal (D492M) cells was combined with the human metabolic reconstruction (RECON2) to make a metabolic model of EMT. The EMT model was further constrained with differential expression from microarray data and mass spectrometry data to afford two genome scale models descriptive of metabolism in D492 and D492M. **B)** Details of the model reconstruction. RECON2 was combined with an RNA-seq dataset containing 36450 unique transcripts, of which 18334 were protein coding. Transcripts with expression values above a given threshold in either cell were included, leaving 1617 genes of which 1284 were present in RECON2. Microarray expression data was then used to define genes that were upregulated or downregulated in D492 vs. D492M. The fluxes in the EMT model were then constrained using this information together with cell specific metabolomics data to generate phenotype specific models referred to as the EPI and MES models. The arcs in blue and red represent fraction of genes upregulated in D492 and D492M respectively. **C)** Overlap of reactions, metabolites and subsystems between the generic RECON2 model and the EMT model.

Altered mitochondrial activity and validation of predicted differences in energy metabolism

In order to validate whether the computational models were descriptive of D492 and D492M cell growth, we compared the predicted maximum growth rates of the EPI and MES models obtained with FBA (0.115 h^{-1} and 0.080 h^{-1}, respectively) to the measured growth rates (**Figure 1b**). The predicted growth

rates were not expected to match the experimental values quantitatively since the biomass function is not necessarily representative of breast epithelial cells (Lee et al., 2012) and maximizing biomass may not be the “true” cellular objective of the D492 and D492M cells. However, although these values are approximately 4 times higher than the measured values, the corresponding ratio between the growth rates of the EPI and MES models is 1.4. This ratio is in agreement with the measured growth rates ratio of 1.3 between D492 and D492M.

The difference in predicted growth rates between the EPI and MES models was traced to decreased activity of cardiolipin synthase in MES model. A demand for mitochondrial ATP was added to the EPI and MES models and FBA was used to estimate the maximum ATP generation. According to these estimates, maximal mitochondrial ATP production is 4.4 times higher in the EPI model than in the MES model. Mitochondrial staining of D492 and D492M did not reveal apparent differences in overall mitochondrial abundance (**Figure 4a**). This was further confirmed with flow cytometry (data not shown). The D492 cells show a strong perinuclear mitochondrial staining while D492M cells show mitochondria placement within the cytosol indicative of mesenchymal front-rear polarity. These data suggest altered mitochondrial function in D492 vs. D492M as opposed to a quantitative effect. Differences in energy metabolism were further confirmed through measurements of the glycolytic vs. oxidative phosphorylation contribution to ATP generation. Both glycolytic and oxidative phosphorylation activity was increased in D492 cells as compared to D492M cells (**Figure 4b**). Furthermore, these data showed that D492 cells have higher spare capacity to perform oxidative phosphorylation as compared to the D492M cells (**Figure 4c**) and corroborate the metabolic phenotypes captured by the EPI and MES models.

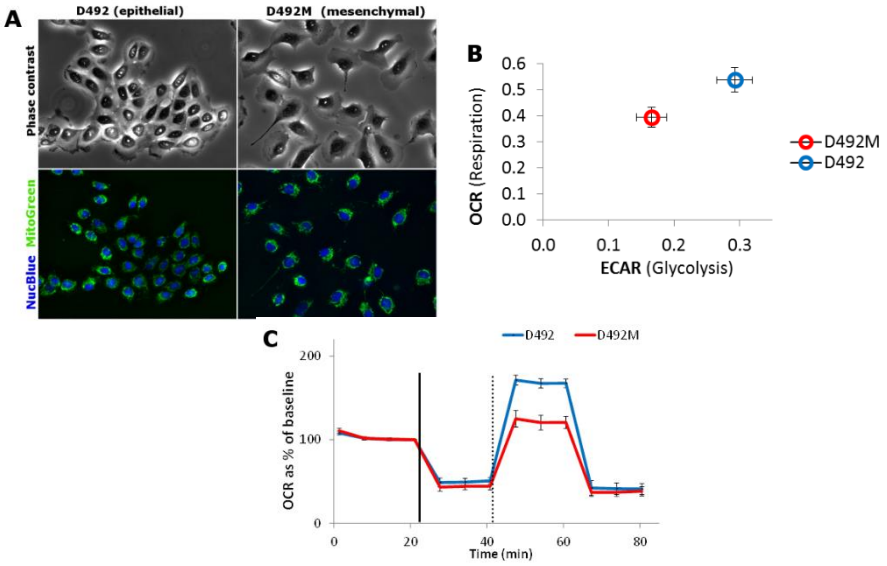

Figure 4. A) Mitochondrial staining of D492 (epithelial) cells and D492M (mesenchymal) cells. Although distribution and staining intensity of individual mitochondria appear different in the two cell lines, flow cytometry of stained cells did not indicate significant differences in total mitochondrial staining. **B)** Oxygen consumption rate (OCR) and extracellular acidification rate (ECAR) of D492 (blue circle) and D492M cells (red circle) as measured in a Seahorse XF analyzer. OCR is presented as pmol/min and normalized for cell density. ECAR measures the medium acidification (in mpH/hour) do to lactate secretion and is as such a proxy for glycolysis. Data represent 15 technical replicates in 4 separate experiments, error bars represent standard deviation, n = 4. **C)** Maximum respiratory capacity in D492 and D492M cells. OCR of D492 (blue line) and D492M (red line) presented over 80 minutes as percentage of baseline. The solid vertical line marks the time of oligomycin injection, a potent inhibitor of ATP-synthase, and the subsequent drop in oxygen consumption indicates that a similar percentage of ATP is generated via OXPHOS in both cell lines. The dotted vertical line marks the time of FCCP injection, an ETC un-coupler, and the subsequent rise in oxygen consumption indicates that D492 cells have far greater spare respiratory capacity than D492M cells. Data represent one of four separate experiments giving comparable results. Error bars represent standard deviation of 15 technical replicates.

These measurements along with the metabolic phenotypes predicted by the EPI and MES models suggest altered energy metabolism in the two cell lines. In order to validate the proposed metabolic phenotypes, we measured selected energy metabolites using enzyme assays (**Table 1)**. ATP concentration in D492 was significantly higher than in D492M. Total NAD(H) concentration and the ratio of NAD^+/NADH were also higher in D492 as compared to D492M (5.66 vs. 4.52). Measurements of NADPH were noisy but were indicative of a lower $NADP^+$/NADPH ratio in D492 (0.25 vs. 0.643). Glutathione was found to be primarily in the non-oxidized form in both cell lines although the total concentration was considerably higher in D492.

	D492 Epithelial		**D492M Mesenchymal**	
	fmol per cell	concentration (mM)	fmol per cell	concentration (mM)
ATP	12.4±0.95	7.29±0.56	7.54±0.44	5.39±0.31
NAD^+	0.85±0.16	0.503±0.096	0.303±0.020	0.216±0.014
NADH	0.15±0.01	0.089±0.004	0.067±0.009	0.048±0.006
$NADP^+$	0.007±0.006	0.004±0.004	0.009±0.014	0.007±0.01
NADPH	0.028±0.008	0.016±0.005	0.014±0.015	0.01±0.011
GSH	25.42±0.41	14.952±0.239	15.15±0.54	10.82±0.39
GSSG	1.26±0.32	0.740±0.190	0.70±0.38	0.50±0.27

Table 1. Energy metabolite (ATP, NAD(H) and NADP(H)) and glutathione (reduced (GSH) and oxidized (GSSG)) concentrations in D492 epithelial and D492M mesenchymal cells. Values represented as fmol per cell and intracellular concentration in mM ± standard deviation (n=3).

TCA cycle flux and oxidative phosphorylation is altered following EMT in D492

Random sampling was used to estimate flux distributions in the EPI and MES models. Comparisons of flux distributions using two-sample Kolmogorov-Smirnov test identified the metabolic reactions and pathways with altered activity between the two models. The predicted global metabolic alterations that occur in D492 following EMT are shown in **SI Figure 5**. Reactions involved in the N- and O-glycan metabolism are highly upregulated in the MES model, along with keratan sulfate metabolism while all the reactions involved in purine synthesis and cysteine metabolism were more active in the EPI model.

Figure 5 shows specific differences in calculated flux distributions through reactions in central carbon metabolism. In the MES model, glycolytic flux is reversed through phosphoglucomutase resulting in more 3-phosphoglycerate diversion to one carbon metabolism, which is one of the contributors to the production of cytosolic NADPH. Triose phosphate isomerase flux was also reversed in the MES model indicative of a demand for the lipid precursor glycerol phosphate through dihydroxyacetone phosphate.

In the TCA cycle, citrate synthase activity was increased in the MES model. This was due to increased oxidation of (iso)-leucine forming acetyl-CoA equivalents to a greater degree in the MES model. Glutamine was metabolised differently in the EPI and MES models. In the EPI model, glutamine was utilized for purine biosynthesis, while in MES model it contributed to alpha-ketoglutarate in the TCA cycle. Increased activity of argininosuccinate lyase in the MES model provided anaplerotic carbons via fumarate. Combined, the glycolytic and TCA cycle metabolic phenotypes provide a description of TCA cycle flux rewiring that occurs following EMT.

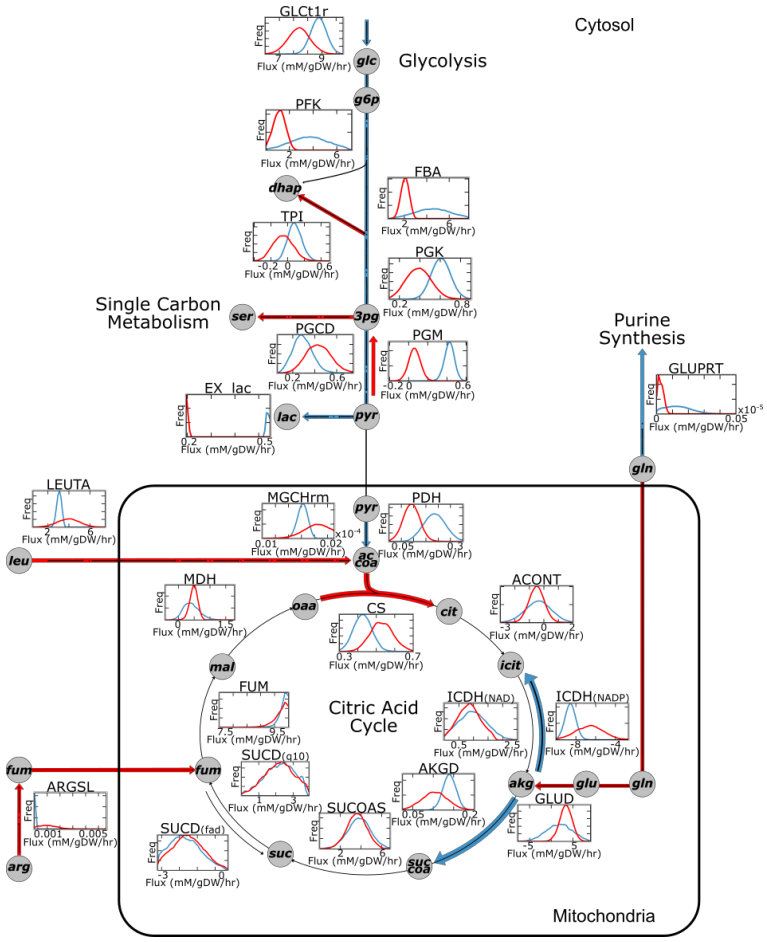

Figure 5: Predicted flux differences in D492 epithelial and D492M mesenchymal cell lines: Reactions highlighted in blue are more active in the EPI model while the red reactions are more active in the MES model. The EPI model has active glycolysis while in MES model 3pg is diverted to serine metabolism. Amino acids feed into Citric acid cycle in MES model. Abb.: glc: glucose; g6p: glucose-6-phosphate; dhap: dihydroxyacetone phosphate; 3pg: 3-phosphoglycerate; ser: serine; pyr: pyruvate; lac: lactate; accoa: acetyl-CoA; cit: citrate; akg: alpha-ketoglutarate; suc: succinate; mal: malate; oaa: oxaloacetate; leu: leucine; gln: glutamine; GLCt1r: Glucose transport; FBA: fructose-bisphosphate aldolase; TPI: triose-phosphate isomerase; PGK: phosphoglycerate kinase; PGM: phosphoglycerate mutase; EX_lac : exchange lactate; PGCD: phosphoglycerate dehydrogenase; CS: citrate synthase; ACONT: aconitase; ICDH(NAD): isocitrate dehydrogenase (NAD dependent); ICDH(NADP): isocitrate dehydrogenase (NADP dependent); AKGD: alphaketoglutarate dehydrogenase; SUCOAS: succinyl-CoA synthetase; SUCD(fad): succinate dehydrogenase (FAD dependent); SUCD(q10): succinate dehydrogenase (ubiquinone dependent); FUM: fumarase; MDH: malate dehydrogenase; LEUTA: leucine transaminase; MGHCrm: methylglutaconyl-CoA hydratase; GLUPRT: glutamine phosphoribosyldiphosphate amidotransferase; GLUN: glutaminase; ARGSL: argininosuccinate lyase.

Identification of metabolic and regulatory genes required for EMT and MET in D492

Having validated the proposed metabolic phenotypes in the EPI and MES models we next identified specific reactions responsible for the metabolic differences observed in the two models. To do this, we calculated which reaction constraints needed to be regulated in the EPI model in order to transform the epithelial phenotype to the mesenchymal phenotype and vice versa for MET. **Figure 6** shows the metabolic subsystems that required regulation, the number of reactions within these subsystems and the number of corresponding genes. The reactions along with their gene identifiers are reported in **SI Table 3 and 4.** A total of 88 target reactions required modification for EMT while this number was 335 to revert the mesenchymal phenotype to epithelial. For EMT (**Figure 6A**), the highest number of reactions requiring regulation were involved in N-glycan degradation, more specifically keratan sulfate degradation. Most genes requiring regulation were however associated with complex III of the electron transport chain. Other subsystems involved included valine, leucine and isoleucine metabolism and fatty acid oxidation. Out of the 335 target reactions predicted by the models to revert mesenchymal phenotype to epithelial, 288 represented extracellular transport reactions associated with only 5 genes (**Figure 6B**). Other important subsystems with altered activity following MET included nucleotide interconversion, glycine, serine, alanine and threonine metabolism and arginine and proline metabolism.

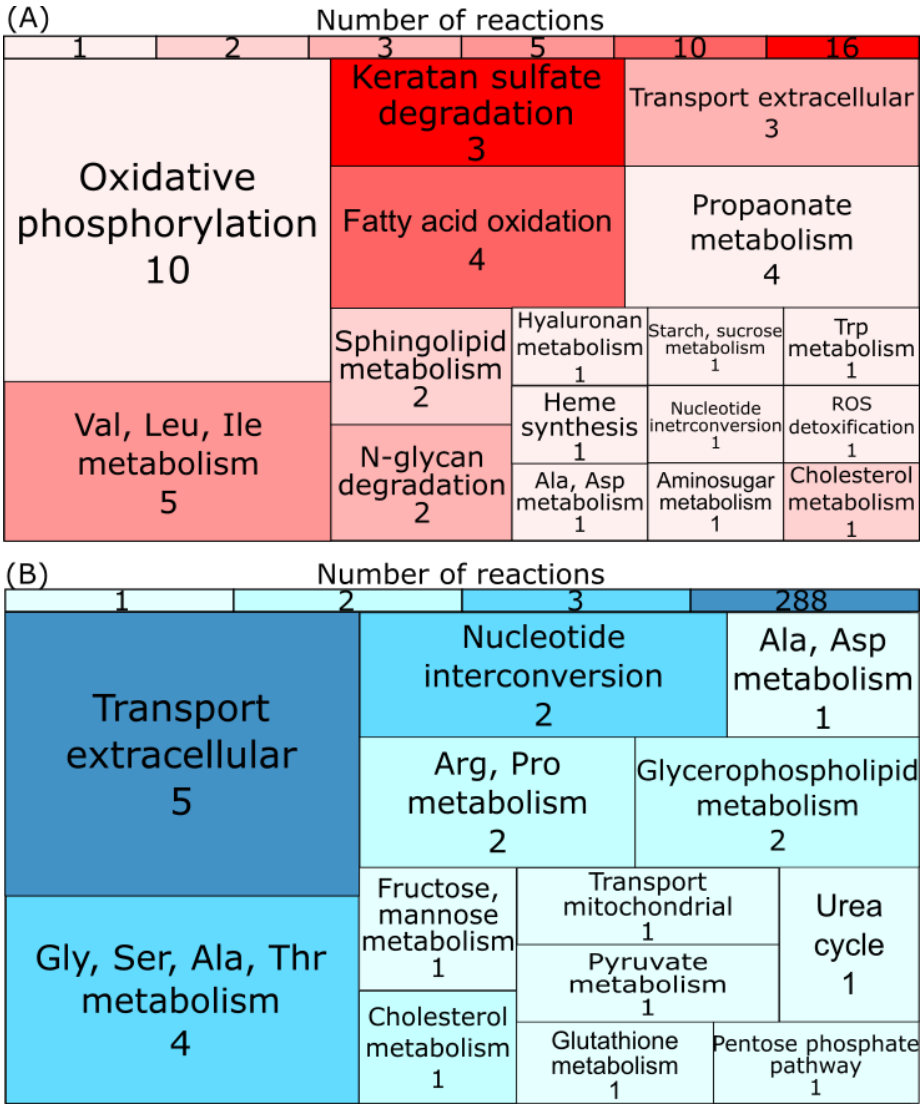

Figure 6. Tree maps for reaction subsystems involved in EMT (A) and MET (B): The color scale above represents the number of reactions in each subsystem while the size and numbers in the boxes represent the number of genes affecting these reactions.

Regulation of transcription is of importance in EMT. We identified transcription factors (TFs) that have been associated with the genes required for EMT and MET in the D492 models using SABiosciences' proprietary database (http://www.sabiosciences.com/chipqpcrsearch). The TFs associated with the genes for EMT and MET overlapped with small differences (**SI Table 3, 4 and 5**) PPAR-gamma1, PPAR-gamma2 and AP-1 were found to be the most relevant for both EMT and MET. Sp1 and TFIID exhibit binding to genes associated with EMT while C/EBPbeta, Msx-1, N-Myc and HFH-1 were predicted to bind to genes associated with MET. While many of these transcription factors have been shown previously to be of importance in the context of EMT (Fuxe, Vincent, & Garcia de Herreros, 2010; Kolesnikoff et al., 2014) the results represent hypothesis of transcription factors important for developmental regulation in the D492 cell model.

Identification of essential genes in the EPI and MES models

Using gene essentiality analysis, we next identified specific metabolic genes in the EPI and MES models that, when knocked out, are likely to be lethal in one cell but not the other (**Table 2**). Gene targets that are lethal for the EPI model are genes required for reactions of the TCA cycle (fumarase) and oxidative phosphorylation (succinate dehydrogenase (complex II) and ATP synthase) while the genes identified as lethal in the MES model fuel anaplerotic reactions for the TCA cycle. This included a sub-unit of the large neutral amino acid transporter LAT1 and reactions involved acetyl-CoA and fumarate production. These results predict that D492M cells can bypass the electron transport chain by supplying mitochondria with TCA cycle intermediates derived from branched chain or other non-polar amino acids.

Genes essential for EPI model	
ATP5B	ATP synthase, H+ transporting, mitochondrial F1 complex, beta polypeptide
ATP5I	ATP synthase, H+ transporting, mitochondrial Fo complex subunit E
FH	fumarate hydratase
GCDH	glutaryl-CoA dehydrogenase
GSS	glutathione synthetase
HEXA	hexosaminidase subunit alpha
NSF	N-ethylmaleimide sensitive factor
SDHA	succinate dehydrogenase complex flavoprotein subunit A
SDHB	succinate dehydrogenase complex iron sulfur subunit B
SDHC	succinate dehydrogenase complex subunit C
SDHD	succinate dehydrogenase complex subunit D, integral membrane protein
ATP5L	ATP synthase, H+ transporting, mitochondrial Fo complex subunit G
SLC16A10	solute carrier family 16 member 10
Genes Essential for MES model	
PDHX	pyruvate dehydrogenase complex component X
ASL	argininosuccinate lyase
SLC7A5	solute carrier family 7 member 5
OAT	ornithine aminotransferase

Table 2. Genes essential for EPI and MES model: The 13 and 4 genes listed in the table are exclusively essential for the biomass production of EPI model and MES model, respectively.

Based on the findings above, we argued that high expression of genes predicted to be essential for a mesenchymal phenotype to survive would contribute to cancer relapse or metastasis formation. To investigate whether our predicted lethal genes had relevance to cancer progression, we compared target gene expression in tumors and risk of remission or distant metastasis

over a period of 10 years in a cohort of 3557 breast cancer patients using the Kaplan-Meier Plotter web-tool (Gyorffy et al., 2010). In particular, risk of remission and distant metastasis formation were found to be consistently higher in patients with high expression of the SLC7A5 sub-unit of the LAT1 transporter (**Figure 7**).

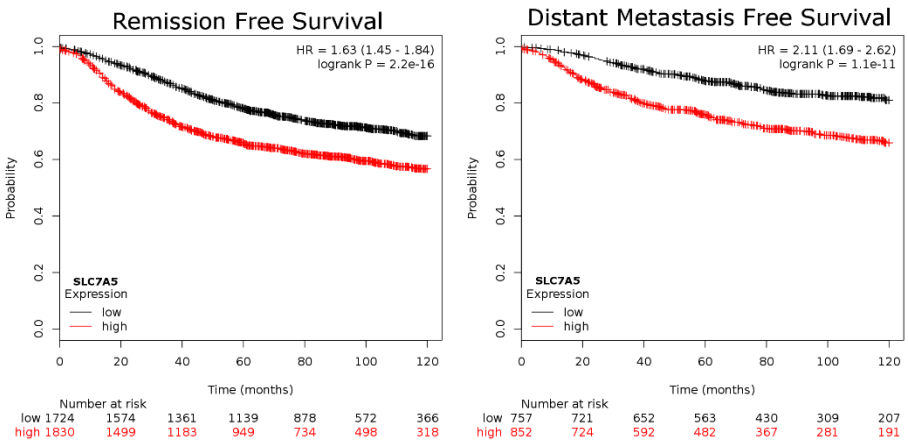

Figure 7. Kaplan-Meier survival curves for remission free and distant metastasis free survival based on high or low SLC7A5 expression. 3554 tumors were evaluated for SLC7A5 expression and correlated with risk of remission (left), 1609 tumors were evaluated for SLC7A5 expression and risk of developing cancers elsewhere in the body. In both cases, high expression of SLC7A5 predicts worse prognosis.

Discussion

Here we set out to identify modulators of EMT through metabolic systems analysis of the isogenic breast epithelial cell line D492 and its EMT-derivative daughter cell line D492M. Analysis of transcriptomic data and measurements of nutrient uptake/secretion rates were used to generate a GEM descriptive of D492 metabolism pre and post EMT. The GEMs represent the integrated analysis of 1304 genes and 43 extracellular metabolites and afford a snapshot of D492 metabolism. GEM based metabolic phenotypes were validated and then used to identify reactions, genes and associated transcription factors that

act to discriminate between D492 epithelial and mesenchymal metabolism. Finally, we used the GEMs to identify genes that when knocked down discriminate between epithelial vs. mesenchymal cell growth. These represent hypotheses of biomarkers or drug targets that could be pursued for anti-metastatic therapy.

Measured uptake rates of metabolites from media were on average higher in D492 and different nutrient distribution profiles within the metabolic networks were observed (**Figures 3 and 7**). In particular, altered utilization of carbons originating from glucose, glutamine, arginine and the branched chain amino acids was apparent in the two cell lines on account of altered gene expression in glycolysis and the TCA cycle. Calculation of the most likely carbon flux through metabolic pathways thus showed that D492 relies more on aerobic glycolysis and that activity of anaplerotic reactions associated with the TCA cycle is altered in D492M. Measurements of energy metabolites and the measured respiration capacity were consistent with the computed alterations in glycolysis, TCA cycle and pentose phosphate pathway activity. A comparison of reaction flux in the EPI and MES models through reactions corresponding to the mesenchymal metabolic signature (MMS) gene set identified by Shaul et al (Shaul et al., 2014), showed that out of 19 reactions encoded by the 28 MMS genes present in the two GEMs, 11 had higher flux in the MES model (**SI Figure 6**). D492 mesenchymal metabolism thus adheres to the general mesenchymal phenotype although deviations are observed. These deviations are to be expected due to the lack of measurements of metabolites in specific metabolic pathways that contain the MMS encoding reactions and the fact that MMS genes were identified based solely on expression data.

Flux balance analysis of the EPI and MES models suggested that lower proliferation rates of D492M vs. D492 is due to lower cardiolipin synthase activity in the MES model. Cardiolipin is a lipid exclusively found in the inner mitochondrial membrane and is important for mitochondrial function with regard to the formation and maintenance of cristae and formation and

stabilization of protein complexes comprising the electron transport chain (Mejia & Hatch, 2016). Although wary of this being a modelling artifact as cardiolipin is part of the biomass function used to optimize model flux, this finding focused our investigation on core energy metabolism. Differences in D492 cell size, weight, mitochondrial staining and respiratory capacity confirmed altered mitochondrial activity (that may or may not arise from altered cardiolipin content), as opposed to a purely quantitative effect induced by fewer mitochondria in D492M. The models therefore correctly accounted for differences in proliferation due to altered mitochondrial activity.

Sampling analysis of the flux space of the D492 GEMs highlighted changes in metabolic pathways (**Figure 6**) that have previously been attributed to increased invasiveness of cancer stem cells and EMT including fatty acid oxidation (Buchheit, Weigel, & Schafer, 2014), nucleotide interconversions (Shaul et al., 2014) and glycan metabolism (Shaul et al., 2014). Fatty acid oxidation in particular has been shown to be altered upon loss of attachment of the cells during EMT (Buchheit et al., 2014). Fatty acids are however not equivalent in their impact on cell proliferation (Hardy et al., 2003; Schug et al., 2015) and more detailed lipid analysis of D492 is required as the D492 models lack intracellular flux measurements of fatty acid oxidation. Regardless, analysis of gene expression data in the context of the models indicate that D492M cells rely considerably more on fatty acid oxidation than D492. Malonyl-CoA decarboxylase is important for breast cancer invasiveness (Yizhak et al., 2014) and lipidomic analysis of EMT show vast reorganization of the lipidome consistent with altered membrane fluidity and function following EMT (Zhao et al., 2016). Expanding the understanding of changes in the lipidome during and following EMT are thus important.

We used the models to identify reactions of importance for EMT and MET. For this purpose, reactions who´s flux requires regulation in order to switch between the EPI and MES model phenotypes were identified (**Figure 6**). Inspection of these reactions and the tracing of calculated metabolite flux values affords mechanistic insight into altered metabolism into the D492 EMT

model. For example, the upregulation of complex III required for EMT is a direct consequence of increased activity of the electron transfer flavoprotein in the MES model that transports electrons originating from fatty acid oxidation in the form of FADH to complex III. Complex III upregulation is therefore required for EMT in D492 to account for increased FADH oxidation. The modelling results suggest the increased oxidative capacity in D492 (Figure 4) is due to enhanced activity of complex I and/or II in D492. Suppression of complex I activity has recently been shown to induce metastatic properties in a series of mammary gland derived cell lines (He et al., 2013).

The altered activity of TCA anaplerosis predicted by the models was traced to amino acid metabolism arising from differential uptake rates of arginine, threonine, lysine and leucine and/or isoleucine. Leucine/isoleucine and arginine induce the activation of mTOR that is associated with enhanced proliferation which we did not observe in D2492M. AMPK overrides mTOR activation. In light of the lower ATP concentration in D492M and lower proliferation rate we conclude that increased uptake of leucine/isoleucine (and arginine) in D492M reflects altered metabolism in D492 associated with differentiation rather than proliferation. Indeed, these metabolites are metabolized differently within the two cell lines. Arginine was used to generate fumarate and proline through citruline and ornithine respectively. In D492 however, arginine fuels polyamine synthesis through ornithine, consistent with enhanced polyamine requirement for proliferation (Soda, 2011). Lysine is oxidized in both models to acetyl CoA in the mitochondria through 2-oxoadipate, however only in D492M was lysine utilized to generate allysine, a component of elastin and collagen. Threonine was oxidized through propanoyl-CoA in both models, but again appears to be more important in the fueling of the TCA cycle in D492M.

We also identified enzymatic reactions of interest outside central carbon metabolism that have previously been associated with EMT. Specifically, for glycan and keratan sulfate degradation we identified FucA1. FucA1 is de-regulated in TGF-β induced EMT in bladder epithelial cells (Guo et al., 2014)

and fucosylation of E-cadherin has been shown to impact cell migration in lung cancer cells (Shao et al., 2016) and is a biomarker for cellular senescence (Hildebrand et al., 2013). The proposed increased flux through glycan degradation pathways in D492M is consistent with these results. Similarly, delta (14)sterol reductase, a key enzyme in cholesterol synthesis, encoded by TM7SF2, previously identified as a signature mesenchymal marker(Shaul et al., 2014), was identified as important for EMT reflecting the increased requirement for membrane fluidity in mesenchymal cells. Prolonged statin therapy has previously been shown to increase breast cancer incidence (McDougall et al., 2013). However our results support epidemiologic evidence of the protective effect of statins on breast cancer recurrence (Ahern, Lash, Damkier, Christiansen, & Cronin-Fenton, 2014) presumably through inhibition of EMT. These findings require follow up molecular biology based investigation. Interestingly, TM7SF2 was recently found to correlate with NFKB and TNF-α expression in mouse fibroblasts (Bellezza et al., 2013). TNF-α induces EMT through upregulation of TWIST via NFKB.

Reports on alterations in core energy metabolism in cells undergoing EMT are conflicting and have been associated with both increased and decreased anaerobic glycolysis and increased and decreased proliferation (Jerby et al., 2012; Thomson et al., 2011). Specifically, our results do not agree with similar investigations of EMT using the HER2 positive BT-474 and ER positive MCF7 EMT cell culture models that found increased proliferation and a switch to aerobic glycolysis following EMT (Kondaveeti, Guttilla Reed, & White, 2015) . This highlights the metabolic diversity of EMT cell models that we have recently shown is influenced by heterogeneous expression profiles in EGFR signaling and is consistent with the inherent flexibility and variation characteristic of EMT (Lamouille, Xu, & Derynck, 2014). D492 presents an alternative to the more studied HMLE, BT-474 and MCF7 cell models (Mani et al., 2008) (Kondaveeti et al., 2015; Tam et al., 2013), of importance given the heterogeneity of cell models used to study EMT (Choudhary et al., 2016) and contribute to the understanding of EMT metabolic diversity. Altered metabolism may also relate to the breast cancer sub-type under study. D492 is representative of basal like

breast cancer that has similarities to triple negative breast cancer (Badve et al., 2011). Ultimately, because the D492 cell model allows investigation of epithelial cells pre and post EMT, our results suggest that in the context of D492, enhanced glycolysis is not a required for maintaining the mesenchymal phenotype.

Importantly, neither D492 nor D492M cells are tumorigenic. D492 originates from reduction mammoplasty, immortalized with E6/E7 viral transduction (Gudjonsson et al., 2002). D492M has a distinct mesenchymal-like phenotype and does not revert back to the original epithelial phenotype. It should be kept in mind that although tumor development is associated with increased cell proliferation and growth, the change to an invasive, mesenchymal phenotype is not (Funasaka, Hu, Yanagawa, Hogan, & Raz, 2007). While EMT is believed to be a pre-requisite to tumor invasion and metastasis, the reversion of mesenchymal cells back to epithelial (MET) is thought to be a crucial step in the formation of secondary tumors (Luo, Brooks, & Wicha, 2015). The D492/D492M cell model is therefore an ideal system to explore the metabolic re-wiring that takes place during EMT and should not be viewed as a tool to examine secondary tumor growth.

The curated GEMs of D492 are the first that are representative of metabolism of EMT generated to date and serve to characterize the metabolism of the D492 EMT cell model. Although the generation of metabolic models is now commonplace using automated algorithms (Jerby & Ruppin, 2012), the model generated here was manually curated and the computed metabolic phenotypes were experimentally validated. These GEMs therefore represent a foundation for future constraint based analysis of epithelial and mesenchymal metabolism within or outside the context of EMT. Furthermore, the methodology used to generate the two models is novel and presents an alternative approach to building context-specific GEMs. As opposed to directly constraining a generic reaction knowledgebase such as RECON2 or the human metabolic atlas (Machado & Herrgard, 2014), we used a combined transcriptomic dataset descriptive of metabolic reaction content in both cell

lines as a basis for model construction (the EMT model) that we then further constrained to generate the GEMs descriptive of D492 and D492M metabolism (the EPI and MES models). The approach allows direct comparison of metabolic phenotypes upon a curated context specific reconstruction that is of value when modeling biological events such as EMT where alternative expression off the same genetic background is being investigated, for example during embryonic development and stem cell differentiation.

Conclusion

Our findings demonstrate a novel approach to define metabolic differences between epithelial and mesenchymal phenotypes of a breast epithelial cell line. The epithelial phenotype was tuned to aerobic glycolysis and oxidative phosphorylation to fuel rapid proliferation while the mesenchymal phenotype relied on anaplerotic reactions to fuel the TCA cycle. The phenotype specific GEMs were used to identify critical metabolic nodes, in particular the LAT1 transport system, that may specifically target EMT derived mesenchymal cells and inhibit metastatic dissemination. In broader terms, the tools we provide showcase how metabolic models can be applied to study cellular development, serve as a platform for further studies of EMT and aid the development of novel cancer therapeutics.

Acknowledgements

We thank Dr. Giuseppe Paglia for valuable discussions on metabolomics experimental design and Dr. Guðmundur Logi Norddahl for help with flow cytometry. Financial support for this work was provided by the Icelandic Research Council (Grants number: 130591-051, 130816-051 and 152358-051).

Availability of data and materials

The datasets supporting the conclusions of this article are included within the supplementary files.

Authors' contributions

SH, NR, SG and OR designed the study, collected the data, analyzed the data and wrote the manuscript. MM, KSC, TG, EK, AB, BH, MP and GMM contributed to data collection, data analysis and the writing of the manuscript.

Competing interests

The authors declare that they have no competing interests.

References

Acloque, H., Adams, M. S., Fishwick, K., Bronner-Fraser, M., & Nieto, M. A. (2009). Epithelial-mesenchymal transitions: the importance of changing cell state in development and disease. *J Clin Invest, 119*(6), 1438-1449. doi:10.1172/JCI38019

Ahern, T. P., Lash, T. L., Damkier, P., Christiansen, P. M., & Cronin-Fenton, D. P. (2014). Statins and breast cancer prognosis: evidence and opportunities. *Lancet Oncol, 15*(10), e461-468. doi:10.1016/s1470-2045(14)70119-6

Badve, S., Dabbs, D. J., Schnitt, S. J., Baehner, F. L., Decker, T., Eusebi, V., . . . Reis-Filho, J. S. (2011). Basal-like and triple-negative breast cancers: a critical review with an emphasis on the implications for pathologists and oncologists. *Mod Pathol, 24*(2), 157-167. doi:10.1038/modpathol.2010.200

Barriere, G., Fici, P., Gallerani, G., Fabbri, F., & Rigaud, M. (2015). Epithelial Mesenchymal Transition: a double-edged sword. *Clin Transl Med, 4*, 14. doi:10.1186/s40169-015-0055-4

Bellezza, I., Roberti, R., Gatticchi, L., Del Sordo, R., Rambotti, M. G., Marchetti, M. C., . . . Minelli, A. (2013). A novel role for Tm7sf2 gene in regulating TNFalpha expression. *PLoS One, 8*(7), e68017. doi:10.1371/journal.pone.0068017

Buchheit, C. L., Weigel, K. J., & Schafer, Z. T. (2014). OPINION Cancer cell survival during detachment from the ECM: multiple barriers to tumour progression. *Nature Reviews Cancer, 14*(9), 632-641. doi:10.1038/nrc3789

Choudhary, K., Rohatgi, N., Halldorsson, S., Briem, E., Gudjonsson, T., Gudmundsson, S., & Rolfsson, O. (2016). EGFR Signal-Network Reconstruction Demonstrates Metabolic Crosstalk in EMT. *PLoS computational biology*.

Dong, C., Yuan, T., Wu, Y., Wang, Y., Fan, T. W., Miriyala, S., . . . Zhou, B. P. (2013). Loss of FBP1 by Snail-mediated repression provides metabolic advantages in basal-like breast cancer. *Cancer Cell, 23*(3), 316-331. doi:10.1016/j.ccr.2013.01.022

Fell, D. A., & Small, J. R. (1986). Fat synthesis in adipose tissue. An examination of stoichiometric constraints. *Biochem J, 238*(3), 781-786.

Funasaka, T., Hu, H., Yanagawa, T., Hogan, V., & Raz, A. (2007). Down-regulation of phosphoglucose isomerase/autocrine motility factor results in mesenchymal-to-epithelial transition of human lung fibrosarcoma cells. *Cancer Res, 67*(9), 4236-4243. doi:10.1158/0008-5472.CAN-06-3935

Fuxe, J., Vincent, T., & Garcia de Herreros, A. (2010). Transcriptional crosstalk between TGF-beta and stem cell pathways in tumor cell invasion: role of EMT promoting Smad complexes. *Cell Cycle, 9*(12), 2363-2374. doi:10.4161/cc.9.12.12050

Gudjonsson, T., Villadsen, R., Nielsen, H. L., Ronnov-Jessen, L., Bissell, M. J., & Petersen, O. W. (2002). Isolation, immortalization, and characterization of a human breast epithelial cell line with stem cell properties. *Genes Dev, 16*(6), 693-706. doi:10.1101/gad.952602

Guo, J., Li, X., Tan, Z., Lu, W., Yang, G., & Guan, F. (2014). Alteration of N-glycans and expression of their related glycogenes in the epithelial-mesenchymal transition of HCV29 bladder epithelial cells. *Molecules, 19*(12), 20073-20090. doi:10.3390/molecules191220073

Gyorffy, B., Lanczky, A., Eklund, A. C., Denkert, C., Budczies, J., Li, Q., & Szallasi, Z. (2010). An online survival analysis tool to rapidly assess the effect of 22,277 genes on breast cancer prognosis using microarray data of 1,809 patients. *Breast Cancer Res Treat, 123*(3), 725-731. doi:10.1007/s10549-009-0674-9

Hanai, J., Doro, N., Sasaki, A. T., Kobayashi, S., Cantley, L. C., Seth, P., & Sukhatme, V. P. (2012). Inhibition of lung cancer growth: ATP citrate lyase knockdown and statin treatment leads to dual blockade of mitogen-activated protein kinase (MAPK) and phosphatidylinositol-3-kinase (PI3K)/AKT pathways. *J Cell Physiol, 227*(4), 1709-1720. doi:10.1002/jcp.22895

Hardy, S., El-Assaad, W., Przybytkowski, E., Joly, E., Prentki, M., & Langelier, Y. (2003). Saturated fatty acid-induced apoptosis in MDA-MB-231 breast cancer cells. A role for cardiolipin. *J Biol Chem, 278*(34), 31861-31870. doi:10.1074/jbc.M300190200

He, X., Zhou, A., Lu, H., Chen, Y., Huang, G., Yue, X., . . . Wu, Y. (2013). Suppression of mitochondrial complex I influences cell metastatic properties. *PLoS One, 8*(4), e61677. doi:10.1371/journal.pone.0061677

Hildebrand, D., Lehle, S., Borst, A., Haferkamp, S., Essmann, F., & Schulze-Osthoff, K. (2013). α-Fucosidase as a novel convenient biomarker for cellular senescence. *Cell Cycle, 12*(12), 1922-1927. doi:10.4161/cc.24944

Jain, M., Nilsson, R., Sharma, S., Madhusudhan, N., Kitami, T., Souza, A. L., . . . Mootha, V. K. (2012). Metabolite profiling identifies a key role for glycine in rapid cancer cell proliferation. *Science, 336*(6084), 1040-1044. doi:10.1126/science.1218595

Jerby, L., & Ruppin, E. (2012). Predicting Drug Targets and Biomarkers of Cancer via Genome-Scale Metabolic Modeling. *Clinical Cancer Research, 18*(20), 5572-5584. doi:10.1158/1078-0432.Ccr-12-1856

Jerby, L., Wolf, L., Denkert, C., Stein, G. Y., Hilvo, M., Oresic, M., . . . Ruppin, E. (2012). Metabolic associations of reduced proliferation and oxidative stress in advanced breast cancer. *Cancer Res, 72*(22), 5712-5720. doi:10.1158/0008-5472.can-12-2215

Kalluri, R. (2009). EMT: when epithelial cells decide to become mesenchymal-like cells. *J Clin Invest, 119*(6), 1417-1419. doi:10.1172/JCI39675

Kalluri, R., & Weinberg, R. A. (2009). The basics of epithelial-mesenchymal transition. *J Clin Invest, 119*(6), 1420-1428. doi:10.1172/JCI39104

Kolesnikoff, N., Attema, J. L., Roslan, S., Bert, A. G., Schwarz, Q. P., Gregory, P. A., & Goodall, G. J. (2014). Specificity protein 1 (Sp1) maintains basal epithelial expression of the miR-200 family: implications for epithelial-mesenchymal transition. *J Biol Chem, 289*(16), 11194-11205. doi:10.1074/jbc.M113.529172

Kondaveeti, Y., Guttilla Reed, I. K., & White, B. A. (2015). Epithelial-mesenchymal transition induces similar metabolic alterations in two independent breast cancer cell lines. *Cancer Lett, 364*(1), 44-58. doi:10.1016/j.canlet.2015.04.025

Lamouille, S., Xu, J., & Derynck, R. (2014). Molecular mechanisms of epithelial-mesenchymal transition. *Nat Rev Mol Cell Biol, 15*(3), 178-196. doi:10.1038/nrm3758

Lee, D., Smallbone, K., Dunn, W. B., Murabito, E., Winder, C. L., Kell, D. B., . . . Swainston, N. (2012). Improving metabolic flux predictions using absolute gene expression data. *BMC systems biology, 6*. doi:Artn 73

10.1186/1752-0509-6-73

Luo, M., Brooks, M., & Wicha, M. S. (2015). Epithelial-mesenchymal plasticity of breast cancer stem cells: implications for metastasis and therapeutic resistance. *Curr Pharm Des, 21*(10), 1301-1310.

Machado, D., & Herrgard, M. (2014). Systematic Evaluation of Methods for Integration of Transcriptomic Data into Constraint-Based Models of Metabolism. *PLoS computational biology, 10*(4). doi:ARTN e1003580

10.1371/journal.pcbi.1003580

Mani, S. A., Guo, W., Liao, M. J., Eaton, E. N., Ayyanan, A., Zhou, A. Y., . . . Weinberg, R. A. (2008). The epithelial-mesenchymal transition generates cells with properties of stem cells. *Cell, 133*(4), 704-715. doi:10.1016/j.cell.2008.03.027

McDougall, J. A., Malone, K. E., Daling, J. R., Cushing-Haugen, K. L., Porter, P. L., & Li, C. I. (2013). Long-term statin use and risk of ductal and

lobular breast cancer among women 55 to 74 years of age. *Cancer Epidemiol Biomarkers Prev, 22*(9), 1529-1537. doi:10.1158/1055-9965.epi-13-0414

Mejia, E. M., & Hatch, G. M. (2016). Mitochondrial phospholipids: role in mitochondrial function. *J Bioenerg Biomembr, 48*(2), 99-112. doi:10.1007/s10863-015-9601-4

O'Brien, E. J., Monk, J. M., & Palsson, B. O. (2015). Using Genome-scale Models to Predict Biological Capabilities. *Cell, 161*(5), 971-987. doi:10.1016/j.cell.2015.05.019

Paglia, G., Sigurjonsson, O. E., Rolfsson, O., Valgeirsdottir, S., Hansen, M. B., Brynjolfsson, S., . . . Palsson, B. O. (2014). Comprehensive metabolomic study of platelets reveals the expression of discrete metabolic phenotypes during storage. *Transfusion*. doi:10.1111/trf.12710

Palsson, B. O. (2015). *Systems Biology: Constraint-based Reconstruction and Analysis*: Cambridge University Press.

Petersen, O. W., Nielsen, H. L., Gudjonsson, T., Villadsen, R., Rank, F., Niebuhr, E., . . . Ronnov-Jessen, L. (2003). Epithelial to mesenchymal transition in human breast cancer can provide a nonmalignant stroma. *Am J Pathol, 162*(2), 391-402. doi:10.1016/S0002-9440(10)63834-5

Polyak, K., & Weinberg, R. A. (2009). Transitions between epithelial and mesenchymal states: acquisition of malignant and stem cell traits. *Nat Rev Cancer, 9*(4), 265-273. doi:10.1038/nrc2620

Savinell, J. M., & Palsson, B. O. (1992). Network analysis of intermediary metabolism using linear optimization. I. Development of mathematical formalism. *J Theor Biol, 154*(4), 421-454.

Schellenberger, J., & Palsson, B. O. (2009). Use of randomized sampling for analysis of metabolic networks. *J Biol Chem, 284*(9), 5457-5461. doi:10.1074/jbc.R800048200

Schug, Z. T., Peck, B., Jones, D. T., Zhang, Q., Grosskurth, S., Alam, I. S., . . . Gottlieb, E. (2015). Acetyl-CoA synthetase 2 promotes acetate

utilization and maintains cancer cell growth under metabolic stress. *Cancer Cell, 27*(1), 57-71. doi:10.1016/j.ccell.2014.12.002

Shao, K., Chen, Z. Y., Gautam, S., Deng, N. H., Zhou, Y., & Wu, X. Z. (2016). Posttranslational modification of E-cadherin by core fucosylation regulates Src activation and induces epithelial-mesenchymal transition-like process in lung cancer cells. *Glycobiology, 26*(2), 142-154. doi:10.1093/glycob/cwv089

Shaul, Y. D., Freinkman, E., Comb, W. C., Cantor, J. R., Tam, W. L., Thiru, P., . . . Sabatini, D. M. (2014). Dihydropyrimidine Accumulation Is Required for the Epithelial-Mesenchymal Transition. *Cell, 158*(5), 1094-1109. doi:10.1016/j.cell.2014.07.032

Sigurdsson, V., Hilmarsdottir, B., Sigmundsdottir, H., Fridriksdottir, A. J., Ringner, M., Villadsen, R., . . . Gudjonsson, T. (2011). Endothelial induced EMT in breast epithelial cells with stem cell properties. *PLoS One, 6*(9), e23833. doi:10.1371/journal.pone.0023833

Soda, K. (2011). The mechanisms by which polyamines accelerate tumor spread. *Journal of experimental & clinical cancer research : CR, 30*, 95. doi:10.1186/1756-9966-30-95

Tam, W. L., Lu, H., Buikhuisen, J., Soh, B. S., Lim, E., Reinhardt, F., . . . Weinberg, R. A. (2013). Protein kinase C alpha is a central signaling node and therapeutic target for breast cancer stem cells. *Cancer Cell, 24*(3), 347-364. doi:10.1016/j.ccr.2013.08.005

Thiele, I., Swainston, N., Fleming, R. M., Hoppe, A., Sahoo, S., Aurich, M. K., . . . Palsson, B. O. (2013). A community-driven global reconstruction of human metabolism. *Nat Biotechnol, 31*(5), 419-425. doi:10.1038/nbt.2488

Thomson, S., Petti, F., Sujka-Kwok, I., Mercado, P., Bean, J., Monaghan, M., . . . Haley, J. D. (2011). A systems view of epithelial-mesenchymal transition signaling states. *Clin Exp Metastasis, 28*(2), 137-155. doi:10.1007/s10585-010-9367-3

Vlassis, N., Pacheco, M. P., & Sauter, T. (2014). Fast reconstruction of compact context-specific metabolic network models. *PLoS Comput Biol, 10*(1), e1003424. doi:10.1371/journal.pcbi.1003424

Yizhak, K., Gaude, E., Le Devedec, S., Waldman, Y. Y., Stein, G. Y., van de Water, B., . . . Ruppin, E. (2014). Phenotype-based cell-specific metabolic modeling reveals metabolic liabilities of cancer. *Elife, 3*. doi:10.7554/eLife.03641

Zhao, W., Prijic, S., Urban, B. C., Tisza, M. J., Zuo, Y., Li, L., . . . Chang, J. T. (2016). Candidate Antimetastasis Drugs Suppress the Metastatic Capacity of Breast Cancer Cells by Reducing Membrane Fluidity. *Cancer Res, 76*(7), 2037-2049. doi:10.1158/0008-5472.can-15-1970

Supplementary Information

Materials and Methods

RNA sequencing

Ribosomal RNA was depleted from total RNA using RiboMinus™ Eukaryote Kit for RNA-Seq (Thermo Fisher Scientific, A1083708), and barcoded ribo-minus RNA libraries were prepared according to the SOLiD™ Total RNA-Seq Kit Protocol (Thermo Fisher Scientific, 4445374). In short, 500 ng rRNA depleted RNA was fragmented using RNase III. Fragments of desired length were enriched and ligated with adaptors before cDNA synthesis. Libraries were amplified by PCR with barcoded SOLiD™ 3' Primers from the SOLiD™ RNA Barcoding Kit, Module 1-16 (Thermo Fisher Scientific, 4427046). Equal molar amounts of each barcoded sample were pooled together in one library, which subsequently were used in emulsion PCR to a total concentration of 0.5 pM. Approximately 1 billion enriched beads were deposited on a full glass slide. High-throughput sequencing was performed using the SOLiD5500 platform. RNA-seq analyses were performed with the CLC Genomic Workbench 8 with forward specific mapping in color space (human reference sequence GRCh37.78). Expression values were normalized by totals and log2 transformed.

Metabolomics

Spent medium supernatant was separated by centrifugation (1600 g, 22°C, 5 min). Medium blanks were used as controls. 200 µL of medium sample were processed adding 30 µL of internal standard mixture (supplemental data) and 0.5 mL of MeOH. Samples were vortexed and centrifuged (15000 g, 4°C, 15 min). Supernatant was transferred into a new tube and dried using vacuum concentrator. Samples were reconstituted in 600 µL of H2O:ACN (50:50) and filtered by using a Pierce protein 96 well precipitation plate by centrifugation (2000 g, 4°C, 15 min). Pooled quality control (QC) samples were prepared by pooling 20 µL for each processed sample. Spiked pooled QC samples were prepared by spiking pooled QC samples with a mix containing 17 standard compounds.

Metabolomics analysis was performed using a modified version of the method presented by Paglia et al. (Paglia et al. 2014).

UPLC-MS

Ultra performance liquid chromatography (UPLC) (Acquity, Waters, Manchester, UK) was coupled with a quadrupole-time of flight mass spectrometer (Synapt G2, Waters, Manchester, UK). Chromatographic separation was achieved by hydrophilic interaction liquid chromatography (HILIC) using an Acquity amide column, 1.7 µm (2.1 x 150 mm) (Waters, Manchester, UK). All samples were analyzed three times: once in positive ionization mode and twice in negative ionization mode using acidic and basic chromatographic conditions. In positive mode and in negative acidic conditions, mobile phase A was 100% ACN and B was 100% H2O both containing 0.1% formic acid. The following elution gradient was used: 0 min 99% A; 7 min 30% A; 7.1 min 99% A; 10 min 99% A. In negative mode basic conditions, mobile phase A contained ACN:sodium bicarbonate 10 mM (95:5) and mobile phase B contained ACN:sodium bicarbonate 10 mM (5:95). The following elution gradient was used: 0 min 99% A; 6 min 30% A; 6.5 min 99% A; 10 min 99 % A. In all conditions, the flow rate was 0.4 mL/min, the column temperature was 45°C, and the injection volume was 3.5 µL.

The mass spectrometer was operated using a capillary voltage of 1.5 kV, the sampling cone and the extraction cone were of 30 V and 5 V. The cone and the desolvation gas flow were 50 L/h and 800 L/h, while the source and desolvation gas temperature were 120 and 500 °C. MS spectra were acquired in centroid mode from m/z 50 to 1000 using scan time of 0.3 s. Leucine enkephalin (2 ng/µL) was used as lock mass (m/z 556.2771 and 554.2615 in positive and negative experiments respectively). A typical analytical block consisted of: pooled QC samples to equilibrate the system; calibrators; samples and spiked pooled QC samples; calibrators.

TargetLynx (v4.1, Waters) was used to integrate chromatograms of targeted metabolites. Extracted ion chromatograms (EICs) were extracted using a 0.02 mDa window centered on the expected m/z for each targeted compound. Quantitation was performed by external calibration with reference standards.

Seahorse metabolic profiling

The D492 and D492M cells were seeded into a 96-well XF cell culture microplate using 14000 and 12000 cells/well respectively the day before the assay. 1 hour prior to the beginning of the assay, the growth medium was replaced with non-buffered serum-free DMEM assay medium (Seahorse Biosciences), supplemented with 10 mM glucose, 1 mM sodium pyruvate and 2 mM (Sigma); the pH was adjusted to 7.4. The plate was then placed in a CO_2-free incubator. During the assay, each cycle included 3 minutes long data acquisition points with 3-minute mixing and 3-minute waiting periods in between. In all experiments there were 4 measurements at the basal level and 3 measurements after injections of each of the metabolic modulators; oligomycin (1 μM; Sigma), FCCP (1 μM; Sigma) and a mixture of antimycin and rotenone (1 μM each; Seahorse Biosciences). At the end of the assay, ECAR and OCR measurements were normalized to cell density, evaluated using an Incucyte Live Cell Imaging instrument (Essen BioScience).

Constraint-based reconstruction and analysis

The stoichiometric matrix containing n reactions and m metabolites is denoted by $\boldsymbol{S}$ and the flux values by vector $\boldsymbol{v}=(v_1, ..., v_n)$. The flux values and stoichiometric matrix are connected via the equation $\boldsymbol{Sv} = \boldsymbol{0}$ under the assumption of steady-state mass conservation. In addition, lower and upper bounds are placed on the fluxes, $l_i \leq v_i \leq u_i$ for i=1, ..., n with a lower bound of zero corresponding to an irreversible reaction. Flux Balance Analysis (FBA) seeks to fulfill these constraints while optimizing a user-specified cellular objective, e.g. maximizing the growth rate, resulting in a single flux value for each reaction, in contrast, Random sampling returns multiple flux vectors, sampled from the set of feasible fluxes (satisfying the model constraints). The flux vectors can then be used to estimate the *distribution* of flux values. Gene essentiality analysis is a FBA-based technique which helps in identifying the weak links in the metabolic network.

Generation of a breast tissue specific metabolic model

The Ensembl gene IDs in the RNA-seq data set were mapped to the Entrez IDs used in RECON2.04 using the David gene ID conversion tool (Huang et al. 2009b; Huang et al. 2009a). Genes with expression values exceeding 1 read per million in either D492 or D492M or both were selected for inclusion in the model and the gene-protein-rules (GPRs) of RECON2.04 were used to identify all the reactions catalyzed by the corresponding genes. This was done by evaluating the GPR for each reaction with respect to the set of included genes. A cut-off value of one read per million for the expression values was selected on the basis of sensitivity analysis **(Figure S2)**, the noise level in the expression data and the aim to obtain a model of manageable size that could be curated and analyzed fairly easily. If one or both of the cell lines had an expression value exceeding the cut-off value, the corresponding gene was included in the model. The "core" set of reactions thus identified did not correspond to a functional network because of incomplete overlap between the RNA-seq data and RECON2 and some reactions being omitted because of the expression value cut-off. The core set of reactions was used as input to the FASTCORE algorithm (Vlassis et al. 2014) which identified a minimal set of additional reactions from RECON2.04 which was needed to obtain a functional network.

The results of the FASTCORE algorithm depend on the boundary conditions of the model, i.e. definition of exchange rates (uptake or secretion of metabolites) in RECON2. The exchange rates were obtained from the metabolomics data as follows. Out of the 44 extracellular metabolites that were quantified with UPLC-MS, 5 metabolites were left out because they were either not present in RECON2.04 or the measurements were deemed to be too noisy upon visual inspection (**Figure 2** in the main text). For each of the remaining 39 metabolites, exchange rates for each cell line were defined as:

$$v_k = V([M_k]_f - [M_k]_i) / (Aw)$$

where v_k is the exchange rate (flux) of metabolite k, V is the volume of the culture, $[M_k]_0$ and $[M_k]_{48}$ are metabolite concentrations at time points 0 and 48 hours respectively, A is the area under the growth curve and w is the weight of a single

cell (Jain et al. 2012). The cell weights correspond to the dry weight values (see results section of the main text) and the flux units are $\mu M \cdot gDW^{-1} \cdot h^{-1}$. Upper and lower bounds for the exchange reaction corresponding to metabolite *k* was obtained by adding and subtracting 10% to/from the value of v_k. To ensure that the tissue specific model obtained with FASTCORE reflected both cell lines, the upper bound for the exchange flux for metabolite *k* in RECON2 was set to max (v_k^{EPI}, v_k^{MES}) and the lower bound to min(v_k^{EPI}, v_k^{MES}) where v_k^{EPI} and v_k^{MES} refer to exchange fluxes in the epithelial and mesenchymal models respectively. All other exchange reactions were disabled (flux set equal to zero), except for water, carbon dioxide, oxygen, urea, ammonia, and ions which were freely available in the media. When this particular set of exchanges was applied to RECON2, flux balance analysis predicted no growth. This was caused by conflicts in uptake and secretion rates which were partly due to noise in the measurements and also because the targeted metabolomics did not capture all the changes that occurred in the medium over time. To resolve these conflicts, the optimization algorithm described in the next section was used to minimally adjust the exchanges in order to obtain a model able to growth. The adjusted exchange bounds, the core reactions derived from the expression data were used as inputs to FASTCORE after placing a lower bound on the biomass function (50% of the maximum) to ensure that the resulting model would be able to generate all components of the biomass. The model produced by FASTCORE was inspected manually and analyzed using flux balance analysis to check for missing exchanges, missing metabolites, missing pathways and aberrant fluxes (e.g. CO_2 fixation). Upon fixing each issue, FASTCORE was run again and the process repeated until no more issues could be identified. The resulting model will be referred to as the EMT model in the following.

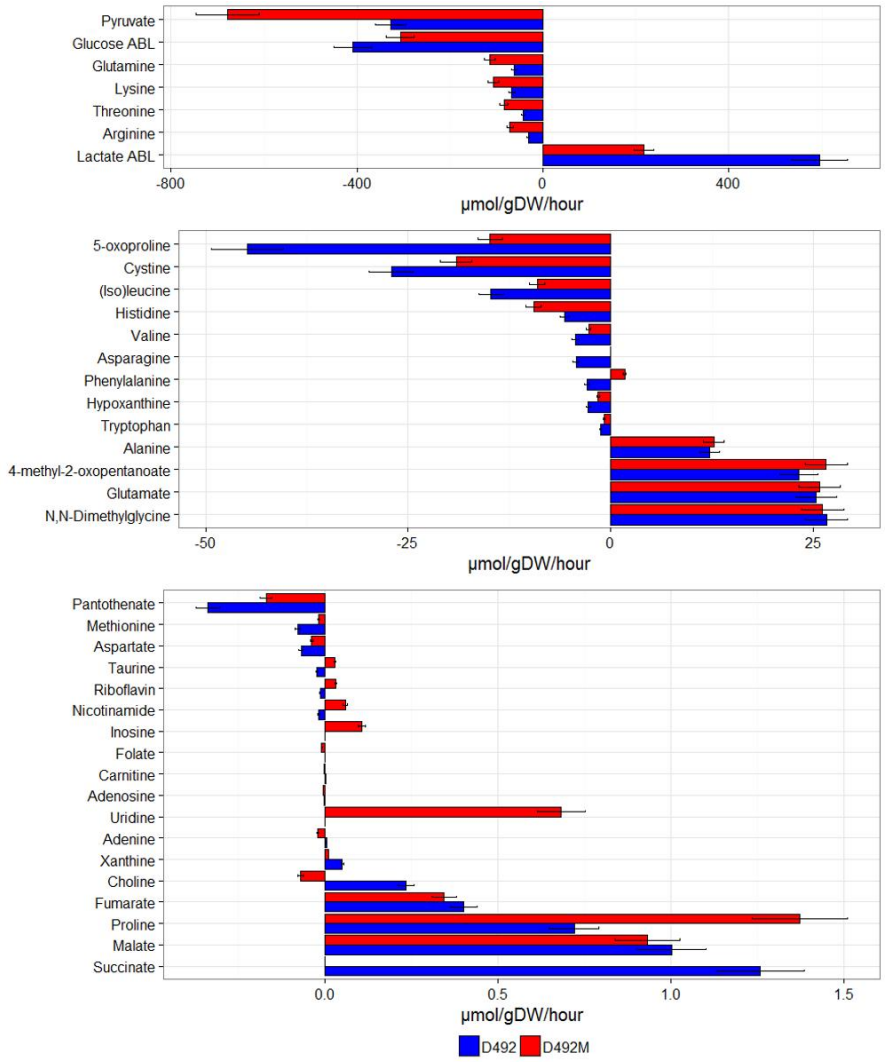

SI Figure 1. Uptake and secretion rates of metabolites in D492 cells (blue) versus D492M cells (red) during culture as used for constraint-based modelling. Mean metabolite uptake and secretion rates presented *as µmol per grams dry-weight per hour* were calculated as described in (Jain et al. 2012), based on the UPLC-MS results, ABL90 measurements, growth rates and dry-weight calculations. Uptake rates are represented as negative values, secretion as positive values.

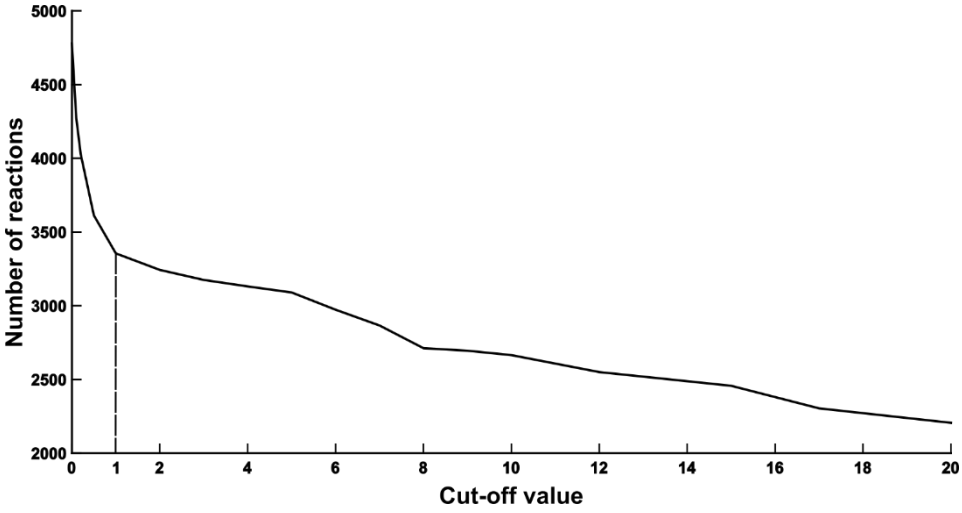

SI Figure 2. The effects of the gene expression cut-off on model size (RNA-seq data). The cut-off value was varied between 0.1 and 20 reads per million and a breast tissue specific model was generated for each value. There is a sharp drop in model size up to 1 read per million but after that, the model size decreases fairly slowly.

Relaxation of exchange bounds to obtain a feasible model

When metabolomics data is used to fix exchange reactions in a metabolic model it may become infeasible, i.e. no set of flux values exist which fulfill the model constraints, for the reasons outlined in the previous section. To address this issue we used an optimization algorithm similar to the algorithm used by Choudhary et al. (Choudhary et al. 2016) to minimally adjust the exchanges in order to obtain a feasible model. The algorithm solves the following optimization problem,

$$\text{minimize } \sum_{j \in R_r} (p_j + n_j) \qquad (1)$$

$$\mathbf{Sv} = \mathbf{0} \qquad (2)$$

$$l_j - n_j \le v_j \le u_j + p_j \qquad j \in R_r \qquad (3)$$

$$l_i \le v_i \le u_i \qquad i \in R_n \qquad (4)$$

$$\sum_{j \in R_r} y_j \le k \qquad (5)$$

$$p_j \le M y_j,\ n_j \le M y_j \qquad j \in R_r \qquad (6)$$

$$p_j \ge 0,\ n_j \ge 0 \qquad j \in R_r \qquad (7)$$

$$y_j \in \{ 0, 1 \} \qquad j \in R_r \qquad (8)$$

The objective is to minimize the total adjustment to exchange fluxes (1) by adjusting the amount of upper (p_j) and lower bound relaxations (n_j) and network fluxes ($\boldsymbol{v}$) while fulfilling the steady state mass balance constraints (2). The set of exchange reactions to be relaxed (3) is denoted by R_r and the set R_n represents all the other reactions. Constraints (4) are the usual upper and lower flux bounds. Corresponding to each exchange relaxation is a binary variable y_j which indicates whether reaction j is relaxed or not and constraint (5) provides the option to control the number of relaxed exchanges. If no such control is needed, k is simply set to some large value, e.g. equal to the number of elements in R_r. Constraints (6) tie the binary variables to the relaxation variables, here the constant M was set to 1000. The algorithm was implemented in Matlab (Mathworks, Natick, MA, USA) using a version of the CVX modeling language (CVX Research 2012) which

supports integer constraints and the Gurobi solver (Gurobi Optimization 2015). When constructing the EMT model, a lower bound was placed on the biomass (0.1/h) to ensure that the model would be able to produce all the biomass components.

Construction and analysis of D429 and D492M GEMs

Microarray expression profiles of the D492 and D492M cells (Sigurdsson et al. 2011) were used to identify up- and downregulated genes in the two cell lines after mapping the microarray expression Illumina gene IDs to the Entrez IDs of RECON2 using the David gene ID conversion tool. The identification was based on the relative difference of the expression values in the two cell lines (Tusher et al. 2001). This measure is frequently used instead of fold change since it takes standard deviation into account. A cutoff value of +/- 5 was established based on sensitivity analysis **(Figure S3)**. Genes with a relative difference of more than 5 were considered to be upregulated in the mesenchymal cells and those with relative difference below -5 were considered upregulated in the epithelial cells. The remaining genes were considered as having the same expression in the two cell lines.

Random sampling was used to estimate flux distributions in the EMT model with the gpSampler function in the COBRA toolbox (Schellenberger et al. 2011) after placing a lower limit on the biomass reaction corresponding to 50% of the maximum biomass. A model of the epithelial D492 phenotype (EPI) was created from the EMT model by restricting fluxes in reactions corresponding to upregulated genes in the mesynchymal cells. These genes were considered to be downregulated in the epithelial cells. The reactions were identified via GPRs as described previously. Instead of simulating a complete knockout of these reactions, the fluxes were restricted to the 30^{th} percentile of the values sampled from the EMT model by adjusting the upper and lower flux bounds. Flux bounds for the remaining (unaffected) reactions were set to the minimum and maximum of the sampled values from the EMT model. The bounds for the exchange reactions were obtained as described previously. Construction of a model of the mesenchymal D492M cells (MES) proceeded in the same way, except fluxes in

reactions corresponding to upregulated genes in the epithelial cells were restricted in this case.

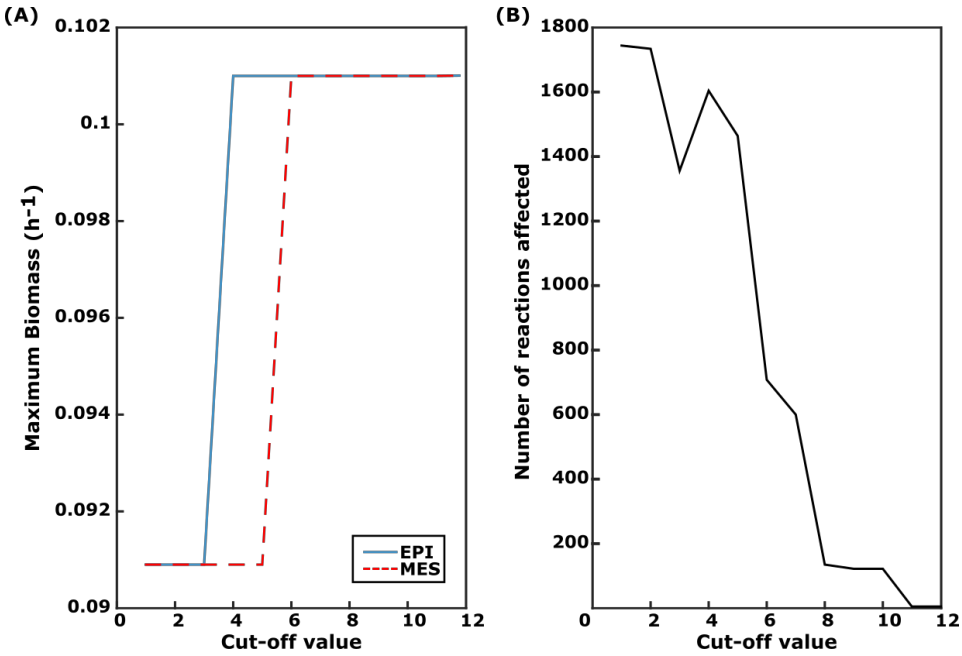

SI Figure 3. The effects of the gene expression cut-off on model properties (microarray data). Epithelial and mesenchymal models were constructed for several different cut-off values. The left panel shows the effects of the cut-off value on the maximum growth rate in the EPI and MES models. The right panel shows the number of reactions having different minimum and/or maximum flux values, as determined by flux variability analysis (Mahadevan and Schilling 2003).

Analysis of the EPI and MES models

Random sampling was used to estimate flux distributions for the EPI and MES models using the gpSampler function after placing a lower bound on the biomass, corresponding to 50% of the maximum. The mean flux of all the reactions in each model was computed and the relative difference (v^{MES} - v^{EPI}) / $|v^{EPI}|$ used to compare the two models. Gene essentiality analysis was performed by searching for single gene knockouts which result in zero growth rate. This was done using the singleGeneKnockout function in COBRA. Identification of targets that revert

the mesenchymal phenotype to the epithelial phenotype was done by solving an optimization problem identical to the one above, except for a different objective function,

$$\text{minimize } \alpha|| \boldsymbol{v} - \boldsymbol{v}_E ||_1 + (1 - \alpha)\sum j \in R_r (p_j + n_j) \qquad (1a)$$

where $\boldsymbol{v}$, p_j and n_j are decision variables as before, $\boldsymbol{v}_E$ are fixed values representing the mean flux distribution of the EPI model, obtained from random sampling, $|| \cdot ||_1$ represents the Manhattan norm (1-norm) of a vector and α is a user-specified parameter that controls the tradeoff between minimizing the distance between the two flux distributions and the amount of relaxation. A value of $\alpha = 1$ was used since the goal was to completely revert the mesenchymal phenotype (**Figure S4**). The upper and lower bounds for each flux in (3) and (4) correspond to the values from the MES model. The algorithm returns a set of reactions in MES whose bounds can be relaxed in order to obtain a flux distribution that resembles that of EPI. The targets for the epithelial to mesenchymal transition were determined analogously, with $\mathbf{v}_M$ used instead of $\boldsymbol{v}_E$ and the flux bounds corresponding to the EPI model.

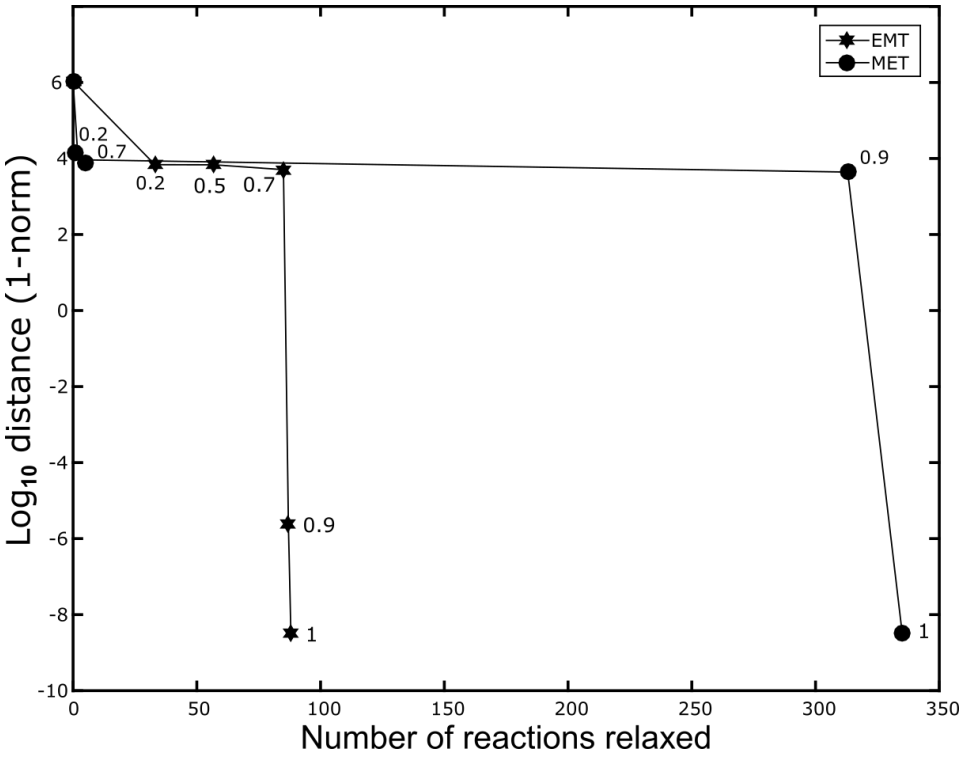

SI Figure 4. The effects of the trade-off parameter (α) on the distance between two models and the number of reactions that need to be relaxed. For α close to zero, the number of relaxed reactions is low while the distance between the models is large. With increasing values of α, the model behavior becomes more similar at the cost of an increasing number of relaxed reactions.

Results

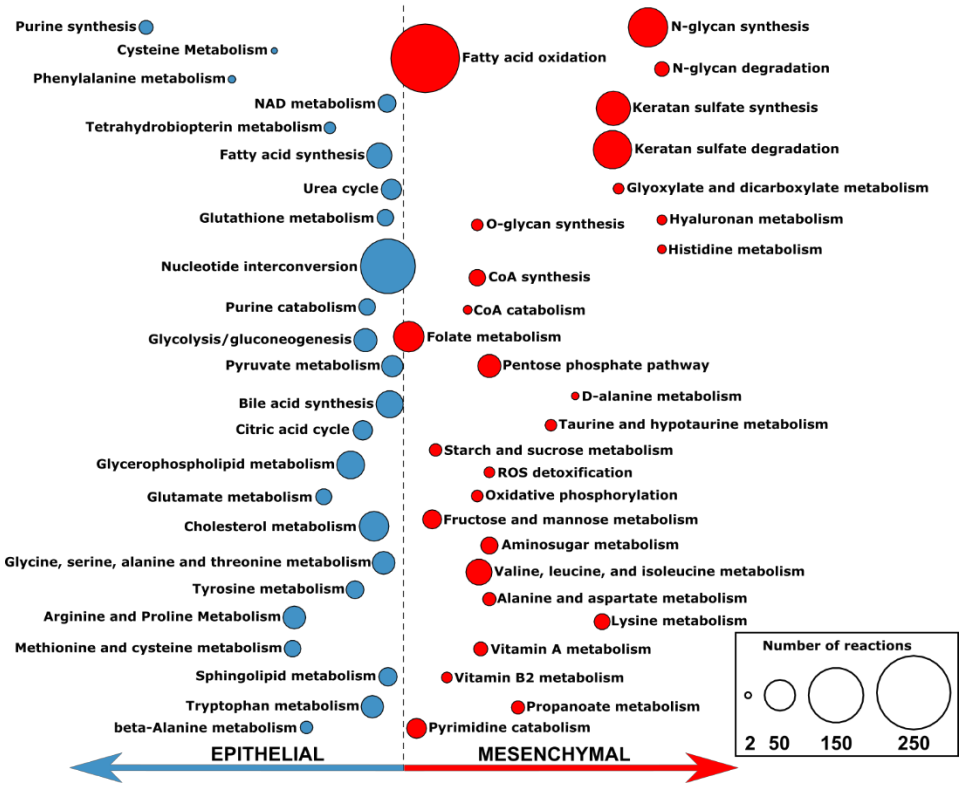

SI Figure 5: Differences in pathway utilization of the two phenotypes. The plot shows the differences in the flux distribution of the two models. The distance of the circles to the left or right from the dotted vertical line represents the proportion of the pathway upregulated in EPI or MES models. The proportion was calculated by subtracting the number of reactions upregulated in EPI from the number of reactions upregulated in MES and dividing by the total number of reactions in the pathway. For example, purine synthesis in the upper left corner indicates that all the reactions in this pathway are upregulated in EPI model. The size of the circles represents the total number of reactions in the pathway.

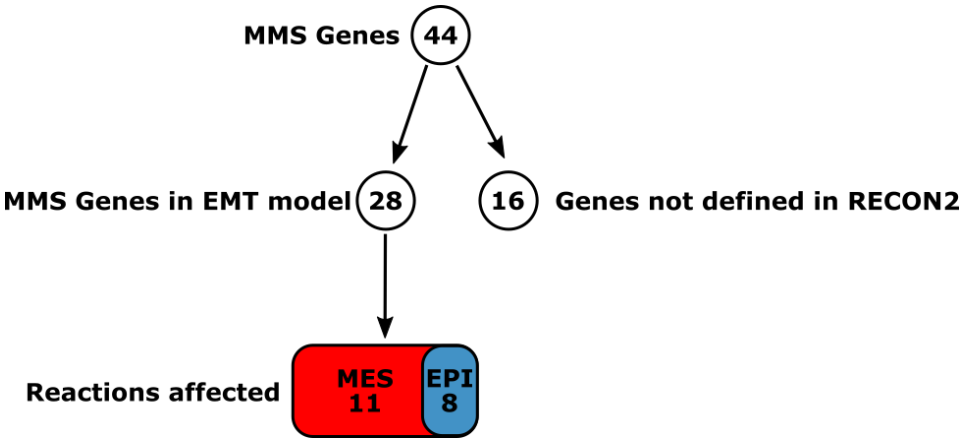

SI Figure 6. Comparison of the model predictions of this study with Mesenchymal Metabolic Signature (MMS) genes as predicted by Shaul *et al*. 28 out of 44 MMS genes predicted by the Shaul et al are present in the EMT model. These genes affect 19 reactions in the model out of which 11 are upregulated in MES model.

Subsystem	Number of reactions	Number of genes
Alanine and aspartate metabolism	1	1
Aminosugar metabolism	1	1
Cholesterol metabolism	2	1
Fatty acid oxidation	10	4
Heme synthesis	1	1
Hyaluronan metabolism	1	1
Keratan sulfate degradation	16	3
N-glycan degradation	3	2
Nucleotide interconversion	1	1
Oxidative phosphorylation	1	10
Propanoate metabolism	1	4
ROS detoxification	1	1
Sphingolipid metabolism	2	2
Starch and sucrose metabolism	1	1
Valine, leucine, and isoleucine metabolism	5	5
Transport, extracellular	3	3
Tryptophan metabolism	1	1
Exchange/demand reaction	31	0

SI Table 1. Number of reactions that have to be relaxed to convert the epithelial phenotype to the mesenchymal phenotype, as predicted by the models.

Subsystems	Number of reactions	Number of genes
Alanine and aspartate metabolism	1	1
Arginine and Proline Metabolism	2	2
Cholesterol metabolism	2	1
Fructose and mannose metabolism	1	1
Glutathione metabolism	1	1
Glycerophospholipid metabolism	2	2
Glycine, serine, alanine and threonine metabolism	3	4
Nucleotide interconversion	3	2
Pentose phosphate pathway	1	1
Pyruvate metabolism	1	1
Urea cycle	1	1
Transport, mitochondrial	1	1
Transport, extracellular	288	5
Exchange/demand reaction	28	0

SI Table 2. The number of reactions that have to be relaxed to revert the mesenchymal phenotype to the epithelial phenotype, as predicted by the models.

References:

Choudhary KS, Rohatgi N, Halldorsson S, Briem E, Gudjonsson T, Gudmundsson S, Rolfsson O. 2016. EGFR Signal-Network Reconstruction Demonstrates Metabolic Crosstalk in EMT. *PLoS Comput Biol* **12**: e1004924.

CVX Research I. 2012. CVX: Matlab Software for Disciplined Convex Programming, version 2.0. *http://cvxrcom/cvx*.

Gurobi Optimization I. 2015. Gurobi Optimizer Reference Manual. *http://wwwgurobicom*.

Huang DW, Sherman BT, Lempicki RA. 2009a. Bioinformatics enrichment tools: paths toward the comprehensive functional analysis of large gene lists. *Nucleic Acids Res* **37**: 1-13.

Huang DW, Sherman BT, Lempicki RA. 2009b. Systematic and integrative analysis of large gene lists using DAVID bioinformatics resources. *Nature Protocols* **4**: 44-57.

Jain M, Nilsson R, Sharma S, Madhusudhan N, Kitami T, Souza AL, Kafri R, Kirschner MW, Clish CB, Mootha VK. 2012. Metabolite profiling identifies a key role for glycine in rapid cancer cell proliferation. *Science* **336**: 1040-1044.

Mahadevan R, Schilling CH. 2003. The effects of alternate optimal solutions in constraint-based genome-scale metabolic models. *Metab Eng* **5**: 264-276.

Paglia G, Sigurjonsson OE, Rolfsson O, Valgeirsdottir S, Hansen MB, Brynjolfsson S, Gudmundsson S, Palsson BO. 2014. Comprehensive metabolomic study of platelets reveals the expression of discrete metabolic phenotypes during storage. *Transfusion*.

Schellenberger J, Que R, Fleming RMT, Thiele I, Orth JD, Feist AM, Zielinski DC, Bordbar A, Lewis NE, Rahmanian S et al. 2011. Quantitative prediction of cellular metabolism with constraint-based models: the COBRA Toolbox v2.0. *Nature protocols* **6**: 1290-1307.

Sigurdsson V, Hilmarsdottir B, Sigmundsdottir H, Fridriksdottir AJR, Ringnér M, Villadsen R, Borg A, Agnarsson Ba, Petersen OW, Magnusson MK et al. 2011. Endothelial induced EMT in breast epithelial cells with stem cell properties. *PloS one* **6**: e23833.

Tusher VG, Tibshirani R, Chu G. 2001. Significance analysis of microarrays applied to the ionizing radiation response. *Proceedings of the National Academy of Sciences of the United States of America* **98**: 5116-5121.

Vlassis N, Pacheco MP, Sauter T. 2014. Fast Reconstruction of Compact Context-Specific Metabolic Network Models. *Plos Computational Biology* **10**.

SI Table 3. Detailed description of the reactions required to convert epithelial phenotype to mesenchymal predicted by the models

Reaction Abbreviation	Reaction Names	Model Subsystem	Reaction formula	Gene ID	Transcription Factors
ARGSS	argininosuccinate synthase	Alanine and aspartate metabolism	atp[c] + asp_L[c] + citr_L[c] -> h[c] + amp[c] + ppi[c] + argsuc[c]	ASS1	Sp1, NF-E2, NF-E2p45, N-Myc, c-Myc, Max, RP58, c-Fos, c-Jun, AP-1
ACGAMK	N-acetylglucosamine kinase	Aminosugar metabolism	atp[c] + acgam[c] -> adp[c] + h[c] + acgam6p[c]	nagK	Brachyury, LUN-1, HNF-1, HNF-1A, PPAR-gamma1, PPAR-gamma2, MRF-2, STAT5A, Elk-1, NF-kappaB
C14STRr	C-14 sterol reductase	Cholesterol metabolism	h[r] + 44mctr[r] + nadph[r] -> 44mzym[r] + nadp[r]	tm7sf2	AP-1, c-Myc, Max, Max1, c-Fos, c-Jun, Nkx5-1, GR-alpha, GR, Roaz
r0780	4,4-dimethyl-5a-cholesta-8,24-dien-3b-ol:NADP+ D14-oxidoreductase Biosynthesis of steroids EC:1.3.1.70	Cholesterol metabolism	44mzym[r] + nadp[r] <=> h[r] + 44mctr[r] + nadph[r]	tm7sf2	AP-1, c-Myc, Max, Max1, c-Fos, c-Jun, Nkx5-1, GR-alpha, GR, Roaz
FACOAL1812	fatty-acid--CoA ligase	Fatty acid oxidation	amp[c] + ppi[c] + vacccoa[c] <=> atp[c] + coa[c] + vacc[c]	ACSL1	PPAR-alpha, AP-2alpha, AP-2alphaisoform2, AP-2alphaisoform3, AP-2alphaisoform4, AP-2alphaA, PPAR-gamma1, PPAR-gamma2
FACOAL200	fatty-acid--CoA ligase	Fatty acid oxidation	atp[c] + coa[c] + arach[c] -> amp[c] + ppi[c] + arachcoa[c]	ACSL1	PPAR-alpha, AP-2alpha, AP-2alphaisoform2, AP-2alphaisoform3, AP-2alphaisoform4, AP-2alphaA, PPAR-gamma1, PPAR-gamma2
FAOXC141C121m	fatty acid beta oxidation(C14:1->C12:1)m	Fatty acid oxidation	h2o[m] + coa[m] + nad[m] + fad[m] + tetd7ecoa[m] -> h[m] + nadh[m] + accoa[m] + fadh2[m] + dd5ecoa[m]	hadhb	p53
				HADHA	HNF-4alpha1, HNF-4alpha2
				ACADVL	PPAR-alpha, AP-2alpha, AP-2alphaisoform2, AP-2alphaisoform3, AP-2alphaisoform4, AP-2alphaA
FAOXC14C12m	fatty acid beta oxidation(C14-->C12)m	Fatty acid oxidation	h2o[m] + coa[m] + nad[m] + fad[m] + tdcoa[m] -> h[m] + nadh[m] + accoa[m] + fadh2[m] + ddcacoa[m]	hadhb	p53
				HADHA	HNF-4alpha1, HNF-4alpha2
				ACADVL	PPAR-alpha, AP-2alpha, AP-2alphaisoform2, AP-2alphaisoform3, AP-2alphaisoform4, AP-2alphaA
FAOXC161C141m	fatty acid beta oxidation(C16:1->C14:1)m	Fatty acid oxidation	h2o[m] + coa[m] + nad[m] + fad[m] + hdcoa[m] -> h[m] + nadh[m] + accoa[m] + fadh2[m] + tetd7ecoa[m]	hadhb	p53
				HADHA	HNF-4alpha1, HNF-4alpha2
				ACADVL	PPAR-alpha, AP-2alpha, AP-2alphaisoform2, AP-2alphaisoform3, AP-2alphaisoform4, AP-2alphaA
FAOXC16C14m	fatty acid beta oxidation(C16-->C14)m	Fatty acid oxidation	h2o[m] + coa[m] + nad[m] + fad[m] + pmtcoa[m] -> h[m] + nadh[m] + accoa[m] + fadh2[m] + tdcoa[m]	hadhb	p53
				HADHA	HNF-4alpha1, HNF-4alpha2
				ACADVL	PPAR-alpha, AP-2alpha, AP-2alphaisoform2, AP-2alphaisoform3, AP-2alphaisoform4, AP-2alphaA
FAOXC181C161m	fatty acid beta oxidation(C18:1->C16:1)m	Fatty acid oxidation	h2o[m] + coa[m] + nad[m] + fad[m] + octd11ecoa[m] -> h[m] + nadh[m] + accoa[m] + fadh2[m] + hdcoa[m]	hadhb	p53
				HADHA	HNF-4alpha1, HNF-4alpha2
				ACADVL	PPAR-alpha, AP-2alpha, AP-2alphaisoform2, AP-2alphaisoform3, AP-2alphaisoform4, AP-2alphaA
FAOXTC142TC122m	fatty acid beta oxidation trans(C14:2-->C12:2)m	Fatty acid oxidation	h2o[m] + coa[m] + nad[m] + fad[m] + ttetddcoa[m] -> h[m] + nadh[m] + accoa[m] + fadh2[m] + tddedicoa[m]	hadhb	p53
				HADHA	HNF-4alpha1, HNF-4alpha2
				ACADVL	PPAR-alpha, AP-2alpha, AP-2alphaisoform2, AP-2alphaisoform3, AP-2alphaisoform4, AP-2alphaA
FAOXTC162TC142m	fatty acid beta oxidation trans(C16:2-->C14:2)m	Fatty acid oxidation	h2o[m] + coa[m] + nad[m] + fad[m] + thexddcoa[m] -> h[m] + nadh[m] + accoa[m] + fadh2[m] + ttetddcoa[m]	hadhb	p53
				HADHA	HNF-4alpha1, HNF-4alpha2
				ACADVL	PPAR-alpha, AP-2alpha, AP-2alphaisoform2, AP-2alphaisoform3, AP-2alphaisoform4, AP-2alphaA
FAOXTC182TC162m	fatty acid beta oxidation trans(C18:2-->C16:2)m	Fatty acid oxidation	h2o[m] + coa[m] + nad[m] + fad[m] + lneldccoa[m] -> h[m] + nadh[m] + accoa[m] + fadh2[m] + thexddcoa[m]	hadhb	p53
				HADHA	HNF-4alpha1, HNF-4alpha2
				ACADVL	PPAR-alpha, AP-2alpha, AP-2alphaisoform2, AP-2alphaisoform3, AP-2alphaisoform4, AP-2alphaA

FE3R2e	Fe(III) reduction (ascorbate)	Heme synthesis	ascb_L[e] + 2 fe3[e] -> h[e] + dhdascb[e] + 2 fe2[e]	cybrd1	SRF, SRF(54AA), Egr-4, HSF1(long), HSF1short, En-1, p53, Egr-2, Elk-1, RORalpha1
GLCAASE9ly	beta-glucuronidase, lysosomal	Hyaluronan metabolism	2 h2o[l] + ha_pre1[l] -> acgam[l] + glcur[l]	GUSB	Sp1, TBP, TFIID
FUCASE2ly	alpha-fucosidase, lysosomal	Keratan sulfate degradation	h2o[l] + ksi[l] -> fuc_L[l] + ksi_deg1[l]	fucA1	Evi-1, GCNF, GCNF-1, GCNF-2, Gfi-1, ER-alpha, TBP, TFIID, CUTL1, NF-1
GASNASE3ly	glycosylasparaginase, lysosomal	Keratan sulfate degradation	h2o[l] + ksi_deg1[l] -> Asn_X_Ser_Thr[l] + ksi_deg2[l]	aga	GR, GR-alpha, GR-beta, c-Fos
S6TASE11ly	N-acetylglucosamine-6-sulfatase, lysosomal	Keratan sulfate degradation	h2o[l] + ksi_deg6[l] <=> h[l] + so4[l] + ksi_deg7[l]	GNS	Pax-2, Pax-2a, Sp1, Zic1, Pax-4a, Sox5, FOXD1
S6TASE12ly	N-acetylglucosamine-6-sulfatase, lysosomal	Keratan sulfate degradation	h2o[l] + ksi_deg9[l] <=> h[l] + so4[l] + ksi_deg10[l]	GNS	Pax-2, Pax-2a, Sp1, Zic1, Pax-4a, Sox5, FOXD1
S6TASE13ly	N-acetylglucosamine-6-sulfatase, lysosomal	Keratan sulfate degradation	h2o[l] + ksi_deg12[l] <=> h[l] + so4[l] + ksi_deg13[l]	GNS	Pax-2, Pax-2a, Sp1, Zic1, Pax-4a, Sox5, FOXD1
S6TASE14ly	N-acetylglucosamine-6-sulfatase, lysosomal	Keratan sulfate degradation	h2o[l] + ksi_deg15[l] <=> h[l] + so4[l] + ksi_deg16[l]	GNS	Pax-2, Pax-2a, Sp1, Zic1, Pax-4a, Sox5, FOXD1
S6TASE15ly	N-acetylglucosamine-6-sulfatase, lysosomal	Keratan sulfate degradation	h2o[l] + ksi_deg18[l] <=> h[l] + so4[l] + ksi_deg19[l]	GNS	Pax-2, Pax-2a, Sp1, Zic1, Pax-4a, Sox5, FOXD1
S6TASE16ly	N-acetylglucosamine-6-sulfatase, lysosomal	Keratan sulfate degradation	h2o[l] + ksi_deg21[l] <=> h[l] + so4[l] + ksi_deg22[l]	GNS	Pax-2, Pax-2a, Sp1, Zic1, Pax-4a, Sox5, FOXD1
S6TASE17ly	N-acetylglucosamine-6-sulfatase, lysosomal	Keratan sulfate degradation	h2o[l] + ksi_deg24[l] <=> h[l] + so4[l] + ksi_deg25[l]	GNS	Pax-2, Pax-2a, Sp1, Zic1, Pax-4a, Sox5, FOXD1
S6TASE18ly	N-acetylglucosamine-6-sulfatase, lysosomal	Keratan sulfate degradation	h2o[l] + ksi_deg27[l] <=> h[l] + so4[l] + ksi_deg28[l]	GNS	Pax-2, Pax-2a, Sp1, Zic1, Pax-4a, Sox5, FOXD1
S6TASE19ly	N-acetylglucosamine-6-sulfatase, lysosomal	Keratan sulfate degradation	h2o[l] + ksi_deg30[l] <=> h[l] + so4[l] + ksi_deg31[l]	GNS	Pax-2, Pax-2a, Sp1, Zic1, Pax-4a, Sox5, FOXD1
S6TASE20ly	N-acetylglucosamine-6-sulfatase, lysosomal	Keratan sulfate degradation	h2o[l] + ksi_deg33[l] <=> h[l] + so4[l] + ksi_deg34[l]	GNS	Pax-2, Pax-2a, Sp1, Zic1, Pax-4a, Sox5, FOXD1
S6TASE21ly	N-acetylglucosamine-6-sulfatase, lysosomal	Keratan sulfate degradation	h2o[l] + ksi_deg36[l] <=> h[l] + so4[l] + ksi_deg37[l]	GNS	Pax-2, Pax-2a, Sp1, Zic1, Pax-4a, Sox5, FOXD1
S6TASE23ly	N-acetylglucosamine-6-sulfatase, lysosomal	Keratan sulfate degradation	h2o[l] + ksii_core2_deg3[l] <=> h[l] + so4[l] + ksii_core2_deg4[l]	GNS	Pax-2, Pax-2a, Sp1, Zic1, Pax-4a, Sox5, FOXD1
S6TASE24ly	N-acetylglucosamine-6-sulfatase, lysosomal	Keratan sulfate degradation	h2o[l] + ksii_core2_deg6[l] <=> h[l] + so4[l] + ksii_core2_deg7[l]	GNS	Pax-2, Pax-2a, Sp1, Zic1, Pax-4a, Sox5, FOXD1
S6TASE26ly	N-acetylglucosamine-6-sulfatase, lysosomal	Keratan sulfate degradation	h2o[l] + ksii_core4_deg3[l] <=> h[l] + so4[l] + ksii_core4_deg4[l]	GNS	Pax-2, Pax-2a, Sp1, Zic1, Pax-4a, Sox5, FOXD1
FUCASEly	alpha-fucosidase, lysosomal	N-glycan degradation	h2o[l] + s2l2fn2m2masn[l] -> fuc_L[l] + s2l2n2m2masn[l]	fucA1	Evi-1, GCNF, GCNF-1, GCNF-2, Gfi-1, ER-alpha, TBP, TFIID, CUTL1, NF-1
GASNASE2ly	glycosylasparaginase, lysosomal	N-glycan degradation	h2o[l] + n2m2nmasn[l] -> Asn_X_Ser_Thr[l] + n2m2nm[l]	aga	GR, GR-alpha, GR-beta, c-Fos
GASNASEly	glycosylasparaginase, lysosomal	N-glycan degradation	h2o[l] + s2l2n2m2masn[l] -> Asn_X_Ser_Thr[l] + s2l2n2m2m[l]	aga	GR, GR-alpha, GR-beta, c-Fos
TRDR	thioredoxin reductase (NADPH)	Nucleotide interconversion	h[c] + nadph[c] + trdox[c] -> nadp[c] + trdrd[c]	TXNRD1	NF-kappaB, NF-kappaB1, Bach1, p53, PPAR-gamma1, PPAR-gamma2

CYOR_u10m	ubiquinol-6 cytochrome c reductase, Complex III	Oxidative phosphorylation	2 h[m] + 2 ficytC[m] + q10h2[m] -> 4 h[c] + q10[m] + 2 focytC[m]	cyc1	TBP, TFIID, CUTL1, Pax-3, AP-4, CHOP-1, STAT5A, AhR, Arnt, C/EBPalpha
				CYTB	
				UQCRB	Lmo2, PPAR-gamma1, PPAR-gamma2, HNF-3beta, Evi-1, ER-alpha, POU2F1, POU2F1a, SRF, SRF(54AA)
				Uqcrc1	AP-1, RP58, NRSFform1, NRSFform2, MyoD, c-Myc, Max1, HTF, XBP-1, Ik-1
				Uqcrc2	POU2F1, POU2F1a, HNF-1, HNF-1A, Bach1, Cart-1, c-Myb, Pax-5, AREB6, FOXC1
				UQCRFSL1	
				UQCRHL	COUP, COUP-TF, COUP-TF1, HNF-4alpha1, HNF-4alpha2, PPAR-gamma1, PPAR-gamma2, S8, E47, Hand1
				Uqcr11 (also k/a uqcr)	STAT1, STAT1alpha, STAT1beta, Pax-6, NRSFform1, NRSFform2, Nkx5-1, HOXA5, PPAR-gamma1, PPAR-gamma2
				UQCRQ	Evi-1, GATA-1, ISGF-3, STAT1, STAT1alpha, STAT1beta, TBP, TFIID, HNF-1, HNF-1A
				Uqcr10 (also K/a UCRC)	POU3F2, PPAR-gamma1, PPAR-gamma2, TGIF, HNF-4alpha2, COUP, COUP-TF, COUP-TF1, HNF-4alpha1, HOXA9
r1154	EC:1.2.7.2	Propanoate metabolism	co2[m] + nadh[m] + ppcoa[m] <=> coa[m] + nad[m] + 2obut[m]	dld	Max, Max1, NF-kappaB1, AP-1, c-Jun, c-Fos
				DBT	AhR
				BCKDHB	Cart-1, AREB6, POU3F1, E47, MyoD, CBF(2), NF-Y, CUTL1, HOXA3, USF-1
				BCKDHA	AP-1, c-Jun
SPODMm	superoxide dismutase	ROS detoxification	2 h[m] + 2 o2s[m] -> o2[m] + h2o2[m]	Sod2	NF-kappaB, NF-kappaB1, FOXO1, FOXO1a, Sp1, AP-2alphaA, AP-2alphaisoform4, AP-2alphaisoform3, AP-2alphaisoform2, AP-2alpha
GBA	Glucosylceramidase	Sphingolipid metabolism	h2o[c] + gluside_hs[c] -> glc_D[c] + crm_hs[c]	GBA	NF-kappaB, NF-kappaB1, GR, GR-alpha, GR-beta
UGCG	Ceramide glucosyltransferase	Sphingolipid metabolism	crm_hs[r] + udpg[r] -> h[r] + gluside_hs[r] + udp[r]	UGCG	NF-kappaB, NF-kappaB1
UDPGD	UDPglucose 6-dehydrogenase	Starch and sucrose metabolism	h2o[c] + 2 nad[c] + udpg[c] -> 3 h[c] + 2 nadh[c] + udpglcur[c]	UGDH	Sp1
LEUTA	leucine transaminase	Valine, leucine, and isoleucine metabolism	akg[c] + leu_L[c] <=> glu_L[c] + 4mop[c]	BCAT1	FOXO1, FOXO1a
OIVD2m	2-oxoisovalerate dehydrogenase (acylating; 3-methyl-2-oxobutanoate), mitochondrial	Valine, leucine, and isoleucine metabolism	coa[m] + nad[m] + 3mob[m] -> co2[m] + nadh[m] + ibcoa[m]	dld	Max, Max1, NF-kappaB1, AP-1, c-Jun, c-Fos
				DBT	AhR
				BCKDHA	AP-1, c-Jun
				BCKDHB	Cart-1, AREB6, POU3F1, E47, MyoD, CBF(2), NF-Y, CUTL1, HOXA3, USF-1
OIVD3m	2-oxoisovalerate dehydrogenase (acylating; 3-methyl-2-oxopentanoate), mitochondrial	Valine, leucine, and isoleucine metabolism	coa[m] + nad[m] + 3mop[m] -> co2[m] + nadh[m] + 2mbcoa[m]	dld	Max, Max1, NF-kappaB1, AP-1, c-Jun, c-Fos
				DBT	AhR
				BCKDHB	Cart-1, AREB6, POU3F1, E47, MyoD, CBF(2), NF-Y, CUTL1, HOXA3, USF-1
				BCKDHA	AP-1, c-Jun
VALTA	valine transaminase	Valine, leucine, and isoleucine metabolism	akg[c] + val_L[c] <=> glu_L[c] + 3mob[c]	BCAT1	FOXO1, FOXO1a
RE3326M	RE3326	Valine, leucine, and isoleucine metabolism	ibcoa[m] + dhlam[m] <=> coa[m] + 2mpdhl[m]	BCKDHB	Cart-1, AREB6, POU3F1, E47, MyoD, CBF(2), NF-Y, CUTL1, HOXA3, USF-1

r1557	Amino Acid-Polyamine-Organocation (APC) TCDB:2.A.3.8.1	Transport, extracellular	gly[e] + ile_L[c] <=> gly[c] + ile_L[e]	SLC7A5	Pax-3, NF-E2, NF-E2p45, aMEF-2, MEF-2A, FosB, Fra-1, JunB, JunD, AP-1
r1672	Y+LAT2 Utilized transport	Transport, extracellular	na1[e] + ala_L[c] + gly[e] -> na1[c] + ala_L[e] + gly[c]	SLC7A6	CREB, deltaCREB, CUTL1, POU2F1, POU2F1a, Ik-1, SREBP-1c, SREBP-1a, SREBP-1b, HTF
VALLAT1tc	transport of L-Valine by LAT1 in association with 4F2hc, across the apical surface of the memebranes.	Transport, extracellular	val_L[e] + leu_L[c] -> leu_L[e] + val_L[c]	SLC3A2	Egr-1, AP-1, c-Jun
				SLC7A5	Pax-3, NF-E2, NF-E2p45, aMEF-2, MEF-2A, FosB, Fra-1, JunB, JunD, AP-1
5HOXINDACTO2OX	5-Hydroxyindoleacetaldehyde:oxygen oxidoreductase	Tryptophan metabolism	h2o[c] + o2[c] + 5hoxindact[c] -> h2o2[c] + h[c] + 5hoxindoa[c]	AOX1	NRSFform1, NRSFform2, AhR, NF-kappaB, NF-kappB1, Brachyury, GR, GR-alpha, GR-beta
r0386	4-methyl-2-oxopentanoate:[dihydrolipoyllysine-residue (2-methylpropanoyl)transferase] lipoyllysine 2-oxidoreductase (decarboxylating, acceptor-2-methylpropanoylating) EC:1.2.4.4	Unassigned	h[m] + 4mop[m] + lpam[m] -> co2[m] + HC01377[m]	BCKDHA	AP-1, c-Jun
				BCKDHB	Cart-1, AREB6, POU3F1, E47, MyoD, CBF(2), NF-Y, CUTL1, HOXA3, USF-1
				Tmem91	SRF, SRF(54AA), Egr-1, PPAR-gamma1, PPAR-gamma2, AP-1, c-Fos, c-Jun, AhR, HEN1
r0644	(S)-Methylmalonate semialdehyde:oxygen oxidoreductase Valine, leucine and isoleucine degradation EC:1.2.3.1	Unassigned	h2o2[c] + h[c] + HC00900[c] <=> h2o[c] + o2[c] + 2mop[c]	AOX1	NRSFform1, NRSFform2, AhR, NF-kappaB, NF-kappB1, Brachyury, GR, GR-alpha, GR-beta
r0670	(S)-3-Methyl-2-oxopentanoate:[dihydrolipoyllysine-residue (2-methylpropanoyl)transferase] lipoyllysine 2-oxidoreductase (decarboxylating, acceptor-2-methylpropanoylating) EC:1.2.4.4	Unassigned	h[m] + 3mop[m] + lpam[m] -> co2[m] + HC01376[m]	BCKDHB	Cart-1, AREB6, POU3F1, E47, MyoD, CBF(2), NF-Y, CUTL1, HOXA3, USF-1
				BCKDHA	AP-1, c-Jun
				Tmem91	SRF, SRF(54AA), Egr-1, PPAR-gamma1, PPAR-gamma2, AP-1, c-Fos, c-Jun, AhR, HEN1
r1433	NADPH:oxidized-thioredoxin oxidoreductase Pyrimidine metabolism EC:1.8.1.9	Unassigned	nadp[m] + trdrd[m] -> h[m] + nadph[m] + trdox[m]	TXNRD1	NF-kappaB, NF-kappaB1, Bach1, p53, PPAR-gamma1, PPAR-gamma2
				TXNRD2	PPAR-gamma1, PPAR-gamma2, PPAR-alpha, HNF-4alpha1, HNF-4alpha2, NF-1, NF-1/L
TRDR2	Thioredoxin (ubiquinone 10) reductase (NADPH)	Miscellaneous	h[c] + nadph[c] + q10[c] -> nadp[c] + q10h2[c]	TXNRD1	NF-kappaB, NF-kappaB1, Bach1, p53, PPAR-gamma1, PPAR-gamma2
TRDR3	Thioredoxin (ubiquinone 10) reductase (NADH)	Miscellaneous	h[c] + nadh[c] + q10[c] -> nad[c] + q10h2[c]	TXNRD1	NF-kappaB, NF-kappaB1, Bach1, p53, PPAR-gamma1, PPAR-gamma2
EX_ade(e)	Adenine exchange	Exchange/demand reaction	ade[e] <=>		
EX_adn(e)	exchange reaction for Adenosine	Exchange/demand reaction	<=> adn[e]		
EX_arg_L(e)	L-Arginine exchange	Exchange/demand reaction	<=> arg_L[e]		
EX_asn_L(e)	exchange reaction for L-asparagine	Exchange/demand reaction	<=> asn_L[e]		
EX_asp_L(e)	L-Aspartate exchange	Exchange/demand reaction	<=> asp_L[e]		
EX_chol(e)	exchange reaction for Choline	Exchange/demand reaction	chol[e] <=>		
EX_glc(e)	D-Glucose exchange	Exchange/demand reaction	<=> glc_D[e]		
EX_gln_L(e)	exchange reaction for L-glutamine	Exchange/demand reaction	<=> gln_L[e]		
EX_his_L(e)	exchange reaction for L-histidine	Exchange/demand reaction	<=> his_L[e]		
EX_ile_L(e)	L-Isoleucine exchange	Exchange/demand reaction	<=> ile_L[e]		

EX_ins(e)	Inosine exchange	Exchange/demand reaction	ins[e] <=>		
EX_lac_L(e)	L-Lactate exchange	Exchange/demand reaction	lac_L[e] <=>		
EX_lys_L(e)	L-Lysine exchange	Exchange/demand reaction	<=> lys_L[e]		
EX_met_L(e)	L-Methionine exchange	Exchange/demand reaction	<=> met_L[e]		
EX_phe_L(e)	exchange reaction for L-phenylalanine	Exchange/demand reaction	<=> phe_L[e]		
EX_pro_L(e)	L-Proline exchange	Exchange/demand reaction	pro_L[e] <=>		
EX_succ(e)	Succinate exchange	Exchange/demand reaction	succ[e] <=>		
EX_taur(e)	Taurine exchange	Exchange/demand reaction	taur[e] <=>		
EX_thr_L(e)	L-Threonine exchange	Exchange/demand reaction	<=> thr_L[e]		
EX_trp_L(e)	L-Tryptophan exchange	Exchange/demand reaction	<=> trp_L[e]		
EX_5oxpro(e)	Exchange of 5-oxoprolinate	Exchange/demand reaction	<=> 5oxpro[e]		
EX_mal_L(e)	Exchange of L-malate	Exchange/demand reaction	mal_L[e] <=>		
EX_fum(e)	EX_fum(e)	Exchange/demand reaction	fum[e] <=>		
EX_dmgly(e)	EX_dmgly(e)	Exchange/demand reaction	dmgly[e] <=>		
EX_ca2(e)	EX_ca2(e)	Exchange/demand reaction	ca2[e] <=>		
EX_fol(e)	EX_fol(e)	Exchange/demand reaction	<=> fol[e]		
EX_5mthf(e)	EX_5mthf(e)	Exchange/demand reaction	5mthf[e] <=>		
EX_ncam(e)	EX_ncam(e)	Exchange/demand reaction	<=> ncam[e]		
sink_ncam[c]	sink_ncam[c]	Exchange/demand reaction	ncam[c] <=>		
EX_pnto_R(e)	EX_pnto_R(e)	Exchange/demand reaction	<=> pnto_R[e]		
EX_uri(e)	EX_uri(e)	Exchange/demand reaction	uri[e] <=>		

SI Table 4. Detailed description of the reactions required to convert mesenchymal phenotype to epithelial predicted by the models					
Reaction Abbreviation	**Reaction Names**	**Model Subsystem**	**Reaction formula**	**Gene ID**	**Transcription Factors**
ASPTAm	aspartate transaminase	Alanine and aspartate metabolism	akg[m] + asp_L[m] <=> glu_L[m] + oaa[m]	Got2	CUTL1, Msx-1, CP2, PPAR-gamma1, PPAR-gamma2, YY1, MyoD, HSF1short, HSF1(long), GR
AGMTm	agmatinase (m)	Arginine and Proline Metabolism	h2o[m] + agm[m] -> ptrc[m] + urea[m]	agmaT	PPAR-gamma1, PPAR-gamma2, AREB6, Olf-1, N-Myc, Pax-5, COUP-TF1, HNF-4alpha1, HNF-4alpha2, COUP
MTAP	5"-methylthioadenosine phosphorylase	Arginine and Proline Metabolism	pi[c] + 5mta[c] -> ade[c] + 5mdr1p[c]	mtaP	HNF-4alpha1, HNF-4alpha2, c-Myc, p53
C14STRr	C-14 sterol reductase	Cholesterol metabolism	h[r] + 44mctr[r] + nadph[r] -> 44mzym[r] + nadp[r]	tm7sf2	AP-1, c-Myc, Max, Max1, c-Fos, c-Jun, Nkx5-1, GR-alpha, GR, Roaz
r0780	4,4-dimethyl-5a-cholesta-8,24-dien-3b-ol:NADP+ D14-oxidoreductase Biosynthesis of steroids EC:1.3.1.70	Cholesterol metabolism	44mzym[r] + nadp[r] <=> h[r] + 44mctr[r] + nadph[r]	tm7sf2	AP-1, c-Myc, Max, Max1, c-Fos, c-Jun, Nkx5-1, GR-alpha, GR, Roaz
SBTD_D2	D-sorbitol dehydrogenase (D-fructose producing)	Fructose and mannose metabolism	nad[c] + sbt_D[c] -> h[c] + nadh[c] + fru[c]	sorD	GR, GR-alpha, GR-beta, STAT5A
AMPTASECG	alanyl aminopeptidase (cys-gly)	Glutathione metabolism	h2o[c] + cgly[c] -> cys_L[c] + gly[c]	ANPEP	STAT1, STAT1alpha, STA1beta, C/EBPalpha, N-Myc
CLS_hs	cardiolipin synthase (homo sapiens)	Glycerophospholipid metabolism	cdpdag_hs[c] + pglyc_hs[c] -> h[c] + cmp[c] + clpn_hs[c]	CRLS1	GATA-1, MRF-2, C/EBPalpha, HFH-1, Meis-1, Meis-1a, Meis-1b, Cart-1, Msx-1, Evi-1
PSSA2_hs	Phosphatidylserine synthase homo sapiens	Glycerophospholipid metabolism	ser_L[c] + pe_hs[c] <=> etha[c] + ps_hs[c]	PTDSS2	NF-kappaB, NF-kappaB1, PPAR-gamma1, PPAR-gamma2, MIF-1, RFX1, AREB6, C/EBPbeta, LyF-1, Pax-5
GCCam	glycine-cleavage complex (lipoylprotein), mitochondrial	Glycine, serine, alanine and threonine metabolism	h[m] + gly[m] + lpro[m] <=> co2[m] + alpro[m]	dld	Max, Max1, NF-kappaB1, AP-1, c-Jun, c-Fos
				amt	AP-1, Egr-1, MyoD, GR, GR-alpha, SRF, SRF(504AA), PPAR-gamma1, PPAR-gamma2, STAT5A
				Gldc	TGIF, POU3F2, FAC1, c-Myb, POU2F1, POU2F1a, LyF-1, GATA-2, GATA-3, NRSFform1
				GCSH	ARP-1, PPAR-gamma1, PPAR-gamma2, FOXO1, FOXO1a, XBP-1, FOXO4, USF-1, USF1, LCR-F1
GCCbim	glycine-cleavage complex (lipoylprotein) irreversible, mitochondrial	Glycine, serine, alanine and threonine metabolism	thf[m] + alpro[m] -> nh4[m] + mlthf[m] + dhlpro[m]	dld	Max, Max1, NF-kappaB1, AP-1, c-Jun, c-Fos
				amt	AP-1, Egr-1, MyoD, GR, GR-alpha, SRF, SRF(504AA), PPAR-gamma1, PPAR-gamma2, STAT5A
				Gldc	TGIF, POU3F2, FAC1, c-Myb, POU2F1, POU2F1a, LyF-1, GATA-2, GATA-3, NRSFform1
				GCSH	ARP-1, PPAR-gamma1, PPAR-gamma2, FOXO1, FOXO1a, XBP-1, FOXO4, USF-1, USF1, LCR-F1

GCCcm	glycine-cleavage complex (lipoylprotein), mitochondrial	Glycine, serine, alanine and threonine metabolism	nad[m] + dhlpro[m] <=> h[m] + nadh[m] + lpro[m]	dld	Max, Max1, NF-kappaB1, AP-1, c-Jun, c-Fos
				amt	AP-1, Egr-1, MyoD, GR, GR-alpha, SRF, SRF(504AA), PPAR-gamma1, PPAR-gamma2, STAT5A
				Gldc	TGIF, POU3F2, FAC1, c-Myb, POU2F1, POU2F1a, LyF-1, GATA-2, GATA-3, NRSFform1
				GCSH	ARP-1, PPAR-gamma1, PPAR-gamma2, FOXO1, FOXO1a, XBP-1, FOXO4, USF-1, USF1, LCR-F1
NTD2e	5''-nucleotidase (UMP), extracellular	Nucleotide interconversion	h2o[e] + ump[e] -> pi[e] + uri[e]	NT5E	Egr-3, SREBP-1a, SREBP-1b, SREBP-1c, AhR, c-Jun, AP-1, ATF, RORalpha2, GR
r0394	Xanthine:NAD+ oxidoreductase Purine metabolism EC:1.17.1.4	Nucleotide interconversion	h[c] + nadh[c] + xan[c] <=> h2o[c] + nad[c] + hxan[c]	XDH	C/EBPbeta, SRY, AP-1, c-Jun, STAT3, Max1, GR, GR-alpha, GR-beta, p53
r0395	Hypoxanthine:oxygen oxidoreductase Purine metabolism EC:1.17.3.2	Nucleotide interconversion	h2o[c] + o2[c] + hxan[c] -> h2o2[c] + xan[c]	XDH	C/EBPbeta, SRY, AP-1, c-Jun, STAT3, Max1, GR, GR-alpha, GR-beta, p53
TALA	transaldolase	Pentose phosphate pathway	g3p[c] + s7p[c] <=> f6p[c] + e4p[c]	taldo1	CUTL1, FOXF2, HFH-1, Sox5, Pax-2, Pax-2a, LCR-F1, FOXC1, CBF(2), CBF-A
ME1m	malic enzyme (NAD), mitochondrial	Pyruvate metabolism	nad[m] + mal_L[m] -> co2[m] + nadh[m] + pyr[m]	ME2	AP-1, c-Jun
ORNDC	Ornithine Decarboxylase	Urea cycle	h[c] + orn[c] -> co2[c] + ptrc[c]	ODC1	PPAR-gamma1, PPAR-gamma2
AMETt2m	S-Adenosyl-L-methionine reversible transport, mitochondrial	Transport, mitochondrial	amet[c] + ahcys[m] <=> ahcys[c] + amet[m]	Slc25a26	
ESTRADIOLGLCt2	17-beta-D-glucuronide transport (ATP-dependent)	Transport, extracellular	h2o[c] + atp[c] + estradiolglc[c] -> adp[c] + h[c] + pi[c] + estradiolglc[e]	abcc4	E4BP4, N-Myc, Max, Max1, GR, GR-alpha, GR-beta, HNF-4alpha1, HNF-4alpha2
METLEUex	Methionine/Leucine exchange (Met in)	Transport, extracellular	met_L[e] + leu_L[c] -> met_L[c] + leu_L[e]	SLC3A2	Egr-1, AP-1, c-Jun
				SLC7A5	Pax-3, NF-E2, NF-E2p45, aMEF-2, MEF-2A, FosB, Fra-1, JunB, JunD, AP-1
PROSTGD2t	prostaglandin transport via bicarbonate countertransport	Transport, extracellular	hco3[e] + prostgd2[c] <=> hco3[c] + prostgd2[e]	SLCO2A1	Pax-5, GCNF, GCNF-1, GCNF-2, FOXD1, Gfi-1, Pax-4a, AREB6, STAT1, STAT1alpha
PROSTGE2t3	prostaglandine E2 transport (ATP-dependent)	Transport, extracellular	h2o[c] + atp[c] + prostge2[c] -> adp[c] + h[c] + pi[c] + prostge2[e]	abcc4	E4BP4, N-Myc, Max, Max1, GR, GR-alpha, GR-beta, HNF-4alpha1, HNF-4alpha2
r1548	Amino Acid-Polyamine-Organocation (APC) TCDB:2.A.3.8.1	Transport, extracellular	gly[e] + phe_L[c] <=> gly[c] + phe_L[e]	SLC7A5	Pax-3, NF-E2, NF-E2p45, aMEF-2, MEF-2A, FosB, Fra-1, JunB, JunD, AP-1
r1551	Amino Acid-Polyamine-Organocation (APC) TCDB:2.A.3.8.1	Transport, extracellular	gly[c] + leu_L[e] <=> gly[e] + leu_L[c]	SLC7A5	Pax-3, NF-E2, NF-E2p45, aMEF-2, MEF-2A, FosB, Fra-1, JunB, JunD, AP-1

r1553	Amino Acid-Polyamine-Organocation (APC) TCDB:2.A.3.8.1	Transport, extracellular	asn_L[c] + gly[e] <=> asn_L[e] + gly[c]	SLC7A5	Pax-3, NF-E2, NF-E2p45, aMEF-2, MEF-2A, FosB, Fra-1, JunB, JunD, AP-1
r1563	Amino Acid-Polyamine-Organocation (APC) TCDB:2.A.3.8.1	Transport, extracellular	ala_L[e] + tyr_L[c] <=> ala_L[c] + tyr_L[e]	SLC7A5	Pax-3, NF-E2, NF-E2p45, aMEF-2, MEF-2A, FosB, Fra-1, JunB, JunD, AP-1
r1574	Amino Acid-Polyamine-Organocation (APC) TCDB:2.A.3.8.1	Transport, extracellular	gln_L[c] + trp_L[e] <=> gln_L[e] + trp_L[c]	SLC7A5	Pax-3, NF-E2, NF-E2p45, aMEF-2, MEF-2A, FosB, Fra-1, JunB, JunD, AP-1
r1575	Amino Acid-Polyamine-Organocation (APC) TCDB:2.A.3.8.1	Transport, extracellular	gln_L[c] + phe_L[e] <=> gln_L[e] + phe_L[c]	SLC7A5	Pax-3, NF-E2, NF-E2p45, aMEF-2, MEF-2A, FosB, Fra-1, JunB, JunD, AP-1
r1576	Amino Acid-Polyamine-Organocation (APC) TCDB:2.A.3.8.1	Transport, extracellular	gln_L[c] + tyr_L[e] <=> gln_L[e] + tyr_L[c]	SLC7A5	Pax-3, NF-E2, NF-E2p45, aMEF-2, MEF-2A, FosB, Fra-1, JunB, JunD, AP-1
r1578	Amino Acid-Polyamine-Organocation (APC) TCDB:2.A.3.8.1	Transport, extracellular	gln_L[e] + leu_L[c] <=> gln_L[c] + leu_L[e]	SLC7A5	Pax-3, NF-E2, NF-E2p45, aMEF-2, MEF-2A, FosB, Fra-1, JunB, JunD, AP-1
r1579	Amino Acid-Polyamine-Organocation (APC) TCDB:2.A.3.8.1	Transport, extracellular	gln_L[e] + pro_L[c] <=> gln_L[c] + pro_L[e]	SLC7A5	Pax-3, NF-E2, NF-E2p45, aMEF-2, MEF-2A, FosB, Fra-1, JunB, JunD, AP-1
r1603	Amino Acid-Polyamine-Organocation (APC) TCDB:2.A.3.8.1	Transport, extracellular	asn_L[e] + met_L[c] <=> asn_L[c] + met_L[e]	SLC7A5	Pax-3, NF-E2, NF-E2p45, aMEF-2, MEF-2A, FosB, Fra-1, JunB, JunD, AP-1
r1613	Amino Acid-Polyamine-Organocation (APC) TCDB:2.A.3.8.1	Transport, extracellular	asn_L[e] + trp_L[c] <=> asn_L[c] + trp_L[e]	SLC7A5	Pax-3, NF-E2, NF-E2p45, aMEF-2, MEF-2A, FosB, Fra-1, JunB, JunD, AP-1
r1618	Amino Acid-Polyamine-Organocation (APC) TCDB:2.A.3.8.1	Transport, extracellular	phe_L[e] + tyr_L[c] <=> tyr_L[e] + phe_L[c]	SLC7A5	Pax-3, NF-E2, NF-E2p45, aMEF-2, MEF-2A, FosB, Fra-1, JunB, JunD, AP-1
r1622	Amino Acid-Polyamine-Organocation (APC) TCDB:2.A.3.8.1	Transport, extracellular	asn_L[c] + phe_L[e] <=> asn_L[e] + phe_L[c]	SLC7A5	Pax-3, NF-E2, NF-E2p45, aMEF-2, MEF-2A, FosB, Fra-1, JunB, JunD, AP-1
r1636	Amino Acid-Polyamine-Organocation (APC) TCDB:2.A.3.8.1	Transport, extracellular	cys_L[c] + pro_L[e] <=> cys_L[e] + pro_L[c]	SLC7A5	Pax-3, NF-E2, NF-E2p45, aMEF-2, MEF-2A, FosB, Fra-1, JunB, JunD, AP-1
r1637	Amino Acid-Polyamine-Organocation (APC) TCDB:2.A.3.8.1	Transport, extracellular	asn_L[e] + cys_L[c] <=> asn_L[c] + cys_L[e]	SLC7A5	Pax-3, NF-E2, NF-E2p45, aMEF-2, MEF-2A, FosB, Fra-1, JunB, JunD, AP-1

r1638	Amino Acid-Polyamine-Organocation (APC) TCDB:2.A.3.8.1	Transport, extracellular	cys_L[c] + val_L[e] <=> cys_L[e] + val_L[c]	SLC7A5	Pax-3, NF-E2, NF-E2p45, aMEF-2, MEF-2A, FosB, Fra-1, JunB, JunD, AP-1
r1639	Amino Acid-Polyamine-Organocation (APC) TCDB:2.A.3.8.1	Transport, extracellular	cys_L[c] + thr_L[e] <=> cys_L[e] + thr_L[c]	SLC7A5	Pax-3, NF-E2, NF-E2p45, aMEF-2, MEF-2A, FosB, Fra-1, JunB, JunD, AP-1
r1643	Amino Acid-Polyamine-Organocation (APC) TCDB:2.A.3.8.1	Transport, extracellular	asn_L[c] + leu_L[e] <=> asn_L[e] + leu_L[c]	SLC7A5	Pax-3, NF-E2, NF-E2p45, aMEF-2, MEF-2A, FosB, Fra-1, JunB, JunD, AP-1
r1650	Amino Acid-Polyamine-Organocation (APC) TCDB:2.A.3.8.1	Transport, extracellular	thr_L[c] + pro_L[e] <=> thr_L[e] + pro_L[c]	SLC7A5	Pax-3, NF-E2, NF-E2p45, aMEF-2, MEF-2A, FosB, Fra-1, JunB, JunD, AP-1
r1660	Amino Acid-Polyamine-Organocation (APC) TCDB:2.A.3.8.1	Transport, extracellular	thr_L[c] + hom_L[e] <=> thr_L[e] + hom_L[c]	SLC7A5	Pax-3, NF-E2, NF-E2p45, aMEF-2, MEF-2A, FosB, Fra-1, JunB, JunD, AP-1
r1669	Y+LAT2 Utilized transport	Transport, extracellular	arg_L[e] + citr_L[c] <=> arg_L[c] + citr_L[e]	SLC7A6	CREB, deltaCREB, CUTL1, POU2F1, POU2F1a, Ik-1, SREBP-1c, SREBP-1a, SREBP-1b, HTF
r1671	Y+LAT2 Utilized transport	Transport, extracellular	citr_L[c] + his_L[e] <=> his_L[c] + citr_L[e]	SLC7A6	CREB, deltaCREB, CUTL1, POU2F1, POU2F1a, Ik-1, SREBP-1c, SREBP-1a, SREBP-1b, HTF
r1672	Y+LAT2 Utilized transport	Transport, extracellular	na1[e] + ala_L[c] + gly[e] -> na1[c] + ala_L[e] + gly[c]	SLC7A6	CREB, deltaCREB, CUTL1, POU2F1, POU2F1a, Ik-1, SREBP-1c, SREBP-1a, SREBP-1b, HTF
r1673	Y+LAT2 Utilized transport	Transport, extracellular	na1[e] + gln_L[c] + gly[e] -> na1[c] + gln_L[e] + gly[c]	SLC7A6	CREB, deltaCREB, CUTL1, POU2F1, POU2F1a, Ik-1, SREBP-1c, SREBP-1a, SREBP-1b, HTF
r1674	Y+LAT2 Utilized transport	Transport, extracellular	na1[e] + gly[e] + ser_L[c] -> na1[c] + gly[c] + ser_L[e]	SLC7A6	CREB, deltaCREB, CUTL1, POU2F1, POU2F1a, Ik-1, SREBP-1c, SREBP-1a, SREBP-1b, HTF
r1675	Y+LAT2 Utilized transport	Transport, extracellular	na1[e] + gly[e] + met_L[c] -> na1[c] + gly[c] + met_L[e]	SLC7A6	CREB, deltaCREB, CUTL1, POU2F1, POU2F1a, Ik-1, SREBP-1c, SREBP-1a, SREBP-1b, HTF
r1676	Y+LAT2 Utilized transport	Transport, extracellular	na1[e] + gly[e] + trp_L[c] -> na1[c] + gly[c] + trp_L[e]	SLC7A6	CREB, deltaCREB, CUTL1, POU2F1, POU2F1a, Ik-1, SREBP-1c, SREBP-1a, SREBP-1b, HTF
r1677	Y+LAT2 Utilized transport	Transport, extracellular	na1[e] + gly[e] + phe_L[c] -> na1[c] + gly[c] + phe_L[e]	SLC7A6	CREB, deltaCREB, CUTL1, POU2F1, POU2F1a, Ik-1, SREBP-1c, SREBP-1a, SREBP-1b, HTF
r1678	Y+LAT2 Utilized transport	Transport, extracellular	na1[e] + gly[e] + tyr_L[c] -> na1[c] + gly[c] + tyr_L[e]	SLC7A6	CREB, deltaCREB, CUTL1, POU2F1, POU2F1a, Ik-1, SREBP-1c, SREBP-1a, SREBP-1b, HTF
r1679	Y+LAT2 Utilized transport	Transport, extracellular	na1[e] + cys_L[c] + gly[e] -> na1[c] + cys_L[e] + gly[c]	SLC7A6	CREB, deltaCREB, CUTL1, POU2F1, POU2F1a, Ik-1, SREBP-1c, SREBP-1a, SREBP-1b, HTF
r1680	Y+LAT2 Utilized transport	Transport, extracellular	na1[e] + gly[e] + leu_L[c] -> na1[c] + gly[c] + leu_L[e]	SLC7A6	CREB, deltaCREB, CUTL1, POU2F1, POU2F1a, Ik-1, SREBP-1c, SREBP-1a, SREBP-1b, HTF

r1681	Y+LAT2 Utilized transport	Transport, extracellular	na1[e] + gly[e] + pro_L[c] -> na1[c] + gly[c] + pro_L[e]	SLC7A6	CREB, deltaCREB, CUTL1, POU2F1, POU2F1a, Ik-1, SREBP-1c, SREBP-1a, SREBP-1b, HTF
r1682	Y+LAT2 Utilized transport	Transport, extracellular	na1[e] + asn_L[c] + gly[e] -> na1[c] + asn_L[e] + gly[c]	SLC7A6	CREB, deltaCREB, CUTL1, POU2F1, POU2F1a, Ik-1, SREBP-1c, SREBP-1a, SREBP-1b, HTF
r1683	Y+LAT2 Utilized transport	Transport, extracellular	na1[e] + gly[e] + val_L[c] -> na1[c] + gly[c] + val_L[e]	SLC7A6	CREB, deltaCREB, CUTL1, POU2F1, POU2F1a, Ik-1, SREBP-1c, SREBP-1a, SREBP-1b, HTF
r1684	Y+LAT2 Utilized transport	Transport, extracellular	na1[e] + gly[e] + thr_L[c] -> na1[c] + gly[c] + thr_L[e]	SLC7A6	CREB, deltaCREB, CUTL1, POU2F1, POU2F1a, Ik-1, SREBP-1c, SREBP-1a, SREBP-1b, HTF
r1685	Y+LAT2 Utilized transport	Transport, extracellular	na1[e] + gly[e] + hom_L[c] -> na1[c] + gly[c] + hom_L[e]	SLC7A6	CREB, deltaCREB, CUTL1, POU2F1, POU2F1a, Ik-1, SREBP-1c, SREBP-1a, SREBP-1b, HTF
r1686	Y+LAT2 Utilized transport	Transport, extracellular	na1[e] + gly[e] + ile_L[c] -> na1[c] + gly[c] + ile_L[e]	SLC7A6	CREB, deltaCREB, CUTL1, POU2F1, POU2F1a, Ik-1, SREBP-1c, SREBP-1a, SREBP-1b, HTF
r1687	Y+LAT2 Utilized transport	Transport, extracellular	na1[e] + ala_L[e] + gly[c] -> na1[c] + ala_L[c] + gly[e]	SLC7A6	CREB, deltaCREB, CUTL1, POU2F1, POU2F1a, Ik-1, SREBP-1c, SREBP-1a, SREBP-1b, HTF
r1690	Y+LAT2 Utilized transport	Transport, extracellular	na1[e] + ala_L[e] + met_L[c] -> na1[c] + ala_L[c] + met_L[e]	SLC7A6	CREB, deltaCREB, CUTL1, POU2F1, POU2F1a, Ik-1, SREBP-1c, SREBP-1a, SREBP-1b, HTF
r1692	Y+LAT2 Utilized transport	Transport, extracellular	na1[e] + ala_L[e] + phe_L[c] -> na1[c] + ala_L[c] + phe_L[e]	SLC7A6	CREB, deltaCREB, CUTL1, POU2F1, POU2F1a, Ik-1, SREBP-1c, SREBP-1a, SREBP-1b, HTF
r1693	Y+LAT2 Utilized transport	Transport, extracellular	na1[e] + ala_L[e] + tyr_L[c] -> na1[c] + ala_L[c] + tyr_L[e]	SLC7A6	CREB, deltaCREB, CUTL1, POU2F1, POU2F1a, Ik-1, SREBP-1c, SREBP-1a, SREBP-1b, HTF
r1695	Y+LAT2 Utilized transport	Transport, extracellular	na1[e] + ala_L[e] + leu_L[c] -> na1[c] + ala_L[c] + leu_L[e]	SLC7A6	CREB, deltaCREB, CUTL1, POU2F1, POU2F1a, Ik-1, SREBP-1c, SREBP-1a, SREBP-1b, HTF
r1696	Y+LAT2 Utilized transport	Transport, extracellular	na1[e] + ala_L[e] + pro_L[c] -> na1[c] + ala_L[c] + pro_L[e]	SLC7A6	CREB, deltaCREB, CUTL1, POU2F1, POU2F1a, Ik-1, SREBP-1c, SREBP-1a, SREBP-1b, HTF
r1698	Y+LAT2 Utilized transport	Transport, extracellular	na1[e] + ala_L[e] + val_L[c] -> na1[c] + ala_L[c] + val_L[e]	SLC7A6	CREB, deltaCREB, CUTL1, POU2F1, POU2F1a, Ik-1, SREBP-1c, SREBP-1a, SREBP-1b, HTF
r1701	Y+LAT2 Utilized transport	Transport, extracellular	na1[e] + ala_L[e] + ile_L[c] -> na1[c] + ala_L[c] + ile_L[e]	SLC7A6	CREB, deltaCREB, CUTL1, POU2F1, POU2F1a, Ik-1, SREBP-1c, SREBP-1a, SREBP-1b, HTF
r1702	Y+LAT2 Utilized transport	Transport, extracellular	na1[e] + gln_L[e] + gly[c] -> na1[c] + gln_L[c] + gly[e]	SLC7A6	CREB, deltaCREB, CUTL1, POU2F1, POU2F1a, Ik-1, SREBP-1c, SREBP-1a, SREBP-1b, HTF
r1705	Y+LAT2 Utilized transport	Transport, extracellular	na1[e] + gln_L[e] + met_L[c] -> na1[c] + gln_L[c] + met_L[e]	SLC7A6	CREB, deltaCREB, CUTL1, POU2F1, POU2F1a, Ik-1, SREBP-1c, SREBP-1a, SREBP-1b, HTF
r1706	Y+LAT2 Utilized transport	Transport, extracellular	na1[e] + gln_L[e] + trp_L[c] -> na1[c] + gln_L[c] + trp_L[e]	SLC7A6	CREB, deltaCREB, CUTL1, POU2F1, POU2F1a, Ik-1, SREBP-1c, SREBP-1a, SREBP-1b, HTF
r1707	Y+LAT2 Utilized transport	Transport, extracellular	na1[e] + gln_L[e] + phe_L[c] -> na1[c] + gln_L[c] + phe_L[e]	SLC7A6	CREB, deltaCREB, CUTL1, POU2F1, POU2F1a, Ik-1, SREBP-1c, SREBP-1a, SREBP-1b, HTF

r1708	Y+LAT2 Utilized transport	Transport, extracellular	na1[e] + gln_L[e] + tyr_L[c] -> na1[c] + gln_L[c] + tyr_L[e]	SLC7A6	CREB, deltaCREB, CUTL1, POU2F1, POU2F1a, Ik-1, SREBP-1c, SREBP-1a, SREBP-1b, HTF
r1710	Y+LAT2 Utilized transport	Transport, extracellular	na1[e] + gln_L[e] + leu_L[c] -> na1[c] + gln_L[c] + leu_L[e]	SLC7A6	CREB, deltaCREB, CUTL1, POU2F1, POU2F1a, Ik-1, SREBP-1c, SREBP-1a, SREBP-1b, HTF
r1711	Y+LAT2 Utilized transport	Transport, extracellular	na1[e] + gln_L[e] + pro_L[c] -> na1[c] + gln_L[c] + pro_L[e]	SLC7A6	CREB, deltaCREB, CUTL1, POU2F1, POU2F1a, Ik-1, SREBP-1c, SREBP-1a, SREBP-1b, HTF
r1713	Y+LAT2 Utilized transport	Transport, extracellular	na1[e] + gln_L[e] + val_L[c] -> na1[c] + gln_L[c] + val_L[e]	SLC7A6	CREB, deltaCREB, CUTL1, POU2F1, POU2F1a, Ik-1, SREBP-1c, SREBP-1a, SREBP-1b, HTF
r1715	Y+LAT2 Utilized transport	Transport, extracellular	na1[e] + gln_L[e] + hom_L[c] -> na1[c] + gln_L[c] + hom_L[e]	SLC7A6	CREB, deltaCREB, CUTL1, POU2F1, POU2F1a, Ik-1, SREBP-1c, SREBP-1a, SREBP-1b, HTF
r1716	Y+LAT2 Utilized transport	Transport, extracellular	na1[e] + gln_L[e] + ile_L[c] -> na1[c] + gln_L[c] + ile_L[e]	SLC7A6	CREB, deltaCREB, CUTL1, POU2F1, POU2F1a, Ik-1, SREBP-1c, SREBP-1a, SREBP-1b, HTF
r1717	Y+LAT2 Utilized transport	Transport, extracellular	na1[e] + gly[c] + ser_L[e] -> na1[c] + gly[e] + ser_L[c]	SLC7A6	CREB, deltaCREB, CUTL1, POU2F1, POU2F1a, Ik-1, SREBP-1c, SREBP-1a, SREBP-1b, HTF
r1720	Y+LAT2 Utilized transport	Transport, extracellular	na1[e] + ser_L[e] + met_L[c] -> na1[c] + ser_L[c] + met_L[e]	SLC7A6	CREB, deltaCREB, CUTL1, POU2F1, POU2F1a, Ik-1, SREBP-1c, SREBP-1a, SREBP-1b, HTF
r1721	Y+LAT2 Utilized transport	Transport, extracellular	na1[e] + ser_L[e] + trp_L[c] -> na1[c] + ser_L[c] + trp_L[e]	SLC7A6	CREB, deltaCREB, CUTL1, POU2F1, POU2F1a, Ik-1, SREBP-1c, SREBP-1a, SREBP-1b, HTF
r1722	Y+LAT2 Utilized transport	Transport, extracellular	na1[e] + ser_L[e] + phe_L[c] -> na1[c] + ser_L[c] + phe_L[e]	SLC7A6	CREB, deltaCREB, CUTL1, POU2F1, POU2F1a, Ik-1, SREBP-1c, SREBP-1a, SREBP-1b, HTF
r1725	Y+LAT2 Utilized transport	Transport, extracellular	na1[e] + ser_L[e] + leu_L[c] -> na1[c] + ser_L[c] + leu_L[e]	SLC7A6	CREB, deltaCREB, CUTL1, POU2F1, POU2F1a, Ik-1, SREBP-1c, SREBP-1a, SREBP-1b, HTF
r1726	Y+LAT2 Utilized transport	Transport, extracellular	na1[e] + ser_L[e] + pro_L[c] -> na1[c] + ser_L[c] + pro_L[e]	SLC7A6	CREB, deltaCREB, CUTL1, POU2F1, POU2F1a, Ik-1, SREBP-1c, SREBP-1a, SREBP-1b, HTF
r1728	Y+LAT2 Utilized transport	Transport, extracellular	na1[e] + ser_L[e] + val_L[c] -> na1[c] + ser_L[c] + val_L[e]	SLC7A6	CREB, deltaCREB, CUTL1, POU2F1, POU2F1a, Ik-1, SREBP-1c, SREBP-1a, SREBP-1b, HTF
r1730	Y+LAT2 Utilized transport	Transport, extracellular	na1[e] + ser_L[e] + hom_L[c] -> na1[c] + ser_L[c] + hom_L[e]	SLC7A6	CREB, deltaCREB, CUTL1, POU2F1, POU2F1a, Ik-1, SREBP-1c, SREBP-1a, SREBP-1b, HTF
r1731	Y+LAT2 Utilized transport	Transport, extracellular	na1[e] + ser_L[e] + ile_L[c] -> na1[c] + ser_L[c] + ile_L[e]	SLC7A6	CREB, deltaCREB, CUTL1, POU2F1, POU2F1a, Ik-1, SREBP-1c, SREBP-1a, SREBP-1b, HTF
r1733	Y+LAT2 Utilized transport	Transport, extracellular	na1[e] + ala_L[c] + met_L[e] -> na1[c] + ala_L[e] + met_L[c]	SLC7A6	CREB, deltaCREB, CUTL1, POU2F1, POU2F1a, Ik-1, SREBP-1c, SREBP-1a, SREBP-1b, HTF
r1734	Y+LAT2 Utilized transport	Transport, extracellular	na1[e] + gln_L[c] + met_L[e] -> na1[c] + gln_L[e] + met_L[c]	SLC7A6	CREB, deltaCREB, CUTL1, POU2F1, POU2F1a, Ik-1, SREBP-1c, SREBP-1a, SREBP-1b, HTF
r1735	Y+LAT2 Utilized transport	Transport, extracellular	na1[e] + ser_L[c] + met_L[e] -> na1[c] + ser_L[e] + met_L[c]	SLC7A6	CREB, deltaCREB, CUTL1, POU2F1, POU2F1a, Ik-1, SREBP-1c, SREBP-1a, SREBP-1b, HTF

r1736	Y+LAT2 Utilized transport	Transport, extracellular	na1[e] + met_L[e] + trp_L[c] -> na1[c] + met_L[c] + trp_L[e]	SLC7A6	CREB, deltaCREB, CUTL1, POU2F1, POU2F1a, Ik-1, SREBP-1c, SREBP-1a, SREBP-1b, HTF
r1737	Y+LAT2 Utilized transport	Transport, extracellular	na1[e] + met_L[e] + phe_L[c] -> na1[c] + met_L[c] + phe_L[e]	SLC7A6	CREB, deltaCREB, CUTL1, POU2F1, POU2F1a, Ik-1, SREBP-1c, SREBP-1a, SREBP-1b, HTF
r1738	Y+LAT2 Utilized transport	Transport, extracellular	na1[e] + met_L[e] + tyr_L[c] -> na1[c] + met_L[c] + tyr_L[e]	SLC7A6	CREB, deltaCREB, CUTL1, POU2F1, POU2F1a, Ik-1, SREBP-1c, SREBP-1a, SREBP-1b, HTF
r1739	Y+LAT2 Utilized transport	Transport, extracellular	na1[e] + cys_L[c] + met_L[e] -> na1[c] + cys_L[e] + met_L[c]	SLC7A6	CREB, deltaCREB, CUTL1, POU2F1, POU2F1a, Ik-1, SREBP-1c, SREBP-1a, SREBP-1b, HTF
r1740	Y+LAT2 Utilized transport	Transport, extracellular	na1[e] + met_L[e] + leu_L[c] -> na1[c] + met_L[c] + leu_L[e]	SLC7A6	CREB, deltaCREB, CUTL1, POU2F1, POU2F1a, Ik-1, SREBP-1c, SREBP-1a, SREBP-1b, HTF
r1741	Y+LAT2 Utilized transport	Transport, extracellular	na1[e] + met_L[e] + pro_L[c] -> na1[c] + met_L[c] + pro_L[e]	SLC7A6	CREB, deltaCREB, CUTL1, POU2F1, POU2F1a, Ik-1, SREBP-1c, SREBP-1a, SREBP-1b, HTF
r1742	Y+LAT2 Utilized transport	Transport, extracellular	na1[e] + asn_L[c] + met_L[e] -> na1[c] + asn_L[e] + met_L[c]	SLC7A6	CREB, deltaCREB, CUTL1, POU2F1, POU2F1a, Ik-1, SREBP-1c, SREBP-1a, SREBP-1b, HTF
r1743	Y+LAT2 Utilized transport	Transport, extracellular	na1[e] + met_L[e] + val_L[c] -> na1[c] + met_L[c] + val_L[e]	SLC7A6	CREB, deltaCREB, CUTL1, POU2F1, POU2F1a, Ik-1, SREBP-1c, SREBP-1a, SREBP-1b, HTF
r1744	Y+LAT2 Utilized transport	Transport, extracellular	na1[e] + thr_L[c] + met_L[e] -> na1[c] + thr_L[e] + met_L[c]	SLC7A6	CREB, deltaCREB, CUTL1, POU2F1, POU2F1a, Ik-1, SREBP-1c, SREBP-1a, SREBP-1b, HTF
r1745	Y+LAT2 Utilized transport	Transport, extracellular	na1[e] + met_L[e] + hom_L[c] -> na1[c] + met_L[c] + hom_L[e]	SLC7A6	CREB, deltaCREB, CUTL1, POU2F1, POU2F1a, Ik-1, SREBP-1c, SREBP-1a, SREBP-1b, HTF
r1746	Y+LAT2 Utilized transport	Transport, extracellular	na1[e] + met_L[e] + ile_L[c] -> na1[c] + met_L[c] + ile_L[e]	SLC7A6	CREB, deltaCREB, CUTL1, POU2F1, POU2F1a, Ik-1, SREBP-1c, SREBP-1a, SREBP-1b, HTF
r1747	Y+LAT2 Utilized transport	Transport, extracellular	na1[e] + gly[c] + trp_L[e] -> na1[c] + gly[e] + trp_L[c]	SLC7A6	CREB, deltaCREB, CUTL1, POU2F1, POU2F1a, Ik-1, SREBP-1c, SREBP-1a, SREBP-1b, HTF
r1748	Y+LAT2 Utilized transport	Transport, extracellular	na1[e] + ala_L[c] + trp_L[e] -> na1[c] + ala_L[e] + trp_L[c]	SLC7A6	CREB, deltaCREB, CUTL1, POU2F1, POU2F1a, Ik-1, SREBP-1c, SREBP-1a, SREBP-1b, HTF
r1749	Y+LAT2 Utilized transport	Transport, extracellular	na1[e] + gln_L[c] + trp_L[e] -> na1[c] + gln_L[e] + trp_L[c]	SLC7A6	CREB, deltaCREB, CUTL1, POU2F1, POU2F1a, Ik-1, SREBP-1c, SREBP-1a, SREBP-1b, HTF
r1750	Y+LAT2 Utilized transport	Transport, extracellular	na1[e] + ser_L[c] + trp_L[e] -> na1[c] + ser_L[e] + trp_L[c]	SLC7A6	CREB, deltaCREB, CUTL1, POU2F1, POU2F1a, Ik-1, SREBP-1c, SREBP-1a, SREBP-1b, HTF
r1751	Y+LAT2 Utilized transport	Transport, extracellular	na1[e] + met_L[c] + trp_L[e] -> na1[c] + met_L[e] + trp_L[c]	SLC7A6	CREB, deltaCREB, CUTL1, POU2F1, POU2F1a, Ik-1, SREBP-1c, SREBP-1a, SREBP-1b, HTF
r1753	Y+LAT2 Utilized transport	Transport, extracellular	na1[e] + trp_L[e] + tyr_L[c] -> na1[c] + tyr_L[e] + trp_L[c]	SLC7A6	CREB, deltaCREB, CUTL1, POU2F1, POU2F1a, Ik-1, SREBP-1c, SREBP-1a, SREBP-1b, HTF
r1754	Y+LAT2 Utilized transport	Transport, extracellular	na1[e] + cys_L[c] + trp_L[e] -> na1[c] + cys_L[e] + trp_L[c]	SLC7A6	CREB, deltaCREB, CUTL1, POU2F1, POU2F1a, Ik-1, SREBP-1c, SREBP-1a, SREBP-1b, HTF

r1755	Y+LAT2 Utilized transport	Transport, extracellular	na1[e] + trp_L[e] + leu_L[c] -> na1[c] + leu_L[e] + trp_L[c]	SLC7A6	CREB, deltaCREB, CUTL1, POU2F1, POU2F1a, Ik-1, SREBP-1c, SREBP-1a, SREBP-1b, HTF
r1756	Y+LAT2 Utilized transport	Transport, extracellular	na1[e] + trp_L[e] + pro_L[c] -> na1[c] + pro_L[e] + trp_L[c]	SLC7A6	CREB, deltaCREB, CUTL1, POU2F1, POU2F1a, Ik-1, SREBP-1c, SREBP-1a, SREBP-1b, HTF
r1757	Y+LAT2 Utilized transport	Transport, extracellular	na1[e] + asn_L[c] + trp_L[e] -> na1[c] + asn_L[e] + trp_L[c]	SLC7A6	CREB, deltaCREB, CUTL1, POU2F1, POU2F1a, Ik-1, SREBP-1c, SREBP-1a, SREBP-1b, HTF
r1758	Y+LAT2 Utilized transport	Transport, extracellular	na1[e] + trp_L[e] + val_L[c] -> na1[c] + val_L[e] + trp_L[c]	SLC7A6	CREB, deltaCREB, CUTL1, POU2F1, POU2F1a, Ik-1, SREBP-1c, SREBP-1a, SREBP-1b, HTF
r1760	Y+LAT2 Utilized transport	Transport, extracellular	na1[e] + trp_L[e] + hom_L[c] -> na1[c] + hom_L[e] + trp_L[c]	SLC7A6	CREB, deltaCREB, CUTL1, POU2F1, POU2F1a, Ik-1, SREBP-1c, SREBP-1a, SREBP-1b, HTF
r1761	Y+LAT2 Utilized transport	Transport, extracellular	na1[e] + trp_L[e] + ile_L[c] -> na1[c] + ile_L[e] + trp_L[c]	SLC7A6	CREB, deltaCREB, CUTL1, POU2F1, POU2F1a, Ik-1, SREBP-1c, SREBP-1a, SREBP-1b, HTF
r1763	Y+LAT2 Utilized transport	Transport, extracellular	na1[e] + ala_L[c] + phe_L[e] -> na1[c] + ala_L[e] + phe_L[c]	SLC7A6	CREB, deltaCREB, CUTL1, POU2F1, POU2F1a, Ik-1, SREBP-1c, SREBP-1a, SREBP-1b, HTF
r1764	Y+LAT2 Utilized transport	Transport, extracellular	na1[e] + gln_L[c] + phe_L[e] -> na1[c] + gln_L[e] + phe_L[c]	SLC7A6	CREB, deltaCREB, CUTL1, POU2F1, POU2F1a, Ik-1, SREBP-1c, SREBP-1a, SREBP-1b, HTF
r1765	Y+LAT2 Utilized transport	Transport, extracellular	na1[e] + ser_L[c] + phe_L[e] -> na1[c] + ser_L[e] + phe_L[c]	SLC7A6	CREB, deltaCREB, CUTL1, POU2F1, POU2F1a, Ik-1, SREBP-1c, SREBP-1a, SREBP-1b, HTF
r1766	Y+LAT2 Utilized transport	Transport, extracellular	na1[e] + met_L[c] + phe_L[e] -> na1[c] + met_L[e] + phe_L[c]	SLC7A6	CREB, deltaCREB, CUTL1, POU2F1, POU2F1a, Ik-1, SREBP-1c, SREBP-1a, SREBP-1b, HTF
r1767	Y+LAT2 Utilized transport	Transport, extracellular	na1[e] + phe_L[e] + trp_L[c] -> na1[c] + trp_L[e] + phe_L[c]	SLC7A6	CREB, deltaCREB, CUTL1, POU2F1, POU2F1a, Ik-1, SREBP-1c, SREBP-1a, SREBP-1b, HTF
r1768	Y+LAT2 Utilized transport	Transport, extracellular	na1[e] + phe_L[e] + tyr_L[c] -> na1[c] + tyr_L[e] + phe_L[c]	SLC7A6	CREB, deltaCREB, CUTL1, POU2F1, POU2F1a, Ik-1, SREBP-1c, SREBP-1a, SREBP-1b, HTF
r1769	Y+LAT2 Utilized transport	Transport, extracellular	na1[e] + cys_L[c] + phe_L[e] -> na1[c] + cys_L[e] + phe_L[c]	SLC7A6	CREB, deltaCREB, CUTL1, POU2F1, POU2F1a, Ik-1, SREBP-1c, SREBP-1a, SREBP-1b, HTF
r1770	Y+LAT2 Utilized transport	Transport, extracellular	na1[e] + phe_L[e] + leu_L[c] -> na1[c] + leu_L[e] + phe_L[c]	SLC7A6	CREB, deltaCREB, CUTL1, POU2F1, POU2F1a, Ik-1, SREBP-1c, SREBP-1a, SREBP-1b, HTF
r1771	Y+LAT2 Utilized transport	Transport, extracellular	na1[e] + phe_L[e] + pro_L[c] -> na1[c] + pro_L[e] + phe_L[c]	SLC7A6	CREB, deltaCREB, CUTL1, POU2F1, POU2F1a, Ik-1, SREBP-1c, SREBP-1a, SREBP-1b, HTF
r1772	Y+LAT2 Utilized transport	Transport, extracellular	na1[e] + asn_L[c] + phe_L[e] -> na1[c] + asn_L[e] + phe_L[c]	SLC7A6	CREB, deltaCREB, CUTL1, POU2F1, POU2F1a, Ik-1, SREBP-1c, SREBP-1a, SREBP-1b, HTF
r1773	Y+LAT2 Utilized transport	Transport, extracellular	na1[e] + phe_L[e] + val_L[c] -> na1[c] + val_L[e] + phe_L[c]	SLC7A6	CREB, deltaCREB, CUTL1, POU2F1, POU2F1a, Ik-1, SREBP-1c, SREBP-1a, SREBP-1b, HTF
r1774	Y+LAT2 Utilized transport	Transport, extracellular	na1[e] + thr_L[c] + phe_L[e] -> na1[c] + thr_L[e] + phe_L[c]	SLC7A6	CREB, deltaCREB, CUTL1, POU2F1, POU2F1a, Ik-1, SREBP-1c, SREBP-1a, SREBP-1b, HTF

r1775	Y+LAT2 Utilized transport	Transport, extracellular	na1[e] + phe_L[e] + hom_L[c] -> na1[c] + hom_L[e] + phe_L[c]	SLC7A6	CREB, deltaCREB, CUTL1, POU2F1, POU2F1a, Ik-1, SREBP-1c, SREBP-1a, SREBP-1b, HTF
r1776	Y+LAT2 Utilized transport	Transport, extracellular	na1[e] + phe_L[e] + ile_L[c] -> na1[c] + ile_L[e] + phe_L[c]	SLC7A6	CREB, deltaCREB, CUTL1, POU2F1, POU2F1a, Ik-1, SREBP-1c, SREBP-1a, SREBP-1b, HTF
r1777	Y+LAT2 Utilized transport	Transport, extracellular	na1[e] + gly[c] + tyr_L[e] -> na1[c] + gly[e] + tyr_L[c]	SLC7A6	CREB, deltaCREB, CUTL1, POU2F1, POU2F1a, Ik-1, SREBP-1c, SREBP-1a, SREBP-1b, HTF
r1778	Y+LAT2 Utilized transport	Transport, extracellular	na1[e] + ala_L[c] + tyr_L[e] -> na1[c] + ala_L[e] + tyr_L[c]	SLC7A6	CREB, deltaCREB, CUTL1, POU2F1, POU2F1a, Ik-1, SREBP-1c, SREBP-1a, SREBP-1b, HTF
r1780	Y+LAT2 Utilized transport	Transport, extracellular	na1[e] + ser_L[c] + tyr_L[e] -> na1[c] + ser_L[e] + tyr_L[c]	SLC7A6	CREB, deltaCREB, CUTL1, POU2F1, POU2F1a, Ik-1, SREBP-1c, SREBP-1a, SREBP-1b, HTF
r1781	Y+LAT2 Utilized transport	Transport, extracellular	na1[e] + met_L[c] + tyr_L[e] -> na1[c] + met_L[e] + tyr_L[c]	SLC7A6	CREB, deltaCREB, CUTL1, POU2F1, POU2F1a, Ik-1, SREBP-1c, SREBP-1a, SREBP-1b, HTF
r1782	Y+LAT2 Utilized transport	Transport, extracellular	na1[e] + tyr_L[e] + trp_L[c] -> na1[c] + trp_L[e] + tyr_L[c]	SLC7A6	CREB, deltaCREB, CUTL1, POU2F1, POU2F1a, Ik-1, SREBP-1c, SREBP-1a, SREBP-1b, HTF
r1783	Y+LAT2 Utilized transport	Transport, extracellular	na1[e] + tyr_L[e] + phe_L[c] -> na1[c] + phe_L[e] + tyr_L[c]	SLC7A6	CREB, deltaCREB, CUTL1, POU2F1, POU2F1a, Ik-1, SREBP-1c, SREBP-1a, SREBP-1b, HTF
r1784	Y+LAT2 Utilized transport	Transport, extracellular	na1[e] + cys_L[c] + tyr_L[e] -> na1[c] + cys_L[e] + tyr_L[c]	SLC7A6	CREB, deltaCREB, CUTL1, POU2F1, POU2F1a, Ik-1, SREBP-1c, SREBP-1a, SREBP-1b, HTF
r1785	Y+LAT2 Utilized transport	Transport, extracellular	na1[e] + tyr_L[e] + leu_L[c] -> na1[c] + leu_L[e] + tyr_L[c]	SLC7A6	CREB, deltaCREB, CUTL1, POU2F1, POU2F1a, Ik-1, SREBP-1c, SREBP-1a, SREBP-1b, HTF
r1786	Y+LAT2 Utilized transport	Transport, extracellular	na1[e] + tyr_L[e] + pro_L[c] -> na1[c] + pro_L[e] + tyr_L[c]	SLC7A6	CREB, deltaCREB, CUTL1, POU2F1, POU2F1a, Ik-1, SREBP-1c, SREBP-1a, SREBP-1b, HTF
r1787	Y+LAT2 Utilized transport	Transport, extracellular	na1[e] + asn_L[c] + tyr_L[e] -> na1[c] + asn_L[e] + tyr_L[c]	SLC7A6	CREB, deltaCREB, CUTL1, POU2F1, POU2F1a, Ik-1, SREBP-1c, SREBP-1a, SREBP-1b, HTF
r1788	Y+LAT2 Utilized transport	Transport, extracellular	na1[e] + tyr_L[e] + val_L[c] -> na1[c] + val_L[e] + tyr_L[c]	SLC7A6	CREB, deltaCREB, CUTL1, POU2F1, POU2F1a, Ik-1, SREBP-1c, SREBP-1a, SREBP-1b, HTF
r1790	Y+LAT2 Utilized transport	Transport, extracellular	na1[e] + tyr_L[e] + hom_L[c] -> na1[c] + hom_L[e] + tyr_L[c]	SLC7A6	CREB, deltaCREB, CUTL1, POU2F1, POU2F1a, Ik-1, SREBP-1c, SREBP-1a, SREBP-1b, HTF
r1791	Y+LAT2 Utilized transport	Transport, extracellular	na1[e] + tyr_L[e] + ile_L[c] -> na1[c] + ile_L[e] + tyr_L[c]	SLC7A6	CREB, deltaCREB, CUTL1, POU2F1, POU2F1a, Ik-1, SREBP-1c, SREBP-1a, SREBP-1b, HTF
r1792	Y+LAT2 Utilized transport	Transport, extracellular	na1[e] + cys_L[e] + gly[c] -> na1[c] + cys_L[c] + gly[e]	SLC7A6	CREB, deltaCREB, CUTL1, POU2F1, POU2F1a, Ik-1, SREBP-1c, SREBP-1a, SREBP-1b, HTF
r1796	Y+LAT2 Utilized transport	Transport, extracellular	na1[e] + cys_L[e] + met_L[c] -> na1[c] + cys_L[c] + met_L[e]	SLC7A6	CREB, deltaCREB, CUTL1, POU2F1, POU2F1a, Ik-1, SREBP-1c, SREBP-1a, SREBP-1b, HTF
r1797	Y+LAT2 Utilized transport	Transport, extracellular	na1[e] + cys_L[e] + trp_L[c] -> na1[c] + cys_L[c] + trp_L[e]	SLC7A6	CREB, deltaCREB, CUTL1, POU2F1, POU2F1a, Ik-1, SREBP-1c, SREBP-1a, SREBP-1b, HTF

r1798	Y+LAT2 Utilized transport	Transport, extracellular	na1[e] + cys_L[e] + phe_L[c] -> na1[c] + cys_L[c] + phe_L[e]	SLC7A6	CREB, deltaCREB, CUTL1, POU2F1, POU2F1a, Ik-1, SREBP-1c, SREBP-1a, SREBP-1b, HTF
r1799	Y+LAT2 Utilized transport	Transport, extracellular	na1[e] + cys_L[e] + tyr_L[c] -> na1[c] + cys_L[c] + tyr_L[e]	SLC7A6	CREB, deltaCREB, CUTL1, POU2F1, POU2F1a, Ik-1, SREBP-1c, SREBP-1a, SREBP-1b, HTF
r1800	Y+LAT2 Utilized transport	Transport, extracellular	na1[e] + cys_L[e] + leu_L[c] -> na1[c] + cys_L[c] + leu_L[e]	SLC7A6	CREB, deltaCREB, CUTL1, POU2F1, POU2F1a, Ik-1, SREBP-1c, SREBP-1a, SREBP-1b, HTF
r1801	Y+LAT2 Utilized transport	Transport, extracellular	na1[e] + cys_L[e] + pro_L[c] -> na1[c] + cys_L[c] + pro_L[e]	SLC7A6	CREB, deltaCREB, CUTL1, POU2F1, POU2F1a, Ik-1, SREBP-1c, SREBP-1a, SREBP-1b, HTF
r1803	Y+LAT2 Utilized transport	Transport, extracellular	na1[e] + cys_L[e] + val_L[c] -> na1[c] + cys_L[c] + val_L[e]	SLC7A6	CREB, deltaCREB, CUTL1, POU2F1, POU2F1a, Ik-1, SREBP-1c, SREBP-1a, SREBP-1b, HTF
r1805	Y+LAT2 Utilized transport	Transport, extracellular	na1[e] + cys_L[e] + hom_L[c] -> na1[c] + cys_L[c] + hom_L[e]	SLC7A6	CREB, deltaCREB, CUTL1, POU2F1, POU2F1a, Ik-1, SREBP-1c, SREBP-1a, SREBP-1b, HTF
r1806	Y+LAT2 Utilized transport	Transport, extracellular	na1[e] + cys_L[e] + ile_L[c] -> na1[c] + cys_L[c] + ile_L[e]	SLC7A6	CREB, deltaCREB, CUTL1, POU2F1, POU2F1a, Ik-1, SREBP-1c, SREBP-1a, SREBP-1b, HTF
r1807	Y+LAT2 Utilized transport	Transport, extracellular	na1[e] + gly[c] + leu_L[e] -> na1[c] + gly[e] + leu_L[c]	SLC7A6	CREB, deltaCREB, CUTL1, POU2F1, POU2F1a, Ik-1, SREBP-1c, SREBP-1a, SREBP-1b, HTF
r1809	Y+LAT2 Utilized transport	Transport, extracellular	na1[e] + gln_L[c] + leu_L[e] -> na1[c] + gln_L[e] + leu_L[c]	SLC7A6	CREB, deltaCREB, CUTL1, POU2F1, POU2F1a, Ik-1, SREBP-1c, SREBP-1a, SREBP-1b, HTF
r1810	Y+LAT2 Utilized transport	Transport, extracellular	na1[e] + ser_L[c] + leu_L[e] -> na1[c] + ser_L[e] + leu_L[c]	SLC7A6	CREB, deltaCREB, CUTL1, POU2F1, POU2F1a, Ik-1, SREBP-1c, SREBP-1a, SREBP-1b, HTF
r1811	Y+LAT2 Utilized transport	Transport, extracellular	na1[e] + met_L[c] + leu_L[e] -> na1[c] + met_L[e] + leu_L[c]	SLC7A6	CREB, deltaCREB, CUTL1, POU2F1, POU2F1a, Ik-1, SREBP-1c, SREBP-1a, SREBP-1b, HTF
r1812	Y+LAT2 Utilized transport	Transport, extracellular	na1[e] + leu_L[e] + trp_L[c] -> na1[c] + trp_L[e] + leu_L[c]	SLC7A6	CREB, deltaCREB, CUTL1, POU2F1, POU2F1a, Ik-1, SREBP-1c, SREBP-1a, SREBP-1b, HTF
r1813	Y+LAT2 Utilized transport	Transport, extracellular	na1[e] + leu_L[e] + phe_L[c] -> na1[c] + phe_L[e] + leu_L[c]	SLC7A6	CREB, deltaCREB, CUTL1, POU2F1, POU2F1a, Ik-1, SREBP-1c, SREBP-1a, SREBP-1b, HTF
r1814	Y+LAT2 Utilized transport	Transport, extracellular	na1[e] + leu_L[e] + tyr_L[c] -> na1[c] + tyr_L[e] + leu_L[c]	SLC7A6	CREB, deltaCREB, CUTL1, POU2F1, POU2F1a, Ik-1, SREBP-1c, SREBP-1a, SREBP-1b, HTF
r1815	Y+LAT2 Utilized transport	Transport, extracellular	na1[e] + cys_L[c] + leu_L[e] -> na1[c] + cys_L[e] + leu_L[c]	SLC7A6	CREB, deltaCREB, CUTL1, POU2F1, POU2F1a, Ik-1, SREBP-1c, SREBP-1a, SREBP-1b, HTF
r1816	Y+LAT2 Utilized transport	Transport, extracellular	na1[e] + leu_L[e] + pro_L[c] -> na1[c] + pro_L[e] + leu_L[c]	SLC7A6	CREB, deltaCREB, CUTL1, POU2F1, POU2F1a, Ik-1, SREBP-1c, SREBP-1a, SREBP-1b, HTF
r1817	Y+LAT2 Utilized transport	Transport, extracellular	na1[e] + asn_L[c] + leu_L[e] -> na1[c] + asn_L[e] + leu_L[c]	SLC7A6	CREB, deltaCREB, CUTL1, POU2F1, POU2F1a, Ik-1, SREBP-1c, SREBP-1a, SREBP-1b, HTF
r1818	Y+LAT2 Utilized transport	Transport, extracellular	na1[e] + leu_L[e] + val_L[c] -> na1[c] + val_L[e] + leu_L[c]	SLC7A6	CREB, deltaCREB, CUTL1, POU2F1, POU2F1a, Ik-1, SREBP-1c, SREBP-1a, SREBP-1b, HTF

r1819	Y+LAT2 Utilized transport	Transport, extracellular	na1[e] + thr_L[c] + leu_L[e] -> na1[c] + thr_L[e] + leu_L[c]	SLC7A6	CREB, deltaCREB, CUTL1, POU2F1, POU2F1a, Ik-1, SREBP-1c, SREBP-1a, SREBP-1b, HTF
r1820	Y+LAT2 Utilized transport	Transport, extracellular	na1[e] + leu_L[e] + hom_L[c] -> na1[c] + hom_L[e] + leu_L[c]	SLC7A6	CREB, deltaCREB, CUTL1, POU2F1, POU2F1a, Ik-1, SREBP-1c, SREBP-1a, SREBP-1b, HTF
r1822	Y+LAT2 Utilized transport	Transport, extracellular	na1[e] + gly[c] + pro_L[e] -> na1[c] + gly[e] + pro_L[c]	SLC7A6	CREB, deltaCREB, CUTL1, POU2F1, POU2F1a, Ik-1, SREBP-1c, SREBP-1a, SREBP-1b, HTF
r1824	Y+LAT2 Utilized transport	Transport, extracellular	na1[e] + gln_L[c] + pro_L[e] -> na1[c] + gln_L[e] + pro_L[c]	SLC7A6	CREB, deltaCREB, CUTL1, POU2F1, POU2F1a, Ik-1, SREBP-1c, SREBP-1a, SREBP-1b, HTF
r1825	Y+LAT2 Utilized transport	Transport, extracellular	na1[e] + ser_L[c] + pro_L[e] -> na1[c] + ser_L[e] + pro_L[c]	SLC7A6	CREB, deltaCREB, CUTL1, POU2F1, POU2F1a, Ik-1, SREBP-1c, SREBP-1a, SREBP-1b, HTF
r1826	Y+LAT2 Utilized transport	Transport, extracellular	na1[e] + met_L[c] + pro_L[e] -> na1[c] + met_L[e] + pro_L[c]	SLC7A6	CREB, deltaCREB, CUTL1, POU2F1, POU2F1a, Ik-1, SREBP-1c, SREBP-1a, SREBP-1b, HTF
r1827	Y+LAT2 Utilized transport	Transport, extracellular	na1[e] + pro_L[e] + trp_L[c] -> na1[c] + trp_L[e] + pro_L[c]	SLC7A6	CREB, deltaCREB, CUTL1, POU2F1, POU2F1a, Ik-1, SREBP-1c, SREBP-1a, SREBP-1b, HTF
r1828	Y+LAT2 Utilized transport	Transport, extracellular	na1[e] + pro_L[e] + phe_L[c] -> na1[c] + phe_L[e] + pro_L[c]	SLC7A6	CREB, deltaCREB, CUTL1, POU2F1, POU2F1a, Ik-1, SREBP-1c, SREBP-1a, SREBP-1b, HTF
r1829	Y+LAT2 Utilized transport	Transport, extracellular	na1[e] + pro_L[e] + tyr_L[c] -> na1[c] + tyr_L[e] + pro_L[c]	SLC7A6	CREB, deltaCREB, CUTL1, POU2F1, POU2F1a, Ik-1, SREBP-1c, SREBP-1a, SREBP-1b, HTF
r1830	Y+LAT2 Utilized transport	Transport, extracellular	na1[e] + cys_L[c] + pro_L[e] -> na1[c] + cys_L[e] + pro_L[c]	SLC7A6	CREB, deltaCREB, CUTL1, POU2F1, POU2F1a, Ik-1, SREBP-1c, SREBP-1a, SREBP-1b, HTF
r1831	Y+LAT2 Utilized transport	Transport, extracellular	na1[e] + pro_L[e] + leu_L[c] -> na1[c] + leu_L[e] + pro_L[c]	SLC7A6	CREB, deltaCREB, CUTL1, POU2F1, POU2F1a, Ik-1, SREBP-1c, SREBP-1a, SREBP-1b, HTF
r1832	Y+LAT2 Utilized transport	Transport, extracellular	na1[e] + asn_L[c] + pro_L[e] -> na1[c] + asn_L[e] + pro_L[c]	SLC7A6	CREB, deltaCREB, CUTL1, POU2F1, POU2F1a, Ik-1, SREBP-1c, SREBP-1a, SREBP-1b, HTF
r1833	Y+LAT2 Utilized transport	Transport, extracellular	na1[e] + pro_L[e] + val_L[c] -> na1[c] + val_L[e] + pro_L[c]	SLC7A6	CREB, deltaCREB, CUTL1, POU2F1, POU2F1a, Ik-1, SREBP-1c, SREBP-1a, SREBP-1b, HTF
r1836	Y+LAT2 Utilized transport	Transport, extracellular	na1[e] + pro_L[e] + ile_L[c] -> na1[c] + ile_L[e] + pro_L[c]	SLC7A6	CREB, deltaCREB, CUTL1, POU2F1, POU2F1a, Ik-1, SREBP-1c, SREBP-1a, SREBP-1b, HTF
r1837	Y+LAT2 Utilized transport	Transport, extracellular	na1[e] + asn_L[e] + gly[c] -> na1[c] + asn_L[c] + gly[e]	SLC7A6	CREB, deltaCREB, CUTL1, POU2F1, POU2F1a, Ik-1, SREBP-1c, SREBP-1a, SREBP-1b, HTF
r1841	Y+LAT2 Utilized transport	Transport, extracellular	na1[e] + asn_L[e] + met_L[c] -> na1[c] + asn_L[c] + met_L[e]	SLC7A6	CREB, deltaCREB, CUTL1, POU2F1, POU2F1a, Ik-1, SREBP-1c, SREBP-1a, SREBP-1b, HTF
r1842	Y+LAT2 Utilized transport	Transport, extracellular	na1[e] + asn_L[e] + trp_L[c] -> na1[c] + asn_L[c] + trp_L[e]	SLC7A6	CREB, deltaCREB, CUTL1, POU2F1, POU2F1a, Ik-1, SREBP-1c, SREBP-1a, SREBP-1b, HTF
r1843	Y+LAT2 Utilized transport	Transport, extracellular	na1[e] + asn_L[e] + phe_L[c] -> na1[c] + asn_L[c] + phe_L[e]	SLC7A6	CREB, deltaCREB, CUTL1, POU2F1, POU2F1a, Ik-1, SREBP-1c, SREBP-1a, SREBP-1b, HTF

r1844	Y+LAT2 Utilized transport	Transport, extracellular	na1[e] + asn_L[e] + tyr_L[c] -> na1[c] + asn_L[c] + tyr_L[e]	SLC7A6	CREB, deltaCREB, CUTL1, POU2F1, POU2F1a, Ik-1, SREBP-1c, SREBP-1a, SREBP-1b, HTF
r1846	Y+LAT2 Utilized transport	Transport, extracellular	na1[e] + asn_L[e] + leu_L[c] -> na1[c] + asn_L[c] + leu_L[e]	SLC7A6	CREB, deltaCREB, CUTL1, POU2F1, POU2F1a, Ik-1, SREBP-1c, SREBP-1a, SREBP-1b, HTF
r1847	Y+LAT2 Utilized transport	Transport, extracellular	na1[e] + asn_L[e] + pro_L[c] -> na1[c] + asn_L[c] + pro_L[e]	SLC7A6	CREB, deltaCREB, CUTL1, POU2F1, POU2F1a, Ik-1, SREBP-1c, SREBP-1a, SREBP-1b, HTF
r1848	Y+LAT2 Utilized transport	Transport, extracellular	na1[e] + asn_L[e] + val_L[c] -> na1[c] + asn_L[c] + val_L[e]	SLC7A6	CREB, deltaCREB, CUTL1, POU2F1, POU2F1a, Ik-1, SREBP-1c, SREBP-1a, SREBP-1b, HTF
r1850	Y+LAT2 Utilized transport	Transport, extracellular	na1[e] + asn_L[e] + hom_L[c] -> na1[c] + asn_L[c] + hom_L[e]	SLC7A6	CREB, deltaCREB, CUTL1, POU2F1, POU2F1a, Ik-1, SREBP-1c, SREBP-1a, SREBP-1b, HTF
r1851	Y+LAT2 Utilized transport	Transport, extracellular	na1[e] + asn_L[e] + ile_L[c] -> na1[c] + asn_L[c] + ile_L[e]	SLC7A6	CREB, deltaCREB, CUTL1, POU2F1, POU2F1a, Ik-1, SREBP-1c, SREBP-1a, SREBP-1b, HTF
r1852	Y+LAT2 Utilized transport	Transport, extracellular	na1[e] + gly[c] + val_L[e] -> na1[c] + gly[e] + val_L[c]	SLC7A6	CREB, deltaCREB, CUTL1, POU2F1, POU2F1a, Ik-1, SREBP-1c, SREBP-1a, SREBP-1b, HTF
r1853	Y+LAT2 Utilized transport	Transport, extracellular	na1[e] + ala_L[c] + val_L[e] -> na1[c] + ala_L[e] + val_L[c]	SLC7A6	CREB, deltaCREB, CUTL1, POU2F1, POU2F1a, Ik-1, SREBP-1c, SREBP-1a, SREBP-1b, HTF
r1854	Y+LAT2 Utilized transport	Transport, extracellular	na1[e] + gln_L[c] + val_L[e] -> na1[c] + gln_L[e] + val_L[c]	SLC7A6	CREB, deltaCREB, CUTL1, POU2F1, POU2F1a, Ik-1, SREBP-1c, SREBP-1a, SREBP-1b, HTF
r1855	Y+LAT2 Utilized transport	Transport, extracellular	na1[e] + ser_L[c] + val_L[e] -> na1[c] + ser_L[e] + val_L[c]	SLC7A6	CREB, deltaCREB, CUTL1, POU2F1, POU2F1a, Ik-1, SREBP-1c, SREBP-1a, SREBP-1b, HTF
r1856	Y+LAT2 Utilized transport	Transport, extracellular	na1[e] + met_L[c] + val_L[e] -> na1[c] + met_L[e] + val_L[c]	SLC7A6	CREB, deltaCREB, CUTL1, POU2F1, POU2F1a, Ik-1, SREBP-1c, SREBP-1a, SREBP-1b, HTF
r1857	Y+LAT2 Utilized transport	Transport, extracellular	na1[e] + val_L[e] + trp_L[c] -> na1[c] + trp_L[e] + val_L[c]	SLC7A6	CREB, deltaCREB, CUTL1, POU2F1, POU2F1a, Ik-1, SREBP-1c, SREBP-1a, SREBP-1b, HTF
r1858	Y+LAT2 Utilized transport	Transport, extracellular	na1[e] + val_L[e] + phe_L[c] -> na1[c] + phe_L[e] + val_L[c]	SLC7A6	CREB, deltaCREB, CUTL1, POU2F1, POU2F1a, Ik-1, SREBP-1c, SREBP-1a, SREBP-1b, HTF
r1859	Y+LAT2 Utilized transport	Transport, extracellular	na1[e] + val_L[e] + tyr_L[c] -> na1[c] + tyr_L[e] + val_L[c]	SLC7A6	CREB, deltaCREB, CUTL1, POU2F1, POU2F1a, Ik-1, SREBP-1c, SREBP-1a, SREBP-1b, HTF
r1860	Y+LAT2 Utilized transport	Transport, extracellular	na1[e] + cys_L[c] + val_L[e] -> na1[c] + cys_L[e] + val_L[c]	SLC7A6	CREB, deltaCREB, CUTL1, POU2F1, POU2F1a, Ik-1, SREBP-1c, SREBP-1a, SREBP-1b, HTF
r1861	Y+LAT2 Utilized transport	Transport, extracellular	na1[e] + val_L[e] + leu_L[c] -> na1[c] + leu_L[e] + val_L[c]	SLC7A6	CREB, deltaCREB, CUTL1, POU2F1, POU2F1a, Ik-1, SREBP-1c, SREBP-1a, SREBP-1b, HTF
r1862	Y+LAT2 Utilized transport	Transport, extracellular	na1[e] + val_L[e] + pro_L[c] -> na1[c] + pro_L[e] + val_L[c]	SLC7A6	CREB, deltaCREB, CUTL1, POU2F1, POU2F1a, Ik-1, SREBP-1c, SREBP-1a, SREBP-1b, HTF
r1863	Y+LAT2 Utilized transport	Transport, extracellular	na1[e] + asn_L[c] + val_L[e] -> na1[c] + asn_L[e] + val_L[c]	SLC7A6	CREB, deltaCREB, CUTL1, POU2F1, POU2F1a, Ik-1, SREBP-1c, SREBP-1a, SREBP-1b, HTF

r1864	Y+LAT2 Utilized transport	Transport, extracellular	na1[e] + thr_L[c] + val_L[e] -> na1[c] + thr_L[e] + val_L[c]	SLC7A6	CREB, deltaCREB, CUTL1, POU2F1, POU2F1a, Ik-1, SREBP-1c, SREBP-1a, SREBP-1b, HTF
r1865	Y+LAT2 Utilized transport	Transport, extracellular	na1[e] + val_L[e] + hom_L[c] -> na1[c] + hom_L[e] + val_L[c]	SLC7A6	CREB, deltaCREB, CUTL1, POU2F1, POU2F1a, Ik-1, SREBP-1c, SREBP-1a, SREBP-1b, HTF
r1866	Y+LAT2 Utilized transport	Transport, extracellular	na1[e] + val_L[e] + ile_L[c] -> na1[c] + ile_L[e] + val_L[c]	SLC7A6	CREB, deltaCREB, CUTL1, POU2F1, POU2F1a, Ik-1, SREBP-1c, SREBP-1a, SREBP-1b, HTF
r1867	Y+LAT2 Utilized transport	Transport, extracellular	na1[e] + gly[c] + thr_L[e] -> na1[c] + gly[e] + thr_L[c]	SLC7A6	CREB, deltaCREB, CUTL1, POU2F1, POU2F1a, Ik-1, SREBP-1c, SREBP-1a, SREBP-1b, HTF
r1871	Y+LAT2 Utilized transport	Transport, extracellular	na1[e] + thr_L[e] + met_L[c] -> na1[c] + thr_L[c] + met_L[e]	SLC7A6	CREB, deltaCREB, CUTL1, POU2F1, POU2F1a, Ik-1, SREBP-1c, SREBP-1a, SREBP-1b, HTF
r1874	Y+LAT2 Utilized transport	Transport, extracellular	na1[e] + thr_L[e] + tyr_L[c] -> na1[c] + thr_L[c] + tyr_L[e]	SLC7A6	CREB, deltaCREB, CUTL1, POU2F1, POU2F1a, Ik-1, SREBP-1c, SREBP-1a, SREBP-1b, HTF
r1876	Y+LAT2 Utilized transport	Transport, extracellular	na1[e] + thr_L[e] + leu_L[c] -> na1[c] + thr_L[c] + leu_L[e]	SLC7A6	CREB, deltaCREB, CUTL1, POU2F1, POU2F1a, Ik-1, SREBP-1c, SREBP-1a, SREBP-1b, HTF
r1877	Y+LAT2 Utilized transport	Transport, extracellular	na1[e] + thr_L[e] + pro_L[c] -> na1[c] + thr_L[c] + pro_L[e]	SLC7A6	CREB, deltaCREB, CUTL1, POU2F1, POU2F1a, Ik-1, SREBP-1c, SREBP-1a, SREBP-1b, HTF
r1879	Y+LAT2 Utilized transport	Transport, extracellular	na1[e] + thr_L[e] + val_L[c] -> na1[c] + thr_L[c] + val_L[e]	SLC7A6	CREB, deltaCREB, CUTL1, POU2F1, POU2F1a, Ik-1, SREBP-1c, SREBP-1a, SREBP-1b, HTF
r1880	Y+LAT2 Utilized transport	Transport, extracellular	na1[e] + thr_L[e] + hom_L[c] -> na1[c] + thr_L[c] + hom_L[e]	SLC7A6	CREB, deltaCREB, CUTL1, POU2F1, POU2F1a, Ik-1, SREBP-1c, SREBP-1a, SREBP-1b, HTF
r1881	Y+LAT2 Utilized transport	Transport, extracellular	na1[e] + thr_L[e] + ile_L[c] -> na1[c] + thr_L[c] + ile_L[e]	SLC7A6	CREB, deltaCREB, CUTL1, POU2F1, POU2F1a, Ik-1, SREBP-1c, SREBP-1a, SREBP-1b, HTF
r1882	Y+LAT2 Utilized transport	Transport, extracellular	na1[e] + gly[c] + hom_L[e] -> na1[c] + gly[e] + hom_L[c]	SLC7A6	CREB, deltaCREB, CUTL1, POU2F1, POU2F1a, Ik-1, SREBP-1c, SREBP-1a, SREBP-1b, HTF
r1883	Y+LAT2 Utilized transport	Transport, extracellular	na1[e] + ala_L[c] + hom_L[e] -> na1[c] + ala_L[e] + hom_L[c]	SLC7A6	CREB, deltaCREB, CUTL1, POU2F1, POU2F1a, Ik-1, SREBP-1c, SREBP-1a, SREBP-1b, HTF
r1884	Y+LAT2 Utilized transport	Transport, extracellular	na1[e] + gln_L[c] + hom_L[e] -> na1[c] + gln_L[e] + hom_L[c]	SLC7A6	CREB, deltaCREB, CUTL1, POU2F1, POU2F1a, Ik-1, SREBP-1c, SREBP-1a, SREBP-1b, HTF
r1885	Y+LAT2 Utilized transport	Transport, extracellular	na1[e] + ser_L[c] + hom_L[e] -> na1[c] + ser_L[e] + hom_L[c]	SLC7A6	CREB, deltaCREB, CUTL1, POU2F1, POU2F1a, Ik-1, SREBP-1c, SREBP-1a, SREBP-1b, HTF
r1886	Y+LAT2 Utilized transport	Transport, extracellular	na1[e] + met_L[c] + hom_L[e] -> na1[c] + met_L[e] + hom_L[c]	SLC7A6	CREB, deltaCREB, CUTL1, POU2F1, POU2F1a, Ik-1, SREBP-1c, SREBP-1a, SREBP-1b, HTF
r1887	Y+LAT2 Utilized transport	Transport, extracellular	na1[e] + hom_L[e] + trp_L[c] -> na1[c] + trp_L[e] + hom_L[c]	SLC7A6	CREB, deltaCREB, CUTL1, POU2F1, POU2F1a, Ik-1, SREBP-1c, SREBP-1a, SREBP-1b, HTF
r1888	Y+LAT2 Utilized transport	Transport, extracellular	na1[e] + hom_L[e] + phe_L[c] -> na1[c] + phe_L[e] + hom_L[c]	SLC7A6	CREB, deltaCREB, CUTL1, POU2F1, POU2F1a, Ik-1, SREBP-1c, SREBP-1a, SREBP-1b, HTF

r1889	Y+LAT2 Utilized transport	Transport, extracellular	na1[e] + hom_L[e] + tyr_L[c] -> na1[c] + tyr_L[e] + hom_L[c]	SLC7A6	CREB, deltaCREB, CUTL1, POU2F1, POU2F1a, Ik-1, SREBP-1c, SREBP-1a, SREBP-1b, HTF
r1890	Y+LAT2 Utilized transport	Transport, extracellular	na1[e] + cys_L[c] + hom_L[e] -> na1[c] + cys_L[e] + hom_L[c]	SLC7A6	CREB, deltaCREB, CUTL1, POU2F1, POU2F1a, Ik-1, SREBP-1c, SREBP-1a, SREBP-1b, HTF
r1891	Y+LAT2 Utilized transport	Transport, extracellular	na1[e] + hom_L[e] + leu_L[c] -> na1[c] + leu_L[e] + hom_L[c]	SLC7A6	CREB, deltaCREB, CUTL1, POU2F1, POU2F1a, Ik-1, SREBP-1c, SREBP-1a, SREBP-1b, HTF
r1892	Y+LAT2 Utilized transport	Transport, extracellular	na1[e] + hom_L[e] + pro_L[c] -> na1[c] + pro_L[e] + hom_L[c]	SLC7A6	CREB, deltaCREB, CUTL1, POU2F1, POU2F1a, Ik-1, SREBP-1c, SREBP-1a, SREBP-1b, HTF
r1893	Y+LAT2 Utilized transport	Transport, extracellular	na1[e] + asn_L[c] + hom_L[e] -> na1[c] + asn_L[e] + hom_L[c]	SLC7A6	CREB, deltaCREB, CUTL1, POU2F1, POU2F1a, Ik-1, SREBP-1c, SREBP-1a, SREBP-1b, HTF
r1894	Y+LAT2 Utilized transport	Transport, extracellular	na1[e] + hom_L[e] + val_L[c] -> na1[c] + val_L[e] + hom_L[c]	SLC7A6	CREB, deltaCREB, CUTL1, POU2F1, POU2F1a, Ik-1, SREBP-1c, SREBP-1a, SREBP-1b, HTF
r1895	Y+LAT2 Utilized transport	Transport, extracellular	na1[e] + thr_L[c] + hom_L[e] -> na1[c] + thr_L[e] + hom_L[c]	SLC7A6	CREB, deltaCREB, CUTL1, POU2F1, POU2F1a, Ik-1, SREBP-1c, SREBP-1a, SREBP-1b, HTF
r1896	Y+LAT2 Utilized transport	Transport, extracellular	na1[e] + hom_L[e] + ile_L[c] -> na1[c] + ile_L[e] + hom_L[c]	SLC7A6	CREB, deltaCREB, CUTL1, POU2F1, POU2F1a, Ik-1, SREBP-1c, SREBP-1a, SREBP-1b, HTF
r1897	Y+LAT2 Utilized transport	Transport, extracellular	na1[e] + gly[c] + ile_L[e] -> na1[c] + gly[e] + ile_L[c]	SLC7A6	CREB, deltaCREB, CUTL1, POU2F1, POU2F1a, Ik-1, SREBP-1c, SREBP-1a, SREBP-1b, HTF
r1898	Y+LAT2 Utilized transport	Transport, extracellular	na1[e] + ala_L[c] + ile_L[e] -> na1[c] + ala_L[e] + ile_L[c]	SLC7A6	CREB, deltaCREB, CUTL1, POU2F1, POU2F1a, Ik-1, SREBP-1c, SREBP-1a, SREBP-1b, HTF
r1899	Y+LAT2 Utilized transport	Transport, extracellular	na1[e] + gln_L[c] + ile_L[e] -> na1[c] + gln_L[e] + ile_L[c]	SLC7A6	CREB, deltaCREB, CUTL1, POU2F1, POU2F1a, Ik-1, SREBP-1c, SREBP-1a, SREBP-1b, HTF
r1900	Y+LAT2 Utilized transport	Transport, extracellular	na1[e] + ser_L[c] + ile_L[e] -> na1[c] + ser_L[e] + ile_L[c]	SLC7A6	CREB, deltaCREB, CUTL1, POU2F1, POU2F1a, Ik-1, SREBP-1c, SREBP-1a, SREBP-1b, HTF
r1902	Y+LAT2 Utilized transport	Transport, extracellular	na1[e] + ile_L[e] + trp_L[c] -> na1[c] + trp_L[e] + ile_L[c]	SLC7A6	CREB, deltaCREB, CUTL1, POU2F1, POU2F1a, Ik-1, SREBP-1c, SREBP-1a, SREBP-1b, HTF
r1904	Y+LAT2 Utilized transport	Transport, extracellular	na1[e] + ile_L[e] + tyr_L[c] -> na1[c] + tyr_L[e] + ile_L[c]	SLC7A6	CREB, deltaCREB, CUTL1, POU2F1, POU2F1a, Ik-1, SREBP-1c, SREBP-1a, SREBP-1b, HTF
r1905	Y+LAT2 Utilized transport	Transport, extracellular	na1[e] + cys_L[c] + ile_L[e] -> na1[c] + cys_L[e] + ile_L[c]	SLC7A6	CREB, deltaCREB, CUTL1, POU2F1, POU2F1a, Ik-1, SREBP-1c, SREBP-1a, SREBP-1b, HTF
r1906	Y+LAT2 Utilized transport	Transport, extracellular	na1[e] + ile_L[e] + leu_L[c] -> na1[c] + leu_L[e] + ile_L[c]	SLC7A6	CREB, deltaCREB, CUTL1, POU2F1, POU2F1a, Ik-1, SREBP-1c, SREBP-1a, SREBP-1b, HTF
r1907	Y+LAT2 Utilized transport	Transport, extracellular	na1[e] + ile_L[e] + pro_L[c] -> na1[c] + pro_L[e] + ile_L[c]	SLC7A6	CREB, deltaCREB, CUTL1, POU2F1, POU2F1a, Ik-1, SREBP-1c, SREBP-1a, SREBP-1b, HTF
r1908	Y+LAT2 Utilized transport	Transport, extracellular	na1[e] + asn_L[c] + ile_L[e] -> na1[c] + asn_L[e] + ile_L[c]	SLC7A6	CREB, deltaCREB, CUTL1, POU2F1, POU2F1a, Ik-1, SREBP-1c, SREBP-1a, SREBP-1b, HTF

r1909	Y+LAT2 Utilized transport	Transport, extracellular	na1[e] + ile_L[e] + val_L[c] -> na1[c] + val_L[e] + ile_L[c]	SLC7A6	CREB, deltaCREB, CUTL1, POU2F1, POU2F1a, Ik-1, SREBP-1c, SREBP-1a, SREBP-1b, HTF
r1910	Y+LAT2 Utilized transport	Transport, extracellular	na1[e] + thr_L[c] + ile_L[e] -> na1[c] + thr_L[e] + ile_L[c]	SLC7A6	CREB, deltaCREB, CUTL1, POU2F1, POU2F1a, Ik-1, SREBP-1c, SREBP-1a, SREBP-1b, HTF
r1911	Y+LAT2 Utilized transport	Transport, extracellular	na1[e] + ile_L[e] + hom_L[c] -> na1[c] + hom_L[e] + ile_L[c]	SLC7A6	CREB, deltaCREB, CUTL1, POU2F1, POU2F1a, Ik-1, SREBP-1c, SREBP-1a, SREBP-1b, HTF
r1912	Y+LAT2 Utilized transport	Transport, extracellular	na1[e] + gly[e] + lys_L[c] -> na1[c] + gly[c] + lys_L[e]	SLC7A6	CREB, deltaCREB, CUTL1, POU2F1, POU2F1a, Ik-1, SREBP-1c, SREBP-1a, SREBP-1b, HTF
r1913	Y+LAT2 Utilized transport	Transport, extracellular	na1[e] + gly[e] + arg_L[c] -> na1[c] + gly[c] + arg_L[e]	SLC7A6	CREB, deltaCREB, CUTL1, POU2F1, POU2F1a, Ik-1, SREBP-1c, SREBP-1a, SREBP-1b, HTF
r1915	Y+LAT2 Utilized transport	Transport, extracellular	na1[e] + gly[e] + his_L[c] -> na1[c] + gly[c] + his_L[e]	SLC7A6	CREB, deltaCREB, CUTL1, POU2F1, POU2F1a, Ik-1, SREBP-1c, SREBP-1a, SREBP-1b, HTF
r1917	Y+LAT2 Utilized transport	Transport, extracellular	na1[e] + ala_L[e] + lys_L[c] -> na1[c] + ala_L[c] + lys_L[e]	SLC7A6	CREB, deltaCREB, CUTL1, POU2F1, POU2F1a, Ik-1, SREBP-1c, SREBP-1a, SREBP-1b, HTF
r1918	Y+LAT2 Utilized transport	Transport, extracellular	na1[e] + ala_L[e] + arg_L[c] -> na1[c] + ala_L[c] + arg_L[e]	SLC7A6	CREB, deltaCREB, CUTL1, POU2F1, POU2F1a, Ik-1, SREBP-1c, SREBP-1a, SREBP-1b, HTF
r1922	Y+LAT2 Utilized transport	Transport, extracellular	na1[e] + gln_L[e] + lys_L[c] -> na1[c] + gln_L[c] + lys_L[e]	SLC7A6	CREB, deltaCREB, CUTL1, POU2F1, POU2F1a, Ik-1, SREBP-1c, SREBP-1a, SREBP-1b, HTF
r1923	Y+LAT2 Utilized transport	Transport, extracellular	na1[e] + gln_L[e] + arg_L[c] -> na1[c] + gln_L[c] + arg_L[e]	SLC7A6	CREB, deltaCREB, CUTL1, POU2F1, POU2F1a, Ik-1, SREBP-1c, SREBP-1a, SREBP-1b, HTF
r1924	Y+LAT2 Utilized transport	Transport, extracellular	na1[e] + orn[c] + gln_L[e] -> na1[c] + gln_L[c] + orn[e]	SLC7A6	CREB, deltaCREB, CUTL1, POU2F1, POU2F1a, Ik-1, SREBP-1c, SREBP-1a, SREBP-1b, HTF
r1925	Y+LAT2 Utilized transport	Transport, extracellular	na1[e] + gln_L[e] + his_L[c] -> na1[c] + gln_L[c] + his_L[e]	SLC7A6	CREB, deltaCREB, CUTL1, POU2F1, POU2F1a, Ik-1, SREBP-1c, SREBP-1a, SREBP-1b, HTF
r1926	Y+LAT2 Utilized transport	Transport, extracellular	na1[e] + gln_L[e] + citr_L[c] -> na1[c] + gln_L[c] + citr_L[e]	SLC7A6	CREB, deltaCREB, CUTL1, POU2F1, POU2F1a, Ik-1, SREBP-1c, SREBP-1a, SREBP-1b, HTF
r1928	Y+LAT2 Utilized transport	Transport, extracellular	na1[e] + ser_L[e] + arg_L[c] -> na1[c] + ser_L[c] + arg_L[e]	SLC7A6	CREB, deltaCREB, CUTL1, POU2F1, POU2F1a, Ik-1, SREBP-1c, SREBP-1a, SREBP-1b, HTF
r1930	Y+LAT2 Utilized transport	Transport, extracellular	na1[e] + ser_L[e] + his_L[c] -> na1[c] + ser_L[c] + his_L[e]	SLC7A6	CREB, deltaCREB, CUTL1, POU2F1, POU2F1a, Ik-1, SREBP-1c, SREBP-1a, SREBP-1b, HTF
r1931	Y+LAT2 Utilized transport	Transport, extracellular	na1[e] + ser_L[e] + citr_L[c] -> na1[c] + ser_L[c] + citr_L[e]	SLC7A6	CREB, deltaCREB, CUTL1, POU2F1, POU2F1a, Ik-1, SREBP-1c, SREBP-1a, SREBP-1b, HTF
r1932	Y+LAT2 Utilized transport	Transport, extracellular	na1[e] + lys_L[c] + met_L[e] -> na1[c] + lys_L[e] + met_L[c]	SLC7A6	CREB, deltaCREB, CUTL1, POU2F1, POU2F1a, Ik-1, SREBP-1c, SREBP-1a, SREBP-1b, HTF
r1934	Y+LAT2 Utilized transport	Transport, extracellular	na1[e] + orn[c] + met_L[e] -> na1[c] + met_L[c] + orn[e]	SLC7A6	CREB, deltaCREB, CUTL1, POU2F1, POU2F1a, Ik-1, SREBP-1c, SREBP-1a, SREBP-1b, HTF

r1935	Y+LAT2 Utilized transport	Transport, extracellular	na1[e] + met_L[e] + his_L[c] -> na1[c] + met_L[c] + his_L[e]	SLC7A6	CREB, deltaCREB, CUTL1, POU2F1, POU2F1a, Ik-1, SREBP-1c, SREBP-1a, SREBP-1b, HTF
r1936	Y+LAT2 Utilized transport	Transport, extracellular	na1[e] + citr_L[c] + met_L[e] -> na1[c] + met_L[c] + citr_L[e]	SLC7A6	CREB, deltaCREB, CUTL1, POU2F1, POU2F1a, Ik-1, SREBP-1c, SREBP-1a, SREBP-1b, HTF
r1937	Y+LAT2 Utilized transport	Transport, extracellular	na1[e] + lys_L[c] + trp_L[e] -> na1[c] + lys_L[e] + trp_L[c]	SLC7A6	CREB, deltaCREB, CUTL1, POU2F1, POU2F1a, Ik-1, SREBP-1c, SREBP-1a, SREBP-1b, HTF
r1938	Y+LAT2 Utilized transport	Transport, extracellular	na1[e] + arg_L[c] + trp_L[e] -> na1[c] + arg_L[e] + trp_L[c]	SLC7A6	CREB, deltaCREB, CUTL1, POU2F1, POU2F1a, Ik-1, SREBP-1c, SREBP-1a, SREBP-1b, HTF
r1939	Y+LAT2 Utilized transport	Transport, extracellular	na1[e] + orn[c] + trp_L[e] -> na1[c] + orn[e] + trp_L[c]	SLC7A6	CREB, deltaCREB, CUTL1, POU2F1, POU2F1a, Ik-1, SREBP-1c, SREBP-1a, SREBP-1b, HTF
r1940	Y+LAT2 Utilized transport	Transport, extracellular	na1[e] + trp_L[e] + his_L[c] -> na1[c] + his_L[e] + trp_L[c]	SLC7A6	CREB, deltaCREB, CUTL1, POU2F1, POU2F1a, Ik-1, SREBP-1c, SREBP-1a, SREBP-1b, HTF
r1941	Y+LAT2 Utilized transport	Transport, extracellular	na1[e] + citr_L[c] + trp_L[e] -> na1[c] + trp_L[c] + citr_L[e]	SLC7A6	CREB, deltaCREB, CUTL1, POU2F1, POU2F1a, Ik-1, SREBP-1c, SREBP-1a, SREBP-1b, HTF
r1942	Y+LAT2 Utilized transport	Transport, extracellular	na1[e] + lys_L[c] + phe_L[e] -> na1[c] + lys_L[e] + phe_L[c]	SLC7A6	CREB, deltaCREB, CUTL1, POU2F1, POU2F1a, Ik-1, SREBP-1c, SREBP-1a, SREBP-1b, HTF
r1943	Y+LAT2 Utilized transport	Transport, extracellular	na1[e] + arg_L[c] + phe_L[e] -> na1[c] + arg_L[e] + phe_L[c]	SLC7A6	CREB, deltaCREB, CUTL1, POU2F1, POU2F1a, Ik-1, SREBP-1c, SREBP-1a, SREBP-1b, HTF
r1944	Y+LAT2 Utilized transport	Transport, extracellular	na1[e] + orn[c] + phe_L[e] -> na1[c] + orn[e] + phe_L[c]	SLC7A6	CREB, deltaCREB, CUTL1, POU2F1, POU2F1a, Ik-1, SREBP-1c, SREBP-1a, SREBP-1b, HTF
r1945	Y+LAT2 Utilized transport	Transport, extracellular	na1[e] + phe_L[e] + his_L[c] -> na1[c] + his_L[e] + phe_L[c]	SLC7A6	CREB, deltaCREB, CUTL1, POU2F1, POU2F1a, Ik-1, SREBP-1c, SREBP-1a, SREBP-1b, HTF
r1946	Y+LAT2 Utilized transport	Transport, extracellular	na1[e] + citr_L[c] + phe_L[e] -> na1[c] + phe_L[c] + citr_L[e]	SLC7A6	CREB, deltaCREB, CUTL1, POU2F1, POU2F1a, Ik-1, SREBP-1c, SREBP-1a, SREBP-1b, HTF
r1947	Y+LAT2 Utilized transport	Transport, extracellular	na1[e] + lys_L[c] + tyr_L[e] -> na1[c] + lys_L[e] + tyr_L[c]	SLC7A6	CREB, deltaCREB, CUTL1, POU2F1, POU2F1a, Ik-1, SREBP-1c, SREBP-1a, SREBP-1b, HTF
r1948	Y+LAT2 Utilized transport	Transport, extracellular	na1[e] + arg_L[c] + tyr_L[e] -> na1[c] + arg_L[e] + tyr_L[c]	SLC7A6	CREB, deltaCREB, CUTL1, POU2F1, POU2F1a, Ik-1, SREBP-1c, SREBP-1a, SREBP-1b, HTF
r1949	Y+LAT2 Utilized transport	Transport, extracellular	na1[e] + orn[c] + tyr_L[e] -> na1[c] + orn[e] + tyr_L[c]	SLC7A6	CREB, deltaCREB, CUTL1, POU2F1, POU2F1a, Ik-1, SREBP-1c, SREBP-1a, SREBP-1b, HTF
r1950	Y+LAT2 Utilized transport	Transport, extracellular	na1[e] + tyr_L[e] + his_L[c] -> na1[c] + his_L[e] + tyr_L[c]	SLC7A6	CREB, deltaCREB, CUTL1, POU2F1, POU2F1a, Ik-1, SREBP-1c, SREBP-1a, SREBP-1b, HTF
r1951	Y+LAT2 Utilized transport	Transport, extracellular	na1[e] + citr_L[c] + tyr_L[e] -> na1[c] + tyr_L[c] + citr_L[e]	SLC7A6	CREB, deltaCREB, CUTL1, POU2F1, POU2F1a, Ik-1, SREBP-1c, SREBP-1a, SREBP-1b, HTF
r1952	Y+LAT2 Utilized transport	Transport, extracellular	na1[e] + cys_L[e] + lys_L[c] -> na1[c] + cys_L[c] + lys_L[e]	SLC7A6	CREB, deltaCREB, CUTL1, POU2F1, POU2F1a, Ik-1, SREBP-1c, SREBP-1a, SREBP-1b, HTF

r1953	Y+LAT2 Utilized transport	Transport, extracellular	na1[e] + cys_L[e] + arg_L[c] -> na1[c] + cys_L[c] + arg_L[e]	SLC7A6	CREB, deltaCREB, CUTL1, POU2F1, POU2F1a, Ik-1, SREBP-1c, SREBP-1a, SREBP-1b, HTF
r1954	Y+LAT2 Utilized transport	Transport, extracellular	na1[e] + orn[c] + cys_L[e] -> na1[c] + cys_L[c] + orn[e]	SLC7A6	CREB, deltaCREB, CUTL1, POU2F1, POU2F1a, Ik-1, SREBP-1c, SREBP-1a, SREBP-1b, HTF
r1955	Y+LAT2 Utilized transport	Transport, extracellular	na1[e] + cys_L[e] + his_L[c] -> na1[c] + cys_L[c] + his_L[e]	SLC7A6	CREB, deltaCREB, CUTL1, POU2F1, POU2F1a, Ik-1, SREBP-1c, SREBP-1a, SREBP-1b, HTF
r1956	Y+LAT2 Utilized transport	Transport, extracellular	na1[e] + cys_L[e] + citr_L[c] -> na1[c] + cys_L[c] + citr_L[e]	SLC7A6	CREB, deltaCREB, CUTL1, POU2F1, POU2F1a, Ik-1, SREBP-1c, SREBP-1a, SREBP-1b, HTF
r1957	Y+LAT2 Utilized transport	Transport, extracellular	na1[e] + lys_L[c] + leu_L[e] -> na1[c] + lys_L[e] + leu_L[c]	SLC7A6	CREB, deltaCREB, CUTL1, POU2F1, POU2F1a, Ik-1, SREBP-1c, SREBP-1a, SREBP-1b, HTF
r1958	Y+LAT2 Utilized transport	Transport, extracellular	na1[e] + arg_L[c] + leu_L[e] -> na1[c] + arg_L[e] + leu_L[c]	SLC7A6	CREB, deltaCREB, CUTL1, POU2F1, POU2F1a, Ik-1, SREBP-1c, SREBP-1a, SREBP-1b, HTF
r1959	Y+LAT2 Utilized transport	Transport, extracellular	na1[e] + orn[c] + leu_L[e] -> na1[c] + orn[e] + leu_L[c]	SLC7A6	CREB, deltaCREB, CUTL1, POU2F1, POU2F1a, Ik-1, SREBP-1c, SREBP-1a, SREBP-1b, HTF
r1960	Y+LAT2 Utilized transport	Transport, extracellular	na1[e] + leu_L[e] + his_L[c] -> na1[c] + his_L[e] + leu_L[c]	SLC7A6	CREB, deltaCREB, CUTL1, POU2F1, POU2F1a, Ik-1, SREBP-1c, SREBP-1a, SREBP-1b, HTF
r1961	Y+LAT2 Utilized transport	Transport, extracellular	na1[e] + citr_L[c] + leu_L[e] -> na1[c] + leu_L[c] + citr_L[e]	SLC7A6	CREB, deltaCREB, CUTL1, POU2F1, POU2F1a, Ik-1, SREBP-1c, SREBP-1a, SREBP-1b, HTF
r1962	Y+LAT2 Utilized transport	Transport, extracellular	na1[e] + lys_L[c] + pro_L[e] -> na1[c] + lys_L[e] + pro_L[c]	SLC7A6	CREB, deltaCREB, CUTL1, POU2F1, POU2F1a, Ik-1, SREBP-1c, SREBP-1a, SREBP-1b, HTF
r1965	Y+LAT2 Utilized transport	Transport, extracellular	na1[e] + pro_L[e] + his_L[c] -> na1[c] + his_L[e] + pro_L[c]	SLC7A6	CREB, deltaCREB, CUTL1, POU2F1, POU2F1a, Ik-1, SREBP-1c, SREBP-1a, SREBP-1b, HTF
r1966	Y+LAT2 Utilized transport	Transport, extracellular	na1[e] + citr_L[c] + pro_L[e] -> na1[c] + pro_L[c] + citr_L[e]	SLC7A6	CREB, deltaCREB, CUTL1, POU2F1, POU2F1a, Ik-1, SREBP-1c, SREBP-1a, SREBP-1b, HTF
r1968	Y+LAT2 Utilized transport	Transport, extracellular	na1[e] + asn_L[e] + arg_L[c] -> na1[c] + asn_L[c] + arg_L[e]	SLC7A6	CREB, deltaCREB, CUTL1, POU2F1, POU2F1a, Ik-1, SREBP-1c, SREBP-1a, SREBP-1b, HTF
r1969	Y+LAT2 Utilized transport	Transport, extracellular	na1[e] + orn[c] + asn_L[e] -> na1[c] + asn_L[c] + orn[e]	SLC7A6	CREB, deltaCREB, CUTL1, POU2F1, POU2F1a, Ik-1, SREBP-1c, SREBP-1a, SREBP-1b, HTF
r1970	Y+LAT2 Utilized transport	Transport, extracellular	na1[e] + asn_L[e] + his_L[c] -> na1[c] + asn_L[c] + his_L[e]	SLC7A6	CREB, deltaCREB, CUTL1, POU2F1, POU2F1a, Ik-1, SREBP-1c, SREBP-1a, SREBP-1b, HTF
r1971	Y+LAT2 Utilized transport	Transport, extracellular	na1[e] + asn_L[e] + citr_L[c] -> na1[c] + asn_L[c] + citr_L[e]	SLC7A6	CREB, deltaCREB, CUTL1, POU2F1, POU2F1a, Ik-1, SREBP-1c, SREBP-1a, SREBP-1b, HTF
r1972	Y+LAT2 Utilized transport	Transport, extracellular	na1[e] + lys_L[c] + val_L[e] -> na1[c] + lys_L[e] + val_L[c]	SLC7A6	CREB, deltaCREB, CUTL1, POU2F1, POU2F1a, Ik-1, SREBP-1c, SREBP-1a, SREBP-1b, HTF
r1973	Y+LAT2 Utilized transport	Transport, extracellular	na1[e] + arg_L[c] + val_L[e] -> na1[c] + arg_L[e] + val_L[c]	SLC7A6	CREB, deltaCREB, CUTL1, POU2F1, POU2F1a, Ik-1, SREBP-1c, SREBP-1a, SREBP-1b, HTF

r1974	Y+LAT2 Utilized transport	Transport, extracellular	na1[e] + orn[c] + val_L[e] -> na1[c] + orn[e] + val_L[c]	SLC7A6	CREB, deltaCREB, CUTL1, POU2F1, POU2F1a, Ik-1, SREBP-1c, SREBP-1a, SREBP-1b, HTF
r1975	Y+LAT2 Utilized transport	Transport, extracellular	na1[e] + val_L[e] + his_L[c] -> na1[c] + his_L[e] + val_L[c]	SLC7A6	CREB, deltaCREB, CUTL1, POU2F1, POU2F1a, Ik-1, SREBP-1c, SREBP-1a, SREBP-1b, HTF
r1976	Y+LAT2 Utilized transport	Transport, extracellular	na1[e] + citr_L[c] + val_L[e] -> na1[c] + citr_L[e] + val_L[c]	SLC7A6	CREB, deltaCREB, CUTL1, POU2F1, POU2F1a, Ik-1, SREBP-1c, SREBP-1a, SREBP-1b, HTF
r1977	Y+LAT2 Utilized transport	Transport, extracellular	na1[e] + thr_L[e] + lys_L[c] -> na1[c] + thr_L[c] + lys_L[e]	SLC7A6	CREB, deltaCREB, CUTL1, POU2F1, POU2F1a, Ik-1, SREBP-1c, SREBP-1a, SREBP-1b, HTF
r1978	Y+LAT2 Utilized transport	Transport, extracellular	na1[e] + thr_L[e] + arg_L[c] -> na1[c] + thr_L[c] + arg_L[e]	SLC7A6	CREB, deltaCREB, CUTL1, POU2F1, POU2F1a, Ik-1, SREBP-1c, SREBP-1a, SREBP-1b, HTF
r1979	Y+LAT2 Utilized transport	Transport, extracellular	na1[e] + orn[c] + thr_L[e] -> na1[c] + thr_L[c] + orn[e]	SLC7A6	CREB, deltaCREB, CUTL1, POU2F1, POU2F1a, Ik-1, SREBP-1c, SREBP-1a, SREBP-1b, HTF
r1980	Y+LAT2 Utilized transport	Transport, extracellular	na1[e] + thr_L[e] + his_L[c] -> na1[c] + thr_L[c] + his_L[e]	SLC7A6	CREB, deltaCREB, CUTL1, POU2F1, POU2F1a, Ik-1, SREBP-1c, SREBP-1a, SREBP-1b, HTF
r1981	Y+LAT2 Utilized transport	Transport, extracellular	na1[e] + thr_L[e] + citr_L[c] -> na1[c] + thr_L[c] + citr_L[e]	SLC7A6	CREB, deltaCREB, CUTL1, POU2F1, POU2F1a, Ik-1, SREBP-1c, SREBP-1a, SREBP-1b, HTF
r1982	Y+LAT2 Utilized transport	Transport, extracellular	na1[e] + lys_L[c] + hom_L[e] -> na1[c] + lys_L[e] + hom_L[c]	SLC7A6	CREB, deltaCREB, CUTL1, POU2F1, POU2F1a, Ik-1, SREBP-1c, SREBP-1a, SREBP-1b, HTF
r1983	Y+LAT2 Utilized transport	Transport, extracellular	na1[e] + arg_L[c] + hom_L[e] -> na1[c] + arg_L[e] + hom_L[c]	SLC7A6	CREB, deltaCREB, CUTL1, POU2F1, POU2F1a, Ik-1, SREBP-1c, SREBP-1a, SREBP-1b, HTF
r1984	Y+LAT2 Utilized transport	Transport, extracellular	na1[e] + orn[c] + hom_L[e] -> na1[c] + orn[e] + hom_L[c]	SLC7A6	CREB, deltaCREB, CUTL1, POU2F1, POU2F1a, Ik-1, SREBP-1c, SREBP-1a, SREBP-1b, HTF
r1985	Y+LAT2 Utilized transport	Transport, extracellular	na1[e] + hom_L[e] + his_L[c] -> na1[c] + his_L[e] + hom_L[c]	SLC7A6	CREB, deltaCREB, CUTL1, POU2F1, POU2F1a, Ik-1, SREBP-1c, SREBP-1a, SREBP-1b, HTF
r1986	Y+LAT2 Utilized transport	Transport, extracellular	na1[e] + citr_L[c] + hom_L[e] -> na1[c] + hom_L[c] + citr_L[e]	SLC7A6	CREB, deltaCREB, CUTL1, POU2F1, POU2F1a, Ik-1, SREBP-1c, SREBP-1a, SREBP-1b, HTF
r1987	Y+LAT2 Utilized transport	Transport, extracellular	na1[e] + lys_L[c] + ile_L[e] -> na1[c] + lys_L[e] + ile_L[c]	SLC7A6	CREB, deltaCREB, CUTL1, POU2F1, POU2F1a, Ik-1, SREBP-1c, SREBP-1a, SREBP-1b, HTF
r1988	Y+LAT2 Utilized transport	Transport, extracellular	na1[e] + arg_L[c] + ile_L[e] -> na1[c] + arg_L[e] + ile_L[c]	SLC7A6	CREB, deltaCREB, CUTL1, POU2F1, POU2F1a, Ik-1, SREBP-1c, SREBP-1a, SREBP-1b, HTF
r1990	Y+LAT2 Utilized transport	Transport, extracellular	na1[e] + ile_L[e] + his_L[c] -> na1[c] + his_L[e] + ile_L[c]	SLC7A6	CREB, deltaCREB, CUTL1, POU2F1, POU2F1a, Ik-1, SREBP-1c, SREBP-1a, SREBP-1b, HTF
r1991	Y+LAT2 Utilized transport	Transport, extracellular	na1[e] + citr_L[c] + ile_L[e] -> na1[c] + ile_L[c] + citr_L[e]	SLC7A6	CREB, deltaCREB, CUTL1, POU2F1, POU2F1a, Ik-1, SREBP-1c, SREBP-1a, SREBP-1b, HTF
r2326	Resistance-Nodulation-Cell Division (RND) TCDB:2.A.60.1.2	Transport, extracellular	hco3[c] + gthrd[c] + prostgd2[e] <=> hco3[e] + gthrd[e] + prostgd2[c]	SLCO2A1	Pax-5, GCNF, GCNF-1, GCNF-2, FOXD1, Gfi-1, Pax-4a, AREB6, STAT1, STAT1alpha

lILELAT1tc	transport of L-Isoleucine by LAT1 in association with 4F2hc, across the apical surface of the memebranes.	Transport, extracellular	ile_L[e] + leu_L[c] -> leu_L[e] + ile_L[c]	SLC3A2	Egr-1, AP-1, c-Jun
				SLC7A5	
EX_ade(e)	Adenine exchange	Exchange/demand reaction	ade[e] <=>		
EX_adn(e)	exchange reaction for Adenosine	Exchange/demand reaction	<=> adn[e]		
EX_ala_L(e)	exchange reaction for L-alanine	Exchange/demand reaction	ala_L[e] <=>		
EX_arg_L(e)	L-Arginine exchange	Exchange/demand reaction	<=> arg_L[e]		
EX_asn_L(e)	exchange reaction for L-asparagine	Exchange/demand reaction	asn_L[e] <=>		
EX_asp_L(e)	L-Aspartate exchange	Exchange/demand reaction	<=> asp_L[e]		
EX_chol(e)	exchange reaction for Choline	Exchange/demand reaction	<=> chol[e]		
EX_glc(e)	D-Glucose exchange	Exchange/demand reaction	<=> glc_D[e]		
EX_gln_L(e)	exchange reaction for L-glutamine	Exchange/demand reaction	<=> gln_L[e]		
EX_glu_L(e)	L-Glutamate exchange	Exchange/demand reaction	glu_L[e] <=>		
EX_his_L(e)	exchange reaction for L-histidine	Exchange/demand reaction	<=> his_L[e]		
EX_lac_L(e)	L-Lactate exchange	Exchange/demand reaction	lac_L[e] <=>		
EX_Lcystin(e)	L-Cystine exchange	Exchange/demand reaction	<=> Lcystin[e]		
EX_lys_L(e)	L-Lysine exchange	Exchange/demand reaction	<=> lys_L[e]		
EX_met_L(e)	L-Methionine exchange	Exchange/demand reaction	<=> met_L[e]		
EX_phe_L(e)	exchange reaction for L-phenylalanine	Exchange/demand reaction	phe_L[e] <=>		
EX_pro_L(e)	L-Proline exchange	Exchange/demand reaction	pro_L[e] <=>		
EX_succ(e)	Succinate exchange	Exchange/demand reaction	succ[e] <=>		
EX_taur(e)	Taurine exchange	Exchange/demand reaction	taur[e] <=>		
EX_thr_L(e)	L-Threonine exchange	Exchange/demand reaction	<=> thr_L[e]		
EX_trp_L(e)	L-Tryptophan exchange	Exchange/demand reaction	<=> trp_L[e]		
EX_val_L(e)	L-Valine exchange	Exchange/demand reaction	<=> val_L[e]		

EX_5oxpro(e)	Exchange of 5-oxoprolinate	Exchange/demand reaction	<=> 5oxpro[e]		
EX_ca2(e)	EX_ca2(e)	Exchange/demand reaction	ca2[e] <=>		
EX_fol(e)	EX_fol(e)	Exchange/demand reaction	<=> fol[e]		
EX_ncam(e)	EX_ncam(e)	Exchange/demand reaction	ncam[e] <=>		
EX_pnto_R(e)	EX_pnto_R(e)	Exchange/demand reaction	<=> pnto_R[e]		
EX_uri(e)	EX_uri(e)	Exchange/demand reaction	uri[e] <=>		

SI Table 5. Transcription Factors associated with EMT and MET			
Transcription Factors	**Random (frequency)**	**EMT (frequency)**	**MET (frequency)**
AhR	0.08	0.11	0.04
aMEF-2	0.09	0.03	0.04
AML1a	0.01	0.00	0.00
AP-1	0.09	0.21	0.35
AP-2alpha	0.01	0.08	0.00
AP-2alphaA	0.01	0.08	0.00
AP-2alphaisoform2	0.00	0.08	0.00
AP-2alphaisoform3	0.00	0.08	0.00
AP-2alphaisoform4	0.00	0.08	0.00
AP-2beta	0.01	0.00	0.00
AP-2gamma	0.01	0.00	0.00
AP-2rep	0.03	0.00	0.00
AP-4	0.00	0.03	0.00
AREB6	0.01	0.05	0.13
Arnt	0.08	0.03	0.00
ARP-1	0.04	0.00	0.04
ATF	0.03	0.00	0.04
ATF-2	0.06	0.00	0.00
Bach1	0.03	0.05	0.00
Bach2	0.03	0.00	0.00
Brachyury	0.01	0.05	0.00
c/EBPalpha	0.11	0.03	0.09
C/EBPbeta	0.03	0.00	0.09
Cart-1	0.04	0.05	0.04
CBF(2)	0.03	0.03	0.04
CBF-A	0.01	0.00	0.04
CBF-B	0.01	0.00	0.00
c-Fos	0.03	0.13	0.09
CHOP-10	0.05	0.03	0.00
Chx10	0.03	0.00	0.00
c-Jun	0.09	0.16	0.26
c-Myb	0.00	0.03	0.04
c-Myc	0.09	0.08	0.09
COMP1	0.03	0.00	0.00
COUP	0.00	0.05	0.04
COUP-TF	0.00	0.05	0.00
COUP-TF1	0.00	0.05	0.04
CP2	0.01	0.00	0.04
CREB	0.06	0.03	0.04
CRE-BP1	0.03	0.00	0.00
CUTL1	0.13	0.11	0.13
deltaCREB	0.05	0.03	0.04
E2F	0.04	0.00	0.00
E2F-1	0.03	0.00	0.00
E47	0.04	0.05	0.00
E4BP4	0.03	0.00	0.04
Egr-1	0.00	0.05	0.09
Egr-2	0.01	0.03	0.00
Egr-3	0.00	0.00	0.04
Egr-4	0.01	0.03	0.00
Elk-1	0.04	0.05	0.00
En-1	0.04	0.03	0.00
ER-alpha	0.03	0.05	0.00
Evi-1	0.13	0.08	0.04
FAC1	0.03	0.00	0.04
FosB	0.01	0.03	0.04
FOXC1	0.03	0.03	0.04

FOXC2	0.01	0.00	0.00
FOXD1	0.00	0.03	0.04
FOXD3	0.01	0.00	0.00
FOXF2	0.03	0.00	0.04
FOXI1	0.01	0.00	0.00
FOXJ2	0.01	0.00	0.00
FOXO1	0.05	0.05	0.04
FOXO1a	0.04	0.05	0.04
FOXO3	0.04	0.00	0.00
FOXO3a	0.04	0.00	0.00
FOXO3b	0.03	0.00	0.00
FOXO4	0.06	0.00	0.04
Fra-1	0.01	0.03	0.04
GATA-1	0.06	0.03	0.04
GATA-2	0.00	0.00	0.04
GATA-3	0.01	0.00	0.04
GCNF	0.04	0.03	0.04
GCNF-1	0.03	0.03	0.04
GCNF-2	0.03	0.03	0.04
Gfi-1	0.01	0.03	0.04
GR	0.06	0.11	0.30
GR-alpha	0.06	0.11	0.22
GR-beta	0.01	0.08	0.13
Hand1	0.03	0.03	0.00
HEN1	0.01	0.03	0.00
HFH-1	0.00	0.00	0.09
HFH-3	0.01	0.00	0.00
Hlf	0.06	0.00	0.00
HNF-1	0.06	0.08	0.00
HNF-1A	0.06	0.08	0.00
HNF-3beta	0.00	0.03	0.00
HNF-4alpha1	0.03	0.11	0.13
HNF-4alpha2	0.03	0.11	0.13
HOXA3	0.05	0.03	0.00
HOXA5	0.01	0.03	0.00
HOXA9	0.04	0.03	0.00
HOXA9B	0.05	0.00	0.00
HSF1(long)	0.03	0.03	0.04
HSF1short	0.03	0.03	0.04
HSF2	0.03	0.00	0.00
HTF	0.01	0.05	0.04
Ik-1	0.00	0.05	0.04
Ik-3	0.05	0.00	0.00
IRF-1	0.03	0.00	0.00
IRF-2	0.03	0.00	0.00
IRF-7A	0.01	0.00	0.00
ISGF-3	0.00	0.03	0.00
JunB	0.01	0.03	0.04
JunD	0.01	0.03	0.04
LCR-F1	0.05	0.00	0.09
LHX3a/Lhx3a	0.01	0.00	0.00
LHX3b/Lhx3b	0.01	0.00	0.00
Lmo2	0.01	0.03	0.00
LUN-1	0.04	0.03	0.00
LyF-1	0.04	0.00	0.09
Max	0.06	0.08	0.13
Max1	0.09	0.08	0.17
MEF-2	0.04	0.00	0.00
MEF-2A	0.09	0.03	0.04

Meis-1	0.06	0.00	0.04
Meis-1a	0.06	0.00	0.04
Meis-1b	0.04	0.00	0.04
MIF-1	0.01	0.00	0.04
MRF-2	0.03	0.03	0.04
Msx-1	0.00	0.00	0.09
MyoD	0.04	0.05	0.09
MZF-1	0.01	0.00	0.00
NCX/Ncx	0.01	0.00	0.00
NF-1	0.04	0.05	0.00
NF-1/L	0.03	0.03	0.00
NF-E2	0.03	0.05	0.04
NF-E2p45	0.03	0.05	0.04
NF-kappaB	0.11	0.16	0.04
NF-kappaB1	0.11	0.13	0.09
NF-kappaB2	0.01	0.00	0.00
NF-kappB1	0.00	0.03	0.00
NF-Y	0.01	0.03	0.00
NF-YA	0.01	0.00	0.00
NF-YB	0.01	0.00	0.00
Nkx2-2	0.01	0.00	0.00
Nkx2-5	0.04	0.00	0.00
Nkx3-1	0.01	0.00	0.00
Nkx3-1v1	0.03	0.00	0.00
Nkx3-1v2	0.03	0.00	0.00
Nkx3-1v3	0.03	0.00	0.00
Nkx3-1v4	0.01	0.00	0.00
Nkx5-1	0.06	0.05	0.04
Nkx6-1	0.01	0.00	0.00
N-Myc	0.04	0.03	0.13
NRSFform	0.01	0.00	0.00
NRSFform1	0.08	0.08	0.04
NRSFform2	0.09	0.08	0.00
Oct-B1	0.04	0.00	0.00
oct-B2	0.03	0.00	0.00
oct-B3	0.04	0.00	0.00
OLF-1	0.01	0.00	0.04
p300	0.06	0.00	0.00
p53	0.13	0.08	0.09
Pax-2	0.01	0.03	0.04
Pax-2a	0.01	0.03	0.04
Pax-3	0.03	0.05	0.04
Pax-4a	0.10	0.03	0.04
Pax-5	0.01	0.03	0.13
Pax-6	0.05	0.03	0.00
Pbx1a	0.04	0.00	0.00
POU2F1	0.14	0.08	0.09
POU2F1a	0.13	0.08	0.09
POU2F1b	0.01	0.00	0.00
POU2F1c	0.01	0.00	0.00
POU2F2	0.05	0.00	0.00
POU2F2(Oct-2.1)	0.04	0.00	0.00
POU2F2B	0.04	0.00	0.00
POU2F2C	0.03	0.00	0.00
POU3F1	0.03	0.03	0.00
POU3F2	0.08	0.03	0.04
POU3F2(N-Oct-5a)	0.03	0.00	0.00
POU3F2(N-Oct-5b)	0.03	0.00	0.00
POUF2F1	0.01	0.00	0.00

PPAR-alpha	0.10	0.08	0.00
PPAR-gamma1	0.13	0.24	0.26
PPAR-gamma2	0.13	0.24	0.26
RelA	0.01	0.00	0.00
RFX1	0.06	0.00	0.04
Roaz	0.00	0.03	0.04
RORalpha1	0.06	0.03	0.00
RORalpha2	0.06	0.00	0.04
RP58	0.01	0.05	0.00
RREB-1	0.03	0.00	0.00
RSRFC4	0.03	0.00	0.00
S8	0.03	0.03	0.00
SEF-1(1)	0.05	0.00	0.00
Sox5	0.01	0.03	0.04
Sox9	0.01	0.00	0.00
Sp1	0.03	0.13	0.00
SREBP-1a	0.03	0.03	0.09
SREBP-1b	0.03	0.03	0.09
SREBP-1c	0.03	0.03	0.09
SRF	0.06	0.08	0.04
SRF(504AA)	0.05	0.08	0.04
SRY	0.01	0.00	0.04
STA1beta	0.01	0.00	0.04
STAT1	0.08	0.05	0.09
STAT1alpha	0.06	0.05	0.09
STAT1beta	0.04	0.05	0.00
STAT2	0.03	0.00	0.00
STAT3	0.10	0.00	0.04
STAT4	0.01	0.00	0.00
STAT5A	0.06	0.05	0.09
STAT5B	0.05	0.00	0.00
STAT6	0.01	0.00	0.00
TBP	0.06	0.11	0.00
TFIID	0.04	0.11	0.00
TGIF	0.00	0.03	0.04
USF1	0.04	0.00	0.04
USF-1	0.05	0.03	0.04
USF2	0.01	0.00	0.00
XBP-1	0.01	0.03	0.04
YY1	0.04	0.00	0.04
Zic1	0.01	0.03	0.00
ZIC2/Zic2	0.01	0.00	0.00
ZID	0.01	0.00	0.00

Frequency = Genes affected by TF / Total Number of Genes

MET

EMT

Both MET and EMT

Paper II

OPEN ACCESS Freely available online

PLOS ONE

Biochemical Characterization of Human Gluconokinase and the Proposed Metabolic Impact of Gluconic Acid as Determined by Constraint Based Metabolic Network Analysis

Neha Rohatgi[1,2], Tine Kragh Nielsen[3], Sara Petersen Bjørn[3], Ivar Axelsson[1], Giuseppe Paglia[1], Bjørn Gunnar Voldborg[3], Bernhard O. Palsson[1], Óttar Rolfsson[1,2]*

1 Center for Systems Biology, University of Iceland, Reykjavik, Iceland, **2** University of Iceland Biomedical Center, Reykjavik, Iceland, **3** Center for Protein Research, Faculty of Health Sciences, University of Copenhagen, Copenhagen, Denmark

Abstract

The metabolism of gluconate is well characterized in prokaryotes where it is known to be degraded following phosphorylation by gluconokinase. Less is known of gluconate metabolism in humans. Human gluconokinase activity was recently identified proposing questions about the metabolic role of gluconate in humans. Here we report the recombinant expression, purification and biochemical characterization of isoform I of human gluconokinase alongside substrate specificity and kinetic assays of the enzyme catalyzed reaction. The enzyme, shown to be a dimer, had ATP dependent phosphorylation activity and strict specificity towards gluconate out of 122 substrates tested. In order to evaluate the metabolic impact of gluconate in humans we modeled gluconate metabolism using steady state metabolic network analysis. The results indicate that significant metabolic flux changes in anabolic pathways linked to the hexose monophosphate shunt (HMS) are induced through a small increase in gluconate concentration. We argue that the enzyme takes part in a context specific carbon flux route into the HMS that, in humans, remains incompletely explored. Apart from the biochemical description of human gluconokinase, the results highlight that little is known of the mechanism of gluconate metabolism in humans despite its widespread use in medicine and consumer products.

Citation: Rohatgi N, Nielsen TK, Bjørn SP, Axelsson I, Paglia G, et al. (2014) Biochemical Characterization of Human Gluconokinase and the Proposed Metabolic Impact of Gluconic Acid as Determined by Constraint Based Metabolic Network Analysis. PLoS ONE 9(6): e98760. doi:10.1371/journal.pone.0098760

Editor: Mark R. Muldoon, Manchester University, United Kingdom

Received December 19, 2013; **Accepted** May 6, 2014; **Published** June 4, 2014

Funding: This work was supported by the European Research Council grant proposal no. 232816. The funders had no role in study design, data collection and analysis.

Competing Interests: The authors have declared that no competing interests exist.

* E-mail: ottarr@hi.is

Introduction

Gluconate is a C-1 oxidized derivative of glucose, widely distributed in nature and commonly used as an acidity regulator in both food and drugs [1]. Gluconate is an excellent chelator of calcium ions and calcium gluconate is often given intravenously in order to regulate intravenous Ca^{2+} levels. While this clinical measure undoubtedly focuses on replenishing Ca^{2+}, gluconate and its chemical counterpart gluconolactone against which it exists in chemical equilibrium, have in fact been shown to exhibit antioxidant properties and result in increased plasma levels of glutathione [2]. Lowered plasma levels of gluconate have also been associated with Alzheimer's disease [3] and increased oxidative stress [4].

We recently highlighted that gluconate metabolism in humans is unaccounted for using a computational network gap filling approach of the human metabolic network Recon 1. Gluconate catabolism was computed to take place through phosphorylation of gluconate to generate 6-phosphogluconate which could then be further degraded through the hexose monophosphate shunt (HMS) via 6-phosphogluconate dehydrogenase [5]. This catabolic route has indeed been shown to take place in rat liver perfusions [6] and corresponds to well researched degradation routes of gluconate in microorganisms. These involve metabolism via (I) direct internalization from the environment, (II) conversion from L-idonic acid or (III) by direct oxidation of glucose via glucono-1,5-lactone [7–9]. A key enzyme in all the gluconate degradation routes is gluconokinase (GntK) which phosphorylates gluconate at the C-6 position thereby priming its catabolism through the HMS or the Entner-Doudoroff pathway in prokaryotes.

The human gene C9orf103 was identified through a metabolic network gap filling effort of Recon 1 and through amino acid sequence alignment as a likely kinase responsible for the initial step in gluconate catabolism in humans [5]. C9orf103 had previously been cloned and sequenced in relation to it being a plausible tumor suppressor gene associated with acute myeloid leukemia [10]. *In vitro* assays of isoforms I and II of C9orf103 expressed in human HeLa cell lysates showed that only isoform I had ATP dependant phosphorylation activity consistent with the absence of a phosphate binding loop domain in isoform II. Isoform I shows 35% sequence similarity to both GntKs encoded within the *E.coli* genome. A defining structural difference is an 18 amino acid insert that is found in various NMP kinases that have similar protein

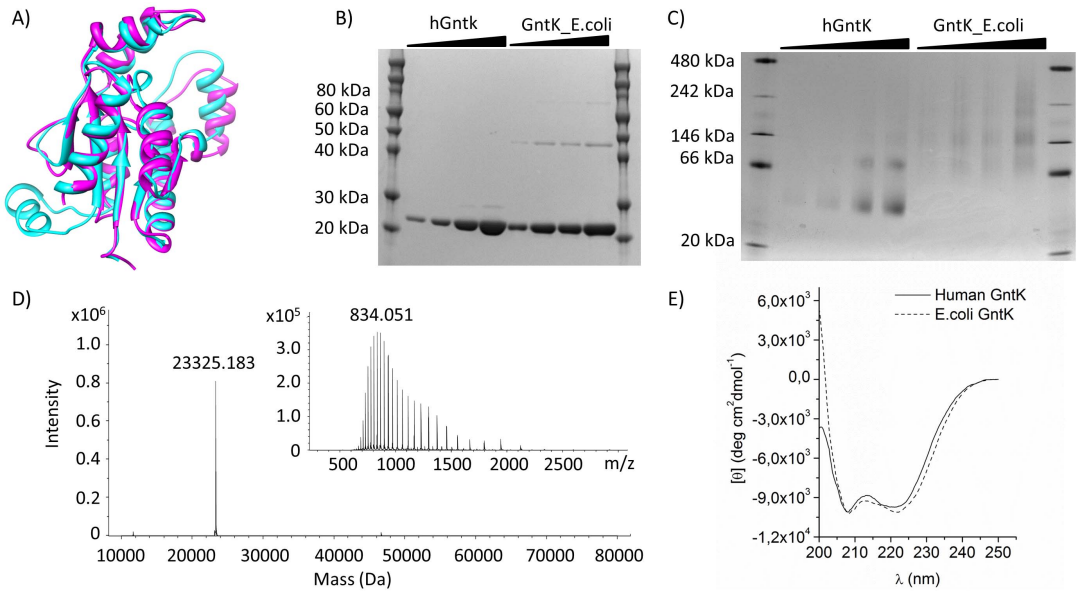

Figure 1. Structural comparison of human GntK to *E.coli* GntK. A) An iTasser [44] structural model of human GntK (cyan) superimposed on E.coli GntK (magenta) to which it shows 34% sequence homology. The 18 a.a. insert observed in human GntK is predicted to form a protruding α-helix. **B**) SDS-PAGE of purified human GntK vs. *E.coli* GntK. **C**) Human GntK was observed to oligomerize as multiples of protein dimers. **D**) The ionization pattern (inset) and deconvoluted mass spectrum of purified human GntK **E**) Circular dichroism spectra of the two proteins are indicative of a similar tertiary structure.
doi:10.1371/journal.pone.0098760.g001

structure to *E.coli* GntK and of which many are known and act on a broad variety of substrates [5,11] (**Figure 1A**).

The presence of a functional human GntK is interesting. Publically available expression and proteomic profiling datasets show that human GntK is differentially expressed in the thyroid and brain amongst others tissues [12,13]. This implies an unknown or expanded role for the protein outside its proposed catabolic role in the mammalian kidney and liver. Direct oxidation of glucose to generate gluconate is generally not perceived to take place in humans where phosphorylation precedes the oxidization step. Excluding dietary origins, the metabolic origins of gluconate remain unknown in humans. The notion that GntK activity is encoded within the human genome however highlights a carbon flux route into the HMS with possible implications for human energy metabolism given the central role that the pathway plays in fatty acid, nucleotide and amino acid synthesis and in combating oxidative stress [14]. In order to further characterize human GntK and gluconate metabolism, we report the expression, kinetic characterisation and substrate specificity of a recombinant human GntK isoform I expressed in *E.coli*. Furthermore, we assessed the contribution of gluconate to human central metabolism through constraint based modeling of the curated erythrocyte metabolic model iARB-RBC-283 [15] and discuss its effect on human metabolism.

Experimental

Expression and purification

Cloning expression and purification of C9orf103 was carried out at the Center for protein research at the University of Copenhagen. C9orf103 isoform I (BI826543, IMAGE ID: 5168613) was inserted into an in-house expression vector pCPR0011 downstream of a 6xHIS and STREPII affinity tags generating pCPR_GNTK-1 which, following sequence confirmation, was transformed into Rosetta cells. The clone was inoculated in 50 ml of TB media with kanamycin (50 μg/ml) and chloramphenicol (25 μg/ml) and incubated overnight at 37°C at 180 rpm. 7 ml of overnight culture was added to 750 ml of media with kanamycin (50 μg/ml), and expression induced with 0.5 mM IPTG at approximately $OD_{600} = 1.5$. Cells were then incubated further at 18°C overnight and harvested by centrifugation at 4000 g for 10 min (culture $OD_{600} = 13.5$ at harvest). A 4.5 L culture resulted in a 110 g cell pellet that was stored at −20°C until purification at which point it was thawed, resuspended in 400 ml of running buffer (50 mM sodium phosphate, 0.3 mM NaCl, 10 mM imidazole, 10% glycerol and 0.5 mM TCEP at pH 7.5) containing protease inhibitors and benzonase, and lysed using french press. The lysate was cleared by centrifugation at 18000 g for 30 min and filtered through a 0.22 μm filter and run through a Nickel HiTrap column at a flow rate of 0.8 ml/min. The protein was eluted off the column with running buffer containing 0.5 M imidazole. Following dialysis and concentration, the eluate was further purified using a 120 ml HiLoad 16/60 superdex 200 size exclusion column eluted with 50 mM sodium phosphate, 150 mM NaCl, 10% glycerol, 0.5 mM TCEP, pH 7.5. 2 ml fractions were collected and samples pooled affording 14 ml of 5.8 mg/ml protein using a calculated molar absorption coefficient of 22461 $Lmol^{-1}cm$ The enzyme was aliquoted and stored in −80°C in 50 mM sodium phosphate, 150 mM NaCl, 10% glycerol and 0.5 mM TCEP at pH 7.5. PAGE was carried out on NuPAGE 12% Bis-tris gels and NativePAGE 4–16%

Bis-Tris Gels using Novex Sharp pre-stained protein markers and NativeMark unstained native markers as size markers, respectively. Protein aliquots were removed from −80°C and thawed on ice prior to enzyme assays. Loss of activity was not observed after storage at 4°C for two weeks.

Circular Dichroism

Samples containing human GntK enzymes were dialyzed into 100 mM phosphate, 40 mM NaCl, 2.5 mM $MgCl_2$ pH 7.2 and a A J-810 CD spectrometer from Jasco (Tokyo, Japan) was used to obtain CD spectra from 190 to 260 nm. For the Tm experiments, the CD signal at 222 nm was monitored as the temperature increased by 1°C/min. The protein concentration was in the range 0.05–0.1 mg/mL.

Kinetic assays

The rate of gluconate phosphorylation was evaluated by coupling GntK activity with that of 6-phosphogluconate oxidation by 6-phosphogluconate dehydrogenase (6PGDH, Megazyme) and monitoring the absorbance increase at 340 nm over time corresponding to the accumulation of NADPH. Assays were carried out in 100 mM phosphate, 40 mM NaCl, 2.5 mM $MgCl_2$ pH 7.2 (Buffer A) taking into account assays reported by Leder [16]. Glukonokinase was kept at 0.25 µM. 0.03 units of 6PGDH were used per reaction. ATP final concentration was 1 mM and gluconate concentration varied from 0.1–10 mM in order to determine gluconate kinetic parameters but vice versa for ATP. $NADP^+$ concentration was 0.65 mM. Reactions were initiated by addition of the target substrate. Reactions were carried out in 96 well clear, flat bottom plates and absorbance values were correlated to NADPH concentration by extrapolation off a freshly diluted NADPH standard curve. Initial reaction rates were obtained from reaction progress curves and plotted against substrate concentration and the resulting data fit to the Michaelis Menten model using Softmax Pro. The values shown represent average values from six biological replicates, performed in technical triplicate.

Substrate specificity assays

Reactions were carried out in 96 well plates in buffer A with ligand concentration at 0.5 mM, ATP at 0.1 mM and human GntK at 250 nM in 50 µl total volume. Following a 30 min incubation time at room temperature, ATP dependant phosphorylation of substrates by human GntK was estimated by measuring the drop in ATP concentration using the Promega Cell Titer Glo assay according to the manufacturers' protocol. Data is portrayed as the difference in luminescence obtained for a substrate from the average luminescence of all compounds. **File S1** gives luminescence values in each reaction subtracted from no GlcnK control luminescence along with calculated z-scores and p-values for each compound [17].

Modelling the uptake of gluconate metabolism in erythrocytes

Modelling of gluconate metabolism was done using the erythrocyte metabolic model iARB-RBC-283 [15] available through the biomodels database as MODEL1106080000. iARB-RBC-283 is a genome scale metabolic model generated and curated by mining red blood cell literature and red cell proteomic datasets. It represents the most complete representation of human red cell metabolism in SBML format and is comprised of 283 genes, 267 unique small metabolites and 469 reactions. Gluconate was introduced into the iARB-RBC-283 model by adding three reactions, namely, for exchange, transport and for conversion of D-gluconate to 6-phospho-D-gluconate using the COBRA toolbox [18]. It is important to state that addition of the exchange and transport reactions are only done in order to introduce gluconate into the metabolic network so that the effect of varying intracellular gluconate concentration on metabolism can be modeled. Flux variability analysis (FVA) was utilized to determine the changes in flux in reactions within the network. FVA calculates the maximum and minimum possible flux through each reaction under the given constraints [19]. A reaction was considered to be effected if the change in the flux range upon gluconate consumption was equal to or more than 40% of the flux range in the absence of gluconate [15]. The flux range is the absolute difference between the maximum and minimum fluxes of a reaction. Flux variability analysis results are given in **File S1** along with calculated shadow prices of each reaction in iARB-RBC-283 in the presence and absence of the added gluconate reactions. Shadow prices are indicator of how a metabolite affects the set objective, which is to be maximized or minimized [20]. Flux balance analysis, following relaxation of each transport reaction bound are also given. All analysis of metabolic network properties were carried out using the COBRA toolbox v.2.0 [18]. Abbreviations of all metabolites are according to the BiGG database [21].

Results

Characterisation of human GntK

Human GntK was over expressed and purified as described in materials and methods. The vector construct expressed a protein product of 208 a.a. compared to the 187 a.a. residue wild type protein due to N-terminal hexahistidine and strep tags. SDS-PAGE showed the protein to be more than 95% pure and migrated to a similar extent as commercially available *E.coli* GntK (**Figure 1B**). Both of these were immunogenic towards a polyclonal antibody against human GntK. The major band migrated with an observed molecular mass of 21,825±0.7 Da having a calculated mass of 23,326 Da. This corresponds well with the mass spectrometry result of 23,325.2 Da (**Figure 1C**). Native gel electrophoresis showed that the protein exists as dimers and oligomerizes as such. The calculated molecular weight of the two most prominent bands in lanes 4 and 5 in **Figure 1D** were 41.785±1.9 kDa and 85.03±3.3 kDa corresponding to a GntK dimer and tetramer. The *E.coli* GntK was similarly observed to oligomerize as multiples of dimers and has been shown to exist as a homodimer in solution [8]. The circular dichroism spectra, an indicator of protein secondary structure [22], of the recombinant forms of both GntKs was similar. Defining negative bands at 208 nm and 222 nm were observed indicative of an α-helical structure although differences were seen in their intensities hinting at conformational differences. A negative band was observed in the human GntK at 200 nm which was not observed in the *E.coli* GntK a difference that was accredited to the unstructured N-terminal region containing the His and Strep tags.

Kinetics of GntK

The steady state kinetics of GntK was investigated by coupling 6-phosphogluconate formation to consumption by 6-phosphogluconate dehydrogenase and measuring the resulting increase in NADPH formation spectrophotometrically at 340 nm (**Figure 2**). Initial rates were calculated and plotted against substrate concentration and the resulting data fit to the Michaelis Menten equation. A double reciprocal plot of initial reaction rates at varied gluconate and ATP concentrations, respectively, is shown in **Figure 2B**. The experimental kinetic parameters for phosphorylation of gluconate

are given in **Table 1**. The affinity of the GntK for gluconate was roughly 3 times that for ATP while the turnover numbers for both substrates were the same. Phosphorylation of gluconate by the nucleoside triphosphates GTP, CTP and UTP was observed. The kinetic parameters for these were not accurately determined. Initial rate data however implied that the Michaelis constant for UTP is roughly five orders of magnitude higher than that of ATP and ten orders higher for GTP and CTP. Nucleotide hydrolysis in the absence of gluconate was not detected.

Substrate specificity of GntK

The annotation of C9orf103 encoding GntK activity was tested further by investigating substrate dependent ATP phosphorylation against an in-house metabolic library composed of a broad spectrum of metabolites involved in core metabolism (**Figure 3**). Following incubation of human GntK with the substrates at a fixed ATP concentration, the drop in ATP concentration was detected spectrophotometrically. The enzyme showed little activity above background for any of the substrates tested apart from gluconate and glucono-1,5-lactone. Included in this list were twenty five carbohydrate/carbohydrate conjugates and twenty four organic acids, including known substrates of closely related carbohydrate kinases [23] such as D-ribulose, meso-erythrose and glycerol. A full list of all compounds screened is given in **File S1**.

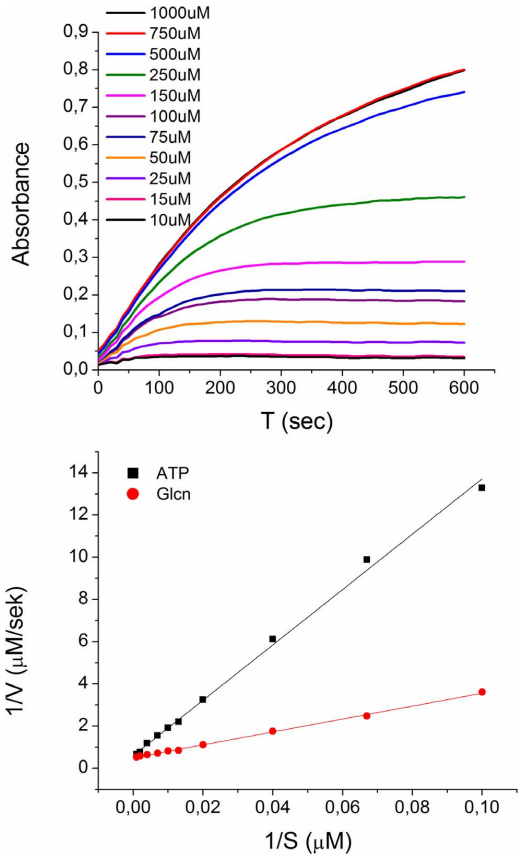

Figure 2. Reaction kinetics of the phosphorylation of gluconate by human GntK. A) Reaction progression curves at increasing gluconate concentration. Initial rates were plotted against substrate concentrations and fit to the Michaelis Menten model using nonlinear regression to afford kinetic parameters shown in **Table 1**. **B**) Double reciprocal representation of the kinetic data.
doi:10.1371/journal.pone.0098760.g002

The effects of gluconate on core metabolism

Flux variability analysis of the erythrocyte metabolic model iAB-RBC-283 [15] was utilized in order to evaluate changes in cellular core metabolism induced by gluconate degradation. Gluconate was fed into the HMS via 6-phosphogluconate by relaxing the bounds on exchange for gluconate at a fixed glucose uptake rate of 1.12 mmol/gDW/h [24]. This resulted in a 0.06 mmol/gDW/h flux increase through the ATP dependent Na^{2+}/K^{+} pump that was set as the objective function. The flux through GntK spanned 0.20–4.46 mmol/gDW/h. An increase in the flux range of all reactions in both the HMS and glycolysis was also observed upon uptake of gluconate (**Figure 4a**). Accordingly, production of NADPH increased that in turn increased production of reduced glutathione and flux through reactions associated with fatty acid metabolism in the model. As glycolysis is interconnected to the HMS, this also led to increased pyruvate and lactate production. In fact, flux ranges for roughly 80% of all the reactions in the metabolic network were perturbed upon gluconate metabolism by more than 40% of the initial flux range in the absence of gluconate. Out of the reactions showing a change in flux ranges, multiple reactions were activated in the presence of gluconate meaning that no flux through these reactions takes place prior to gluconate metabolism in the metabolic model (**Figure 4b**).

The effect of GntK flux on the objective was investigated further employing robustness analysis. Flux balance analysis was performed at forced and increasing rates (0–20 mmol/gDW/h) of gluconate uptake, at a fixed glucose uptake rate of 1.12 mmol/gDW/h [24] (**Figure 5**). As expected, based on the FVA analysis, the objective maximum was reached at a flux of 0.2 mmol/gDW/h through GntK, which is roughly 18% of the set glucose uptake rate. Increasing the GntK flux rate past 4.5 mmol/gDW/h resulted in a sharp drop in the objective as metabolites required for gluconate catabolism became limiting due to physiologically determined model constraints [24]. In order to pinpoint these metabolites we calculated shadow prices for each metabolite in the metabolic network in the presence and absence of gluconate (**File S1**). In the absence of gluconate, 89 out of the 267 unique metabolites within iAB-RBC-283 had an effect on flux through the ATP dependent Na^{2+}/K^{+} pump while in the presence of gluconate this number was reduced to 10. These metabolites were all ultimately associated with either bicarbonate transport/exchange (bicarbonate, chloride, potassium, bilirubin monoglucuronide, bilirubin, biliverdin and carbon monoxide) or glutathione synthesis (L-cysteine, γ-L-glutamyl-L-cysteine and glycine) and became limiting on the account of increased levels of NADPH and carbon dioxide generated from gluconate catabolism.

Further investigation into the limiting factor of gluconate metabolism was performed by relaxing bounds constraining each exchange reaction followed by flux variability analysis (**File S1**). In the absence of gluconate, a total of 7 reactions, including exchange of glucose, galactose, glucosamine mannose, fructose, inosine and adenosine were observed to affect the objective function. In the presence of gluconate however there was only one reaction, namely bicarbonate exchange. The modeling results indicate that metabolism of gluconate via the HMS compensates for the aforementioned metabolites. This occurs until transport of bicarbonate, generated from increased levels of carbon dioxide

Table 1. Human GntK kinetic properties.

	K_m (μM)	V_{max} (μM/s)	k_{cat} (s^{-1})	k_{cat}/K_m ($s^{-1}\mu M^{-1}$)	R^2
Gluconate	106.4±18.5	2.3±0.1	9.3±0.5	0.089±0.013	0.98±0.008
ATP	343.8±13.9	2.4±0.1	9.5±0.5	0.028±0.002	0.99±0.002

doi:10.1371/journal.pone.0098760.t001

that in turn originate from increased dehydrogenase activity, limit metabolism.

Discussion

Gluconate metabolism is well characterized in microorganisms due to bioengineering efforts to enhance production of gluconate for industry. In humans, studies have been carried out that have shown the compound to be safe and degraded via core metabolic pathways [25]. Crucially, Stetten demonstrated that gluconate is metabolized differently than glucose in rats and contributes to glycogen and CO_2 production [6]. In humans however gluconate metabolism remains under-explored in light of its potential role in metabolism. The molecular details of gluconate metabolism and how it might contribute to energy metabolism have not been characterized in humans. Here we employed a combined approach composed of traditional molecular biology and computational network modeling methods to gain information on GntK and gluconate metabolism in humans, respectively. We characterized isoform I of human GntK in terms of structure, kinetic properties and substrate specificity. Metabolic network analysis, designed to afford ideas on the contribution of gluconate to core metabolism was performed on the genome scale metabolic network iAB-RBC-283 encompassing red cell metabolism. These show that combined glucose and gluconate metabolism is likely to result in beneficial effects on cellular anabolism.

Isoform I of human GntK was characterized in terms of structure, kinetic properties and substrate specificity. Denaturing gel electrophoresis and mass spectrometry confirmed the purity and identity of the recombinant enzyme which was shown to conform to a dimer structure using native gel electrophoresis (**Figure 1**). Indeed, many of the carbohydrate kinases including, glycerol kinase, shikimate kinase, xylulokinase and GntK are known to be active as dimers [23] and this appears to be the case for human GntK as well. The 18 a.a. insertion found in human GntK which is likely the defining structural difference between human GntK and prokaryotic GntK, does therefore not affect the dimerization properties of the enzyme. This corresponds with the electronic structural proposal of human GntK indicating that the insert is located away from the dimer interaction interface of the protein. We obtained CD spectra, a method for determining the secondary structure of proteins [22]. The CD spectra of GntK and *E.coli* GntK provided further confirmation of structural similarities and suggested that the enzyme most likely adheres to the α/β structure and topology solved for *E.coli* GntK. More focused

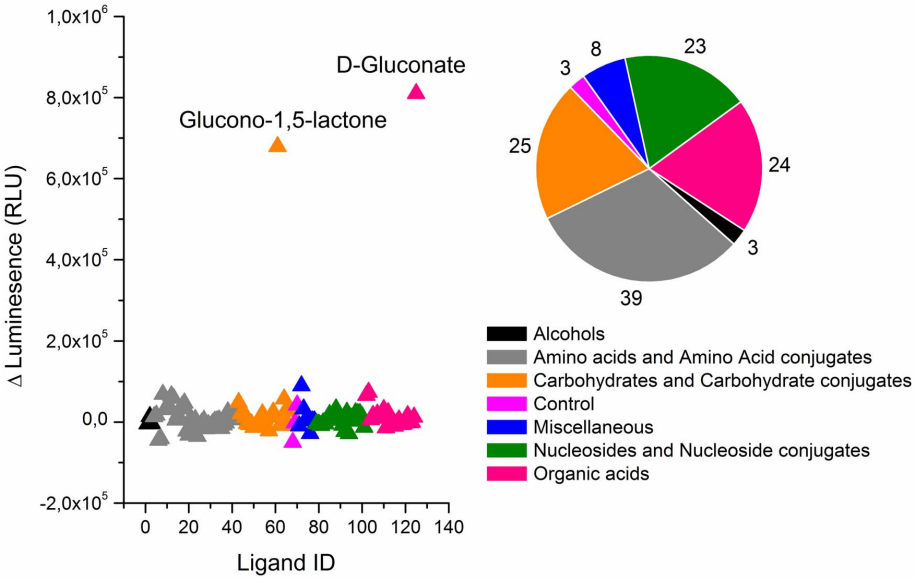

Figure 3. Human GntK showed strict substrate specificity for D-gluconate out of 122 common metabolites involved in human core metabolism. Activity was only observed for D-gluconate and its lactone derivative. These had calculated p-values of 9.5×10^{-17} and 3.4×10^{-12} based on Z-scores of −8.2 and −6.7 respectively. The pie chart shows the number of compounds tested according to their taxonomy class.
doi:10.1371/journal.pone.0098760.g003

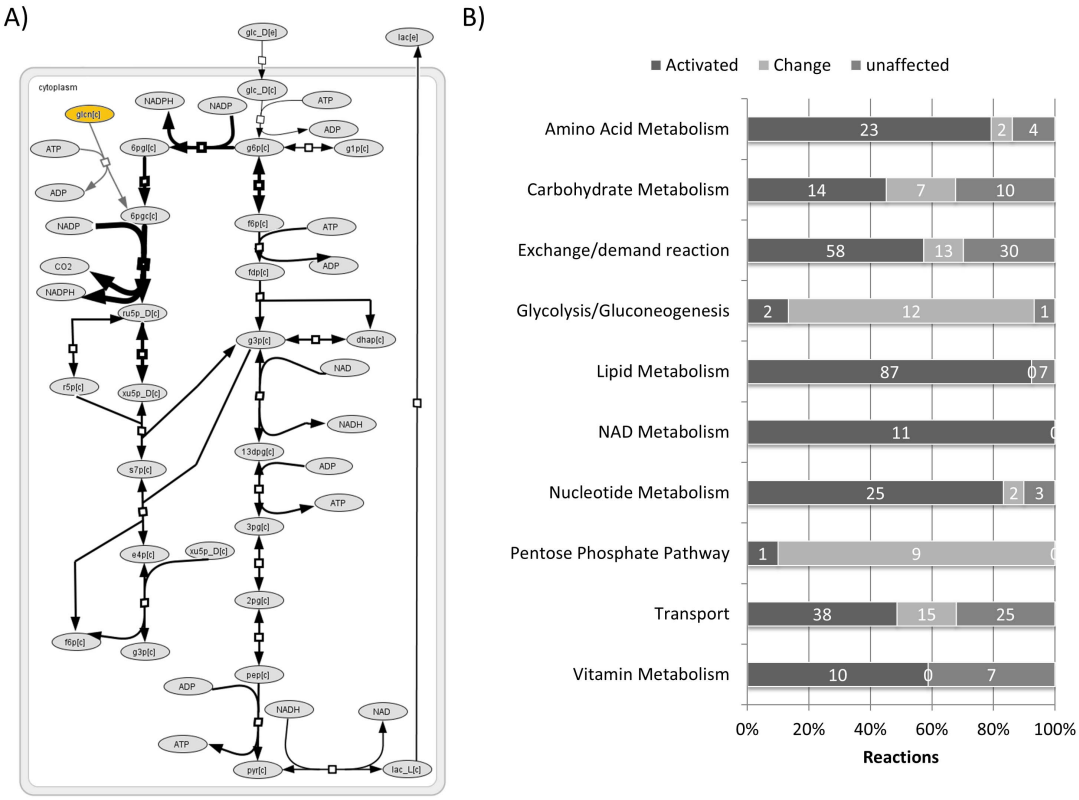

Figure 4. Modelling the contribution of gluconate to core metabolism. A) Metabolic flux through glycolysis and the HMS is affected upon gluconate (yellow) consumption via GntK. The two added reactions (grey) feed gluconate into the HMS as described in the text. Reactions in the HMS and glycolysis with changed flux ranges upon gluconate uptake are indicated by arrow thickness as defined in **File S1**. Metabolite abbreviations are consistent with the BiGG database. **B**) Flux variability analysis showed changes in the flux ranges of 329 out of the 416 reactions in the RBC model upon incorporation of gluconate. 56 miscellaneous reactions, which were not defined properly in the model, have been removed from this graph to simplify the graph. Gluconate degradation also activated reactions that otherwise did not carry flux due to constraints imposed by flux into the HMS through glucose-6-phosphate dehydrogenase which was floated at physiological 5–10% of glucose uptake.
doi:10.1371/journal.pone.0098760.g004

structural biology methods are however required to deduce the fine details of the structure of human GntK.

Apart from non-cognate GntKs, human GntK shows sequence similarity to various NMP kinases known to catalyze the phosphorylation of a broad range of substrates [11]. We found that recombinant human GntK showed strict substrate specificity for gluconate. ATP dependant phosphorylation activity was also observed for glucono-1,5-lactone as it exists in equilibrium with gluconate in aqueous conditions. The enzyme was inactive against the hexoses D-glucose, D-galactose, D-fructose, D-mannose and D-glucosamine. Similarly no activity was observed against the pentoses D-ribose, D-ribulose, D-arabinose, D-xylulose, D-xylose and D-erythrose. Finally no activity was observed against various polyols and carboxylic acids which differ from gluconate in terms of carbon chain length and in their degree of saturation. Previously, for hog GntK, substrate specificity analyses were focused on compounds similar in structure to gluconate. The substrates tested in this study were structurally more diverse. These results refute automated electronic annotations of this enzyme having shikimate kinase and adenylate kinase activity and imply that the phosphorylation activity of human GntK is indeed specific for gluconate. This is in line with the findings for hog GntK [16] and the constraints on substrate binding implied from the crystal structure solved for *E.coli* GntK [11].

The estimated Michaelis constant obtained for human GntK towards gluconate was similar to that found for hog GntK, $K_m = 140$ μM, but higher than those reported for *E.coli* GntK, $K_m = 20$ μM [8,9]. The ratio of K_{mGlcn}/K_{mATP} is however similar between human GntK and *E.coli* GntK, 3.2 vs. 3.0 and implies that the reaction dynamics are similar for these enzymes. The turnover numbers for both gluconate and ATP were nearly identical (**Table 1**) however the catalytic efficiency (k_{cat}/K_m) for gluconate was slightly higher than for ATP indicative of a sequential reaction mechanism. The order of substrate binding was however not determined. The reaction mechanism for GntK from *E.coli* and *S. pombe* have been proposed, and while both found that the reaction takes place via a transition state following sequential binding, the binding order of substrates was proposed to be ordered for *E.coli* GntK as opposed to random for *S.pombe* GntK. The results reported here do not allow the reaction

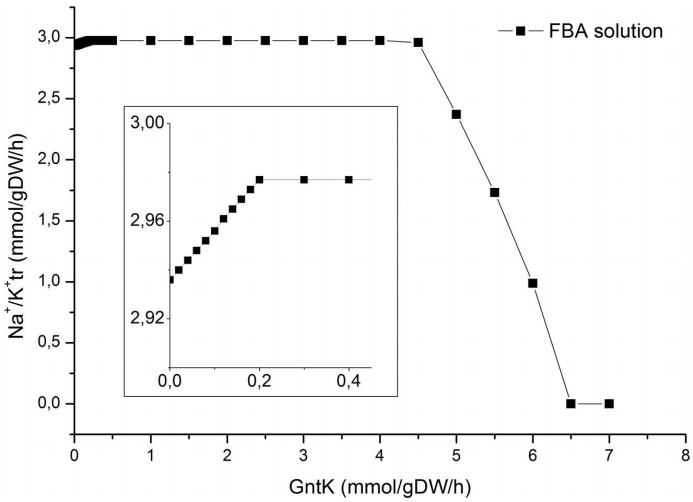

Figure 5. Robustness analysis of gluconate flux through GntK vs. the Na^{2+}/K^{+} transporter pump set as the objective in iAB-RBC-283. A slight increase in flux through the Na^{2+}/K^{+} transporter pump that then became constant up to a gluconate flux rate of 4.5 mmol/gDW/h was observed upon gluconate addition. This resulted in an increase (defined as >40%) in the flux range of multiple reactions in iAB-RBC-283. At GntK flux rates above 4.5 mmol/gDW/h bicarbonate exchange becomes limiting and as a result flux through the Na^{2+}/K^{+} transporter pump drops. The figure inset is the same as the above but with a modified scale.
doi:10.1371/journal.pone.0098760.g005

mechanism for human GntK to be determined. A detailed report on the kinetics and thermodynamics of the human GntK reaction will be reported separately.

The only reported degradation route of gluconate in vertebrates is via the HMS [16,26,27]. In order to assess how gluconate contributes to global metabolism, its degradation through the HMS was modeled using FVA of the erythrocyte metabolic model iAB-RBC-283. Although human genome scale cell and tissue specific metabolic models have been generated for a variety of context specific applications [28–32], this model was chosen to model metabolism for several reasons. Firstly the model is small with few components, uncluttered with minimum possibilities of false positives introduced by metabolic gaps, dead ends and flux loops [30,33,34] and the model has defined metabolite exchange constraints [15]. Secondly the Na^{+}/K^{+} pump is a realistic objective function, the maintenance of the Na^{+} concentration gradient has been shown to account for up to 70% of cell ATP expenditure [35]. Finally, erythrocytes have a very active HMS so any observed flux changes were likely to be emphasized with a minimum of false positives. A drawback of this model is the absence of core metabolic pathways downstream of glycolysis namely the TCA cycle and oxidative phosphorylation that are indeed central to cells that carry out aerobic glycolysis.

Introducing gluconate had an effect on flux through reactions within the model. 269 reactions were activated and 60 reactions showed changes in their flux range out of a total of 472 reactions in iAB-RBC-283. In the HMS, 9 out of 10 reactions had increased flux ranges, however the biggest effect was observed in metabolic pathways involving metabolites/reactions derived from the HMS. These included nucleotide, carbohydrate, amino acid and lipid metabolic pathways due to increased levels of ribose-5-phosphate, xylulose-5-phosphate, erythrose-4-phosphate and NADPH, respectively. This suggests that the metabolic repertoire/capacity of the model is significantly increased upon gluconate degradation. Increasing flux through the HMS in the form of gluconate relieves constraints on these pathways imposed by the glucose uptake rate and the HMS split ratio. Indeed a similar effect would be observed if the flux into the HMS would be increased through glucose-6-phosphate dehydrogenase. In erythrocytes glucose-6-phosphate deyhydrogenase is the main source of NADPH and is the most common enzyme deficiency known and has deleterious effects when homozygous [36]. The modeling results here simply demonstrate that considerable control of key metabolic pathways can be achieved by bypassing this regulatory enzyme into the HMS. There is little apparent energetic gain to feeding the HMS through GntK or through hexokinase. Both pathways supposedly result in the same use and production of ATP and NADPH. We propose that GntK or enzymes upstream of it are involved in context specific regulation of carbon flux into the HMS. A gene co-expression analysis or knockdown study of the effect of GntK on core metabolism could help shed light on a novel flux route into the HMS in humans.

There are several ways in which gluconate could be generated endogenously. It could be formed by spontaneous oxidation of glucose, as a product of advance glycation end-product formation [37], as a product of microbiota [38], through undiscovered anabolism of complex glycans or simply by dephosphorylation of 6-phosphogluconate. In these cases GntK might function as a salvaging enzyme, re-routing gluconate back into central carbon metabolism through the HMS. Another route of gluconate formation is its production through direct oxidation of glucose via glucose dehydrogenase (EC 1.1.1.47) and gluconolactonase (EC 3.1.1.17). Glucose dehydrogenase activity is not generally believed to be a central part of human metabolism. Although the endoplasmic reticulum localized hexose-6-phosphate dehydrogenase has been reported to carry out the direct oxidation of glucose, generating D-glucono-1,5-lactone, its main substrate is glucose-6-phosphate [39,40]. D-gluconolactonase activity, affording gluconate

from D-glucono-1,5-lactone, has been shown to be encoded by the microsomal enzyme SMP30 in the context of ascorbic acid synthesis in rats [41]. Given that humans do not synthesize ascorbic acid it is likely that SMP30 has a different metabolic role in humans. In an attempt to address this, over expression of SMP30 in HEPG2 cells has been shown to result in significant reduction in reactive oxygen species with associated decreases in lipid peroxidation levels and superoxide dismutase activity. The effects were attributed to intracellular [Ca^{2+}] modulation brought about by increased SMP30. SMP30 itself was shown not to have radical scavenging ability and *Handa et al.* proposed an indirect antioxidant ability of SMP30 [42]. In light of our modeling results, which indicate how human GntK activity affects the global metabolic phenotype, we propose that the effect observed upon SMP30 over expression and later complemented by knockdown experiments of SMP30, is brought about by modulating flux into the HMS through gluconate thereby promoting NADPH formation.

Herein we have described the biochemical characterization of human GntK, an enzyme flagged in two network gap filling analyses of Recon 1 [5,43] and employed constraint based network analysis to assess how gluconate might impact human metabolism. The results advance knowledge of the biochemical properties of isoform I of human GntK and suggest that considerable perturbation of metabolic pathways associated with the HMS result given that gluconate degradation follows similar routes in humans as reported in vertebrates. Furthermore, these data serve to highlight an overlooked carbon flux pathway into the HMS in humans which could be of significance given the pathways central anabolic role and importance in combating oxidative stress. Finally the results demonstrate the application of human metabolic models to assess metabolic phenotypes and how these can be put into context with existing biological data to advance functional genomic hypotheses.

Supporting Information

File S1 The file contains five worksheets that report the following 1: measured luminesence values from the substrate specificity assays 2: results from flux variability analysis of in iAB-RBC-283 with and without gluconate. 3: how flux values relate to arrow thickness as portrayed in figure 4. 4: Calculated shadow prices in the presence and absence of gluconate. 5: FBA solutions obtained upon relaxing transport/exchange flux boundaries in the presence and absence of gluconate.
(XLSX)

Author Contributions

Conceived and designed the experiments: BOP OR. Performed the experiments: NR TKN SPB IA GP OR. Analyzed the data: NR TKN SPB GP OR. Contributed reagents/materials/analysis tools: BOP SPB BGV GP OR. Wrote the paper: NR OR.

References

1. Ramachandran S, Fontanille P, Pandey A, Larroche C (2006) Gluconic acid: Properties, applications and microbial production. Food Technology and Biotechnology 44: 185–195.
2. Kolodziejczyk J, Saluk-Juszczak J, Wachowicz B (2011) In vitro study of the antioxidative properties of the glucose derivatives against oxidation of plasma components. J Physiol Biochem 67: 175–183.
3. Hu ZP, Browne ER, Liu T, Angel TE, Ho PC, et al. (2012) Metabonomic profiling of TASTPM transgenic Alzheimer's disease mouse model. J Proteome Res 11: 5903–5913.
4. Oresic M, Hyotylainen T, Herukka SK, Sysi-Aho M, Mattila I, et al. (2011) Metabolome in progression to Alzheimer's disease. Transl Psychiatry 1: e57.
5. Rolfsson O, Paglia G, Magnusdottir M, Palsson BO, Thiele I (2013) Inferring the metabolism of human orphan metabolites from their metabolic network context affirms human gluconokinase activity. Biochemical Journal 449: 427–435.
6. Bloom B, Stetten D, Jr. (1955) The fraction of glucose catabolized via the glycolytic pathway. The Journal of Biological Chemistry 212: 555–563.
7. Peekhaus N, Conway T (1998) What's for dinner?: Entner-Doudoroff metabolism in Escherichia coli. Journal of Bacteriology 180: 3495–3502.
8. Izu H, Adachi O, Yamada M (1996) Purification and characterization of the Escherichia coli thermoresistant glucokinase encoded by the gntK gene. FEBS Letters 394: 14–16.
9. Tong S, Porco A, Isturiz T, Conway T (1996) Cloning and molecular genetic characterization of the Escherichia coli gntR, gntK, and gntU genes of GntI, the main system for gluconate metabolism. Journal of Bacteriology 178: 3260–3269.
10. Sweetser DA, Peniket AJ, Haaland C, Blomberg AA, Zhang Y, et al. (2005) Delineation of the minimal commonly deleted segment and identification of candidate tumor-suppressor genes in del(9q) acute myeloid leukemia. Genes, Chromosomes & Cancer 44: 279–291.
11. Kraft L, Sprenger GA, Lindqvist Y (2002) Conformational changes during the catalytic cycle of gluconate kinase as revealed by X-ray crystallography. Journal of molecular biology 318: 1057–1069.
12. Uhlen M, Oksvold P, Fagerberg L, Lundberg E, Jonasson K, et al. (2010) Towards a knowledge-based Human Protein Atlas. Nat Biotechnol 28: 1248–1250.
13. Kupershmidt I, Su QJ, Grewal A, Sundaresh S, Halperin I, et al. (2010) Ontology-based meta-analysis of global collections of high-throughput public data. PLoS ONE 5.
14. Riganti C, Gazzano E, Polimeni M, Aldieri E, Ghigo D (2012) The pentose phosphate pathway: an antioxidant defense and a crossroad in tumor cell fate. Free Radic Biol Med 53: 421–436.
15. Bordbar A, Jamshidi N, Palsson BO (2011) iAB-RBC-283: A proteomically derived knowledge-base of erythrocyte metabolism that can be used to simulate its physiological and patho-physiological states. BMC systems biology 5: 110–110.
16. Leder IG (1957) Hog kidney gluconokinase. The Journal of Biological Chemistry 225: 125–136.
17. Zhang J-H, Chung TDY, Oldenburg KR (1999) A Simple Statistical Parameter for Use in Evaluation and Validation of High Throughput Screening Assays. Journal of Biomolecular Screening 4: 67–73.
18. Schellenberger J, Que R, Fleming RMT, Thiele I, Orth JD, et al. (2011) Quantitative prediction of cellular metabolism with constraint-based models: the COBRA Toolbox v2.0. Nature protocols 6: 1290–1307.
19. Mahadevan R, Schilling CH (2003) The effects of alternate optimal solutions in constraint-based genome-scale metabolic models. Metabolic Engineering 5: 264–276.
20. Palsson BO (2006) Systems Biology: Properties of Reconstructed Networks: Cambridge University Press.
21. Schellenberger J, Park J, Conrad T, Palsson B (2010) BiGG: a Biochemical Genetic and Genomic knowledgebase of large scale metabolic reconstructions. BMC Bioinformatics 11: 213–213.
22. Greenfield NJ (2006) Using circular dichroism spectra to estimate protein secondary structure. Nat Protoc 1: 2876–2890.
23. Zhang Y, Zagnitko O, Rodionova I, Osterman A, Godzik A (2011) The FGGY carbohydrate kinase family: insights into the evolution of functional specificities. PLoS Comput Biol 7: e1002318.
24. Joshi A, Palsson BO (1990) Metabolic dynamics in the human red cell. Part III—Metabolic reaction rates. J Theor Biol 142: 41–68.
25. UNEPreport (2004) Gluconic acid and derivatives. OECD SIDS. http://www.oecd.org/env/hazard/data: UNEP Publications. Accessed: May 15 2014.
26. Stetten MR, Topper YJ (1953) Pathways from Gluconic Acid to Glucose in Vivo. Journal of Biological Chemistry 203: 653–664.
27. Birnesser H, Reinauer H, Hollmann S (1973) Comparative study of enzyme activities degrading sorbitol, ribitol, xylitol and gluconate in guinea pig tissues. Diabetologia 9: 30–33.
28. Mardinoglu A, Agren R, Kampf C, Asplund A, Nookaew I, et al. (2013) Integration of clinical data with a genome-scale metabolic model of the human adipocyte. Mol Syst Biol 9: 649.
29. Karlstadt A, Fliegner D, Kararigas G, Ruderisch HS, Regitz-Zagrosek V, et al. (2012) CardioNet: a human metabolic network suited for the study of cardiomyocyte metabolism. BMC Syst Biol 6: 114.
30. Agren R, Bordel S, Mardinoglu A, Pornputtapong N, Nookaew I, et al. (2012) Reconstruction of genome-scale active metabolic networks for 69 human cell types and 16 cancer types using INIT. PLoS Comput Biol 8: e1002518.
31. Bordbar A, Feist AM, Usaite-Black R, Woodcock J, Palsson BO, et al. (2011) A multi-tissue type genome-scale metabolic network for analysis of whole-body systems physiology. BMC Systems Biology 5: 180–180.
32. Gille C, Bolling C, Hoppe A, Bulik S, Hoffmann S, et al. (2010) HepatoNet1: a comprehensive metabolic reconstruction of the human hepatocyte for the analysis of liver physiology. Mol Syst Biol 6.

33. Thiele I, Swainston N, Fleming RM, Hoppe A, Sahoo S, et al. (2013) A community-driven global reconstruction of human metabolism. Nat Biotechnol 31: 419–425.
34. Gebauer J, Schuster S, de Figueiredo LF, Kaleta C (2012) Detecting and investigating substrate cycles in a genome-scale human metabolic network. FEBS J 279: 3192–3202.
35. Dahl JL, Hokin LE (1974) SODIUM-POTASSIUM ADENOSINE-TRIPHOSPHATASE. Annual Review of Biochemistry 43: 327–356.
36. Frank JE (2005) Diagnosis and management of G6PD deficiency. Am Fam Physician 72: 1277–1282.
37. Thornalley PJ (1998) Cell activation by glycated proteins. AGE receptors, receptor recognition factors and functional classification of AGEs. Cell Mol Biol (Noisy-le-grand) 44: 1013–1023.
38. Behrends V, Bell TJ, Liebeke M, Cordes-Blauert A, Ashraf SN, et al. (2013) Metabolite profiling to characterize disease-related bacteria: gluconate excretion by Pseudomonas aeruginosa mutants and clinical isolates from cystic fibrosis patients. J Biol Chem 288: 15098–15109.
39. Bublitz C, Steavenson S (1988) The pentose phosphate pathway in the endoplasmic reticulum. J Biol Chem 263: 12849–12853.
40. Senesi S, Csala M, Marcolongo P, Fulceri R, Mandl J, et al. (2010) Hexose-6-phosphate dehydrogenase in the endoplasmic reticulum. Biological Chemistry 391: 1–8.
41. Kondo Y, Inai Y, Sato Y, Handa S, Kubo S, et al. (2006) Senescence marker protein 30 functions as gluconolactonase in l-ascorbic acid biosynthesis, and its knockout mice are prone to scurvy. 103: 5723–5728.
42. Handa S, Maruyama N, Ishigami A (2009) Over-expression of Senescence Marker Protein-30 decreases reactive oxygen species in human hepatic carcinoma Hep G2 cells. Biol Pharm Bull 32: 1645–1648.
43. Rolfsson O, Palsson BØ, Thiele I (2011) The human metabolic reconstruction Recon 1 directs hypotheses of novel human metabolic functions. BMC Systems Biology 5: 155–155.
44. Roy A, Kucukural A, Zhang Y (2010) I-TASSER: a unified platform for automated protein structure and function prediction. Nat Protocols 5: 725–738.

Substrate specificty of human gluconokinase					
Tested Substrates	**HMDB metabolites.taxonomy_super_class**	**HMDB metabolites.taxonomy_class**	**Cntrl (Luminesence) - GlcnK (Luminesence)**	**Z-score**	**P-value**
Ribitol	Alcohols and Polyols	Alcohols	4364.625	0.251581869	0.599317863
Erythritol	Alcohols and Polyols	Alcohols	-13867.938	0.061751245	0.524619535
D-arabitol	Alcohols and Polyols	Alcohols	3987.375	0.247654083	0.597798969
nicotinic acid	Amino Acids	Amino acids and Amino Acid conjugates	-13227.625	0.068417944	0.527273531
L-Phenylalanine	Amino Acids	Amino acids and Amino Acid conjugates	-17415	0.024820562	0.509900955
L-Isoleucine	Amino Acids	Amino acids and Amino Acid conjugates	44931.688	0.673950952	0.749828751
N-acetyl-L-methionine	Amino Acids	Amino acids and Amino Acid conjugates	40341.062	0.626155071	0.734393383
L-Carnitine	Quaternary Amines; Amino Acids	Amino acids and Amino Acid conjugates	-68682.813	-0.508960726	0.305389877
L-Valine	Amino Acids	Amino acids and Amino Acid conjugates	-30609.562	-0.112556281	0.455191174
Oxidized glutathione	Polypeptides	Amino acids and Amino Acid conjugates	-31019.062	-0.116819842	0.45350141
L-Methionine	Amino Acids	Amino acids and Amino Acid conjugates	-38801.625	-0.197848976	0.421581613
L-Glutamine	Amino Acids	Amino acids and Amino Acid conjugates	-64966	-0.47026266	0.319083686
L-Cystine	Amino Acids	Amino acids and Amino Acid conjugates	-58849.063	-0.4065754	0.342159934
L-Tyrosine	Amino Acids	Amino acids and Amino Acid conjugates	-4903.25	0.155088222	0.561624116
3-Methylhistidine	Amino Acids	Amino acids and Amino Acid conjugates	-17635.938	0.022520238	0.508983516
L-Aspartic acid	Amino Acids	Amino acids and Amino Acid conjugates	-32468.001	-0.131905652	0.447529459
L-Glutamic acid	Amino Acids	Amino acids and Amino Acid conjugates	-40031.937	-0.210658524	0.416576871
L-Leucine	Amino Acids	Amino acids and Amino Acid conjugates	-47088.626	-0.28413013	0.388155329
L-Histidine	Amino Acids	Amino acids and Amino Acid conjugates	22013.374	0.435334041	0.66834001
L-Asparagine	Amino Acids	Amino acids and Amino Acid conjugates	32112.563	0.540483018	0.705568015
L-Tryptophan	Amino Acids; Indoles and Indole Derivatives	Amino acids and Amino Acid conjugates	-9783.876	0.10427297	0.541523636
L-Serine	Amino Acids	Amino acids and Amino Acid conjugates	15783	0.370465718	0.644482242
L-Cysteine	Amino Acids	Amino acids and Amino Acid conjugates	-6736.75	0.135998506	0.554088769
Sarcosine	Quaternary Amines; Amino Acids	Amino acids and Amino Acid conjugates	34989.312	0.570434653	0.715808534
citrulline	Amino Acids	Amino acids and Amino Acid conjugates	11820	0.329204444	0.628999418
L-Alanine	Amino Acids	Amino acids and Amino Acid conjugates	2032.688	0.227302614	0.58990578
L-Acetylcarnitine	Quaternary Amines	Amino acids and Amino Acid conjugates	-4608.625	0.158155747	0.562832963
Ornithine	Amino Acids	Amino acids and Amino Acid conjugates	16312.875	0.375982578	0.646535076
Glycine	Amino Acids	Amino acids and Amino Acid conjugates	5862.312	0.267175226	0.605332875
L-Threonine	Amino Acids	Amino acids and Amino Acid conjugates	10535.75	0.315833314	0.623935485
L-Arginine	Amino Acids	Amino acids and Amino Acid conjugates	3279.063	0.240279404	0.59494317
L-Lysine	Amino Acids	Amino acids and Amino Acid conjugates	-2253.563	0.182675772	0.572473786
Taurine	Amino Acids	Amino acids and Amino Acid conjugates	-3328.5	0.17148393	0.568078367
L-Proline	Amino Acids	Amino acids and Amino Acid conjugates	-5516.125	0.148707197	0.559107659
Pyroglutamic acid	Amino Acids; Amino Ketones	Amino acids and Amino Acid conjugates	15827.187	0.370925776	0.644653592

Creatine	Amino Acids	Amino acids and Amino Acid conjugates	6884.562	0.27781851	0.609424159
N-Acetyl-L-alanine	Amino Acids	Amino acids and Amino Acid conjugates	2271.624	0.229790326	0.590872649
4-Hydroxy-L-proline	Amino Acids	Amino acids and Amino Acid conjugates	-25493.562	-0.059290403	0.476360403
dimethylglycine	Amino Acids	Amino acids and Amino Acid conjugates	-12713.813	0.073767562	0.529402331
Phosphocreatine	Amino Acid Phosphates	Amino acids and Amino Acid conjugates	-20830.25	-0.010737743	0.495716343
Glutathione	Polypeptides	Amino acids and Amino Acid conjugates	-21614.437	-0.018902405	0.492459481
Symmetric dimethylarginine	Amino Acids	Amino acids and Amino Acid conjugates	-5802.063	0.145730117	0.557932778
D-fructose	Carbohydrates	Carbohydrates and Carbohydrate conjugates	-48569.874	-0.29955233	0.382259325
fructose 1-phosphate	Sugar Phosphates	Carbohydrates and Carbohydrate conjugates	-20522.937	-0.007538115	0.496992756
mannose 6-phosphate	Sugar Phosphates	Carbohydrates and Carbohydrate conjugates	-26716.249	-0.072020563	0.471292772
D-mannose	Carbohydrates	Carbohydrates and Carbohydrate conjugates	-11915.125	0.082083203	0.532709725
galactose 1-phosphate	Sugar Phosphates	Carbohydrates and Carbohydrate conjugates	3189.062	0.239342347	0.594579934
6-phosphogluconic acid	Sugar Phosphates	Carbohydrates and Carbohydrate conjugates	5902.25	0.267591045	0.605492938
D-ribose 5-phosphate	Sugar Phosphates	Carbohydrates and Carbohydrate conjugates	4371.25	0.251650846	0.599344523
D-Ribose	Carbohydrates	Carbohydrates and Carbohydrate conjugates	12960.188	0.341075655	0.633476686
D-arabinose	Carbohydrates	Carbohydrates and Carbohydrate conjugates	9589.125	0.305977409	0.620189077
glucosamine 6-phosphate	Sugar Phosphates	Carbohydrates and Carbohydrate conjugates	3460.376	0.242167167	0.595674683
D-Xylose	Carbohydrates	Carbohydrates and Carbohydrate conjugates	12553.687	0.336843319	0.631882492
Fructose 1,6-bisphosphate	Sugar Phosphates	Carbohydrates and Carbohydrate conjugates	-20554.75	-0.00786934	0.49686062
glucose 6-phosphate	Sugar Phosphates	Carbohydrates and Carbohydrate conjugates	-6866	0.134652803	0.553556805
fructose 6-phosphate	Sugar Phosphates	Carbohydrates and Carbohydrate conjugates	10485.125	0.315306225	0.623735421
Beta-D-Galactose	Carbohydrates	Carbohydrates and Carbohydrate conjugates	21406.125	0.429011591	0.666042605
N-Acetyl-D-glucosamine	Carbohydrates	Carbohydrates and Carbohydrate conjugates	-15316.562	0.046668714	0.518611367
Erythrose	Carbohydrates	Carbohydrates and Carbohydrate conjugates	-24711.75	-0.051150469	0.47960281
D-Xylulose	Carbohydrates	Carbohydrates and Carbohydrate conjugates	-13238.84056	0.068301172	0.527227054
gluconolactone	Carbohydrates	Carbohydrates and Carbohydrate conjugates	-678998.172	-6.863335906	3.36354E-12
D-Glucuronic acid	Carbohydrates	Carbohydrates and Carbohydrate conjugates	8372.188	0.293307116	0.615356292
glucose 1-phosphate	Sugar Phosphates	Carbohydrates and Carbohydrate conjugates	-12143.125	0.079709352	0.531765789
D-Ribulose	Carbohydrates	Carbohydrates and Carbohydrate conjugates	-57093.126	-0.388293241	0.348899519
D-Ribulose 5-phosphate	Sugar Phosphates	Carbohydrates and Carbohydrate conjugates	-29922.187	-0.10539959	0.458029371
Glucosamine-1P	Sugar Phosphates	Carbohydrates and Carbohydrate conjugates	7596.624	0.285232234	0.612266887
Xylulose 5-phosphate	Sugar Phosphates	Carbohydrates and Carbohydrate conjugates	-26791.75	-0.072806651	0.470979989
H2O	Control	Control	49988.938	0.726605147	0.766266063
H2O	Control	Control	1701.626	0.22385572	0.588565214
H2O	Control	Control	-42190.687	-0.233134622	0.407828436
Folic acid	Pterins; Benzamides	Miscellaneous	9210.125	0.302031402	0.618685938
Dimethylallylpyrophosphate	Acyl Phosphates	Miscellaneous	-89707.406	-0.727860922	0.233349363
Glycerol 3-phosphate	Acyl Phosphates	Miscellaneous	-32499.687	-0.132235555	0.44739899
Phosphoenolpyruvic acid	Acyl Phosphates	Miscellaneous	-6517.688	0.138279298	0.554990157
Serotonin	Indoles and Indole Derivatives	Miscellaneous	-6861.437	0.134700312	0.553575587
Cyanocobalamin	Cobalamin Derivatives	Miscellaneous	28113.68	0.498848145	0.691056816

Mevalonic acid-5P	Acyl Phosphates	Miscellaneous	-3029.75	0.174594403	0.569300827
3-Phosphoglyceric acid	Acyl Phosphates	Miscellaneous	-2948.063	0.175444898	0.569634968
Cytidine monophosphate	Nucleotides	Nucleosides and Nucleoside conjugates	3739.437	0.245072646	0.596799909
Adenosine monophosphate	Nucleotides	Nucleosides and Nucleoside conjugates	4852.324	0.256659609	0.601279223
Uridine diphosphate glucose	Nucleotides	Nucleosides and Nucleoside conjugates	8202.938	0.291544948	0.614682714
Uridine 5'-diphosphate	Nucleotides	Nucleosides and Nucleoside conjugates	1607.5	0.222875715	0.588183881
GDP	Nucleotides	Nucleosides and Nucleoside conjugates	4243.312	0.250318804	0.598829592
UMP	Nucleotides	Nucleosides and Nucleoside conjugates	-4567.249	0.158586539	0.563002682
Inosine 2'-phosphate	Nucleotides	Nucleosides and Nucleoside conjugates	-18794.125	0.010461629	0.50417351
Guanosine monophosphate	Nucleotides	Nucleosides and Nucleoside conjugates	-7146.687	0.131730395	0.552401229
Guanosine triphosphate	Nucleotides	Nucleosides and Nucleoside conjugates	-5581.251	0.148029129	0.55884011
Cytidine	Nucleoside Analogues	Nucleosides and Nucleoside conjugates	-32723.312	-0.134563855	0.446478361
ADP	Nucleotides	Nucleosides and Nucleoside conjugates	-6896.562	0.134334603	0.553431004
Adenylsuccinic acid	Nucleotides	Nucleosides and Nucleoside conjugates	-5056.563	0.153491985	0.560994845
CDP	Nucleotides	Nucleosides and Nucleoside conjugates	7640.438	0.285688409	0.612441608
S-Adenosylmethionine	Nucleoside Analogues	Nucleosides and Nucleoside conjugates	23144.875	0.447114806	0.672603915
Propionyl-CoA	Coenzyme A Derivatives	Nucleosides and Nucleoside conjugates	-24328.563	-0.047160869	0.481192507
Malonyl-CoA	Coenzyme A Derivatives	Nucleosides and Nucleoside conjugates	28553.813	0.503430645	0.692669235
Acetoacetyl-coA	Coenzyme A Derivatives	Nucleosides and Nucleoside conjugates	-9381.562	0.108461713	0.543185275
acetyl-coA	Coenzyme A Derivatives	Nucleosides and Nucleoside conjugates	-2205.625	0.183174884	0.5726696
Butyryl-CoA	Coenzyme A Derivatives	Nucleosides and Nucleoside conjugates	-22951.501	-0.032823415	0.486907703
Cytidine triphosphate	Nucleotides	Nucleosides and Nucleoside conjugates	-20926.813	-0.011743121	0.49531528
ADP-glucose	Nucleotides	Nucleosides and Nucleoside conjugates	-21011.125	-0.012620946	0.494965105
Coenzyme A	Coenzyme A Derivatives	Nucleosides and Nucleoside conjugates	-13756.875	0.062907591	0.525079955
3-Hydroxy-3-methylglutaryl-CoA	Coenzyme A Derivatives	Nucleosides and Nucleoside conjugates	12746.937	0.338855366	0.632640655
4-Hydroxyphenylpyruvic acid	Aromatic Acids	Organic acids	-65860.25	-0.479573256	0.315765433
methylmalonic acid	Dicarboxylic Acids	Organic acids	-73484.375	-0.558952793	0.288096969
salicylic acid	Salicylates	Organic acids	-5952.125	0.144167728	0.557315988
fumaric acid	Dicarboxylic Acids	Organic acids	-16470.625	0.034653041	0.513821797
Protocatechuic acid	Aromatic Acids	Organic acids	-11062.75	0.090957813	0.536236944
arabinonic acid	Hydroxy Acids	Organic acids	-19875.312	-0.000795286	0.499682727
Hydrocinnamic acid	Aromatic Acids	Organic acids	-10370.125	0.098169165	0.539101017
Shikimic acid	Hydroxy Acids	Organic acids	-9296.376	0.109348638	0.543537015
Ascorbic acid	Hydroxy Acids	Organic acids	-31265.5	-0.119385662	0.45248491
Isocitric acid	Tricarboxylic Acids	Organic acids	13927.312	0.351144989	0.637260211
itaconic acid	Dicarboxylic Acids	Organic acids	-23247.687	-0.035907193	0.48567818
glyceric acid	Hydroxy Acids	Organic acids	1043.875	0.217007463	0.585898735
oxalic acid	Dicarboxylic Acids	Organic acids	6709.625	0.275997132	0.608724865
Alpha-ketoisovaleric acid	Keto-Acids	Organic acids	10047.125	0.310745933	0.622003112
3-hydroxyphenylacetic acid	Hydroxy Acids	Organic acids	2415.562	0.231288954	0.591454836
Oxalacetic acid	Dicarboxylic Acids	Organic acids	-5515.499	0.148713715	0.559110231
3-Methyl-2-oxovaleric acid	Keto-Acids	Organic acids	6181.437	0.270497836	0.606611359
D-xylonate	Hydroxy Acids	Organic acids	5415.063	0.262518637	0.60353919
cis-aconitic acid	Tricarboxylic Acids	Organic acids	2115.563	0.228165477	0.590241201
glutaric acid	Dicarboxylic Acids	Organic acids	-15933.125	0.04024929	0.516052809
oxoglutaric acid	Dicarboxylic Acids	Organic acids	1605.75	0.222857495	0.588176791

3,5-dinitrosalicylic acid	Salicylates	Organic acids	212.249	0.208348884	0.582521717
mevalonic acid	Hydroxy Acids	Organic acids	-12398.937	0.077045933	0.530706498
Gluconic acid	Hydroxy Acids	Organic acids	-810096.844	-8.22828623	9.49554E-17

Flux variability analysis results before and after adding gluconate												
Reaction No.	Reaction Abbreviation	Subsystem	Reaction Formula	Minflux_glcn0	Maxflux_glcn0	Range	Minflux_glcn	Maxflux_glcn	Minflux_diff	Maxflux_diff	Minfluxdiff %	Maxfluxdiff %
1	EX_35cgmp(e)	Exchange/demand reaction	35cgmp[e] ->	0.000	0.000	0.000	0.000	0.024	0.000	0.024	0	29000752.1
2	EX_3moxtyr(e)	Exchange/demand reaction	3moxtyr[e] ->	0.000	0.000	0.000	0.000	0.032	0.000	0.032	0	2699979.51
3	EX_4pyrdx(e)	Exchange/demand reaction	4pyrdx[e] ->	0.000	0.000	0.000	0.000	0.000	0.000	0.000	0	47776.4098
4	EX_5aop(e)	Exchange/demand reaction	-> 5aop[e]	0.000	0.000	0.000	-0.020	-0.020	-0.020	-0.020	-1249937.4	-1249570.7
5	EX_ac(e)	Exchange/demand reaction	ac[e] ->	0.000	0.000	0.000	0.000	0.000	0.000	0.000	-9250.2759	0
6	EX_acald(e)	Exchange/demand reaction	acald[e] <=>	0.000	0.000	0.000	0.000	0.000	0.000	0.000	-9250.2753	0
7	EX_acnam(e)	Exchange/demand reaction	-> acnam[e]	0.000	0.000	0.000	0.000	0.000	0.000	0.000	0	9250.27588
8	EX_ade(e)	Exchange/demand reaction	ade[e] <=>	-0.014	0.010	0.024	-0.014	0.010	0.000	0.000	0	0
9	EX_adn(e)	Exchange/demand reaction	adn[e] <=>	-0.010	-0.010	0.000	-0.010	0.014	0.000	0.024	0	8000135.06
10	EX_adrnl(e)	Exchange/demand reaction	-> adrnl[e]	0.000	0.000	0.000	-0.038	0.000	-0.038	0.000	-3149992.8	0
11	EX_ala-L(e)	Exchange/demand reaction	ala-L[e] ->	0.000	0.000	0.000	0.055	0.080	0.055	0.080	23997085.9	35000930.7
12	EX_arg-L(e)	Exchange/demand reaction	-> arg-L[e]	-0.115	0.000	0.115	-0.115	0.000	0.000	0.000	0	0
13	EX_ascb-L(e)	Exchange/demand reaction	ascb-L[e] ->	0.000	0.111	0.111	0.000	0.111	0.000	0.000	0	0
14	EX_bilglcur(e)	Exchange/demand reaction	bilglcur[e] ->	0.000	0.000	0.000	0.002	0.003	0.002	0.002	1249570.73	1249937.38
15	EX_ca2(e)	Exchange/demand reaction	ca2[e] <=>	0.000	0.000	0.000	0.000	0.000	0.000	0.000	#DIV/0!	#DIV/0!
16	EX_camp(e)	Exchange/demand reaction	camp[e] ->	0.000	0.000	0.000	0.000	0.024	0.000	0.024	0	20000487.8
17	EX_chol(e)	Exchange/demand reaction	-> chol[e]	0.000	0.000	0.000	-0.012	0.000	-0.012	0.000	-10500209	0
18	EX_cl(e)	Exchange/demand reaction	cl[e] <=>	0.000	0.000	0.000	0.000	0.000	0.000	0.000	#DIV/0!	#DIV/0!
19	EX_co(e)	Exchange/demand reaction	co[e] ->	0.000	0.000	0.000	0.002	0.003	0.002	0.002	1249570.73	1249937.38
20	EX_co2(e)	Exchange/demand reaction	co2[e] <=>	-5.778	-4.913	0.865	-5.657	2.286	0.120	7.198	13.9167812	831.989221
21	EX_cys-L(e)	Exchange/demand reaction	-> cys-L[e]	0.000	0.000	0.000	-0.080	-0.080	-0.080	-0.080	-35000931	-35000622
22	EX_dhdascb(e)	Exchange/demand reaction	-> dhdascb[e]	-0.111	0.000	0.111	-0.111	0.000	0.000	0.000	0	0
23	EX_dopa(e)	Exchange/demand reaction	-> dopa[e]	0.000	0.000	0.000	-0.032	0.000	-0.032	0.000	-2699979.5	0
24	EX_etha(e)	Exchange/demand reaction	-> etha[e]	0.000	0.000	0.000	-0.012	0.000	-0.012	0.000	-10500209	0
25	EX_fe2(e)	Exchange/demand reaction	fe2[e] <=>	0.000	0.000	0.000	0.000	0.000	0.000	0.000	#DIV/0!	#DIV/0!
26	EX_fru(e)	Exchange/demand reaction	fru[e] <=>	-0.008	-0.007	0.000	-0.008	1.120	0.000	1.127	0	281883193
27	EX_fum(e)	Exchange/demand reaction	fum[e] <=>	-0.250	0.500	0.750	-0.250	0.500	0.000	0.000	0	0
28	EX_gal(e)	Exchange/demand reaction	-> gal[e]	-0.317	-0.317	0.000	-0.317	0.000	0.000	0.317	0	79227237.6
29	EX_gam(e)	Exchange/demand reaction	-> gam[e]	0.000	0.000	0.000	0.000	0.000	0.000	0.000	0	2400.07361
30	EX_glc(e)	Exchange/demand reaction	-> glc-D[e]	-1.120	-1.120	0.000	-1.120	0.000	0.000	1.120	0	280008139
31	EX_gln-L(e)	Exchange/demand reaction	gln-L[e] <=>	0.000	0.000	0.000	-0.025	0.000	-0.025	0.000	-14147830	0
32	EX_gluala(e)	Exchange/demand reaction	-> gluala[e]	0.000	0.000	0.000	-0.080	-0.055	-0.080	-0.055	-35000931	-23997086
33	EX_gly(e)	Exchange/demand reaction	-> gly[e]	0.000	0.000	0.000	-0.080	-0.080	-0.080	-0.080	-35000931	-35000622
34	EX_glyc(e)	Exchange/demand reaction	-> glyc[e]	0.000	0.000	0.000	-0.012	0.000	-0.012	0.000	-10500209	0
35	EX_gthox(e)	Exchange/demand reaction	gthox[e] ->	0.000	0.000	0.000	0.040	0.040	0.040	0.040	35000621.5	35000929.9
36	EX_h(e)	Exchange/demand reaction	h[e] <=>	7.851	10.000	2.149	5.582	10.000	-2.270	0.000	-105.65181	0
37	EX_h2o(e)	Exchange/demand reaction	h2o[e] <=>	-6.289	4.712	11.001	-6.457	10.000	-0.168	5.288	-1.5246074	48.0662713
38	EX_h2o2(e)	Exchange/demand reaction	h2o2[e] <=>	-10.000	0.000	10.000	-10.000	0.001	0.000	0.001	0	0.006102
39	EX_hco3(e)	Exchange/demand reaction	hco3[e] <=>	5.834	5.834	0.000	5.871	5.871	0.037	0.037	2041775.76	2041726.8
40	EX_hcyst-L(e)	Exchange/demand reaction	hcys-L[e] ->	0.000	0.000	0.000	0.000	0.010	0.000	0.010	0	3750010.33
41	EX_hdca(e)	Exchange/demand reaction	-> hdca[e]	0.000	0.000	0.000	-0.012	0.000	-0.012	0.000	-5250054.3	0

42	EX_hxan(e)	Exchange/demand reaction	hxan[e] ->	0.000	0.024	0.024	0.000	0.024	0.000	0.000	0	0
43	EX_ins(e)	Exchange/demand reaction	ins[e] ->	0.000	0.000	0.000	0.000	0.024	0.000	0.024	0	8000135.06
44	EX_k(e)	Exchange/demand reaction	k[e] <=>	0.000	0.000	0.000	0.000	0.000	0.000	0.000	#DIV/0!	#DIV/0!
45	EX_lac-D(e)	Exchange/demand reaction	lac-D[e] ->	0.000	0.000	0.000	0.000	1.468	0.000	1.468	0	366955881
46	EX_lac-L(e)	Exchange/demand reaction	lac-L[e] ->	1.833	3.657	1.824	1.075	3.676	-0.757	0.019	-41.512364	1.02288341
47	EX_leuktrA4(e)	Exchange/demand reaction	-> leuktrA4[e]	0.000	0.000	0.000	0.000	0.000	0.000	0.000	0	0
48	EX_leuktrB4(e)	Exchange/demand reaction	leuktrB4[e] ->	0.000	0.000	0.000	0.000	0.000	0.000	0.000	0	0
49	EX_lnlc(e)	Exchange/demand reaction	-> lnlc[e]	0.000	0.000	0.000	-0.006	0.000	-0.006	0.000	-4875043.2	0
50	EX_mal-L(e)	Exchange/demand reaction	mal-L[e] <=>	-0.500	0.250	0.750	-0.500	0.250	0.000	0.000	0	0
51	EX_man(e)	Exchange/demand reaction	-> man[e]	-0.010	-0.010	0.000	-0.010	0.000	0.000	0.010	0	2499973.76
52	EX_mepi(e)	Exchange/demand reaction	mepi[e] ->	0.000	0.000	0.000	0.000	0.038	0.000	0.038	0	3149992.76
53	EX_met-L(e)	Exchange/demand reaction	-> met-L[e]	0.000	0.000	0.000	-0.010	0.000	-0.010	0.000	-3750010.5	0
54	EX_na1(e)	Exchange/demand reaction	na1[e] <=>	0.000	0.000	0.000	0.000	0.000	0.000	0.000	#DIV/0!	#DIV/0!
55	EX_nac(e)	Exchange/demand reaction	-> nac[e]	0.000	0.000	0.000	-0.001	0.000	-0.001	0.000	-499914.69	0
56	EX_ncam(e)	Exchange/demand reaction	ncam[e] ->	0.000	0.000	0.000	0.000	0.001	0.000	0.001	0	499914.691
57	EX_nh4(e)	Exchange/demand reaction	nh4[e] <=>	0.000	0.024	0.024	0.009	0.034	0.009	0.010	37.2867478	42.0778963
58	EX_normete-L(e)	Exchange/demand reaction	normete-L[e] ->	0.000	0.000	0.000	0.000	0.029	0.000	0.029	0	2399970.67
59	EX_nrpphr(e)	Exchange/demand reaction	-> nrpphr[e]	0.000	0.000	0.000	-0.029	0.000	-0.029	0.000	-2399970.7	0
60	EX_o2(e)	Exchange/demand reaction	o2[e] <=>	0.000	5.000	5.000	-0.039	4.986	-0.039	-0.014	-0.7881644	-0.2733553
61	EX_ocdcea(e)	Exchange/demand reaction	-> ocdcea[e]	0.000	0.000	0.000	-0.006	0.000	-0.006	0.000	-2624977.1	0
62	EX_orot(e)	Exchange/demand reaction	-> orot[e]	0.000	0.000	0.000	-0.010	0.000	-0.010	0.000	-5833405.1	0
63	EX_phe-L(e)	Exchange/demand reaction	phe-L[e] <=>	0.000	0.000	0.000	0.000	0.000	0.000	0.000	#DIV/0!	#DIV/0!
64	EX_pi(e)	Exchange/demand reaction	-> pi[e]	0.000	0.000	0.000	-1.305	0.000	-1.305	0.000	-163092280	0
65	EX_ptrc(e)	Exchange/demand reaction	ptrc[e] ->	0.000	0.115	0.115	0.000	0.115	0.000	0.000	0	0
66	EX_pydam(e)	Exchange/demand reaction	-> pydam[e]	0.000	0.000	0.000	0.000	0.000	0.000	0.000	-12400.368	0
67	EX_pydx(e)	Exchange/demand reaction	pydx[e] <=>	0.000	0.000	0.000	0.000	0.000	0.000	0.000	-9637.7853	14200.4196
68	EX_pydxn(e)	Exchange/demand reaction	pydxn[e] <=>	0.000	0.000	0.000	0.000	0.000	0.000	0.000	-7950.2356	15887.9693
69	EX_pyr(e)	Exchange/demand reaction	pyr[e] ->	0.000	1.824	1.824	0.000	2.933	0.000	1.108	0	60.7631057
70	EX_ribflv(e)	Exchange/demand reaction	ribflv[e] <=>	0.000	0.000	0.000	0.000	0.000	0.000	0.000	#DIV/0!	#DIV/0!
71	EX_spmd(e)	Exchange/demand reaction	spmd[e] ->	0.000	0.000	0.000	0.000	0.025	0.000	0.025	0	20959794.3
72	EX_sprm(e)	Exchange/demand reaction	sprm[e] ->	0.000	0.000	0.000	0.000	0.013	0.000	0.013	0	20959794.7
73	EX_thm(e)	Exchange/demand reaction	-> thm[e]	0.000	0.000	0.000	0.000	0.000	0.000	0.000	-14900.441	0
74	EX_thmmp(e)	Exchange/demand reaction	thmmp[e] ->	0.000	0.000	0.000	0.000	0.000	0.000	0.000	0	14900.4407
75	EX_urea(e)	Exchange/demand reaction	urea[e] ->	0.000	0.115	0.115	0.000	0.115	0.000	0.000	0	0
76	EX_uri(e)	Exchange/demand reaction	uri[e] ->	0.000	0.000	0.000	0.000	0.010	0.000	0.010	0	5833404.73
77	sink_adprbp(c)	Exchange/demand reaction	adprbp[c] <=>	0.000	0.000	0.000	0.000	0.024	0.000	0.024	0	31000811.1
78	sink_akg(c)	Exchange/demand reaction	akg[c] <=>	0.000	0.000	0.000	0.000	0.025	0.000	0.025	0	20959795.1
79	sink_band(c)	Exchange/demand reaction	band[c] <=>	0.000	0.000	0.000	-0.010	0.099	-0.010	0.099	-681820.07	6750116.83
80	sink_bandmt(c)	Exchange/demand reaction	bandmt[c] <=>	0.000	0.000	0.000	-0.099	0.010	-0.099	0.010	-6750116.8	681820.066
81	sink_for(c)	Exchange/demand reaction	for[c] <=>	0.000	0.000	0.000	0.000	0.025	0.000	0.025	0	20959795.1
82	sink_mi1345p(c)	Exchange/demand reaction	mi1345p[c] <=>	0.000	0.000	0.000	-1.133	2.105	-1.133	2.105	-94456871	175419898
83	sink_mi134p(c)	Exchange/demand reaction	mi134p[c] <=>	0.000	0.000	0.000	0.000	2.105	0.000	2.105	0	263129850
84	sink_mi145p(c)	Exchange/demand reaction	mi145p[c] <=>	0.000	0.000	0.000	-4.210	0.378	-4.210	0.378	-247651618	22225147.8
85	sink_mi14p(c)	Exchange/demand reaction	mi14p[c] <=>	0.000	0.000	0.000	0.000	2.105	0.000	2.105	0	263129851

86	sink_pchol_hs_16_0_16_0(c)	Exchange/demand reaction	pchol_hs_16_0_16_0[c] <=>	0.000	0.000	0.000	-0.178	0.178	-0.178	0.178	-89921801	89921785.9
87	sink_pchol_hs_16_0_18_1(c)	Exchange/demand reaction	pchol_hs_16_0_18_1[c] <=>	0.000	0.000	0.000	-0.351	0.351	-0.351	0.351	-131564929	131645288
88	sink_pchol_hs_16_0_18_2(c)	Exchange/demand reaction	pchol_hs_16_0_18_2[c] <=>	0.000	0.000	0.000	-0.351	0.351	-0.351	0.351	-131564932	131618505
89	sink_pchol_hs_18_1_18_1(c)	Exchange/demand reaction	pchol_hs_18_1_18_1[c] <=>	0.000	0.000	0.000	-0.180	0.177	-0.180	0.177	-90695498	89148089.1
90	sink_pchol_hs_18_1_18_2(c)	Exchange/demand reaction	pchol_hs_18_1_18_2[c] <=>	0.000	0.000	0.000	-0.351	0.351	-0.351	0.351	-131564929	131618502
91	sink_pchol_hs_18_2_16_0(c)	Exchange/demand reaction	pchol_hs_18_2_16_0[c] <=>	0.000	0.000	0.000	-0.351	0.351	-0.351	0.351	-131564929	131618502
92	sink_pchol_hs_18_2_18_1(c)	Exchange/demand reaction	pchol_hs_18_2_18_1[c] <=>	0.000	0.000	0.000	-0.351	0.351	-0.351	0.351	-131564928	131618501
93	sink_pe_hs_16_0_16_0(c)	Exchange/demand reaction	pe_hs_16_0_16_0[c] <=>	0.000	0.000	0.000	0.000	0.012	0.000	0.012	0	10500208.5
94	sink_pe_hs_16_0_18_1(c)	Exchange/demand reaction	pe_hs_16_0_18_1[c] <=>	0.000	0.000	0.000	0.000	0.012	0.000	0.012	0	10500208.6
95	sink_pe_hs_16_0_18_2(c)	Exchange/demand reaction	pe_hs_16_0_18_2[c] <=>	0.000	0.000	0.000	0.000	0.012	0.000	0.012	0	10500208.5
96	sink_pe_hs_18_1_18_1(c)	Exchange/demand reaction	pe_hs_18_1_18_1[c] <=>	0.000	0.000	0.000	0.000	0.012	0.000	0.012	0	10500208.5
97	sink_pe_hs_18_1_18_2(c)	Exchange/demand reaction	pe_hs_18_1_18_2[c] ->	0.000	0.000	0.000	0.000	0.012	0.000	0.012	0	10500208.6
98	sink_pe_hs_18_2_16_0(c)	Exchange/demand reaction	pe_hs_18_2_16_0[c] ->	0.000	0.000	0.000	0.000	0.012	0.000	0.012	0	10500208.5
99	sink_pe_hs_18_2_18_1(c)	Exchange/demand reaction	pe_hs_18_2_18_1[c] ->	0.000	0.000	0.000	0.000	0.012	0.000	0.012	0	10500208.6
100	2KMBTA	Amino Acid Metabolism	2kmb[c] + glu-L[c] -> akg[c] + met-L[c]	0.000	0.000	0.000	0.000	0.025	0.000	0.025	0	20959795.1
101	3MOXTYRESSte	Transport	3 3moxtyr[c] + 2 atp[c] + 2 h2o[c] -> 2 adp[c] + 2 h[c] + 2 pi[c] + 3 3moxtyr[e]	0.000	0.000	0.000	0.000	0.011	0.000	0.011	0	2699979.51
102	4PYRDX	Transport	4pyrdx[c] + atp[c] + h2o[c] -> adp[c] + h[c] + pi[c] + 4pyrdx[e]	0.000	0.000	0.000	0.000	0.000	0.000	0.000	0	47776.4098
103	5AOPt2	Transport	5aop[e] + h[e] -> 5aop[c] + h[c]	0.000	0.000	0.000	0.020	0.020	0.020	0.020	1249570.73	1249937.38
104	ACALDt	Transport	acald[e] <=> acald[c]	0.000	0.000	0.000	0.000	0.000	0.000	0.000	0	9250.27532
105	ACGAM2E	Carbohydrate Metabolism	acgam[c] <=> acmana[c]	0.000	0.000	0.000	0.000	0.000	0.000	0.000	0	9250.27588
106	ACGAMK	Carbohydrate Metabolism	acgam[c] + atp[c] -> acgam6p[c] + adp[c] + h[c]	0.000	0.000	0.000	0.000	0.000	0.000	0.000	-9250.2759	0
107	ACNAM9PL	Carbohydrate Metabolism	acmanap[c] + h2o[c] + pep[c] -> acnamp[c] + pi[c]	0.000	0.000	0.000	0.000	1.052	0.000	1.052	0	263129851
108	ACNAMPH	Carbohydrate Metabolism	acnamp[c] + h2o[c] -> acnam[c] + pi[c]	0.000	0.000	0.000	0.000	1.052	0.000	1.052	0	263129851
109	ACNAMt2	Transport	acnam[e] + h[e] -> acnam[c] + h[c]	0.000	0.000	0.000	0.000	0.000	0.000	0.000	-9250.2759	0
110	ACNMLr	Carbohydrate Metabolism	acnam[c] <=> acmana[c] + pyr[c]	0.000	0.000	0.000	0.000	1.053	0.000	1.052	-4625.1376	131564035
111	ACP1(FMN)	Vitamin Metabolism	fmn[c] + h2o[c] -> pi[c] + ribflv[c]	0.000	0.000	0.000	0.000	2.105	0.000	2.105	0	263129850
112	ACt2r	Transport	ac[e] + h[e] <=> ac[c] + h[c]	0.000	0.000	0.000	0.000	0.000	0.000	0.000	0	9250.27588
113	ADA	Nucleotide Metabolism	adn[c] + h[c] + h2o[c] -> ins[c] + nh4[c]	0.000	0.024	0.024	0.000	0.024	0.000	0.000	0	0

114	ADEt	Transport	ade[e] <=> ade[c]	-0.010	0.014	0.024	-0.010	0.014	0.000	0.000	0	0
115	ADK1	Nucleotide Metabolism	amp[c] + atp[c] <=> 2 adp[c]	0.000	0.000	0.000	0.000	1.053	0.000	1.053	0	263134227
116	ADMDC	Amino Acid Metabolism	amet[c] + h[c] -> ametam[c] + co2[c]	0.000	0.000	0.000	0.000	0.025	0.000	0.025	0	20959795.1
117	ADNCYC	Nucleotide Metabolism	atp[c] -> camp[c] + ppi[c]	0.000	0.000	0.000	0.000	1.052	0.000	1.052	0	263129850
118	ADNK1	Nucleotide Metabolism	adn[c] + atp[c] -> adp[c] + amp[c] + h[c]	0.000	0.000	0.000	0.000	2.105	0.000	2.105	0	263129851
119	ADNt	Transport	adn[e] <=> adn[c]	0.010	0.010	0.000	-0.014	0.010	-0.024	0.000	-8000135.1	0
120	ADPT	Nucleotide Metabolism	ade[c] + prpp[c] -> amp[c] + ppi[c]	0.000	0.000	0.000	0.000	1.052	0.000	1.052	0	263129851
121	ADRNLtu	Transport	adrnl[e] <=> adrnl[c]	0.000	0.000	0.000	0.000	0.038	0.000	0.038	0	3149992.76
122	AGDC	Carbohydrate Metabolism	acgam6p[c] + h2o[c] -> ac[c] + gam6p[c]	0.000	0.000	0.000	0.000	0.000	0.000	0.000	-9250.2759	0
123	AGPAT1_16_0_16_0	Lipid Metabolism	alpa_hs_16_0[c] + pmtcoa[c] -> coa[c] + pa_hs_16_0_16_0[c]	0.000	0.000	0.000	0.000	0.351	0.000	0.351	0	263237003
124	AGPAT1_16_0_18_1	Lipid Metabolism	alpa_hs_16_0[c] + odecoa[c] -> coa[c] + pa_hs_16_0_18_1[c]	0.000	0.000	0.000	0.000	0.351	0.000	0.351	0	263290588
125	AGPAT1_16_0_18_2	Lipid Metabolism	alpa_hs_16_0[c] + lnlccoa[c] -> coa[c] + pa_hs_16_0_18_2[c]	0.000	0.000	0.000	0.000	0.351	0.000	0.351	0	263237005
126	AGPAT1_18_1_18_1	Lipid Metabolism	alpa_hs_18_1[c] + odecoa[c] -> coa[c] + pa_hs_18_1_18_1[c]	0.000	0.000	0.000	0.000	0.351	0.000	0.351	0	263183424
127	AGPAT1_18_1_18_2	Lipid Metabolism	alpa_hs_18_1[c] + lnlccoa[c] -> coa[c] + pa_hs_18_1_18_2[c]	0.000	0.000	0.000	0.000	0.351	0.000	0.351	0	263237005
128	AGPAT1_18_2_16_0	Lipid Metabolism	alpa_hs_18_2[c] + pmtcoa[c] -> coa[c] + pa_hs_18_2_16_0[c]	0.000	0.000	0.000	0.000	0.351	0.000	0.351	0	263237006
129	AGPAT1_18_2_18_1	Lipid Metabolism	alpa_hs_18_2[c] + odecoa[c] -> coa[c] + pa_hs_18_2_18_1[c]	0.000	0.000	0.000	0.000	0.351	0.000	0.351	0	263237002
130	AHC	Amino Acid Metabolism	ahcys[c] + h2o[c] <=> adn[c] + hcys-L[c]	0.000	0.000	0.000	0.000	0.010	0.000	0.010	0	3750010.33
131	ALAt4	Transport	ala-L[e] + na1[e] <=> ala-L[c] + na1[c]	0.000	0.000	0.000	-0.080	-0.055	-0.080	-0.055	-35000931	-23997086
132	ALDD2x	Glycolysis/Gluconeogenesis	acald[c] + h2o[c] + nad[c] -> ac[c] + 2 h[c] + nadh[c]	0.000	0.000	0.000	0.000	0.000	0.000	0.000	0	9250.27532
133	AMANK	Carbohydrate Metabolism	acmana[c] + atp[c] -> acmanap[c] + adp[c] + h[c]	0.000	0.000	0.000	0.000	1.052	0.000	1.052	0	263129851
134	AMPDA	Nucleotide Metabolism	amp[c] + h[c] + h2o[c] -> imp[c] + nh4[c]	0.000	0.000	0.000	0.000	0.024	0.000	0.024	0	2999988.27
135	AP4AH1	Nucleotide Metabolism	ap4a[c] + h2o[c] -> amp[c] + atp[c] + 2 h[c]	0.000	0.000	0.000	0.000	0.000	0.000	0.000	#DIV/0!	#DIV/0!
136	ARD1_hs	Amino Acid Metabolism	dhmtp[c] + o2[c] -> 2kmb[c] + for[c] + 2 h[c]	0.000	0.000	0.000	0.000	0.025	0.000	0.025	0	20959795.1

137	ARGN	Amino Acid Metabolism	arg-L[c] + h2o[c] -> orn[c] + urea[c]	0.000	0.115	0.115	0.000	0.115	0.000	0.000	0	0
138	ARGt5r	Transport	arg-L[e] <=> arg-L[c]	0.000	0.115	0.115	0.000	0.115	0.000	0.000	0	0
139	ARS_hs	Amino Acid Metabolism	dkmpp[c] + h2o[c] -> dhmtp[c] + pi[c]	0.000	0.000	0.000	0.000	0.025	0.000	0.025	0	20959795.1
140	ASCBt	Transport	ascb-L[e] <=> ascb-L[c]	-0.111	0.000	0.111	-0.111	0.000	0.000	0.000	0	0
141	BANDMT	Amino Acid Metabolism	amet[c] + band[c] <=> ahcys[c] + bandmt[c] + h[c]	0.000	0.000	0.000	-0.099	0.010	-0.099	0.010	-6750116.8	681820.066
142	BILGLCURt	Transport	hco3[c] + bilglcur[e] <=> bilglcur[c] + hco3[e]	0.000	0.000	0.000	-0.003	-0.002	-0.002	-0.002	-1249937.4	-1249570.7
143	BILIRBU	Miscellaneous	bilirub[c] + 2 h[c] + udpglcur[c] -> bilglcur[c] + udp[c]	0.000	0.000	0.000	0.002	0.003	0.002	0.002	1249570.73	1249937.38
144	BILIRED	Miscellaneous	biliverd[c] + h[c] + nadph[c] -> bilirub[c] + nadp[c]	0.000	0.000	0.000	0.002	0.003	0.002	0.002	1249570.73	1249937.38
145	C160CPT1	Lipid Metabolism	crn[c] + pmtcoa[c] -> coa[c] + pmtcrn[c]	0.000	1000.000	1000.000	0.000	1000.000	0.000	0.000	0	0
146	C160CPT2rbc	Lipid Metabolism	coa[c] + pmtcrn[c] -> crn[c] + pmtcoa[c]	0.000	1000.000	1000.000	0.000	1000.000	0.000	0.000	0	0
147	C181CPT1	Lipid Metabolism	crn[c] + odecoa[c] -> coa[c] + odecrn[c]	0.000	1000.000	1000.000	0.000	1000.000	0.000	0.000	0	0
148	C181CPT2rbc	Lipid Metabolism	coa[c] + odecrn[c] -> crn[c] + odecoa[c]	0.000	1000.000	1000.000	0.000	1000.000	0.000	0.000	0	0
149	CA2t	Transport	ca2[e] <=> ca2[c]	0.000	0.000	0.000	0.000	4.210	0.000	4.210	0	263129850
150	CAATPS	Transport	atp[c] + 2 ca2[c] + h2o[c] -> adp[c] + pi[c] + 2 ca2[e] + h[e]	0.000	0.000	0.000	0.000	2.105	0.000	2.105	0	263129850
151	CAMPt	Transport	atp[c] + camp[c] + h2o[c] -> adp[c] + h[c] + pi[c] + camp[e]	0.000	0.000	0.000	0.000	0.024	0.000	0.024	0	20000487.8
152	CAT	Miscellaneous	2 h2o2[c] -> 2 h2o[c] + o2[c]	0.000	5.000	5.000	0.000	5.000	0.000	0.000	0	0.006102
153	CDIPTr_16_0_16_0	Lipid Metabolism	cdpdag_hs_16_0_16_0[c] + inost[c] <=> cmp[c] + h[c] + pail_hs_16_0_16_0[c]	0.000	0.000	0.000	0.000	0.702	0.000	0.702	0	263129857
154	CDIPTr_16_0_18_1	Lipid Metabolism	cdpdag_hs_16_0_18_1[c] + inost[c] <=> cmp[c] + h[c] + pail_hs_16_0_18_1[c]	0.000	0.000	0.000	0.000	0.702	0.000	0.702	0	263129857
155	CDIPTr_16_0_18_2	Lipid Metabolism	cdpdag_hs_16_0_18_2[c] + inost[c] <=> cmp[c] + h[c] + pail_hs_16_0_18_2[c]	0.000	0.000	0.000	0.000	0.702	0.000	0.702	0	263129851
156	CDIPTr_18_1_18_1	Lipid Metabolism	cdpdag_hs_18_1_18_1[c] + inost[c] <=> cmp[c] + h[c] + pail_hs_18_1_18_1[c]	0.000	0.000	0.000	0.000	0.702	0.000	0.702	0	263129851
157	CDIPTr_18_1_18_2	Lipid Metabolism	cdpdag_hs_18_1_18_2[c] + inost[c] <=> cmp[c] + h[c] + pail_hs_18_1_18_2[c]	0.000	0.000	0.000	0.000	0.702	0.000	0.702	0	263129851

158	CDIPTr_18_2_16_0	Lipid Metabolism	cdpdag_hs_18_2_16_0[c] + inost[c] <=> cmp[c] + h[c] + pail_hs_18_2_16_0[c]	0.000	0.000	0.000	0.000	0.702	0.000	0.702	0	263129851
159	CDIPTr_18_2_18_1	Lipid Metabolism	cdpdag_hs_18_2_18_1[c] + inost[c] <=> cmp[c] + h[c] + pail_hs_18_2_18_1[c]	0.000	0.000	0.000	0.000	0.702	0.000	0.702	0	263129851
160	CDS_16_0_16_0	Lipid Metabolism	ctp[c] + h[c] + pa_hs_16_0_16_0[c] -> cdpdag_hs_16_0_16_0[c] + ppi[c]	0.000	0.000	0.000	0.000	0.702	0.000	0.702	0	263129857
161	CDS_16_0_18_1	Lipid Metabolism	ctp[c] + h[c] + pa_hs_16_0_18_1[c] -> cdpdag_hs_16_0_18_1[c] + ppi[c]	0.000	0.000	0.000	0.000	0.702	0.000	0.702	0	263129857
162	CDS_16_0_18_2	Lipid Metabolism	ctp[c] + h[c] + pa_hs_16_0_18_2[c] -> cdpdag_hs_16_0_18_2[c] + ppi[c]	0.000	0.000	0.000	0.000	0.702	0.000	0.702	0	263129851
163	CDS_18_1_18_1	Lipid Metabolism	ctp[c] + h[c] + pa_hs_18_1_18_1[c] -> cdpdag_hs_18_1_18_1[c] + ppi[c]	0.000	0.000	0.000	0.000	0.702	0.000	0.702	0	263129851
164	CDS_18_1_18_2	Lipid Metabolism	ctp[c] + h[c] + pa_hs_18_1_18_2[c] -> cdpdag_hs_18_1_18_2[c] + ppi[c]	0.000	0.000	0.000	0.000	0.702	0.000	0.702	0	263129851
165	CDS_18_2_16_0	Lipid Metabolism	ctp[c] + h[c] + pa_hs_18_2_16_0[c] -> cdpdag_hs_18_2_16_0[c] + ppi[c]	0.000	0.000	0.000	0.000	0.702	0.000	0.702	0	263129851
166	CDS_18_2_18_1	Lipid Metabolism	ctp[c] + h[c] + pa_hs_18_2_18_1[c] -> cdpdag_hs_18_2_18_1[c] + ppi[c]	0.000	0.000	0.000	0.000	0.702	0.000	0.702	0	263129851
167	CEPTC_16_0_16_0	Lipid Metabolism	cdpchol[c] + dag_hs_16_0_16_0[c] -> cmp[c] + h[c] + pchol_hs_16_0_16_0[c]	0.000	0.000	0.000	0.000	0.351	0.000	0.351	0	263237006
168	CEPTC_16_0_18_1	Lipid Metabolism	cdpchol[c] + dag_hs_16_0_18_1[c] -> cmp[c] + h[c] + pchol_hs_16_0_18_1[c]	0.000	0.000	0.000	0.000	0.351	0.000	0.351	0	263290579
169	CEPTC_16_0_18_2	Lipid Metabolism	cdpchol[c] + dag_hs_16_0_18_2[c] -> cmp[c] + h[c] + pchol_hs_16_0_18_2[c]	0.000	0.000	0.000	0.000	0.351	0.000	0.351	0	263236997
170	CEPTC_18_1_18_1	Lipid Metabolism	cdpchol[c] + dag_hs_18_1_18_1[c] -> cmp[c] + h[c] + pchol_hs_18_1_18_1[c]	0.000	0.000	0.000	0.000	0.351	0.000	0.351	0	263183430
171	CEPTC_18_1_18_2	Lipid Metabolism	cdpchol[c] + dag_hs_18_1_18_2[c] -> cmp[c] + h[c] + pchol_hs_18_1_18_2[c]	0.000	0.000	0.000	0.000	0.351	0.000	0.351	0	263237005
172	CEPTC_18_2_16_0	Lipid Metabolism	cdpchol[c] + dag_hs_18_2_16_0[c] -> cmp[c] + h[c] + pchol_hs_18_2_16_0[c]	0.000	0.000	0.000	0.000	0.351	0.000	0.351	0	263236997

173	CEPTC_18_2_18_1	Lipid Metabolism	cdpchol[c] + dag_hs_18_2_18_1[c] -> cmp[c] + h[c] + pchol_hs_18_2_18_1[c]	0.000	0.000	0.000	0.000	0.351	0.000	0.351	0	263237006
174	CEPTE_16_0_16_0	Lipid Metabolism	cdpea[c] + dag_hs_16_0_16_0[c] -> cmp[c] + h[c] + pe_hs_16_0_16_0[c]	0.000	0.000	0.000	0.000	0.012	0.000	0.012	0	10500208.5
175	CEPTE_16_0_18_1	Lipid Metabolism	cdpea[c] + dag_hs_16_0_18_1[c] -> cmp[c] + h[c] + pe_hs_16_0_18_1[c]	0.000	0.000	0.000	0.000	0.012	0.000	0.012	0	10500208.6
176	CEPTE_16_0_18_2	Lipid Metabolism	cdpea[c] + dag_hs_16_0_18_2[c] -> cmp[c] + h[c] + pe_hs_16_0_18_2[c]	0.000	0.000	0.000	0.000	0.012	0.000	0.012	0	10500208.5
177	CEPTE_18_1_18_1	Lipid Metabolism	cdpea[c] + dag_hs_18_1_18_1[c] -> cmp[c] + h[c] + pe_hs_18_1_18_1[c]	0.000	0.000	0.000	0.000	0.012	0.000	0.012	0	10500208.5
178	CEPTE_18_1_18_2	Lipid Metabolism	cdpea[c] + dag_hs_18_1_18_2[c] -> cmp[c] + h[c] + pe_hs_18_1_18_2[c]	0.000	0.000	0.000	0.000	0.012	0.000	0.012	0	10500208.6
179	CEPTE_18_2_16_0	Lipid Metabolism	cdpea[c] + dag_hs_18_2_16_0[c] -> cmp[c] + h[c] + pe_hs_18_2_16_0[c]	0.000	0.000	0.000	0.000	0.012	0.000	0.012	0	10500208.5
180	CEPTE_18_2_18_1	Lipid Metabolism	cdpea[c] + dag_hs_18_2_18_1[c] -> cmp[c] + h[c] + pe_hs_18_2_18_1[c]	0.000	0.000	0.000	0.000	0.012	0.000	0.012	0	10500208.6
181	CGMPt	Transport	35cgmp[c] + atp[c] + h2o[c] -> adp[c] + h[c] + pi[c] + 35cgmp[e]	0.000	0.000	0.000	0.000	0.024	0.000	0.024	0	29000752.1
182	CHLP	Lipid Metabolism	cholp[c] + h2o[c] -> chol[c] + pi[c]	0.000	0.000	0.000	0.000	2.105	0.000	2.105	0	263129851
183	CHLPCTD	Lipid Metabolism	cholp[c] + ctp[c] + h[c] -> cdpchol[c] + ppi[c]	0.000	0.000	0.000	0.000	0.351	0.000	0.351	0	263344148
184	CHOLK	Lipid Metabolism	atp[c] + chol[c] -> adp[c] + cholp[c] + h[c]	0.000	0.000	0.000	0.000	2.105	0.000	2.105	0	263129851
185	CHOLt4	Transport	chol[e] + na1[e] <=> chol[c] + na1[c]	0.000	0.000	0.000	0.000	0.012	0.000	0.012	0	10500208.5
186	CO2t	Transport	co2[e] <=> co2[c]	4.913	5.778	0.865	-2.286	5.657	-7.198	-0.120	-831.98922	-13.916781
187	COt	Transport	co[c] <=> co[e]	0.000	0.000	0.000	0.002	0.003	0.002	0.002	1249570.73	1249937.38
188	CPPPGO	Miscellaneous	cpppg3[c] + 2 h[c] + o2[c] -> 2 co2[c] + 2 h2o[c] + pppg9[c]	0.000	0.000	0.000	0.002	0.003	0.002	0.002	1249570.73	1249937.38
189	CYStec	Transport	cys-L[e] <=> cys-L[c]	0.000	0.000	0.000	0.080	0.080	0.080	0.080	35000622.4	35000930.7
190	CYTK1	Nucleotide Metabolism	atp[c] + cmp[c] <=> adp[c] + cdp[c]	0.000	0.000	0.000	0.000	0.702	0.000	0.702	0	263129851

191	D-LACt2	Transport	h[e] + lac-D[e] <=> h[c] + lac-D[c]	0.000	0.000	0.000	-1.468	0.000	-1.468	0.000	-366955881	0
192	DAGK_hs_16_0_16_0	Lipid Metabolism	atp[c] + dag_hs_16_0_16_0[c] <=> adp[c] + h[c] + pa_hs_16_0_16_0[c]	0.000	0.000	0.000	-0.351	2.105	-0.351	2.105	-37605285	225539873
193	DAGK_hs_16_0_18_1	Lipid Metabolism	atp[c] + dag_hs_16_0_18_1[c] <=> adp[c] + h[c] + pa_hs_16_0_18_1[c]	0.000	0.000	0.000	-0.351	2.105	-0.351	2.105	-37612939	225539874
194	DAGK_hs_16_0_18_2	Lipid Metabolism	atp[c] + dag_hs_16_0_18_2[c] <=> adp[c] + h[c] + pa_hs_16_0_18_2[c]	0.000	0.000	0.000	-0.351	2.105	-0.351	2.105	-37605285	225539871
195	DAGK_hs_18_1_18_1	Lipid Metabolism	atp[c] + dag_hs_18_1_18_1[c] <=> adp[c] + h[c] + pa_hs_18_1_18_1[c]	0.000	0.000	0.000	-0.351	2.105	-0.351	2.105	-37597632	225539872
196	DAGK_hs_18_1_18_2	Lipid Metabolism	atp[c] + dag_hs_18_1_18_2[c] <=> adp[c] + h[c] + pa_hs_18_1_18_2[c]	0.000	0.000	0.000	-0.351	2.105	-0.351	2.105	-37605285	225539872
197	DAGK_hs_18_2_16_0	Lipid Metabolism	atp[c] + dag_hs_18_2_16_0[c] <=> adp[c] + h[c] + pa_hs_18_2_16_0[c]	0.000	0.000	0.000	-0.351	2.105	-0.351	2.105	-37605285	225539873
198	DAGK_hs_18_2_18_1	Lipid Metabolism	atp[c] + dag_hs_18_2_18_1[c] <=> adp[c] + h[c] + pa_hs_18_2_18_1[c]	0.000	0.000	0.000	-0.351	2.105	-0.351	2.105	-37605285	225539873
199	DGULND	Carbohydrate Metabolism	3dhguln[c] + h[c] <=> co2[c] + xylu-L[c]	0.000	0.000	0.000	0.000	0.417	0.000	0.417	0	121582361
200	DHAAt1r	Transport	dhdascb[e] <=> dhdascb[c]	0.000	0.111	0.111	0.000	0.111	0.000	0.000	0	0
201	DM_nadh	Exchange/demand reaction	nadh[c] -> h[c] + nad[c]	0.000	1.074	1.074	0.000	2.254	0.000	1.179	0	109.787162
202	DOPAMT	Amino Acid Metabolism	amet[c] + dopa[c] -> 3moxtyr[c] + ahcys[c] + h[c]	0.000	0.000	0.000	0.000	0.032	0.000	0.032	0	2699979.51
203	DOPAtu	Transport	dopa[e] <=> dopa[c]	0.000	0.000	0.000	0.000	0.032	0.000	0.032	0	2699979.51
204	DPGM	Glycolysis/Gluconeogenesis	13dpg[c] <=> 23dpg[c] + h[c]	0.000	0.000	0.000	0.000	2.105	0.000	2.105	0	263129851
205	DPGase	Glycolysis/Gluconeogenesis	23dpg[c] + h2o[c] -> 3pg[c] + pi[c]	0.000	0.000	0.000	0.000	2.105	0.000	2.105	0	263129851
206	ENO	Glycolysis/Gluconeogenesis	2pg[c] <=> h2o[c] + pep[c]	2.907	2.907	0.000	3.252	5.578	0.345	2.671	43115485.3	333930789
207	ETHAK	Lipid Metabolism	atp[c] + etha[c] -> adp[c] + ethamp[c] + h[c]	0.000	0.000	0.000	0.000	2.105	0.000	2.105	0	263129851
208	ETHAt	Transport	etha[e] <=> etha[c]	0.000	0.000	0.000	0.000	0.012	0.000	0.012	0	10500208.6

209	ETHP	Lipid Metabolism	ethamp[c] + h2o[c] -> etha[c] + pi[c]	0.000	0.000	0.000	0.000	2.105	0.000	2.105	0	263129851
210	FACOAL160	Lipid Metabolism	atp[c] + coa[c] + hdca[c] <=> amp[c] + pmtcoa[c] + ppi[c]	0.000	0.000	0.000	0.000	0.702	0.000	0.702	0	263237002
211	FACOAL181	Lipid Metabolism	atp[c] + coa[c] + ocdcea[c] <=> amp[c] + odecoa[c] + ppi[c]	0.000	0.000	0.000	0.000	0.702	0.000	0.702	0	263183413
212	FACOAL1821	Lipid Metabolism	atp[c] + coa[c] + lnlc[c] <=> amp[c] + lnlccoa[c] + ppi[c]	0.000	0.000	0.000	0.000	0.351	0.000	0.351	0	263236986
213	FADDP	Vitamin Metabolism	fad[c] + h2o[c] -> amp[c] + fmn[c] + 2 h[c]	0.000	0.000	0.000	0.000	1.052	0.000	1.052	0	263129857
214	FBA	Glycolysis/Gluconeogenesis	fdp[c] <=> dhap[c] + g3p[c]	1.442	1.442	0.000	0.459	2.568	-0.984	1.125	-122974926	140668804
215	FBP26	Carbohydrate Metabolism	f26bp[c] + h2o[c] -> f6p[c] + pi[c]	0.000	0.000	0.000	0.000	2.105	0.000	2.105	0	263129850
216	FCLT	Miscellaneous	fe2[c] + ppp9[c] -> 2 h[c] + pheme[c]	0.000	0.000	0.000	0.002	0.003	0.002	0.002	1249570.73	1249937.38
217	FE2t1	Transport	fe2[e] <=> fe2[c]	0.000	0.000	0.000	0.000	0.000	0.000	0.000	#DIV/0!	#DIV/0!
218	FMNAT	Vitamin Metabolism	atp[c] + fmn[c] + h[c] -> fad[c] + ppi[c]	0.000	0.000	0.000	0.000	1.052	0.000	1.052	0	263129857
219	FRUt1r	Transport	fru[e] <=> fru[c]	0.007	0.008	0.000	-1.120	0.008	-1.127	0.000	-281883193	0
220	FUM	Citric Acid Cycle	fum[c] + h2o[c] <=> mal-L[c]	-0.500	0.250	0.750	-0.500	0.250	0.000	0.000	0	0
221	FUMtr	Transport	fum[e] <=> fum[c]	-0.500	0.250	0.750	-0.500	0.250	0.000	0.000	0	0
222	G6PDA	Carbohydrate Metabolism	gam6p[c] + h2o[c] -> f6p[c] + nh4[c]	0.000	0.000	0.000	0.000	0.000	0.000	0.000	-11750.35	0
223	G6PDH2r	Pentose Phosphate Pathway	g6p[c] + nadp[c] <=> 6pgl[c] + h[c] + nadph[c]	0.056	0.056	0.000	0.000	4.997	-0.056	4.941	-2333402	205892929
224	GALK	Carbohydrate Metabolism	atp[c] + gal[c] -> adp[c] + gal1p[c] + h[c]	0.317	0.317	0.000	0.000	0.317	-0.317	0.000	-79227238	0
225	GALOR	Carbohydrate Metabolism	gal[c] + h[c] + nadph[c] <=> galt[c] + nadp[c]	0.000	0.000	0.000	0.000	0.000	0.000	0.000	#DIV/0!	#DIV/0!
226	GALT	Carbohydrate Metabolism	gal1p[c] + h[c] + utp[c] <=> ppi[c] + udpgal[c]	-999.683	1000.000	1999.683	-999.998	1000.000	-0.314	0.000	-0.0157225	0
227	GALU	Carbohydrate Metabolism	g1p[c] + h[c] + utp[c] <=> ppi[c] + udpg[c]	-1000.000	999.683	1999.683	-999.998	1000.000	0.002	0.317	0.00012497	0.01584749
228	GALt1r	Transport	gal[e] <=> gal[c]	0.317	0.317	0.000	0.000	0.317	-0.317	0.000	-79227238	0
229	GAMt1r	Transport	gam[e] <=> gam[c]	0.000	0.000	0.000	0.000	0.000	0.000	0.000	-2400.0736	0
230	GAPD	Glycolysis/Gluconeogenesis	g3p[c] + nad[c] + pi[c] <=> 13dpg[c] + h[c] + nadh[c]	2.907	2.907	0.000	3.252	5.578	0.345	2.671	43115485.2	333930788
231	GGLUCT	Amino Acid Metabolism	gluala[e] -> 5oxpro[c] + ala-L[c]	0.000	0.000	0.000	0.055	0.080	0.055	0.080	23997085.9	35000930.7
232	GK1	Nucleotide Metabolism	atp[c] + gmp[c] <=> adp[c] + gdp[c]	0.000	0.000	0.000	0.000	0.024	0.000	0.024	0	29000752.1
233	GLCt1r	Transport	glc-D[e] <=> glc-D[c]	1.120	1.120	0.000	0.000	1.120	-1.120	0.000	-280008139	0
234	GLNS	Amino Acid Metabolism	atp[c] + glu-L[c] + nh4[c] -> adp[c] + gln-L[c] + h[c] + pi[c]	0.000	0.000	0.000	0.000	0.560	0.000	0.560	0	209837700
235	GLNt4	Transport	gln-L[e] + na1[e] -> gln-L[c] + na1[c]	0.000	0.000	0.000	0.000	0.025	0.000	0.025	0	14147829.7

236	GLUCYS	Amino Acid Metabolism	atp[c] + cys-L[c] + glu-L[c] -> adp[c] + glucys[c] + h[c] + pi[c]	0.000	0.000	0.000	0.080	0.080	0.080	0.080	35000622.4	35000930.7
237	GLYCt	Transport	glyc[c] <=> glyc[e]	0.000	0.000	0.000	-0.012	0.000	-0.012	0.000	-10500209	0
238	GLYK	Lipid Metabolism	atp[c] + glyc[c] -> adp[c] + glyc3p[c] + h[c]	0.000	0.000	0.000	0.000	0.012	0.000	0.012	0	10500208.5
239	GLYOX	Amino Acid Metabolism	h2o[c] + lgt-S[c] -> gthrd[c] + h[c] + lac-D[c]	0.000	0.000	0.000	0.000	1.468	0.000	1.468	0	366955881
240	GLYt7(211)r	Transport	cl[e] + gly[e] + 2 na1[e] <=> cl[c] + gly[c] + 2 na1[c]	0.000	0.000	0.000	0.080	0.080	0.080	0.080	35000622.4	35000930.7
241	GMPR	Nucleotide Metabolism	gmp[c] + 2 h[c] + nadph[c] -> imp[c] + nadp[c] + nh4[c]	0.000	0.000	0.000	0.000	0.570	0.000	0.570	0	213627294
242	GMPS2	Nucleotide Metabolism	atp[c] + gln-L[c] + h2o[c] + xmp[c] -> amp[c] + glu-L[c] + gmp[c] + 2 h[c] + ppi[c]	0.000	0.000	0.000	0.000	0.570	0.000	0.570	0	213627278
243	GND	Pentose Phosphate Pathway	6pgc[c] + nadp[c] -> co2[c] + nadph[c] + ru5p-D[c]	0.056	0.056	0.000	0.199	7.434	0.143	7.378	5947986.68	307427956
244	GPAM_hs_16_0	Lipid Metabolism	glyc3p[c] + pmtcoa[c] -> alpa_hs_16_0[c] + coa[c]	0.000	0.000	0.000	0.000	0.351	0.000	0.351	0	263344275
245	GPAM_hs_18_1	Lipid Metabolism	glyc3p[c] + odecoa[c] -> alpa_hs_18_1[c] + coa[c]	0.000	0.000	0.000	0.000	0.351	0.000	0.351	0	263237002
246	GPAM_hs_18_2	Lipid Metabolism	glyc3p[c] + lnlccoa[c] -> alpa_hs_18_2[c] + coa[c]	0.000	0.000	0.000	0.000	0.351	0.000	0.351	0	263237002
247	GPDDA1	Lipid Metabolism	g3pc[c] + h2o[c] -> chol[c] + glyc3p[c] + h[c]	0.000	0.000	0.000	0.000	0.351	0.000	0.351	0	263129856
248	GTHDH	Vitamin Metabolism	dhdascb[c] + 2 gthrd[c] -> ascb-L[c] + gthox[c]	0.000	0.111	0.111	0.000	0.111	0.000	0.000	0	0
249	GTHO	Amino Acid Metabolism	gthox[c] + h[c] + nadph[c] -> 2 gthrd[c] + nadp[c]	0.000	0.862	0.862	0.000	10.072	0.000	9.210	0	1068.4055
250	GTHOXti2	Transport	atp[c] + gthox[c] + h2o[c] -> adp[c] + h[c] + pi[c] + gthox[e]	0.000	0.000	0.000	0.040	0.040	0.040	0.040	35000621.5	35000929.9
251	GTHP	Amino Acid Metabolism	2 gthrd[c] + h2o2[c] -> gthox[c] + 2 h2o[c]	0.000	0.862	0.862	0.000	10.001	0.000	9.139	0	1060.15723
252	GTHS	Amino Acid Metabolism	atp[c] + glucys[c] + gly[c] -> adp[c] + gthrd[c] + h[c] + pi[c]	0.000	0.000	0.000	0.080	0.080	0.080	0.080	35000622.4	35000930.7
253	GUACYC	Nucleotide Metabolism	gtp[c] -> 35cgmp[c] + ppi[c]	0.000	0.000	0.000	0.000	0.024	0.000	0.024	0	29000752.1
254	GUAPRT	Nucleotide Metabolism	gua[c] + prpp[c] -> gmp[c] + ppi[c]	0.000	0.000	0.000	0.000	1.052	0.000	1.052	0	263129851
255	GULN3D	Carbohydrate Metabolism	guln[c] + nad[c] <=> 3dhguln[c] + h[c] + nadh[c]	0.000	0.000	0.000	0.000	0.417	0.000	0.417	0	121582361
256	GULND	Carbohydrate Metabolism	glcur[c] + h[c] + nadph[c] <=> guln[c] + nadp[c]	0.000	0.000	0.000	0.000	0.417	0.000	0.417	0	121582361
257	H2O2t	Transport	h2o2[e] <=> h2o2[c]	0.000	10.000	10.000	-0.001	10.000	-0.001	0.000	-0.006102	0
258	H2Ot	Transport	h2o[e] <=> h2o[c]	-4.712	6.289	11.001	-10.000	6.457	-5.288	0.168	-48.066271	1.52460744
259	HCO3E	Miscellaneous	co2[c] + h2o[c] <=> h[c] + hco3[c]	5.834	5.834	0.000	5.871	5.871	0.037	0.037	2041775.76	2041726.8

260	HCO3_CLt	Transport	cl[c] + hco3[e] <=> hco3[c] + cl[e]	-5.834	-5.834	0.000	-5.874	-5.874	-0.040	-0.040	-2178449.6	-2178498.5
261	HCYSte	Transport	hcys-L[e] <=> hcys-L[c]	0.000	0.000	0.000	-0.010	0.000	-0.010	0.000	-3750010.3	0
262	HDCAtr	Transport	hdca[e] <=> hdca[c]	0.000	0.000	0.000	0.000	0.012	0.000	0.012	0	5250054.27
263	HEX1	Glycolysis/Gluconeogenesis	atp[c] + glc-D[c] -> adp[c] + g6p[c] + h[c]	0.258	1.120	0.862	0.000	1.120	-0.258	0.000	-29.929671	0
264	HEX10	Carbohydrate Metabolism	atp[c] + gam[c] -> adp[c] + gam6p[c] + h[c]	0.000	0.000	0.000	0.000	0.000	0.000	0.000	-2400.0736	0
265	HEX4	Carbohydrate Metabolism	atp[c] + man[c] -> adp[c] + h[c] + man6p[c]	0.010	0.010	0.000	0.000	0.010	-0.010	0.000	-2499973.8	0
266	HEX7	Carbohydrate Metabolism	atp[c] + fru[c] -> adp[c] + f6p[c] + h[c]	0.007	0.870	0.862	0.000	1.128	-0.007	0.258	-0.870018	29.9296571
267	HMBS	Miscellaneous	h2o[c] + 4 ppbng[c] -> hmbil[c] + 4 nh4[c]	0.000	0.000	0.000	0.002	0.003	0.002	0.002	1249570.73	1249937.38
268	HOXG	Miscellaneous	5 h[c] + 3 nadph[c] + 3 o2[c] + pheme[c] -> biliverd[c] + co[c] + fe2[c] + 3 h2o[c] + 3 nadp[c]	0.000	0.000	0.000	0.002	0.003	0.002	0.002	1249570.73	1249937.38
269	HXPRT	Nucleotide Metabolism	hxan[c] + prpp[c] -> imp[c] + ppi[c]	0.000	0.000	0.000	0.000	1.052	0.000	1.052	0	263129850
270	HYXNt	Transport	hxan[e] <=> hxan[c]	-0.024	0.000	0.024	-0.024	0.000	0.000	0.000	0	0
271	Ht	Transport	h[c] <=> h[e]	4.219	7.117	2.899	1.049	6.802	-3.170	-0.315	-109.36168	-10.864705
272	ICDHy	Citric Acid Cycle	icit[c] + nadp[c] -> akg[c] + co2[c] + nadph[c]	0.000	0.000	0.000	0.000	0.000	0.000	0.000	#DIV/0!	#DIV/0!
273	IMPD	Nucleotide Metabolism	h2o[c] + imp[c] + nad[c] -> h[c] + nadh[c] + xmp[c]	0.000	0.000	0.000	0.000	0.570	0.000	0.570	0	213627278
274	INSt	Transport	ins[e] <=> ins[c]	0.000	0.000	0.000	-0.024	0.000	-0.024	0.000	-8000135.1	0
275	KCCt	Transport	cl[e] + k[e] <=> cl[c] + k[c]	-5.834	-5.834	0.000	-5.954	-5.954	-0.120	-0.120	-7489803.9	-7489845.5
276	L-LACt2r	Transport	h[e] + lac-L[e] <=> h[c] + lac-L[c]	-3.657	-1.833	1.824	-3.676	-1.075	-0.019	0.757	-1.0228834	41.5123642
277	LDH_L	Glycolysis/Gluconeogenesis	lac-L[c] + nad[c] <=> h[c] + nadh[c] + pyr[c]	-3.657	-1.833	1.824	-3.676	-1.075	-0.019	0.757	-1.0228834	41.5123642
278	LEUKTRA4t	Transport	leuktrA4[e] <=> leuktrA4[c]	0.000	0.000	0.000	0.000	0.000	0.000	0.000	0	0
279	LEUKTRB4t	Transport	leuktrB4[e] <=> leuktrB4[c]	0.000	0.000	0.000	0.000	0.000	0.000	0.000	0	0
280	LGTHL	Amino Acid Metabolism	gthrd[c] + mthgxl[c] -> lgt-S[c]	0.000	0.000	0.000	0.000	1.468	0.000	1.468	0	366955881
281	LNLCCPT1	Lipid Metabolism	crn[c] + lnlccoa[c] -> coa[c] + lnlccrn[c]	0.000	1000.000	1000.000	0.000	1000.000	0.000	0.000	0	0
282	LNLCCPT2rbc	Lipid Metabolism	coa[c] + lnlccrn[c] -> crn[c] + lnlccoa[c]	0.000	1000.000	1000.000	0.000	1000.000	0.000	0.000	0	0
283	LNLCt	Transport	lnlc[e] <=> lnlc[c]	0.000	0.000	0.000	0.000	0.006	0.000	0.006	0	4875043.24
284	LPASE_16_0	Lipid Metabolism	h2o[c] + lpchol_hs_16_0[c] -> g3pc[c] + h[c] + hdca[c]	0.000	0.000	0.000	0.000	0.351	0.000	0.351	0	263129856
285	LPASE_18_1	Lipid Metabolism	h2o[c] + lpchol_hs_18_1[c] -> g3pc[c] + h[c] + ocdcea[c]	0.000	0.000	0.000	0.000	0.351	0.000	0.351	0	263129856
286	LPASE_18_2	Lipid Metabolism	h2o[c] + lpchol_hs_18_2[c] -> g3pc[c] + h[c] + lnlc[c]	0.000	0.000	0.000	0.000	0.351	0.000	0.351	0	263129856
287	LTA4H	Lipid Metabolism	h2o[c] + leuktrA4[c] -> leuktrB4[c]	0.000	0.000	0.000	0.000	0.000	0.000	0.000	0	0
288	MALt	Transport	mal-L[e] <=> mal-L[c]	-0.250	0.500	0.750	-0.250	0.500	0.000	0.000	0	0

289	MAN6PI	Carbohydrate Metabolism	man6p[c] <=> f6p[c]	0.010	0.010	0.000	0.000	0.010	-0.010	0.000	-2499973.8	0
290	MANt1r	Transport	man[e] <=> man[c]	0.010	0.010	0.000	0.000	0.010	-0.010	0.000	-2499973.8	0
291	MDH	Citric Acid Cycle	mal-L[c] + nad[c] <=> h[c] + nadh[c] + oaa[c]	0.000	0.000	0.000	0.000	0.000	0.000	0.000	#DIV/0!	#DIV/0!
292	MDRPD	Amino Acid Metabolism	5mdru1p[c] -> dkmpp[c] + h2o[c]	0.000	0.000	0.000	0.000	0.025	0.000	0.025	0	20959795.1
293	ME2	Amino Acid Metabolism	mal-L[c] + nadp[c] -> co2[c] + nadph[c] + pyr[c]	0.000	0.750	0.750	0.000	0.750	0.000	0.000	0	0
294	MEPIVESTe	Transport	2 atp[c] + 2 h2o[c] + 3 mepi[c] -> 2 adp[c] + 2 h[c] + 2 pi[c] + 3 mepi[e]	0.000	0.000	0.000	0.000	0.013	0.000	0.013	0	3149992.76
295	METAT	Amino Acid Metabolism	atp[c] + h2o[c] + met-L[c] -> amet[c] + pi[c] + ppi[c]	0.000	0.000	0.000	0.000	0.035	0.000	0.035	0	13181962.8
296	METtec	Transport	met-L[e] <=> met-L[c]	0.000	0.000	0.000	0.000	0.010	0.000	0.010	0	3750010.48
297	MGSA	Amino Acid Metabolism	dhap[c] -> mthgxl[c] + pi[c]	0.000	0.000	0.000	0.000	1.468	0.000	1.468	0	366955881
298	MI1345PP	Miscellaneous	h2o[c] + mi1345p[c] -> mi134p[c] + pi[c]	0.000	0.000	0.000	0.000	2.105	0.000	2.105	0	263129850
299	MI145PK	Miscellaneous	atp[c] + mi145p[c] -> adp[c] + h[c] + mi1345p[c]	0.000	0.000	0.000	0.000	2.105	0.000	2.105	0	263129839
300	MI145PP	Miscellaneous	h2o[c] + mi145p[c] -> mi14p[c] + pi[c]	0.000	0.000	0.000	0.000	2.105	0.000	2.105	0	263129850
301	MI1PP	Miscellaneous	h2o[c] + mi1p-D[c] -> inost[c] + pi[c]	0.000	0.000	0.000	0.000	0.702	0.000	0.702	0	263129850
302	MI1PS	Miscellaneous	g6p[c] -> mi1p-D[c]	0.000	0.000	0.000	0.000	0.460	0.000	0.460	0	402917620
303	MTAP	Amino Acid Metabolism	5mta[c] + pi[c] -> 5mdr1p[c] + ade[c]	0.000	0.000	0.000	0.000	0.025	0.000	0.025	0	20959795.1
304	MTRI	Amino Acid Metabolism	5mdr1p[c] <=> 5mdru1p[c]	0.000	0.000	0.000	0.000	0.025	0.000	0.025	0	20959795.1
305	NACt	Transport	nac[e] <=> nac[c]	0.000	0.000	0.000	0.000	0.001	0.000	0.001	0	499914.691
306	NADK	NAD Metabolism	atp[c] + nad[c] -> adp[c] + h[c] + nadp[c]	0.000	0.000	0.000	0.000	0.024	0.000	0.024	0	31000811.1
307	NADPN	NAD Metabolism	h2o[c] + nadp[c] -> adprbp[c] + h[c] + ncam[c]	0.000	0.000	0.000	0.000	0.024	0.000	0.024	0	31000811.1
308	NADS2	NAD Metabolism	atp[c] + dnad[c] + gln-L[c] + h2o[c] -> amp[c] + glu-L[c] + h[c] + nad[c] + ppi[c]	0.000	0.000	0.000	0.000	0.001	0.000	0.001	0	499914.746
309	NAt	Transport	na1[e] <=> na1[c]	8.751	8.751	0.000	8.788	8.850	0.037	0.100	1276717.14	3400684.19
310	NCAMt	Transport	ncam[e] <=> ncam[c]	0.000	0.000	0.000	-0.001	0.000	-0.001	0.000	-499914.69	0
311	NDPK1	Nucleotide Metabolism	atp[c] + gdp[c] <=> adp[c] + gtp[c]	0.000	0.000	0.000	0.000	0.024	0.000	0.024	0	29000752.1
312	NDPK2	Nucleotide Metabolism	atp[c] + udp[c] <=> adp[c] + utp[c]	0.000	0.000	0.000	0.002	0.419	0.002	0.419	728915.969	122311553
313	NDPK3	Nucleotide Metabolism	atp[c] + cdp[c] <=> adp[c] + ctp[c]	0.000	0.000	0.000	0.000	0.702	0.000	0.702	0	263129851
314	NH4t3r	Transport	nh4[c] + h[e] <=> h[c] + nh4[e]	0.000	0.024	0.024	0.009	0.034	0.009	0.010	37.2867478	42.0778963
315	NICRNS	NAD Metabolism	atp[c] + nicrns[c] -> adp[c] + h[c] + nicrnt[c]	0.000	0.000	0.000	0.000	2.105	0.000	2.105	0	263129851
316	NMNATr	NAD Metabolism	atp[c] + h[c] + nmn[c] <=> nad[c] + ppi[c]	0.000	0.000	0.000	-0.001	0.024	-0.001	0.024	-360403.64	8651389.77
317	NNATr	NAD Metabolism	atp[c] + h[c] + nicrnt[c] <=> dnad[c] + ppi[c]	0.000	0.000	0.000	0.000	0.001	0.000	0.001	0	499914.746

318	NORMETEVESSte	Transport	2 atp[c] + 2 h2o[c] + 3 normete-L[c] -> 2 adp[c] + 2 h[c] + 2 pi[c] + 3 normete-L[e]	0.000	0.000	0.000	0.000	0.010	0.000	0.010	0	2399970.67
319	NP1	NAD Metabolism	h[c] + nac[c] + r1p[c] -> nicrns[c] + pi[c]	0.000	0.000	0.000	0.000	0.001	0.000	0.001	0	499914.691
320	NRPPHRtu	Transport	nrpphr[e] <=> nrpphr[c]	0.000	0.000	0.000	0.000	0.029	0.000	0.029	0	2399970.67
321	NT5C	NAD Metabolism	h2o[c] + nicrnt[c] -> nicrns[c] + pi[c]	0.000	0.000	0.000	0.000	2.105	0.000	2.105	0	263129851
322	NTD11	Nucleotide Metabolism	h2o[c] + imp[c] -> ins[c] + pi[c]	0.000	0.000	0.000	0.000	1.064	0.000	1.064	0	133064919
323	NTD2	Nucleotide Metabolism	h2o[c] + ump[c] -> pi[c] + uri[c]	0.000	0.000	0.000	0.000	0.010	0.000	0.010	0	5833404.73
324	NTD5_a	NAD Metabolism	h2o[c] + nmn[c] -> pi[c] + rnam[c]	0.000	0.000	0.000	0.000	2.105	0.000	2.105	0	263129851
325	NTD7	Nucleotide Metabolism	amp[c] + h2o[c] -> adn[c] + pi[c]	0.000	0.000	0.000	0.000	2.105	0.000	2.105	0	263129850
326	NTD9	Nucleotide Metabolism	gmp[c] + h2o[c] -> gsn[c] + pi[c]	0.000	0.000	0.000	0.000	1.052	0.000	1.052	0	263129851
327	NaKt	Transport	atp[c] + h2o[c] + 3 na1[c] + 2 k[e] -> adp[c] + h[c] + 2 k[c] + pi[c] + 3 na1[e]	2.917	2.917	0.000	2.977	2.977	0.060	0.060	7489845.54	7489803.87
328	O2t	Transport	o2[e] <=> o2[c]	-5.000	0.000	5.000	-4.986	0.039	0.014	0.039	0.27335526	0.78816443
329	OCDCEAtr	Transport	ocdcea[e] <=> ocdcea[c]	0.000	0.000	0.000	0.000	0.006	0.000	0.006	0	2624977.14
330	OMPDC	Nucleotide Metabolism	h[c] + orot5p[c] -> co2[c] + ump[c]	0.000	0.000	0.000	0.000	0.010	0.000	0.010	0	5833405.1
331	OPAHir	Amino Acid Metabolism	5oxpro[c] + atp[c] + 2 h2o[c] -> adp[c] + glu-L[c] + h[c] + pi[c]	0.000	0.000	0.000	0.055	0.080	0.055	0.080	23997085.9	35000930.7
332	ORNDC	Amino Acid Metabolism	h[c] + orn[c] -> co2[c] + ptrc[c]	0.000	0.115	0.115	0.000	0.115	0.000	0.000	0	0
333	OROATP	Transport	h[e] + orot[e] -> h[c] + orot[c]	0.000	0.000	0.000	0.000	0.010	0.000	0.010	0	5833405.1
334	ORPT	Nucleotide Metabolism	orot5p[c] + ppi[c] <=> orot[c] + prpp[c]	0.000	0.000	0.000	-0.010	0.000	-0.010	0.000	-5833405.1	0
335	PDE1	Nucleotide Metabolism	camp[c] + h2o[c] -> amp[c] + h[c]	0.000	0.000	0.000	0.000	1.052	0.000	1.052	0	263129851
336	PDX5PO	Vitamin Metabolism	o2[c] + pdx5p[c] <=> h2o2[c] + pydx5p[c]	0.000	0.000	0.000	0.000	0.000	0.000	0.000	-15887.969	7950.23558
337	PDXPP	Vitamin Metabolism	h2o[c] + pdx5p[c] -> pi[c] + pydxn[c]	0.000	0.000	0.000	0.000	2.105	0.000	2.105	0	263130148
338	PETHCT	Lipid Metabolism	ctp[c] + ethamp[c] + h[c] -> cdpea[c] + ppi[c]	0.000	0.000	0.000	0.000	0.012	0.000	0.012	0	10500208.5
339	PFK	Glycolysis/Gluconeogenesis	atp[c] + f6p[c] -> adp[c] + fdp[c] + h[c]	1.442	1.442	0.000	0.459	2.568	-0.984	1.125	-122974926	140668804
340	PFK26	Carbohydrate Metabolism	atp[c] + f6p[c] -> adp[c] + f26bp[c] + h[c]	0.000	0.000	0.000	0.000	2.105	0.000	2.105	0	263129850
341	PGI	Glycolysis/Gluconeogenesis	g6p[c] <=> f6p[c]	0.519	1.381	0.862	-4.879	1.434	-5.397	0.054	-626.15444	6.20655295
342	PGK	Glycolysis/Gluconeogenesis	3pg[c] + atp[c] <=> 13dpg[c] + adp[c]	-2.907	-2.907	0.000	-5.578	-3.252	-2.671	-0.345	-333930789	-43115485
343	PGL	Pentose Phosphate Pathway	6pgl[c] + h2o[c] -> 6pgc[c] + h[c]	0.056	0.056	0.000	0.000	4.997	-0.056	4.941	-2333402	205892929
344	PGM	Glycolysis/Gluconeogenesis	2pg[c] <=> 3pg[c]	-2.907	-2.907	0.000	-5.578	-3.252	-2.671	-0.345	-333930789	-43115485
345	PGMT	Glycolysis/Gluconeogenesis	g1p[c] <=> g6p[c]	0.317	0.317	0.000	-0.419	0.314	-0.736	-0.002	-184065749	-624784.95
346	PHETA1	Amino Acid Metabolism	akg[c] + phe-L[c] <=> glu-L[c] + phpyr[c]	0.000	0.000	0.000	0.000	0.000	0.000	0.000	#DIV/0!	#DIV/0!

347	PHEtec	Transport	phe-L[e] <=> phe-L[c]	0.000	0.000	0.000	0.000	0.000	0.000	0.000	#DIV/0!	#DIV/0!
348	PI45P5P_16_0_16_0	Miscellaneous	h2o[c] + pail45p_hs_16_0_16_0[c] -> pail4p_hs_16_0_16_0[c] + pi[c]	0.000	0.000	0.000	0.000	2.105	0.000	2.105	0	263129851
349	PI45P5P_16_0_18_1	Miscellaneous	h2o[c] + pail45p_hs_16_0_18_1[c] -> pail4p_hs_16_0_18_1[c] + pi[c]	0.000	0.000	0.000	0.000	2.105	0.000	2.105	0	263129851
350	PI45P5P_16_0_18_2	Miscellaneous	h2o[c] + pail45p_hs_16_0_18_2[c] -> pail4p_hs_16_0_18_2[c] + pi[c]	0.000	0.000	0.000	0.000	2.105	0.000	2.105	0	263129851
351	PI45P5P_18_1_18_1	Miscellaneous	h2o[c] + pail45p_hs_18_1_18_1[c] -> pail4p_hs_18_1_18_1[c] + pi[c]	0.000	0.000	0.000	0.000	2.105	0.000	2.105	0	263129851
352	PI45P5P_18_1_18_2	Miscellaneous	h2o[c] + pail45p_hs_18_1_18_2[c] -> pail4p_hs_18_1_18_2[c] + pi[c]	0.000	0.000	0.000	0.000	2.105	0.000	2.105	0	263129851
353	PI45P5P_18_2_16_0	Miscellaneous	h2o[c] + pail45p_hs_18_2_16_0[c] -> pail4p_hs_18_2_16_0[c] + pi[c]	0.000	0.000	0.000	0.000	2.105	0.000	2.105	0	263129851
354	PI45P5P_18_2_18_1	Miscellaneous	h2o[c] + pail45p_hs_18_2_18_1[c] -> pail4p_hs_18_2_18_1[c] + pi[c]	0.000	0.000	0.000	0.000	2.105	0.000	2.105	0	263129851
355	PI45PLC_16_0_16_0	Miscellaneous	h2o[c] + pail45p_hs_16_0_16_0[c] -> dag_hs_16_0_16_0[c] + h[c] + mi145p[c]	0.000	0.000	0.000	0.000	0.378	0.000	0.378	0	377827506
356	PI45PLC_16_0_18_1	Miscellaneous	h2o[c] + pail45p_hs_16_0_18_1[c] -> dag_hs_16_0_18_1[c] + h[c] + mi145p[c]	0.000	0.000	0.000	0.000	0.378	0.000	0.378	0	377827506
357	PI45PLC_16_0_18_2	Miscellaneous	h2o[c] + pail45p_hs_16_0_18_2[c] -> dag_hs_16_0_18_2[c] + h[c] + mi145p[c]	0.000	0.000	0.000	0.000	0.378	0.000	0.378	0	377827506
358	PI45PLC_18_1_18_1	Miscellaneous	h2o[c] + pail45p_hs_18_1_18_1[c] -> dag_hs_18_1_18_1[c] + h[c] + mi145p[c]	0.000	0.000	0.000	0.000	0.378	0.000	0.378	0	377827506
359	PI45PLC_18_1_18_2	Miscellaneous	h2o[c] + pail45p_hs_18_1_18_2[c] -> dag_hs_18_1_18_2[c] + h[c] + mi145p[c]	0.000	0.000	0.000	0.000	0.378	0.000	0.378	0	377827506
360	PI45PLC_18_2_16_0	Miscellaneous	h2o[c] + pail45p_hs_18_2_16_0[c] -> dag_hs_18_2_16_0[c] + h[c] + mi145p[c]	0.000	0.000	0.000	0.000	0.378	0.000	0.378	0	377827506
361	PI45PLC_18_2_18_1	Miscellaneous	h2o[c] + pail45p_hs_18_2_18_1[c] -> dag_hs_18_2_18_1[c] + h[c] + mi145p[c]	0.000	0.000	0.000	0.000	0.378	0.000	0.378	0	377827506
362	PI4P5K_16_0_16_0	Lipid Metabolism	atp[c] + pail4p_hs_16_0_16_0[c] -> adp[c] + h[c] + pail45p_hs_16_0_16_0[c]	0.000	0.000	0.000	0.000	2.105	0.000	2.105	0	263129851

363	PI4P5K_16_0_18_1	Lipid Metabolism	atp[c] + pail4p_hs_16_0_18_1[c] -> adp[c] + h[c] + pail45p_hs_16_0_18_1[c]	0.000	0.000	0.000	0.000	2.105	0.000	2.105	0	263129851
364	PI4P5K_16_0_18_2	Lipid Metabolism	atp[c] + pail4p_hs_16_0_18_2[c] -> adp[c] + h[c] + pail45p_hs_16_0_18_2[c]	0.000	0.000	0.000	0.000	2.105	0.000	2.105	0	263129851
365	PI4P5K_18_1_18_1	Lipid Metabolism	atp[c] + pail4p_hs_18_1_18_1[c] -> adp[c] + h[c] + pail45p_hs_18_1_18_1[c]	0.000	0.000	0.000	0.000	2.105	0.000	2.105	0	263129851
366	PI4P5K_18_1_18_2	Lipid Metabolism	atp[c] + pail4p_hs_18_1_18_2[c] -> adp[c] + h[c] + pail45p_hs_18_1_18_2[c]	0.000	0.000	0.000	0.000	2.105	0.000	2.105	0	263129851
367	PI4P5K_18_2_16_0	Lipid Metabolism	atp[c] + pail4p_hs_18_2_16_0[c] -> adp[c] + h[c] + pail45p_hs_18_2_16_0[c]	0.000	0.000	0.000	0.000	2.105	0.000	2.105	0	263129851
368	PI4P5K_18_2_18_1	Lipid Metabolism	atp[c] + pail4p_hs_18_2_18_1[c] -> adp[c] + h[c] + pail45p_hs_18_2_18_1[c]	0.000	0.000	0.000	0.000	2.105	0.000	2.105	0	263129851
369	PI4PLC_16_0_16_0	Miscellaneous	h2o[c] + pail4p_hs_16_0_16_0[c] -> dag_hs_16_0_16_0[c] + h[c] + mi14p[c]	0.000	0.000	0.000	0.000	0.460	0.000	0.460	0	402917621
370	PI4PLC_16_0_18_1	Miscellaneous	h2o[c] + pail4p_hs_16_0_18_1[c] -> dag_hs_16_0_18_1[c] + h[c] + mi14p[c]	0.000	0.000	0.000	0.000	0.460	0.000	0.460	0	402917621
371	PI4PLC_16_0_18_2	Miscellaneous	h2o[c] + pail4p_hs_16_0_18_2[c] -> dag_hs_16_0_18_2[c] + h[c] + mi14p[c]	0.000	0.000	0.000	0.000	0.460	0.000	0.460	0	402917621
372	PI4PLC_18_1_18_1	Miscellaneous	h2o[c] + pail4p_hs_18_1_18_1[c] -> dag_hs_18_1_18_1[c] + h[c] + mi14p[c]	0.000	0.000	0.000	0.000	0.460	0.000	0.460	0	402917621
373	PI4PLC_18_1_18_2	Miscellaneous	h2o[c] + pail4p_hs_18_1_18_2[c] -> dag_hs_18_1_18_2[c] + h[c] + mi14p[c]	0.000	0.000	0.000	0.000	0.460	0.000	0.460	0	402917621
374	PI4PLC_18_2_16_0	Miscellaneous	h2o[c] + pail4p_hs_18_2_16_0[c] -> dag_hs_18_2_16_0[c] + h[c] + mi14p[c]	0.000	0.000	0.000	0.000	0.460	0.000	0.460	0	402917621
375	PI4PLC_18_2_18_1	Miscellaneous	h2o[c] + pail4p_hs_18_2_18_1[c] -> dag_hs_18_2_18_1[c] + h[c] + mi14p[c]	0.000	0.000	0.000	0.000	0.460	0.000	0.460	0	402917621
376	PI4PP_16_0_16_0	Miscellaneous	h2o[c] + pail4p_hs_16_0_16_0[c] -> pail_hs_16_0_16_0[c] + pi[c]	0.000	0.000	0.000	0.000	2.105	0.000	2.105	0	263129851
377	PI4PP_16_0_18_1	Miscellaneous	h2o[c] + pail4p_hs_16_0_18_1[c] -> pail_hs_16_0_18_1[c] + pi[c]	0.000	0.000	0.000	0.000	2.105	0.000	2.105	0	263129851

378	PI4PP_16_0_18_2	Miscellaneous	h2o[c] + pail4p_hs_16_0_18_2[c] -> pail_hs_16_0_18_2[c] + pi[c]	0.000	0.000	0.000	0.000	2.105	0.000	2.105	0	263129851
379	PI4PP_18_1_18_1	Miscellaneous	h2o[c] + pail4p_hs_18_1_18_1[c] -> pail_hs_18_1_18_1[c] + pi[c]	0.000	0.000	0.000	0.000	2.105	0.000	2.105	0	263129851
380	PI4PP_18_1_18_2	Miscellaneous	h2o[c] + pail4p_hs_18_1_18_2[c] -> pail_hs_18_1_18_2[c] + pi[c]	0.000	0.000	0.000	0.000	2.105	0.000	2.105	0	263129851
381	PI4PP_18_2_16_0	Miscellaneous	h2o[c] + pail4p_hs_18_2_16_0[c] -> pail_hs_18_2_16_0[c] + pi[c]	0.000	0.000	0.000	0.000	2.105	0.000	2.105	0	263129851
382	PI4PP_18_2_18_1	Miscellaneous	h2o[c] + pail4p_hs_18_2_18_1[c] -> pail_hs_18_2_18_1[c] + pi[c]	0.000	0.000	0.000	0.000	2.105	0.000	2.105	0	263129851
383	PIK4_16_0_16_0	Lipid Metabolism	atp[c] + pail_hs_16_0_16_0[c] -> adp[c] + h[c] + pail4p_hs_16_0_16_0[c]	0.000	0.000	0.000	0.000	2.105	0.000	2.105	0	263129851
384	PIK4_16_0_18_1	Lipid Metabolism	atp[c] + pail_hs_16_0_18_1[c] -> adp[c] + h[c] + pail4p_hs_16_0_18_1[c]	0.000	0.000	0.000	0.000	2.105	0.000	2.105	0	263129851
385	PIK4_16_0_18_2	Lipid Metabolism	atp[c] + pail_hs_16_0_18_2[c] -> adp[c] + h[c] + pail4p_hs_16_0_18_2[c]	0.000	0.000	0.000	0.000	2.105	0.000	2.105	0	263129851
386	PIK4_18_1_18_1	Lipid Metabolism	atp[c] + pail_hs_18_1_18_1[c] -> adp[c] + h[c] + pail4p_hs_18_1_18_1[c]	0.000	0.000	0.000	0.000	2.105	0.000	2.105	0	263129851
387	PIK4_18_1_18_2	Lipid Metabolism	atp[c] + pail_hs_18_1_18_2[c] -> adp[c] + h[c] + pail4p_hs_18_1_18_2[c]	0.000	0.000	0.000	0.000	2.105	0.000	2.105	0	263129851
388	PIK4_18_2_16_0	Lipid Metabolism	atp[c] + pail_hs_18_2_16_0[c] -> adp[c] + h[c] + pail4p_hs_18_2_16_0[c]	0.000	0.000	0.000	0.000	2.105	0.000	2.105	0	263129851
389	PIK4_18_2_18_1	Lipid Metabolism	atp[c] + pail_hs_18_2_18_1[c] -> adp[c] + h[c] + pail4p_hs_18_2_18_1[c]	0.000	0.000	0.000	0.000	2.105	0.000	2.105	0	263129851
390	PIPLC_16_0_16_0	Miscellaneous	h2o[c] + pail_hs_16_0_16_0[c] -> dag_hs_16_0_16_0[c] + h[c] + mi1p-D[c]	0.000	0.000	0.000	0.000	0.702	0.000	0.702	0	263129851
391	PIPLC_16_0_18_1	Miscellaneous	h2o[c] + pail_hs_16_0_18_1[c] -> dag_hs_16_0_18_1[c] + h[c] + mi1p-D[c]	0.000	0.000	0.000	0.000	0.702	0.000	0.702	0	263129849
392	PIPLC_16_0_18_2	Miscellaneous	h2o[c] + pail_hs_16_0_18_2[c] -> dag_hs_16_0_18_2[c] + h[c] + mi1p-D[c]	0.000	0.000	0.000	0.000	0.702	0.000	0.702	0	263129849

393	PIPLC_18_1_18_1	Miscellaneous	h2o[c] + pail_hs_18_1_18_1[c] -> dag_hs_18_1_18_1[c] + h[c] + mi1p-D[c]	0.000	0.000	0.000	0.000	0.702	0.000	0.702	0	263129849
394	PIPLC_18_1_18_2	Miscellaneous	h2o[c] + pail_hs_18_1_18_2[c] -> dag_hs_18_1_18_2[c] + h[c] + mi1p-D[c]	0.000	0.000	0.000	0.000	0.702	0.000	0.702	0	263129849
395	PIPLC_18_2_16_0	Miscellaneous	h2o[c] + pail_hs_18_2_16_0[c] -> dag_hs_18_2_16_0[c] + h[c] + mi1p-D[c]	0.000	0.000	0.000	0.000	0.702	0.000	0.702	0	263129849
396	PIPLC_18_2_18_1	Miscellaneous	h2o[c] + pail_hs_18_2_18_1[c] -> dag_hs_18_2_18_1[c] + h[c] + mi1p-D[c]	0.000	0.000	0.000	0.000	0.702	0.000	0.702	0	263129849
397	Plt	Transport	pi[c] <=> pi[e]	0.000	0.000	0.000	-1.305	0.000	-1.305	0.000	-163092280	0
398	PLA2_2_16_0_16_0	Lipid Metabolism	h2o[c] + pchol_hs_16_0_16_0[c] -> h[c] + hdca[c] + lpchol_hs_16_0[c]	0.000	0.000	0.000	0.000	0.351	0.000	0.351	0	263129847
399	PLA2_2_16_0_18_1	Lipid Metabolism	h2o[c] + pchol_hs_16_0_18_1[c] -> h[c] + lpchol_hs_16_0[c] + ocdcea[c]	0.000	0.000	0.000	0.000	0.351	0.000	0.351	0	263129856
400	PLA2_2_16_0_18_2	Lipid Metabolism	h2o[c] + pchol_hs_16_0_18_2[c] -> h[c] + lnlc[c] + lpchol_hs_16_0[c]	0.000	0.000	0.000	0.000	0.351	0.000	0.351	0	263129850
401	PLA2_2_18_1_18_1	Lipid Metabolism	h2o[c] + pchol_hs_18_1_18_1[c] -> h[c] + lpchol_hs_18_1[c] + ocdcea[c]	0.000	0.000	0.000	0.000	0.351	0.000	0.351	0	263129856
402	PLA2_2_18_1_18_2	Lipid Metabolism	h2o[c] + pchol_hs_18_1_18_2[c] -> h[c] + lnlc[c] + lpchol_hs_18_1[c]	0.000	0.000	0.000	0.000	0.351	0.000	0.351	0	263129856
403	PLA2_2_18_2_16_0	Lipid Metabolism	h2o[c] + pchol_hs_18_2_16_0[c] -> h[c] + hdca[c] + lpchol_hs_18_2[c]	0.000	0.000	0.000	0.000	0.351	0.000	0.351	0	263129850
404	PLA2_2_18_2_18_1	Lipid Metabolism	h2o[c] + pchol_hs_18_2_18_1[c] -> h[c] + lpchol_hs_18_2[c] + ocdcea[c]	0.000	0.000	0.000	0.000	0.351	0.000	0.351	0	263129856
405	PMANM	Carbohydrate Metabolism	man1p[c] <=> man6p[c]	0.000	0.000	0.000	0.000	0.000	0.000	0.000	#DIV/0!	#DIV/0!
406	PNP	NAD Metabolism	pi[c] + rnam[c] <=> h[c] + ncam[c] + r1p[c]	0.000	0.000	0.000	-0.024	0.001	-0.024	0.001	-8651389.8	360403.643
407	PPA	Oxidative Phosphorylation	h2o[c] + ppi[c] -> h[c] + 2 pi[c]	0.000	0.000	0.000	0.002	1.056	0.002	1.056	624785.098	263973562
408	PPAP_16_0_16_0	Lipid Metabolism	h2o[c] + pa_hs_16_0_16_0[c] -> dag_hs_16_0_16_0[c] + pi[c]	0.000	0.000	0.000	0.000	2.105	0.000	2.105	0	263129851
409	PPAP_16_0_18_1	Lipid Metabolism	h2o[c] + pa_hs_16_0_18_1[c] -> dag_hs_16_0_18_1[c] + pi[c]	0.000	0.000	0.000	0.000	2.105	0.000	2.105	0	263129851
410	PPAP_16_0_18_2	Lipid Metabolism	h2o[c] + pa_hs_16_0_18_2[c] -> dag_hs_16_0_18_2[c] + pi[c]	0.000	0.000	0.000	0.000	2.105	0.000	2.105	0	263129851

411	PPAP_18_1_18_1	Lipid Metabolism	h2o[c] + pa_hs_18_1_18_1[c] -> dag_hs_18_1_18_1[c] + pi[c]	0.000	0.000	0.000	0.000	2.105	0.000	2.105	0	263129847
412	PPAP_18_1_18_2	Lipid Metabolism	h2o[c] + pa_hs_18_1_18_2[c] -> dag_hs_18_1_18_2[c] + pi[c]	0.000	0.000	0.000	0.000	2.105	0.000	2.105	0	263129851
413	PPAP_18_2_16_0	Lipid Metabolism	h2o[c] + pa_hs_18_2_16_0[c] -> dag_hs_18_2_16_0[c] + pi[c]	0.000	0.000	0.000	0.000	2.105	0.000	2.105	0	263129851
414	PPAP_18_2_18_1	Lipid Metabolism	h2o[c] + pa_hs_18_2_18_1[c] -> dag_hs_18_2_18_1[c] + pi[c]	0.000	0.000	0.000	0.000	2.105	0.000	2.105	0	263129851
415	PPBNGS	Miscellaneous	2 5aop[c] -> h[c] + 2 h2o[c] + ppbng[c]	0.000	0.000	0.000	0.010	0.010	0.010	0.010	1249570.73	1249937.38
416	PPM	Pentose Phosphate Pathway	r1p[c] <=> r5p[c]	0.010	0.010	0.000	-0.063	1.062	-0.073	1.052	-10450426	150359911
417	PPPGO	Miscellaneous	1.5 o2[c] + pppg9[c] -> 3 h2o[c] + ppp9[c]	0.000	0.000	0.000	0.002	0.003	0.002	0.002	1249570.73	1249937.38
418	PRPPS	Pentose Phosphate Pathway	atp[c] + r5p[c] <=> amp[c] + h[c] + prpp[c]	0.000	0.000	0.000	0.000	1.052	0.000	1.052	0	263129857
419	PTRCt	Transport	ptrc[e] <=> ptrc[c]	-0.115	0.000	0.115	-0.115	0.000	0.000	0.000	0	0
420	PUNP1	Nucleotide Metabolism	adn[c] + pi[c] <=> ade[c] + r1p[c]	-0.014	0.010	0.024	-0.039	1.057	-0.025	1.047	-104.79362	4363.84536
421	PUNP3	Nucleotide Metabolism	gsn[c] + pi[c] <=> gua[c] + r1p[c]	0.000	0.000	0.000	0.000	1.052	0.000	1.052	0	263129851
422	PUNP5	Nucleotide Metabolism	ins[c] + pi[c] <=> hxan[c] + r1p[c]	0.000	0.024	0.024	0.000	1.076	0.000	1.052	0	4385.29539
423	PYAM5PO	Vitamin Metabolism	h2o[c] + o2[c] + pyam5p[c] -> h2o2[c] + nh4[c] + pydx5p[c]	0.000	0.000	0.000	0.000	0.000	0.000	0.000	0	12400.3682
424	PYDAMK	Vitamin Metabolism	atp[c] + pydam[c] -> adp[c] + h[c] + pyam5p[c]	0.000	0.000	0.000	0.000	0.000	0.000	0.000	0	12400.3682
425	PYDAMtr	Transport	pydam[e] <=> pydam[c]	0.000	0.000	0.000	0.000	0.000	0.000	0.000	0	12400.3682
426	PYDXDH	Vitamin Metabolism	h2o[c] + o2[c] + pydx[c] -> 4pyrdx[c] + h2o2[c]	0.000	0.000	0.000	0.000	0.000	0.000	0.000	0	47776.4098
427	PYDXK	Vitamin Metabolism	atp[c] + pydx[c] -> adp[c] + h[c] + pydx5p[c]	0.000	0.000	0.000	0.000	2.105	0.000	2.105	0	263129851
428	PYDXNK	Vitamin Metabolism	atp[c] + pydxn[c] -> adp[c] + h[c] + pdx5p[c]	0.000	0.000	0.000	0.000	2.105	0.000	2.105	0	263129851
429	PYDXNtr	Transport	pydxn[e] <=> pydxn[c]	0.000	0.000	0.000	0.000	0.000	0.000	0.000	-15887.969	7950.23557
430	PYDXPP	Vitamin Metabolism	h2o[c] + pydx5p[c] -> pi[c] + pydx[c]	0.000	0.000	0.000	0.000	2.105	0.000	2.105	0	263130148
431	PYDXtr	Transport	pydx[e] <=> pydx[c]	0.000	0.000	0.000	0.000	0.000	0.000	0.000	-14200.42	9637.78527
432	PYK	Glycolysis/Gluconeogenesis	adp[c] + h[c] + pep[c] -> atp[c] + pyr[c]	2.907	2.907	0.000	3.252	5.578	0.345	2.671	43115485.3	333930789
433	PYRt2r	Transport	h[e] + pyr[e] <=> h[c] + pyr[c]	-1.824	0.000	1.824	-2.933	0.000	-1.108	0.000	-60.763106	0
434	RBFK	Vitamin Metabolism	atp[c] + ribflv[c] -> adp[c] + fmn[c] + h[c]	0.000	0.000	0.000	0.000	2.105	0.000	2.105	0	263129850
435	RIBFLVt3	Transport	atp[c] + h2o[c] + ribflv[e] -> adp[c] + h[c] + pi[c] + ribflv[c]	0.000	0.000	0.000	0.000	1.052	0.000	1.052	0	263129851

436	RIBFLVt3o	Transport	atp[c] + h2o[c] + ribflv[c] -> adp[c] + h[c] + pi[c] + ribflv[e]	0.000	0.000	0.000	0.000	1.052	0.000	1.052	0	263129851
437	RNMK	NAD Metabolism	atp[c] + rnam[c] -> adp[c] + h[c] + nmn[c]	0.000	0.000	0.000	0.000	2.105	0.000	2.105	0	263129850
438	RPE	Pentose Phosphate Pathway	ru5p-D[c] <=> xu5p-D[c]	0.044	0.044	0.000	0.139	4.953	0.095	4.909	5287110.41	272738643
439	RPI	Pentose Phosphate Pathway	r5p[c] <=> ru5p-D[c]	-0.012	-0.012	0.000	-2.544	-0.060	-2.532	-0.048	-316503892	-5947986.7
440	SALMCOM	Amino Acid Metabolism	amet[c] + nrpphr[c] -> ahcys[c] + h[c] + normete-L[c]	0.000	0.000	0.000	0.000	0.029	0.000	0.029	0	2399970.67
441	SALMCOM 2	Amino Acid Metabolism	adrnl[c] + amet[c] -> ahcys[c] + h[c] + mepi[c]	0.000	0.000	0.000	0.000	0.038	0.000	0.038	0	3149992.76
442	SBTD_D2	Carbohydrate Metabolism	nad[c] + sbt-D[c] -> fru[c] + h[c] + nadh[c]	0.000	0.862	0.862	0.000	1.120	0.000	0.258	0	29.9296709
443	SBTR	Carbohydrate Metabolism	glc-D[c] + h[c] + nadph[c] -> nadp[c] + sbt-D[c]	0.000	0.862	0.862	0.000	1.120	0.000	0.258	0	29.9296709
444	SPMDt	Transport	spmd[e] <=> spmd[c]	0.000	0.000	0.000	-0.025	0.000	-0.025	0.000	-20959794	0
445	SPMS	Amino Acid Metabolism	ametam[c] + ptrc[c] -> 5mta[c] + h[c] + spmd[c]	0.000	0.000	0.000	0.000	0.025	0.000	0.025	0	20959795.1
446	SPRMS	Amino Acid Metabolism	ametam[c] + spmd[c] -> 5mta[c] + h[c] + sprm[c]	0.000	0.000	0.000	0.000	0.013	0.000	0.013	0	20959794.7
447	SPRMt2r	Transport	h[c] + sprm[e] <=> sprm[c] + h[e]	0.000	0.000	0.000	-0.013	0.000	-0.013	0.000	-20959795	0
448	TALA	Pentose Phosphate Pathway	g3p[c] + s7p[c] <=> e4p[c] + f6p[c]	0.022	0.022	0.000	0.070	2.507	0.048	2.485	5287110.51	276118386
449	TDP	Vitamin Metabolism	h2o[c] + thmpp[c] -> h[c] + pi[c] + thmmp[c]	0.000	0.000	0.000	0.000	0.000	0.000	0.000	0	14900.4407
450	THMMPtrbc	Transport	thmmp[e] <=> thmmp[c]	0.000	0.000	0.000	0.000	0.000	0.000	0.000	-14900.441	0
451	THMTP	Vitamin Metabolism	h2o[c] + thmtp[c] -> h[c] + pi[c] + thmpp[c]	0.000	0.000	0.000	0.000	2.105	0.000	2.105	0	263129850
452	THMtrbc	Transport	thm[e] <=> thm[c]	0.000	0.000	0.000	0.000	0.000	0.000	0.000	0	14900.4407
453	TKT1	Pentose Phosphate Pathway	r5p[c] + xu5p-D[c] <=> g3p[c] + s7p[c]	0.022	0.022	0.000	0.070	2.507	0.048	2.485	5287110.51	276118386
454	TKT2	Pentose Phosphate Pathway	e4p[c] + xu5p-D[c] <=> f6p[c] + g3p[c]	0.022	0.022	0.000	0.070	2.507	0.048	2.485	5287110.51	276118386
455	TMDPK	Vitamin Metabolism	atp[c] + thm[c] -> amp[c] + h[c] + thmpp[c]	0.000	0.000	0.000	0.000	0.000	0.000	0.000	0	14900.4407
456	TMDPPK	Vitamin Metabolism	atp[c] + thmpp[c] -> adp[c] + thmtp[c]	0.000	0.000	0.000	0.000	2.105	0.000	2.105	0	263129850
457	TPI	Glycolysis/Gluconeogenesis	dhap[c] <=> g3p[c]	1.442	1.442	0.000	0.389	2.081	-1.053	0.639	-131684494	79847742.4
458	UDPG4E	Carbohydrate Metabolism	udpg[c] <=> udpgal[c]	-0.317	-0.317	0.000	-0.317	0.000	0.000	0.317	0	79227246.6
459	UDPGD	Carbohydrate Metabolism	h2o[c] + 2 nad[c] + udpg[c] -> 3 h[c] + 2 nadh[c] + udpglcur[c]	0.000	0.000	0.000	0.002	0.419	0.002	0.419	728916.051	122311566
460	UDPGNP	Carbohydrate Metabolism	h2o[c] + udpglcur[c] -> glcur[c] + h[c] + udp[c]	0.000	0.000	0.000	0.000	0.417	0.000	0.417	0	121582361
461	UGLT	Carbohydrate Metabolism	gal1p[c] + udpg[c] <=> g1p[c] + udpgal[c]	-999.683	1000.000	1999.683	-1000.000	1000.000	-0.317	0.000	-0.0158475	0
462	UMPK	Nucleotide Metabolism	atp[c] + ump[c] <=> adp[c] + udp[c]	0.000	0.000	0.000	0.000	0.000	0.000	0.000	#DIV/0!	#DIV/0!

463	UPP3S	Miscellaneous	hmbil[c] -> h2o[c] + uppg3[c]	0.000	0.000	0.000	0.002	0.003	0.002	0.002	1249570.73	1249937.38
464	UPPDC1	Miscellaneous	4 h[c] + uppg3[c] -> 4 co2[c] + cpppg3[c]	0.000	0.000	0.000	0.002	0.003	0.002	0.002	1249570.73	1249937.38
465	UREAt	Transport	urea[e] <=> urea[c]	-0.115	0.000	0.115	-0.115	0.000	0.000	0.000	0	0
466	URIt	Transport	uri[e] <=> uri[c]	0.000	0.000	0.000	-0.010	0.000	-0.010	0.000	-5833404.7	0
467	XYLK	Carbohydrate Metabolism	atp[c] + xylu-D[c] -> adp[c] + h[c] + xu5p-D[c]	0.000	0.000	0.000	0.000	0.417	0.000	0.417	0	121582361
468	XYLTD_Dr	Carbohydrate Metabolism	nad[c] + xylt[c] <=> h[c] + nadh[c] + xylu-D[c]	0.000	0.000	0.000	0.000	0.417	0.000	0.417	0	121582361
469	XYLUR	Carbohydrate Metabolism	h[c] + nadph[c] + xylu-L[c] <=> nadp[c] + xylt[c]	0.000	0.000	0.000	0.000	0.417	0.000	0.417	0	121582361
470	EX_glcn(e)	Exchange/demand reaction	<=> glcn[e]	0	0	0	-4.456	-0.198747	-4.456	-0.19875	0	0
471	GLCNtr	Transport	glcn[e] <=> glcn[c]	0	0	0	0.198747	4.456005	0.1987	4.456	0	0
472	GNTK	Nucleotide Metabolism	atp[c] + glcn[c] -> 6pgc[c] + adp[c] + h[c]	0.000	0.000	0.000	0.199	4.456	0.199	4.456	0	0

The results of FVA for all the reactions :
Minflux_glcn0 , Maxflux_glcn0 = minimum and maximum flux values (mmol/gDW/h) for each reaction when no gluconate was added to the model.
Minflux_glcn , Maxflux_glcn = minimum and maximum flux values for each reaction when gluconate was provided to the model (EX_glcn = 1000).

Range = Maxflux_glcn0 - Minflux_glcn0 (Range of flux possible through the reaction before adding gluconate)

Change in minimum and maximum fluxes :
Minflux_diff = Minflux_glcn - Minflux_glcn0
Maxflux_diff = Maxflux_glcn - Maxflux_glcn0

Reactions used in Figure 4											
Reaction No.	Reaction Abb.	Subsystem	Reaction Formula	Minflux_glcn0	Maxflux_glcn0	Range	Minflux_glcn	Maxflux_glcn	Range after	Range diff	Width
132	ALDD2x	Glycolysis/Gluconeogenesis	acald[c] + h2o[c] + nad[c] -> ac[c] + 2 h[c] + nadh[c]	0.0	0.0	0.0	0.0	0.0	0.0	0	1
263	HEX1	Glycolysis/Gluconeogenesis	atp[c] + glc-D[c] -> adp[c] + g6p[c] + h[c]	0.3	1.1	0.9	0.0	1.1	1.1	0	1
345	PGMT	Glycolysis/Gluconeogenesis	g1p[c] <=> g6p[c]	0.3	0.3	0.0	-0.4	0.3	0.7	1	2
277	LDH_L	Glycolysis/Gluconeogenesis	lac-L[c] + nad[c] <=> h[c] + nadh[c] + pyr[c]	-3.7	-1.8	1.8	-3.7	-1.1	2.6	1	2
418	PRPPS	Pentose Phosphate Pathway	atp[c] + r5p[c] <=> amp[c] + h[c] + prpp[c]	0.0	0.0	0.0	0.0	1.1	1.1	1	2
416	PPM	Pentose Phosphate Pathway	r1p[c] <=> r5p[c]	0.0	0.0	0.0	-0.1	1.1	1.1	1	2
457	TPI	Glycolysis/Gluconeogenesis	dhap[c] <=> g3p[c]	1.4	1.4	0.0	0.4	2.1	1.7	2	3
204	DPGM	Glycolysis/Gluconeogenesis	13dpg[c] <=> 23dpg[c] + h[c]	0.0	0.0	0.0	0.0	2.1	2.1	2	3
205	DPGase	Glycolysis/Gluconeogenesis	23dpg[c] + h2o[c] -> 3pg[c] + pi[c]	0.0	0.0	0.0	0.0	2.1	2.1	2	3
214	FBA	Glycolysis/Gluconeogenesis	fdp[c] <=> dhap[c] + g3p[c]	1.4	1.4	0.0	0.5	2.6	2.1	2	3
339	PFK	Glycolysis/Gluconeogenesis	atp[c] + f6p[c] -> adp[c] + fdp[c] + h[c]	1.4	1.4	0.0	0.5	2.6	2.1	2	3
230	GAPD	Glycolysis/Gluconeogenesis	g3p[c] + nad[c] + pi[c] <=> 13dpg[c] + h[c] + nadh[c]	2.9	2.9	0.0	3.3	5.6	2.3	2	3
342	PGK	Glycolysis/Gluconeogenesis	3pg[c] + atp[c] <=> 13dpg[c] + adp[c]	-2.9	-2.9	0.0	-5.6	-3.3	2.3	2	3
432	PYK	Glycolysis/Gluconeogenesis	adp[c] + h[c] + pep[c] -> atp[c] + pyr[c]	2.9	2.9	0.0	3.3	5.6	2.3	2	3
206	ENO	Glycolysis/Gluconeogenesis	2pg[c] <=> h2o[c] + pep[c]	2.9	2.9	0.0	3.3	5.6	2.3	2	3
344	PGM	Glycolysis/Gluconeogenesis	2pg[c] <=> 3pg[c]	-2.9	-2.9	0.0	-5.6	-3.3	2.3	2	3
448	TALA	Pentose Phosphate Pathway	g3p[c] + s7p[c] <=> e4p[c] + f6p[c]	0.0	0.0	0.0	0.1	2.5	2.4	2	3
453	TKT1	Pentose Phosphate Pathway	r5p[c] + xu5p-D[c] <=> g3p[c] + s7p[c]	0.0	0.0	0.0	0.1	2.5	2.4	2	3
454	TKT2	Pentose Phosphate Pathway	e4p[c] + xu5p-D[c] <=> f6p[c] + g3p[c]	0.0	0.0	0.0	0.1	2.5	2.4	2	3
439	RPI	Pentose Phosphate Pathway	r5p[c] <=> ru5p-D[c]	0.0	0.0	0.0	-2.5	-0.1	2.5	2	3
438	RPE	Pentose Phosphate Pathway	ru5p-D[c] <=> xu5p-D[c]	0.0	0.0	0.0	0.1	5.0	4.8	5	6
223	G6PDH2r	Pentose Phosphate Pathway	g6p[c] + nadp[c] <=> 6pgl[c] + h[c] + nadph[c]	0.1	0.1	0.0	0.0	5.0	5.0	5	6
343	PGL	Pentose Phosphate Pathway	6pgl[c] + h2o[c] -> 6pgc[c] + h[c]	0.1	0.1	0.0	0.0	5.0	5.0	5	6
341	PGI	Glycolysis/Gluconeogenesis	g6p[c] <=> f6p[c]	0.5	1.4	0.9	-4.9	1.4	6.3	5	6
243	GND	Pentose Phosphate Pathway	6pgc[c] + nadp[c] -> co2[c] + nadph[c] + ru5p-D[c]	0.1	0.1	0.0	0.2	7.4	7.2	7	8
276	L-LACt2r	Transport	h[e] + lac-L[e] <=> h[c] + lac-L[c]	-3.7	-1.8	1.8	-3.7	-1.1	2.6	1	2
46	EX_lac-L(e)	Exchange/demand reaction	lac-L[e] ->	1.8	3.7	1.8	1.1	3.7	2.6	1	2

Minflux_glcn0 , Maxflux_glcn0 = minimum and maximum flux values for each reaction when no gluconate was added to the model.
Minflux_glcn , Maxflux_glcn = minimum and maximum flux values for each reaction when gluconate was provided to the model (EX_glcn = 1000).

Range = Maxflux_glcn0 - Minflux_glcn0 (Range of flux possible through the reaction before adding gluconate)
Range after= Maxflux_glcn - Minflux_glcn (Range of flux possible through the reaction after adding gluconate)
Range diff = Range after - Range
Width is the width of the reaction connection in the diagram.

Shadow price for each metabolite			
		FBA.y when glcn is unbounded and PPP split ratio is fixed (solver : glpk)	FBA.y when there is no gluconate provided to the model with PPP split ratio fixed (solver : glpk)
Mets	MetNames	shadow prices w. Glcn	shadow prices without glcn
13dpg[c]	3-Phospho-D-glyceroyl phosphate	0	4.44089E-17
23dpg[c]	2,3-Disphospho-D-glycerate	0	4.44089E-17
2kmb[c]	2-keto-4-methylthiobutyrate	0	-1
2pg[c]	D-Glycerate 2-phosphate	0	9.99201E-17
35cgmp[c]	3',5'-Cyclic GMP	0	-2.666666667
35cgmp[e]	3',5'-Cyclic GMP	0	0
3dhguln[c]	3-Dehydro-L-gulonate	0	-2
3moxtyr[c]	3-Methoxytyramine	0	0
3moxtyr[e]	3-Methoxytyramine	0	0
3pg[c]	3-Phospho-D-glycerate	0	9.99201E-17
4pyrdx[c]	4-Pyridoxate	0	-1.77494E-29
4pyrdx[e]	4-Pyridoxate	0	0
5aop[c]	5-Amino-4-oxopentanoate	0	0
5aop[e]	5-Amino-4-oxopentanoate	0	0
5mdr1p[c]	5-Methylthio-5-deoxy-D-ribose 1-phosphate	0	-1.666666667
5mdru1p[c]	5-Methylthio-5-deoxy-D-ribulose 1-phosphate	0	-1.666666667
5mta[c]	5-Methylthioadenosine	0	-2.666666667
5oxpro[c]	5-Oxoproline	0	4.73317E-29
6pgc[c]	6-Phospho-D-gluconate	0	-1.666666667
6pgl[c]	6-phospho-D-glucono-1,5-lactone	0	-1.666666667
ac[c]	Acetate	0	2
ac[e]	Acetate	0	2
acald[c]	Acetaldehyde	0	0
acald[e]	Acetaldehyde	0	0
acgam[c]	N-Acetyl-D-glucosamine	0	-1.28196E-16
acgam6p[c]	N-Acetyl-D-glucosamine 6-phosphate	0	-1.28196E-16
acmana[c]	N-Acetyl-D-mannosamine	0	-1.28196E-16
acmanap[c]	N-Acetyl-D-mannosamine 6-phosphate	0	-1.28196E-16
acnam[c]	N-Acetylneuraminate	0	0
acnam[e]	N-Acetylneuraminate	0	0
acnamp[c]	N-Acetylneuraminate 9-phosphate	0	1
ade[c]	Adenine	0	0
ade[e]	Adenine	0	0
adn[c]	Adenosine	0	-2.666666667
adn[e]	Adenosine	0	-2.666666667
adp[c]	ADP	0	-1.666666667
adprbp[c]	ADPribose 2'-phosphate	0	0
adrnl[c]	Adrenaline	0	0
adrnl[e]	Adrenaline	0	0
ahcys[c]	S-Adenosyl-L-homocysteine	0	-2.666666667
akg[c]	2-Oxoglutarate	0	0
ala-L[c]	L-Alanine	0	-4.73317E-29
ala-L[e]	L-Alanine	0	0
alpa_hs_16_0[c]	lysophosphatidic acid (homo sapiens, C16:0)	0	-8.14164E-17
alpa_hs_18_1[c]	lysophosphatidic acid (homo sapiens, C18:1)	0	-1.22587E-16
alpa_hs_18_2[c]	lysophosphatidic acid (homo sapiens, C18:2)	0	-1.22587E-16
amet[c]	S-Adenosyl-L-methionine	0	-2.666666667
ametam[c]	S-Adenosylmethioninamine	0	-2.666666667
amp[c]	AMP	0	-1.666666667
ap4a[c]	P1,P4-Bis(5'-adenosyl) tetraphosphate	0	-3.333333333
arg-L[c]	L-Arginine	0	0

arg-L[e]	L-Arginine	0	0
ascb-L[c]	L-Ascorbate	0	0
ascb-L[e]	L-Ascorbate	0	0
atp[c]	ATP	0	-1.666666667
band[c]	Band membrane protein (universal, erythrocyte -> 2.1,3,4.1)	0	0
bandmt[c]	Band membrane protein (methylated, universal, erythrocyte -> 2.1,3,4.1)	0	0
bilglcur[c]	Bilirubin monoglucuronide	-0.5	-6.42922E-29
bilglcur[e]	Bilirubin monoglucuronide	0	0
bilirub[c]	Bilirubin	-0.5	2
biliverd[c]	Biliverdin	-0.5	2
ca2[c]	Calcium	0	0
ca2[e]	Calcium	0	0
camp[c]	cAMP	0	-1.666666667
camp[e]	cAMP	0	0
cdp[c]	CDP	0	8.14164E-17
cdpchol[c]	CDPcholine	0	0
cdpdag_hs_16_0_16_0[c]	CDP diacylglycerol (homo sapiens, C16:0, C16:0)	0	2.59052E-17
cdpdag_hs_16_0_18_1[c]	CDP diacylglycerol (homo sapiens, C16:0, C18:1)	0	2.59052E-17
cdpdag_hs_16_0_18_2[c]	CDP diacylglycerol (homo sapiens, C16:0, C18:2)	0	2.59052E-17
cdpdag_hs_18_1_18_1[c]	CDP diacylglycerol (homo sapiens, C18:1, C18:1)	0	2.59052E-17
cdpdag_hs_18_1_18_2[c]	CDP diacylglycerol (homo sapiens, C18:1, C18:2)	0	2.59052E-17
cdpdag_hs_18_2_16_0[c]	CDP diacylglycerol (homo sapiens, C18:2, C16:0)	0	2.59052E-17
cdpdag_hs_18_2_18_1[c]	CDP diacylglycerol (homo sapiens, C18:2, C18:1)	0	2.59052E-17
cdpea[c]	CDPethanolamine	0	0
chol[c]	Choline	0	2.8399E-29
chol[e]	Choline	0	0
cholp[c]	Choline phosphate	0	-5.55112E-17
cl[c]	Chloride	-0.5	-6.42922E-29
cl[e]	Chloride	0	0
cmp[c]	CMP	0	2.59052E-17
co[c]	Carbon monoxide	0.5	0
co[e]	Carbon monoxide	0.5	0
co2[c]	CO2	0	0
co2[e]	CO2	0	0
coa[c]	Coenzyme A	0	-1.06396E-17
cpppg3[c]	Coproporphyrinogen III	0	-2.61902E-28
crn[c]	L-Carnitine	0	0
ctp[c]	CTP	0	-8.51171E-17
cys-L[c]	L-Cysteine	-0.5	0
cys-L[e]	L-Cysteine	-0.5	0
dag_hs_16_0_16_0[c]	diacylglycerol (homo sapiens, C16:0, C16:0)	0	2.59052E-17
dag_hs_16_0_18_1[c]	diacylglycerol (homo sapiens, C16:0, C18:1)	0	2.59052E-17
dag_hs_16_0_18_2[c]	diacylglycerol (homo sapiens, C16:0, C18:2)	0	2.59052E-17
dag_hs_18_1_18_1[c]	diacylglycerol (homo sapiens, C18:1, C18:1)	0	2.59052E-17
dag_hs_18_1_18_2[c]	diacylglycerol (homo sapiens, C18:1, C18:2)	0	2.59052E-17
dag_hs_18_2_16_0[c]	diacylglycerol (homo sapiens, C18:2, C16:0)	0	2.59052E-17
dag_hs_18_2_18_1[c]	diacylglycerol (homo sapiens, C18:2, C18:1)	0	2.59052E-17
dhap[c]	Dihydroxyacetone phosphate	0	-1
dhdascb[c]	Dehydroascorbate	0	0
dhdascb[e]	Dehydroascorbate	0	0
dhmtp[c]	1,2-Dihydroxy-5-(methylthio)pent-1-en-3-one	0	-2.666666667
dkmpp[c]	2,3-diketo-5-methylthio-1-phosphopentane	0	-1.666666667
dnad[c]	Deamino-NAD+	0	-2.333333333
dopa[c]	Dopamine	0	0
dopa[e]	Dopamine	0	0
e4p[c]	D-Erythrose 4-phosphate	0	-1.333333333

etha[c]	Ethanolamine	0	0
etha[e]	Ethanolamine	0	0
ethamp[c]	Ethanolamine phosphate	0	-5.55112E-17
f26bp[c]	D-Fructose 2,6-bisphosphate	0	-1
f6p[c]	D-Fructose 6-phosphate	0	-2
fad[c]	Flavin adenine dinucleotide oxidized	0	-1.666666667
fdp[c]	D-Fructose 1,6-bisphosphate	0	-2
fe2[c]	Fe2+	0	0
fe2[e]	Fe2+	0	0
fmn[c]	FMN	0	0
for[c]	Formate	0	0
fru[c]	D-Fructose	0	-2
fru[e]	D-Fructose	0	-2
fum[c]	Fumarate	0	-2.01554E-28
fum[e]	Fumarate	0	-2.01554E-28
g1p[c]	D-Glucose 1-phosphate	0	-2
g3p[c]	Glyceraldehyde 3-phosphate	0	-1
g3pc[c]	sn-Glycero-3-phosphocholine	0	-1.33227E-16
g6p[c]	D-Glucose 6-phosphate	0	-2
gal[c]	D-Galactose	0	-2
gal[e]	D-Galactose	0	-2
gal1p[c]	alpha-D-Galactose 1-phosphate	0	-2
galt[c]	Galactitol	0	-2
gam[c]	D-Glucosamine	0	-2
gam[e]	D-Glucosamine	0	-2
gam6p[c]	D-Glucosamine 6-phosphate	0	-2
gdp[c]	GDP	0	-2.666666667
glc-D[c]	D-Glucose	0	-2
glc-D[e]	D-Glucose	0	-2
glcn[c]	glcn[c]	0	-1.666666667
glcn[e]	glcn[e]	0	-1.666666667
glcur[c]	D-Glucuronate	0	-2
gln-L[c]	L-Glutamine	0	9.13106E-29
gln-L[e]	L-Glutamine	0	0
gluala[e]	5-L-Glutamyl-L-alanine	0	0
glucys[c]	gamma-L-Glutamyl-L-cysteine	-0.5	-1.61908E-17
glu-L[c]	L-Glutamate	0	1
gly[c]	Glycine	0.5	6.42922E-29
gly[e]	Glycine	0	0
glyc[c]	Glycerol	0	0
glyc[e]	Glycerol	0	0
glyc3p[c]	Glycerol 3-phosphate	0	-1.33227E-16
gmp[c]	GMP	0	-2.666666667
gsn[c]	Guanosine	0	-3.666666667
gthox[c]	Oxidized glutathione	0	0
gthox[e]	Oxidized glutathione	0	0
gthrd[c]	Reduced glutathione	0	0
gtp[c]	GTP	0	-2.666666667
gua[c]	Guanine	0	-1
guln[c]	L-Gulonate	0	-2
h[c]	H+	0	2.91879E-29
h[e]	H+	0	0
h2o[c]	H2O	0	0
h2o[e]	H2O	0	0
h2o2[c]	Hydrogen peroxide	0	0
h2o2[e]	Hydrogen peroxide	0	0
hco3[c]	Bicarbonate	0	-4.69372E-29

hco3[e]	Bicarbonate	0.5	0
hcys-L[c]	L-Homocysteine	0	0
hcys-L[e]	L-Homocysteine	0	0
hdca[c]	Hexadecanoate (n-C16:0)	0	1.07784E-16
hdca[e]	Hexadecanoate (n-C16:0)	0	1.07784E-16
hmbil[c]	Hydroxymethylbilane	0	-3.97586E-28
hxan[c]	Hypoxanthine	0	-1.11022E-17
hxan[e]	Hypoxanthine	0	-1.11022E-17
icit[c]	Isocitrate	0	1.22125E-16
imp[c]	IMP	0	-1.666666667
inost[c]	myo-Inositol	0	2.59052E-17
ins[c]	Inosine	0	-2.666666667
ins[e]	Inosine	0	-2.666666667
k[c]	potassium	0.5	6.42922E-29
k[e]	potassium	0	0
lac-D[c]	D-Lactate	0	0
lac-D[e]	D-Lactate	0	0
lac-L[c]	L-Lactate	0	1.81438E-29
lac-L[e]	L-Lactate	0	0
leuktrA4[c]	Leukotriene A4	0	0
leuktrA4[e]	Leukotriene A4	0	0
leuktrB4[c]	Leukotriene B4	0	-1.77494E-29
leuktrB4[e]	Leukotriene B4	0	-1.77494E-29
lgt-S[c]	(R)-S-Lactoylglutathione	0	-2
lnlc[c]	linoleic acid (all cis C18:2) n-6	0	6.66134E-17
lnlc[e]	linoleic acid (all cis C18:2) n-6	0	6.66134E-17
lnlccoa[c]	linoleic coenzyme A	0	0
lnlccrn[c]	Linoleyl carnitine	0	1.06396E-17
lpchol_hs_16_0[c]	lysophosphatidylcholine (homo sapiens, C16:0)	0	-1.07784E-16
lpchol_hs_18_1[c]	lysophosphatidylcholine (homo sapiens, C18:1)	0	-6.66134E-17
lpchol_hs_18_2[c]	lysophosphatidylcholine (homo sapiens, C18:2)	0	-6.66134E-17
mal-L[c]	L-Malate	0	0
mal-L[e]	L-Malate	0	0
man[c]	D-Mannose	0	-2
man[e]	D-Mannose	0	-2
man1p[c]	D-Mannose 1-phosphate	0	-2
man6p[c]	D-Mannose 6-phosphate	0	-2
mepi[c]	Metanephrine	0	0
mepi[e]	Metanephrine	0	0
met-L[c]	L-Methionine	0	5.92119E-16
met-L[e]	L-Methionine	0	5.92119E-16
mi1345p[c]	1D-myo-Inositol 1,3,4,5-tetrakisphosphate	0	0
mi134p[c]	1D-myo-Inositol 1,3,4-trisphosphate	0	0
mi145p[c]	1D-myo-Inositol 1,4,5-trisphosphate	0	0
mi14p[c]	1D-myo-Inositol 1,4-bisphosphate	0	0
mi1p-D[c]	1D-myo-Inositol 1-phosphate	0	3.31322E-28
mthgxl[c]	Methylglyoxal	0	-2
na1[c]	Sodium	0	0
na1[e]	Sodium	0	0
nac[c]	Nicotinate	0	0
nac[e]	Nicotinate	0	0
nad[c]	Nicotinamide adenine dinucleotide	0	-3.333333333
nadh[c]	Nicotinamide adenine dinucleotide - reduced	0	-3.333333333
nadp[c]	Nicotinamide adenine dinucleotide phosphate	0	9.38744E-29
nadph[c]	Nicotinamide adenine dinucleotide phosphate - reduced	0	1.22125E-16
ncam[c]	Nicotinamide	0	0
ncam[e]	Nicotinamide	0	0

nh4[c]	Ammonium	0	1.00974E-28
nh4[e]	Ammonium	0	0
nicrns[c]	Nicotinate D-ribonucleoside	0	-0.666666667
nicrnt[c]	Nicotinate D-ribonucleotide	0	-0.666666667
nmn[c]	NMN	0	-1.666666667
normete-L[c]	L-Normetanephrine	0	0
normete-L[e]	L-Normetanephrine	0	0
nrpphr[c]	Norepinephrine	0	0
nrpphr[e]	Norepinephrine	0	0
o2[c]	O2	0	0
o2[e]	O2	0	0
oaa[c]	Oxaloacetate	0	-2.91879E-29
ocdcea[c]	octadecenoate (n-C18:1)	0	6.66134E-17
ocdcea[e]	octadecenoate (n-C18:1)	0	6.66134E-17
odecoa[c]	Octadecenoyl-CoA (n-C18:1CoA)	0	0
odecrn[c]	octadecenoyl carnitine	0	1.06396E-17
orn[c]	Ornithine	0	-1.77494E-29
orot[c]	Orotate	0	2.666666667
orot[e]	Orotate	0	0
orot5p[c]	Orotidine 5'-phosphate	0	1
pa_hs_16_0_16_0[c]	phosphatidic acid (homo sapiens, C16:0, C16:0)	0	-2.96059E-17
pa_hs_16_0_18_1[c]	phosphatidic acid (homo sapiens, C16:0, C18:1)	0	-2.96059E-17
pa_hs_16_0_18_2[c]	phosphatidic acid (homo sapiens, C16:0, C18:2)	0	-2.96059E-17
pa_hs_18_1_18_1[c]	phosphatidic acid (homo sapiens, C18:1, C18:1)	0	-2.96059E-17
pa_hs_18_1_18_2[c]	phosphatidic acid (homo sapiens, C18:1, C18:2)	0	-2.96059E-17
pa_hs_18_2_16_0[c]	phosphatidic acid (homo sapiens, C18:2, C16:0)	0	-2.96059E-17
pa_hs_18_2_18_1[c]	phosphatidic acid (homo sapiens, C18:2, C18:1)	0	-1.11947E-16
pail_hs_16_0_16_0[c]	phosphatidylinositol (homo sapiens, C16:0, C16:0)	0	2.59052E-17
pail_hs_16_0_18_1[c]	phosphatidylinositol (homo sapiens, C16:0, C18:1)	0	2.59052E-17
pail_hs_16_0_18_2[c]	phosphatidylinositol (homo sapiens, C16:0, C18:2)	0	2.59052E-17
pail_hs_18_1_18_1[c]	phosphatidylinositol (homo sapiens, C18:1, C18:1)	0	2.59052E-17
pail_hs_18_1_18_2[c]	phosphatidylinositol (homo sapiens, C18:1, C18:2)	0	2.59052E-17
pail_hs_18_2_16_0[c]	phosphatidylinositol (homo sapiens, C18:2, C16:0)	0	2.59052E-17
pail_hs_18_2_18_1[c]	phosphatidylinositol (homo sapiens, C18:2, C18:1)	0	2.59052E-17
pail45p_hs_16_0_16_0[c]	phosphatidylinositol 4,5-bisphosphate (homo sapiens, C16:0, C16:0)	0	2.59052E-17
pail45p_hs_16_0_18_1[c]	phosphatidylinositol 4,5-bisphosphate (homo sapiens, C16:0, C18:1)	0	2.59052E-17
pail45p_hs_16_0_18_2[c]	phosphatidylinositol 4,5-bisphosphate (homo sapiens, C16:0, C18:2)	0	2.59052E-17
pail45p_hs_18_1_18_1[c]	phosphatidylinositol 4,5-bisphosphate (homo sapiens, C18:1, C18:1)	0	2.59052E-17
pail45p_hs_18_1_18_2[c]	phosphatidylinositol 4,5-bisphosphate (homo sapiens, C18:1, C18:2)	0	2.59052E-17
pail45p_hs_18_2_16_0[c]	phosphatidylinositol 4,5-bisphosphate (homo sapiens, C18:2, C16:0)	0	2.59052E-17
pail45p_hs_18_2_18_1[c]	phosphatidylinositol 4,5-bisphosphate (homo sapiens, C18:2, C18:1)	0	2.59052E-17
pail4p_hs_16_0_16_0[c]	1-Phosphatidyl-1D-myo-inositol 4-phosphate (homo sapiens, C16:0, C16:0)	0	2.59052E-17
pail4p_hs_16_0_18_1[c]	1-Phosphatidyl-1D-myo-inositol 4-phosphate (homo sapiens, C16:0, C18:1)	0	2.59052E-17
pail4p_hs_16_0_18_2[c]	1-Phosphatidyl-1D-myo-inositol 4-phosphate (homo sapiens, C16:0, C18:2)	0	2.59052E-17
pail4p_hs_18_1_18_1[c]	1-Phosphatidyl-1D-myo-inositol 4-phosphate (homo sapiens, C18:1, C18:1)	0	2.59052E-17
pail4p_hs_18_1_18_2[c]	1-Phosphatidyl-1D-myo-inositol 4-phosphate (homo sapiens, C18:1, C18:2)	0	2.59052E-17
pail4p_hs_18_2_16_0[c]	1-Phosphatidyl-1D-myo-inositol 4-phosphate (homo sapiens, C18:2, C16:0)	0	2.59052E-17
pail4p_hs_18_2_18_1[c]	1-Phosphatidyl-1D-myo-inositol 4-phosphate (homo sapiens, C18:2, C18:1)	0	2.59052E-17
pchol_hs_16_0_16_0[c]	phosphatidylcholine (homo sapiens, C16:0, C16:0)	0	0
pchol_hs_16_0_18_1[c]	phosphatidylcholine (homo sapiens, C16:0, C18:1)	0	0
pchol_hs_16_0_18_2[c]	phosphatidylcholine (homo sapiens, C16:0, C18:2)	0	0

pchol_hs_18_1_18_1[c]	phosphatidylcholine (homo sapiens, C18:1, C18:1)	0	0
pchol_hs_18_1_18_2[c]	phosphatidylcholine (homo sapiens, C18:1, C18:2)	0	0
pchol_hs_18_2_16_0[c]	phosphatidylcholine (homo sapiens, C18:2, C16:0)	0	0
pchol_hs_18_2_18_1[c]	phosphatidylcholine (homo sapiens, C18:2, C18:1)	0	0
pdx5p[c]	Pyridoxine 5'-phosphate	0	1
pe_hs_16_0_16_0[c]	phosphatidylethanolamine (homo sapiens, C16:0, C16:0)	0	0
pe_hs_16_0_18_1[c]	phosphatidylethanolamine (homo sapiens, C16:0, C18:1)	0	0
pe_hs_16_0_18_2[c]	phosphatidylethanolamine (homo sapiens, C16:0, C18:2)	0	0
pe_hs_18_1_18_1[c]	phosphatidylethanolamine (homo sapiens, C18:1, C18:1)	0	0
pe_hs_18_1_18_2[c]	phosphatidylethanolamine (homo sapiens, C18:1, C18:2)	0	0
pe_hs_18_2_16_0[c]	phosphatidylethanolamine (homo sapiens, C18:2, C16:0)	0	0
pe_hs_18_2_18_1[c]	phosphatidylethanolamine (homo sapiens, C18:2, C18:1)	0	0
pep[c]	Phosphoenolpyruvate	0	9.99201E-17
phe-L[c]	L-Phenylalanine	0	0
phe-L[e]	L-Phenylalanine	0	0
pheme[c]	Protoheme	0	-1.73549E-28
phpyr[c]	Phenylpyruvate	0	-1
pi[c]	Phosphate	0	1
pi[e]	Phosphate	0	1
pmtcoa[c]	Palmitoyl-CoA (n-C16:0CoA)	0	4.11708E-17
pmtcrn[c]	L-Palmitoylcarnitine	0	5.18104E-17
ppbng[c]	Porphobilinogen	0	6.31089E-30
ppi[c]	Diphosphate	0	-1.40628E-16
ppp9[c]	Protoporphyrin	0	-1.15174E-28
pppg9[c]	Protoporphyrinogen IX	0	-1.68816E-28
prpp[c]	5-Phospho-alpha-D-ribose 1-diphosphate	0	-1.666666667
ptrc[c]	Putrescine	0	1.14385E-29
ptrc[e]	Putrescine	0	1.14385E-29
pyam5p[c]	Pyridoxamine 5'-phosphate	0	1
pydam[c]	Pyridoxamine	0	0
pydam[e]	Pyridoxamine	0	0
pydx[c]	Pyridoxal	0	0
pydx[e]	Pyridoxal	0	0
pydx5p[c]	Pyridoxal 5'-phosphate	0	1
pydxn[c]	Pyridoxine	0	0
pydxn[e]	Pyridoxine	0	0
pyr[c]	Pyruvate	0	1.28196E-16
pyr[e]	Pyruvate	0	1.28196E-16
r1p[c]	alpha-D-Ribose 1-phosphate	0	-1.666666667
r5p[c]	alpha-D-Ribose 5-phosphate	0	-1.666666667
ribflv[c]	Riboflavin	0	-1
ribflv[e]	Riboflavin	0	0
rnam[c]	N-Ribosylnicotinamide	0	-2.666666667
ru5p-D[c]	D-Ribulose 5-phosphate	0	-1.666666667
s7p[c]	Sedoheptulose 7-phosphate	0	-2.333333333
sbt-D[c]	D-Sorbitol	0	-2
spmd[c]	Spermidine	0	1.06396E-17
spmd[e]	Spermidine	0	1.06396E-17
sprm[c]	Spermine	0	-1.89327E-29
sprm[e]	Spermine	0	0
thm[c]	Thiamin	0	0
thm[e]	Thiamin	0	0
thmmp[c]	Thiamin monophosphate	0	0
thmmp[e]	Thiamin monophosphate	0	0
thmpp[c]	Thiamine diphosphate	0	1
thmtp[c]	Thiamin triphosphate	0	1
udp[c]	UDP	0	1

udpg[c]	UDPglucose	0	-1
udpgal[c]	UDPgalactose	0	-1
udpglcur[c]	UDP-D-glucuronate	0	-1
ump[c]	UMP	0	1
uppg3[c]	Uroporphyrinogen III	0	-3.78653E-28
urea[c]	Urea	0	0
urea[e]	Urea	0	0
uri[c]	Uridine	0	0
uri[e]	Uridine	0	0
utp[c]	UTP	0	1
xmp[c]	Xanthosine 5'-phosphate	0	-1.666666667
xu5p-D[c]	D-Xylulose 5-phosphate	0	-1.666666667
xylt[c]	Xylitol	0	-2
xylu-D[c]	D-Xylulose	0	-2
xylu-L[c]	L-Xylulose	0	-2

Exchanges affecting the objective function				
Reaction No	Reaction Names	Reaction Abb.	FBA sol when no glcn (mmol/gDW/h)	FBA sol with glcn (mmol/gDW/h)
1	3',5'-Cyclic GMP exchange	EX_35cgmp(e)	2.936	2.977
2	3-Methoxytyramine exchange	EX_3moxtyr(e)	2.936	2.977
3	4-Pyridoxate exchange	EX_4pyrdx(e)	2.936	2.977
4	5-Amino-4-oxopentanoate exchange	EX_5aop(e)	2.936	2.977
5	Acetate exchange	EX_ac(e)	2.936	2.977
6	Acetaldehyde exchange	EX_acald(e)	2.936	2.977
7	N-Acetylneuraminate exchange	EX_acnam(e)	2.936	2.977
8	Adenine exchange	EX_ade(e)	2.936	2.977
9	Adenosine exchange	EX_adn(e)	2.944	2.977
10	Adrenaline exchange	EX_adrnl(e)	2.936	2.977
11	L-Alanine exchange	EX_ala-L(e)	2.936	2.977
12	L-Arginine exchange	EX_arg-L(e)	2.936	2.977
13	L-Ascorbate exchange	EX_ascb-L(e)	2.936	2.977
14	Bilirubin monoglucuronide exchange	EX_bilglcur(e)	2.936	2.977
15	Calcium exchange	EX_ca2(e)	2.936	2.977
16	cAMP exchange	EX_camp(e)	2.936	2.977
17	Choline exchange	EX_chol(e)	2.936	2.977
18	Chloride exchange	EX_cl(e)	2.936	2.977
19	Carbon monoxide exchange	EX_co(e)	2.936	2.977
20	CO2 exchange	EX_co2(e)	2.936	2.977
21	L-Cysteine exchange	EX_cys-L(e)	2.936	2.977
22	Dehydroascorbate exchange	EX_dhdascb(e)	2.936	2.977
23	Dopamine exchange	EX_dopa(e)	2.936	2.977
24	Ethanolamine exchange	EX_etha(e)	2.936	2.977
25	Fe2+ exchange	EX_fe2(e)	2.936	2.977
26	D-Fructose exchange	EX_fru(e)	2.977	2.977
27	Fumarate exchange	EX_fum(e)	2.936	2.977
28	D-Galactose exchange	EX_gal(e)	2.977	2.977
29	D-Glucosamine exchange	EX_gam(e)	2.944	2.977
30	D-Glucose exchange	EX_glc(e)	2.977	2.977
31	L-Glutamine exchange	EX_gln-L(e)	2.936	2.977
32	5-L-Glutamyl-L-alanine exchange	EX_gluala(e)	2.936	2.977
33	Glycine exchange	EX_gly(e)	2.936	2.977
34	Glycerol exchange	EX_glyc(e)	2.936	2.977
35	Oxidized glutathione exchange	EX_gthox(e)	2.936	2.977
36	H+ exchange	EX_h(e)	2.936	2.977
37	H2O exchange	EX_h2o(e)	2.936	2.977
38	Hydrogen peroxide exchange	EX_h2o2(e)	2.936	2.977
39	Bicarbonate exchange	EX_hco3(e)	2.936	4.289
40	L-homocysteine exchange	EX_hcyst-L(e)	2.936	2.977
41	Hexadecanoate (n-C16:0) exchange	EX_hdca(e)	2.936	2.977
42	Hypoxanthine exchange	EX_hxan(e)	2.936	2.977
43	Inosine exchange	EX_ins(e)	2.944	2.977
44	K+ exchange	EX_k(e)	2.936	2.977
45	D-lactate exchange	EX_lac-D(e)	2.936	2.977
46	L-Lactate exchange	EX_lac-L(e)	2.936	2.977
47	Leukotriene A4 exchange	EX_leuktrA4(e)	2.936	2.977
48	Leukotriene B4 exchange	EX_leuktrB4(e)	2.936	2.977
49	linoleic acid (all cis C18:2) exchange	EX_lnlc(e)	2.936	2.977
50	L-Malate exchange	EX_mal-L(e)	2.936	2.977
51	D-Mannose exchange	EX_man(e)	2.977	2.977

52	Metanephrine exchange	EX_mepi(e)	2.936	2.977
53	L-Methionine exchange	EX_met-L(e)	2.936	2.977
54	Sodium exchange	EX_na1(e)	2.936	2.977
55	Nicotinate exchange	EX_nac(e)	2.936	2.977
56	Nicotinamide exchange	EX_ncam(e)	2.936	2.977
57	Ammonia exchange	EX_nh4(e)	2.936	2.977
58	L-Normetanephrine exchange	EX_normete-L(e)	2.936	2.977
59	Norepinephrine exchange	EX_nrpphr(e)	2.936	2.977
60	O2 exchange	EX_o2(e)	2.936	2.977
61	octadecenoate (n-C18:1) exchange	EX_ocdcea(e)	2.936	2.977
62	Orotate exchange	EX_orot(e)	2.936	2.977
63	L-Phenylalanine exchange	EX_phe-L(e)	2.936	2.977
64	Phosphate exchange	EX_pi(e)	2.936	2.977
65	Putrescine exchange	EX_ptrc(e)	2.936	2.977
66	Pyridoxamine exchange	EX_pydam(e)	2.936	2.977
67	Pyridoxal exchange	EX_pydx(e)	2.936	2.977
68	Pyridoxine exchange	EX_pydxn(e)	2.936	2.977
69	Pyruvate exchange	EX_pyr(e)	2.936	2.977
70	Riboflavin exchange	EX_ribflv(e)	2.936	2.977
71	Spermidine exchange	EX_spmd(e)	2.936	2.977
72	Spermine exchange	EX_sprm(e)	2.936	2.977
73	Thiamin exchange	EX_thm(e)	2.936	2.977
74	Thiamin monophosphate exchange	EX_thmmp(e)	2.936	2.977
75	Urea exchange	EX_urea(e)	2.936	2.977
76	Uridine exchange	EX_uri(e)	2.936	2.977
77	sink adprbp(c)	sink_adprbp(c)	2.936	2.977
78	sink akg(c)	sink_akg(c)	2.936	2.977
79	sink band(c)	sink_band(c)	2.936	2.977
80	sink bandmt(c)	sink_bandmt(c)	2.936	2.977
81	sink for(c)	sink_for(c)	2.936	2.977
82	sink mi1345p(c)	sink_mi1345p(c)	2.936	2.977
83	sink mi134p(c)	sink_mi134p(c)	2.936	2.977
84	sink mi145p(c)	sink_mi145p(c)	2.936	2.977
85	sink mi14p(c)	sink_mi14p(c)	2.936	2.977
86	sink pchol hs 16 0 16 0(c)	sink_pchol_hs_16_0_16_0(c)	2.936	2.977
87	sink pchol hs 16 0 18 1(c)	sink_pchol_hs_16_0_18_1(c)	2.936	2.977
88	sink pchol hs 16 0 18 2(c)	sink_pchol_hs_16_0_18_2(c)	2.936	2.977
89	sink pchol hs 18 1 18 1(c)	sink_pchol_hs_18_1_18_1(c)	2.936	2.977
90	sink pchol hs 18 1 18 2(c)	sink_pchol_hs_18_1_18_2(c)	2.936	2.977
91	sink pchol hs 18 2 16 0(c)	sink_pchol_hs_18_2_16_0(c)	2.936	2.977
92	sink pchol hs 18 2 18 1(c)	sink_pchol_hs_18_2_18_1(c)	2.936	2.977
93	sink pe hs 16 0 16 0(c)	sink_pe_hs_16_0_16_0(c)	2.936	2.977
94	sink pe hs 16 0 18 1(c)	sink_pe_hs_16_0_18_1(c)	2.936	2.977
95	sink pe hs 16 0 18 2(c)	sink_pe_hs_16_0_18_2(c)	2.936	2.977
96	sink pe hs 18 1 18 1(c)	sink_pe_hs_18_1_18_1(c)	2.936	2.977
97	sink pe hs 18 1 18 2(c)	sink_pe_hs_18_1_18_2(c)	2.936	2.977
98	sink pe hs 18 2 16 0(c)	sink_pe_hs_18_2_16_0(c)	2.936	2.977
99	sink pe hs 18 2 18 1(c)	sink_pe_hs_18_2_18_1(c)	2.936	2.977
201	demand NADH	DM_nadh	2.936	2.977
470	EX_glcn(e)	EX_glcn(e)	2.977	2.977

Paper III

FEBS Letters 589 (2015) 3548–3555

journal homepage: www.FEBSLetters.org

Kinetic analysis of gluconate phosphorylation by human gluconokinase using isothermal titration calorimetry

Neha Rohatgi [a,b], Steinn Guðmundsson [a], Óttar Rolfsson [a,b,*]

[a] Center for Systems Biology, University of Iceland, Sturlugata 8, 101 Reykjavik, Iceland
[b] University of Iceland Biomedical Center, Laeknagardur, 101 Reykjavik, Iceland

ARTICLE INFO

Article history:
Received 15 July 2015
Revised 15 October 2015
Accepted 16 October 2015
Available online 23 October 2015

Edited by Judit Ovádi

Keywords:
Enzyme kinetics
Isothermal titration calorimetry
Gluconate (Glcn)
Human gluconokinase (hGntK, IdnK)
Human metabolism

ABSTRACT

Gluconate is a commonly encountered nutrient, which is degraded by the enzyme gluconokinase to generate 6-phosphogluconate. Here we used isothermal titration calorimetry to study the properties of this reaction. ΔH, K_M and k_{cat} are reported along with substrate binding data. We propose that the reaction follows a ternary complex mechanism, with ATP binding first. The reaction is inhibited by gluconate, as it binds to an Enzyme–ADP complex forming a dead-end complex. The study exemplifies that ITC can be used to determine mechanisms of enzyme catalyzed reactions, for which it is currently not commonly applied.

1. Introduction

Gluconate (Glcn) is a naturally occurring carboxylic acid that is found abundantly in various fruits, vegetables and dairy products as well as being added to processed foods and pharmaceuticals due to its refreshing taste. Gluconate has also found use in formulation chemistry, both in industry and in the health sector on account of its metal chelating properties. In the clinic, calcium gluconate is used for treating calcium deficiency, hydrofluoric acid burns and as dietary supplements in the form of zinc gluconate and iron gluconate derivatives [1,2]. Despite widespread use of the compound across diverse sectors and its presence in human bio-fluids [3,4] the details of gluconate production and consumption in humans remain relatively unexplored as highlighted in a recent metabolic network gap analysis of human metabolism [5].

Phosphorylated gluconate is an intermediate of the pentose phosphate pathway. The oxidation of 6-phosphogluconate contributes to NADPH formation in the cytosol and thus to both anabolic reactions and the recycling of glutathione, ultimately combating oxidative stress [6,7]. Metabolism of gluconate is likely to follow this pathway given that consumed gluconate is absorbed and subsequently phosphorylated (Fig. 1). Indeed, isoform I of the human gene C9orf103 was recently shown to encode gluconokinase activity [5]. Through a computational metabolic modeling approach, the metabolic contribution of gluconate has also been estimated to have broad impact on cellular metabolism in accordance with its contribution to NADPH formation [8]. It is likely that gluconate follows this metabolic route in humans. Early biochemical investigations into the fate of gluconate added to rat liver perfusions strengthen this hypothesis. These studies showed that gluconate is internalized but is metabolized differently as compared to glucose [9]. In addition, gluconate metabolism in prokaryotes and lower eukaryotes is very well characterized where it is metabolized following phosphorylation by gluconokinase [10]. The biological conditions under which human gluconokinase (hGntK) is active have not been deduced. Analysis of publically accessible gene expression profiles indicate that these are likely context specific with the gene primarily expressed in brain, lymph node, kidney and hepatic tissue. Despite incomplete understanding of its metabolic context, human gluconokinase activity is encoded within the human genome and this enzyme is likely to play a pivotal role in the metabolism of gluconate in humans.

Gluconokinase belongs to the family of FGGY carbohydrate domain containing kinases [11] of which gluconokinase from *Escherichia coli* is one of the best described [12–14]. We recently

Author contributions: N.R. designed the study, carried out the experiments, performed the data analysis and wrote the paper, S.G. performed data analysis and O.R. designed the study, carried out experiments and wrote the paper.

* Corresponding author at: Center for Systems Biology, University of Iceland, Sturlugata 8, 101 Reykjavik, Iceland.
E-mail address: ottarr@hi.is (Ó. Rolfsson).

http://dx.doi.org/10.1016/j.febslet.2015.10.024
0014-5793/

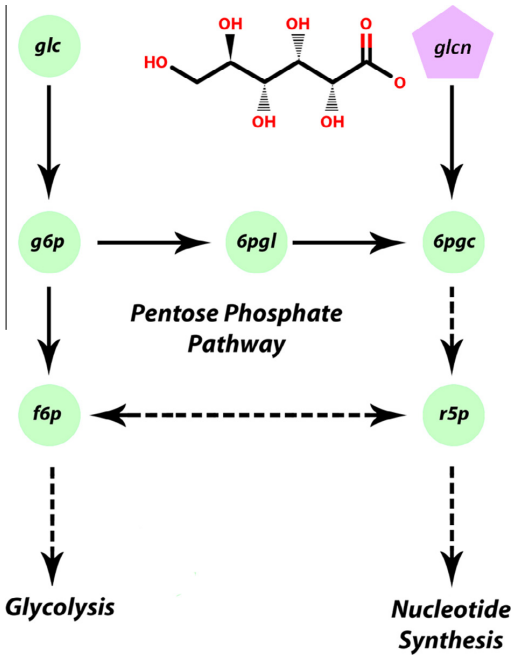

Fig. 1. Overview of the gluconate metabolism in humans. Gluconate is phosphorylated by gluconokinase (EC 2.7.1.12). 6-Phosphogluconate can then be degraded through the pentose phosphate pathway although the biological context in which this occurs in humans has not been demonstrated.

reported the biochemical characterization of a recombinantly produced isoform I of human gluconokinase (hGntK) encoded by the gene IDNK (Uniprot id: Q5T6J7). Human gluconokinase is a dimer, each monomer weighing 23.33kDa, that catalyzes ATP dependent phosphorylation of gluconate to 6-phosphogluconate. The enzyme was shown to be similar in secondary structure to its *E. coli* counterpart and was specific towards the phosphorylation of gluconate. The kinetics of the enzymatic reaction was characterized spectrophotometrically by coupling 6-phosphogluconate formation with consumption by 6-phosphogluconate dehydrogenase.

Here we report the kinetic characterization of the gluconokinase catalyzed reaction using isothermal titration calorimetry (ITC). The kinetic and thermodynamic characterization of metabolic enzymes has recently gained interest from the computational metabolic modeling community where kinetic parameters are required for models that accurately capture genotype/phenotype relationships [15]. Employing ITC we were able to study the reaction without any coupling of the reaction or tagging of the substrates. ITC was used to determine kinetic parameters of the reaction under varying concentrations of each substrate. Kinetic data was fit to equations descriptive of relevant reaction models to deduce the reaction mechanism. The results suggest that the gluconokinase reaction follows a ternary complex mechanism and is inhibited at high concentrations of gluconate.

2. Materials and methods

Recombinant human gluconokinase was prepared as described previously [8]. Protein concentration was estimated using Beer–Lambert's Law from measured absorbance at 280 nm. Molar absorption coefficient was calculated using Tyr, Trp and Cys content of the protein [16]. MicroCal iTC200 (MicroCal, Northampton, MA, USA) was used to monitor enzymatic activity directly by detecting heat flow during the reaction at 25 °C. All the experiments were performed in a kinase assay buffer composed of 100 mM sodium phosphate, 40 mM NaCl, 2.5 mM $MgCl_2$ (unless otherwise stated) and at pH 7.2. All enzyme and substrate solutions were prepared in this buffer, in order to minimize the heat of dilution during injection. The reaction cell was filled with 200 μL of the reaction mixture, with stirring speed 1000 rpm and each reaction had an initial delay of 60 s. All the experiments were performed in triplicates. These assays were based on the principles of implementations of ITC described by Wiseman et al. [17]. The raw ITC data was analyzed using the MicroCal iTC200 Origin Software package and MATLAB (Mathworks, Natick, MA, USA) was used for fitting and plotting the data.

2.1. Determination of enthalpy change (ΔH)

We measured the enthalpy using the multiple injection ITC method [18,19]. The experiment was carried out by titrating 0.7 μL of 20 mM Glcn into the reaction cell containing 33.5 nM hGntK and 1 mM ATP, at 40 min intervals. A total of 20 injections were done which continued for 13 h. The enthalpy of the reaction (ΔH) was then determined by dividing total heat change in each injection by the amount of substrate in the cell after the injection.

$$\Delta H = \frac{1}{[S]_{\text{Total}} \cdot V} \int_{t=0}^{t=\infty} \frac{dQ(t)}{dt} dt \tag{1}$$

where $[S]_{\text{Total}}$ is the concentration of the limiting substrate, V is the volume of the reaction mixture and dQ is the heat change measured at time t. The determination of ΔH and the data fitting was done in MicroCal iTC200 Origin Software package for experiments performed at 25 and 37 °C. As after a few injections product concentration increased significantly and started affecting the rate, average of first few ΔH values was calculated [18]. For blanks, the substrate was injected in cell containing reaction mixtures without the enzyme and the blanks were then subtracted.

2.2. Kinetic experiments to study mechanism of reaction

ITC enables the determination of enzymatic parameters of the reaction under study as the rate of the reaction is proportional to the measured heat flow, according to:

$$\frac{dQ}{dt} = \frac{d[P]}{dt} \cdot V \cdot \Delta H \tag{2}$$

In the experimental conditions where one substrate is at a saturating concentration, the enzymatic reaction can be described in terms of first-order kinetics in relation to the other substrate. The heat flow is given by:

$$\frac{dQ}{dt} = \Delta H V k [S]_0 \exp(-kt) \tag{3}$$

where, k is the rate constant, and $[S]_0$ is the initial concentration of the limiting substrate, ΔH is the experimentally determined molar enthalpy for the reaction.

Kinetic parameters were determined under pseudo steady-state conditions [20]. The sample cell was loaded with a solution containing hGntK (67 nM) and a fixed concentration of Glcn. Sixteen injections of 1.5 μL (20 mM) ATP were done every 60 s at 25 °C. The saturating concentration of the fixed substrate is important for the estimation of kinetic parameters but for determining the mechanism, the fixed substrate has to vary over a broader range, from sub-saturated to saturated concentrations. Thus for these experiments, Glcn was fixed from 0.5 mM to 12.5 mM. As the concentration of ATP in the cell increases from 0.15 mM to 2.4 mM, the

concentration of $MgCl_2$ was maintained at 6 mM to maintain a steady amount of $MgATP^{2-}$. All experiments were done in triplicates or more. Analogous experiments were done for Glcn (20 mM), where 1.2 μL of Glcn was injected (16 injections) into the reaction solution containing 67 nM hGntK and 0.5 mM of fixed ATP concentration. The experiments for the other fixed ATP concentration values (1–7.5 mM) were performed at an enzyme concentration of 53.6 nM. The enzyme concentration in these experiments was reduced in order to attain a pseudo steady state condition after every injection. The $MgCl_2$ in these experiments was maintained at 5 mM excess of ATP. Enzyme blanks were carried out for each experiment. Reaction rates were obtained by dividing the measured baseline heat flow by the ΔH of the reaction (evaluated as described above). Primary plots for the kinetic data were plotted and analyzed in Origin.

2.3. Substrate binding

Substrate binding experiments were performed to add more experimental support to the kinetic mechanism. For this, 36 injections of 1 μL of ATP (1 mM) were done every 120 s, in a cell containing 52.3 μM of hGntK. Similarly for Glcn, 36 injections of 1 μL (1 mM) were done every 120 s, in a cell containing 52.3 μM of hGntK. The basic principle behind these experiments is explained in detail in the book "Methods in cell biology" [21]. The heat change measured after every injection is proportional to the level of binding of the substrate to the enzyme. "Single Set of Identical Sites" model in the MicroCal iTC200 Origin Software was used to calculate change in enthalpy, change in entropy during binding and the binding constant. Experiments without enzyme in the cell were performed in order to get the blank values.

MicroScale Thermophoresis (MST) experiments were carried out with fluorescently labeled hGntK. MST is based on the principle that molecules move within a temperature gradient based on their charge, size and hydration shell, a property called thermophoresis. The movement is traced by measuring fluorescence. A fluorescent label (NT-647) was covalently attached to the protein using NHS coupling using a Monolith NT Protein Labeling Kit (NanoTemper Technologies GmbH, Munich, Germany). Labeled hGntK was kept constant at 10 nM, while the concentration of the non-labeled ATP was varied between 3 mM and 0.09 μM. The assay was performed in an assay buffer with 0.05% Tween-20 and prepared in protein low-binding tubes. After a short incubation, the samples were loaded into MST NT.115 hydrophilic glass capillaries and the MST analysis was performed using the Monolith NT.115. Similar experiments were performed for measuring the binding of Glcn, where the concentration of the non-labeled Glcn was varied between 50 mM and 1.5 μM.

2.4. Data fitting to estimate the kinetic parameters

In order to calculate the kinetic parameters, reaction rates obtained from the kinetic experiments were fitted to relevant equations, using a non-linear least-squares procedure in MATLAB. As substrate inhibition by Glcn was observed, the data was fitted to a compulsory-order ternary complex mechanism with substrate inhibition equation [Eq. (4)] and substituted enzyme mechanism with substrate inhibition [Eq. (5)].

$$\text{Rate } (v_i) = \frac{k_{cat}E_0[A][G]}{K_{iA}K_{mG} + K_{mG}[A] + K_{mA}[G] + [A][G]\left(1 + \frac{[G]}{K_{siG}}\right)} \quad (4)$$

$$\text{Rate } (v_i) = \frac{k_{cat}E_0[A][G]}{K_{mG}[A] + K_{mA}[G]\left(1 + \frac{[G]}{K_{siG}}\right) + [A][G]} \quad (5)$$

In the above equations v_i (mM/s) is the reaction rate, k_{cat} is turnover number, E_0 is the initial enzyme concentration, $[A]$ and $[G]$ (mM) are concentrations of ATP and Glcn respectively, K_{mA} and K_{mG} (mM) are the Michaelis–Menten constants for ATP and Glcn respectively, K_{iA} (mM) is the dissociation constant of Enzyme–ATP (this was determined experimentally), and K_{siG} (mM) is a constant that defines the strength of inhibition. The equations are taken from Fundamentals of Enzyme kinetics [22]. The model having the smallest residual sum of squares is then selected as best fit. When analysis of the residuals does not reveal a significant difference between models, the model with the fewest number of parameters is chosen.

3. Results

3.1. Determination of ΔH at 25 and 37 °C

The amount of heat exchanged by the reaction system with the surroundings over time was measured using ITC [21]. A prerequisite for determining kinetic parameters using ITC was the determination of reaction enthalpy (ΔH). This was required in order to relate heat change, the parameter measured by ITC, to product/-substrate concentration, allowing the reaction rate to be calculated through changes in concentration over time [Eq. (1)]. The heat flow (μcal/s) was measured as a function of time, following multiple injections of Glcn into the calorimeter cell containing the reaction mixture as described in the materials and methods section. Fig. 2 shows a thermogram resulting from the injections of 0.7 μL of 20 mM Glcn, into the cell containing ATP (1 mM) and 33.5 nM of hGntK. Each injection resulted in an exothermic reaction as observed from a negative value of the heat flow. After complete consumption of Glcn, the heat flow returned to the baseline level, indicating that the substrate had been used up. The enthalpy change (ΔH) of the reaction was calculated under these experimental conditions, with the Origin Software. The average enthalpy change of first seven injections was -8.04 ± 1.09 kcal/mol at 25 °C. In similar manner, the ΔH of hGntK was also determined at 37 °C, a physiologically more realistic temperature. ΔH at 37 °C was measured to be -8.22 ± 0.15 kcal/mol, by injecting 1 μL of Glcn (20 mM) into the cell containing 1 mM ATP and 33.5 nM hGntK.

3.2. Kinetics of gluconate phosphorylation

In order to determine the rate of Glcn phosphorylation by hGntK, the heat flow was measured as a function of time under pseudo steady-state conditions. In order to maintain pseudo steady-state conditions in ITC, a large amount of the substrate is injected into the reaction cell containing much lower concentration of the enzyme, thus there is negligible depletion in substrate concentration and the reaction proceeds at a steady rate. This was achieved using a multiple injection method where either substrate (ATP or Glcn) at known concentrations was titrated into the reaction mixture at time intervals that prevented the titrated substrate being totally consumed. Fig. 3A shows the thermograms resulting from injections of ATP into the sample cell containing hGntK and Glcn at fixed concentrations, ranging from 0.5 to 12.5 mM. Upon titration with ATP, heat was initially consumed by the reaction mixture (heat of dilution), followed immediately by a drop in thermal power, with respect to the baseline, indicating heat released by the reaction mixture. The output then became steady, corresponding to the point at which the hGntK catalytic rate is at its maximum, up until additional ATP was titrated into the cell and a new rate maximum was achieved, as defined by altered substrate concentrations. Human GntK reaction rates following each injection were calculated from Eq. (2). At Glcn a

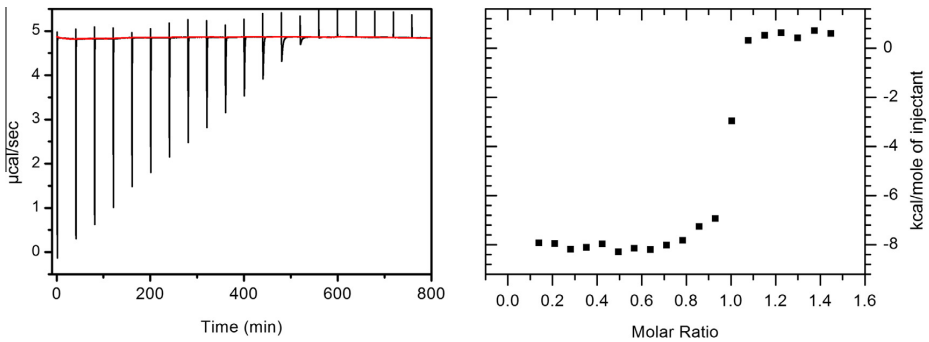

Fig. 2. Micro-calorimetric titration isotherm for determination of enthalpy of the hGntK reaction. Injections of 0.7 µL gluconate (20 mM) were done every 40 min, into a cell containing hGntK (33.5 nM) and an excess of ATP (1 mM). Each peak in the left graph corresponds to the heat released on addition of gluconate to the reaction cell. The total heat accumulated up to a particular injection is normalized to the total gluconate concentration at that step and is plotted against the ratio of the total gluconate concentration at that step to the total ATP concentration. This yields the titration curve shown in the right graph.

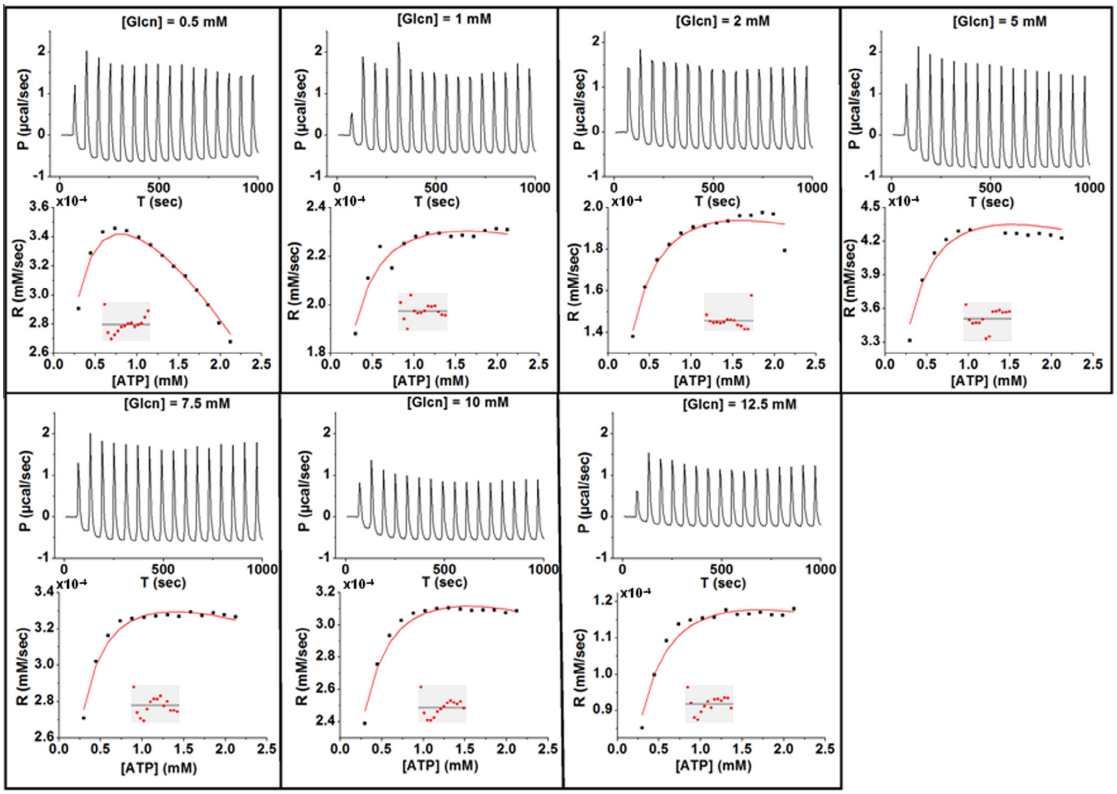

Fig. 3A. Determination of the kinetic parameters for ATP. The graphs on the top of each panel show the raw ITC data, where heat flow is measured while maintaining pseudo steady-state conditions. Injections of 1.5 µL of ATP (20 mM) were done every 60 s, in a cell containing 67 nM of hGntK and varying concentrations of Glcn. The lower graphs show the measured rate vs. substrate concentration at 25 °C. Red lines indicate data fitted with ternary complex mechanism with second substrate inhibition [Eq. (4)]. Inset in these graphs show the residuals from the fitting procedure.

concentration of 0.5 mM, the rate of reaction decreased after a few injections of ATP. This was caused by depletion of Glcn in the reaction mixture. At all other Glcn concentrations, this effect was not observed and the reaction rate increased until maximum rate was achieved.

Analogous experiments were done to determine the kinetics of Glcn. Glcn was injected into the sample cell containing a solution of hGntK with a constant ATP concentration (Fig. 3B). Upon titration of Glcn, we observed smaller injection peaks associated with substrate dilution than compared to ATP injection. A subsequent

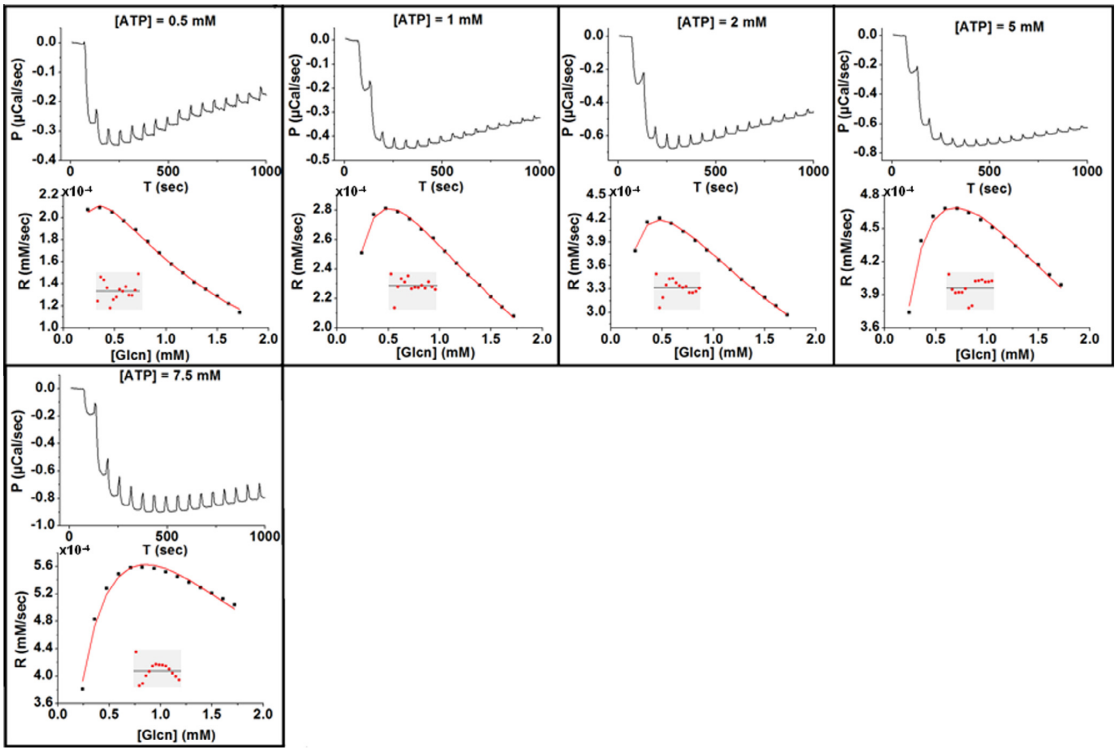

Fig. 3B. Determination of the kinetic parameters for gluconate. The top graphs in each panel show the enzyme assay where the reaction mixture had varying concentrations of ATP (0.5–7.5 mM). Sixteen injections of 1.2 µL Glcn (20 mM) were done every 60 s. In contrast with ATP, high Glcn concentrations slowed down the reaction leading to an apparent inhibition by excess substrate. This is seen in the lower graphs in each panel. Red lines are fitted data with ternary complex mechanism taking inhibition by gluconate into account [Eq. (4)]. Each graph has inset showing the residuals.

drop in thermal power indicative of an increase in reaction rate followed immediately thereafter, but after only a few injections of Glcn, the rate of reaction was reduced. This reduction in reaction rate was observed at all constant ATP concentrations (Fig. 3B, lower panels) as opposed to when Glcn was kept constant (Fig. 3A, lower panels) and was indicative of reaction inhibition due to excess Glcn.

3.3. Mechanism of Glcn phosphorylation by hGntK

Bimolecular reactions can be catalyzed through two distinct molecular mechanisms. We used the substrate inhibition observed to differentiate between a ternary-complex mechanism and a substituted-enzyme mechanism. Thus there was no need to do product inhibition studies in order to differentiate between different mechanisms [22]. Hanes-Woolf plots were generated, where the ratio of substrate concentration to reaction rate $[S]/V$ is plotted against substrate concentration $[S]$. Fig. 4A shows that for ATP injections at variable Glcn concentration, a linear trend is observed with lines having no common point of intersection. The Hanes-Woolf plot of kinetic data series for Glcn injections in Fig. 4B shows non-linear curves that all intersect at a single point. These figures confirm that the reaction is inhibited by Glcn [21]. Hanes-Woolf plots for both the substrates together suggest a ternary complex mechanism with ATP binding first and inhibited by Glcn. For Glcn to inhibit the reaction following a ternary complex mechanism it will have to bind to the ADP–Enzyme complex forming a dead-end ADP–Enzyme–Glcn complex. Intrinsically, this also means that 6-phosphogluconate is the first product to leave.

3.4. Substrate binding

In order to add support to our hypothesis about the mechanism of the reaction we performed substrate-binding experiments. Employing ITC, ATP and Glcn were injected into the cell containing hGntK at a fixed concentration. The heat changes during binding were measured for each substrate and the binding constants were calculated. These experiments indicated that ATP binds to the free enzyme but due to low heat of interaction these experiments were not accurate enough for K_d measurements. Binding of Glcn to the free enzyme could not be confirmed using ITC experiments. Thus, in order to obtain an accurate measure of K_d, MST experiments were done.

In MST experiments the movement of fluorescently labeled enzyme was measured with ATP and Glcn. The K_d value for ATP measured by MST was 90.5 µM ± 9.5 µM. The binding for Glcn was again too low to obtain an accurate estimate be measured accurately. K_d for Glcn was estimated nearly equal to 1.6 ± 0.3 mM. This shows that Glcn has very low affinity for the free enzyme in absence of ATP. Fig. 5(A) shows the thermogram of ATP from ITC and Fig. 5(B) shows the graph of concentrations versus normalized fluorescence from MST. Figures for Glcn are not provided because the binding was too low. These results support the hypothesis that the reaction adheres to an ordered binding of substrates, with ATP binding first.

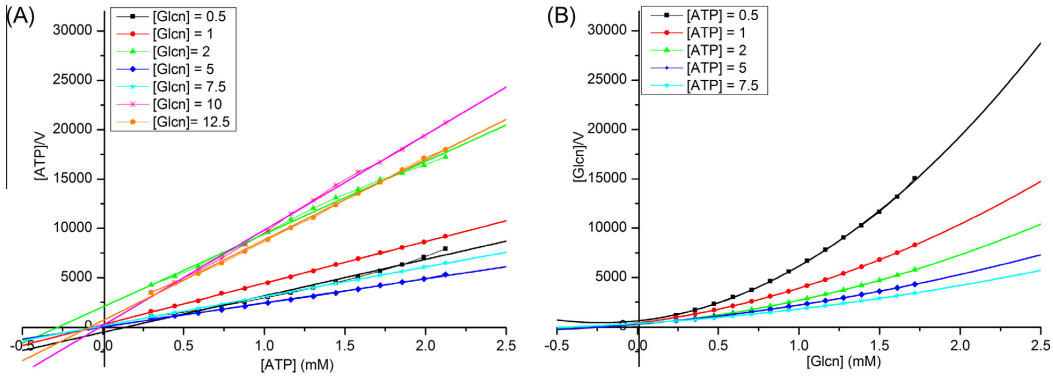

Fig. 4. Hanes-Woolf plots of hGntK catalyzed reaction at altering Glcn and ATP concentrations. (A) For ATP at fixed concentrations of Glcn 0.5 mM (black; square), Glcn 1 mM (red; circle), 2 mM (green; triangle), 5 mM (blue; diamond), 7.5 mM (cyan; star), 10 mM (magenta; star), 12.5 mM (orange; pentagon). The curves are linear and do not have a common point of intersection. (B) Analogous plots for Glcn at fixed concentrations of ATP: 0.5 mM (black; square), 7.5 mM (cyan; star), 10 mM (magenta; star). The curves here are parabolic in contrast to the first graph and have a single intersection point. These two graphs together, point towards a ternary complex mechanism, with Glcn inhibition.

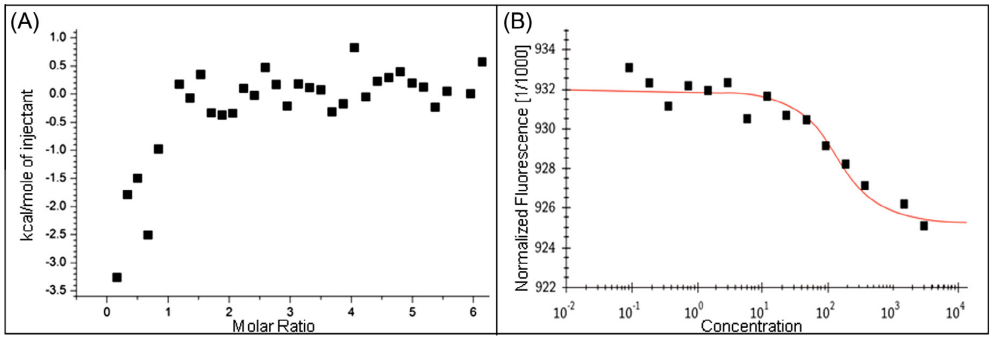

Fig. 5. (A) Binding of ATP and hGntK. Left graph is a thermogram showing the binding of ATP to the enzyme. 36 injections of 1 μL of ATP (1 mM) were done every 120 s, into a cell containing 52.3 μM of hGntK (4 outlier data points were removed) (B) Binding of ATP and hGntK (MST). Concentrations on the horizontal axis are plotted in μM, with normalized fluorescence on the vertical axis. A K_d of 90.5 μM ± 9.5 μM was determined for this interaction. For Glcn binding to hGntK in the absence of ATP, binding detected was too low.

Table 1
Kinetic parameters for ATP. The parameter values are obtained by fitting measurements to Eq. (4) (Fig. 3A). The values listed are average ± standard deviation from three replicates.

	k_{cat} (s^{-1})	K_MA (mM)	Residual error
[Glcn] = 0.5 mM	14.95 ± 9.28	0.16 ± 0.04	0.002109
[Glcn] = 1 mM	9.75 ± 1.65	0.28 ± 0.11	0.000333
[Glcn] = 2 mM	8.95 ± 2.78	0.89 ± 0.80	0.000351
[Glcn] = 5 mM	9.35 ± 1.46	0.12 ± 0.01	0.003564
[Glcn] = 7.5 mM	9.17 ± 3.78	0.11 ± 0.02	0.000681
[Glcn] = 10 mM	5.47 ± 0.39	0.20 ± 0.07	0.000466
[Glcn] = 12.5 mM	6.38 ± 2.02	0.30 ± 0.16	0.001012

Table 2
Kinetic parameters for Glcn. The parameter values are obtained by fitting measurements to Eq. (4) (Fig. 3B). The values listed are average ± standard deviation from three replicates.

	k_{cat} (s^{-1})	K_MG (mM)	K_{si} (mM)	Residual error
[ATP] = 0.5 mM	15.08 ± 3.60	0.33 ± 0.09	0.38 ± 0.13	0.000082
[ATP] = 1 mM	15.47 ± 6.38	0.20 ± 0.02	1.15 ± 0.45	0.000049
[ATP] = 2 mM	14.69 ± 2.14	0.16 ± 0.02	1.52 ± 0.23	0.000116
[ATP] = 5 mM	15.64 ± 1.38	0.22 ± 0.02	2.85 ± 0.55	0.000781
[ATP] = 7.5 mM	16.01 ± 4.51	0.34 ± 0.03	2.30 ± 0.62	0.000766

3.5. Data fitting to calculate kinetic parameters (K_M and k_{cat})

In order to calculate the kinetic parameters, the data was fitted to equations describing ternary complex and substituted enzyme complex reaction mechanisms [Eqs. (4) and (5)]. By comparing the residual errors and parameter estimates it was concluded that the data better corresponded to a compulsory-order ternary complex mechanism with substrate inhibition [Eq. (4)]. This was also supported by Hanes-Woolf plots of the data. The estimated kinetic parameters are shown in Tables 1 and 2. The kinetic parameters at sub-saturated concentrations are not accurate but just an estimate as explained in materials and methods. These experiments were done to get the mechanism. As seen in Table 1, k_{cat} decreases with increasing constant Glcn when ATP is being injected into the cell. On the other hand with ATP being kept fixed at increasing levels, it remains un-changed when Glcn is being injected, as seen in Table 2. We also observed that K_{si}, which is a constant that defines the strength of inhibition by Glcn, increases with increasing ATP. Combined, this further supports inhibition by Glcn.

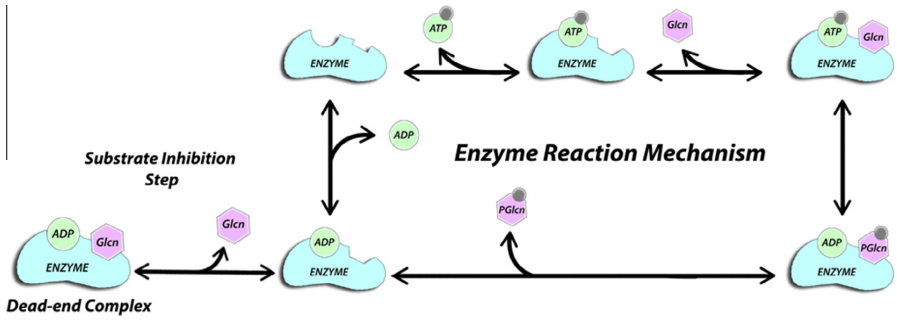

Fig. 6. Proposed mechanism of hGntK catalysis (start from top left). The reaction follows a compulsory-order ternary-complex mechanism, with ATP binding first. Glcn then binds to form 6-pglcn. Glcn also binds to the Enzyme–ADP complex to form a non-productive dead-end complex, which results in reduction of the reaction rate.

4. Discussion

Determining kinetic and thermodynamic properties of enzyme catalyzed reactions using ITC is fairly common but to the best of our knowledge, it has never been utilized to understand kinetics of a reaction beyond Michaelis–Menten mechanism of reaction. Here we have demonstrated that ITC can be used to get a complete understanding of kinetic properties of an enzyme catalyzed reaction, including the mechanism of reaction.

Determination of the change in enthalpy was a prerequisite for the determination of hGntK kinetic parameters with ITC [21]. In Fig. 2 the isotherm shows that the reaction peaks were not consistent in shape which indicates product inhibition. Therefore the average of first seven injections where the inhibition was not significant was used to estimate ΔH for fitting the kinetic data [18]. The ΔH of the reaction at 25 °C and 37 °C were indicative of an exothermic reaction as expected accompanying the hydrolysis of ATP. The enthalpy change observed at 37 °C was slightly higher than the enthalpy change at 25 °C. The measured enthalpy change was nearly −8 kcal/mol, which is similar to reactions catalyzed by other small molecule phosphotransferases such as yeast hexokinase (−10.75 to −12.18 kcal/mol) [23], serine/threonine phosphatase (−8.7 kcal/mol) and Ap4A hydrolase (−8.6 kcal/mol) [18] whose reaction enthalpies have been determined by ITC.

The mechanism of the enzyme catalyzed reaction was determined to be a compulsory-ordered ternary complex mechanism. A Hanes-Woolf plot for Glcn revealed that Glcn inhibited the reaction, as the plots were parabolic. Similar plots for ATP were straight lines that had no common point of intersection. These two graphs together are typically seen when reactions follows compulsory-ordered ternary complex mechanism and are inhibited by the second substrate, in this case Glcn [21]. We performed substrate-binding experiments to add more experimental support to the sequential binding kinetic mechanism. As the heat of interaction is too low in order to obtain an accurate measure of K_d we confirmed this data with additional experiments in microscale thermophoresis. Data from ITC and MST show that Glcn has very low to negligible binding to the free enzyme in the absence of ATP. These results confirm that the reaction likely adheres to a ternary complex mechanism with ATP binding first.

A structural study of GntK in *E. coli* revealed that the ATP binding site is accessible in the absence of Glcn, whereas, Glcn cannot bind in absence of ATP [14]. Collectively all this data serves to confirm the previously proposed structural similarity between human and *E. coli* GntK and furthermore that the catalytic mechanism of these two enzymes is similar, where ATP binding induces a conformational change required to allow gluconate to bind. As Glcn inhibits the reaction, it implies Glcn also binds to the ADP–Enzyme complex forming a non-productive complex. This suggests that 6-phosphogluconate is the first product to leave. Fig. 6 shows the proposed mechanism of the reaction. Gluconokinase from *Pseudomonad* and *Schizosaccharomyces pombe* both have been reported to follow ternary complex mechanism [24,25]. Additionally, *S. pombe* gluconokinase was reported to form E-ADP-Gluconate complex meaning it also has substrate inhibition [26]. However, while *S. pombe* gluconokinase was reported to have random order of substrate binding, our results indicate that human gluconokinase has sequential binding of substrates, by substrate binding studies.

Kinetic data for the enzyme under varying substrate concentrations was fitted Eqs. (4) and (5) to get more evidence for the predicted model and to calculate the kinetic parameters. The parameter estimates and residual analysis from the data fitting suggested that the data fitted better to Eq. (4), which represents compulsory-order ternary-complex mechanism. The K_M for ATP, as calculated from data fitting, lies in the range 0.1 to 0.3 mM at varying concentrations of Glcn. Although when Glcn is 2 mM, there is a large error in the parameter estimates. The K_M of Glcn is in the range 0.2 to 0.3 mM. The values of K_M's of substrates for the structurally similar FGGY carbohydrate kinases lie in the range of 0.1 to 0.3 mM at 37 °C although with exceptions, the K_M for L-fuculokinase is for example 1.4 mM. The value of K_M of ATP and Glcn for *E. coli* GntK is reported to be 0.123 mM and 0.04 mM respectively at 25 °C. Earlier we reported kinetic parameters of hGntK using spectrophotometric assays. The K_M for ATP in previous study was calculated to be 0.34 ± 0.01 mM and k_{cat} to be $9.5 \pm 0.5\ s^{-1}$ at a Glcn concentration 1 mM. This is comparable to K_M and k_{cat} in this study at Glcn 1 mM, the values for which are 0.28 ± 0.11 mM and $9.75 \pm 1.65\ s^{-1}$. For Glcn however, the data do not correspond to our earlier study as the range of Glcn concentrations tested earlier was not high enough to detect substrate inhibition. The parameters for Glcn are therefore not comparable [8].

Holistic approaches to modeling the metabolic states of cells are rapidly moving from static stoichiometric models of metabolism to dynamic kinetic models. Computational biologists have expressed a shortage in detailed biochemical data for organisms of interest required to build context specific dynamic metabolic models required to explain complex genotype phenotype relationships [26]. In this respect elucidating the kinetic parameters of enzymes has recently gained increased importance and attention because the descriptive and predictive capabilities of these models are dependent upon accurate biochemical information [27,28]. Spectroscopic techniques determine kinetic parameters, with the need to couple the enzyme or labeling the substrate. This is not required in ITC. Thus isothermal calorimetry has the advantage of determining enzymatic activity and thermodynamic parameters directly

and simultaneously [29]. Knowledge of these parameters is the key to understanding bioenergetics of metabolism and is used increasingly to compute metabolic flux phenotypes [30,31]. Here we have reported the kinetic and mechanism of reaction of isoform I of hGntK encoded by the gene IDNK that was recently highlighted to be incompletely characterized in a metabolic systems analysis of human metabolic reactions.

Acknowledgements

This study was funded by an ERC advanced grant number: 232816 and RANNIS grant number: 130591-053. The authors would like to thank Bjarni Asgeirsson at the Icelandic Science Institute for help with ITC and Athel-Cornish Bowden for his help and support in data analysis. The authors would also like thank the reviewers for critically reading the manuscript and providing helpful comments.

References

[1] Ramachandran, S., Fontanille, P., Pandey, A. and Larroche, C. (2006) Gluconic acid: properties, applications and microbial production. Food Technol. Biotechnol. 44 (2), 185–195.
[2] Singh, O.V. and Kumar, R. (2007) Biotechnological production of gluconic acid: future implications. Appl. Microbiol. Biotechnol. 75 (4), 713–722.
[3] Psychogios, N., Hau, D.D., Peng, J., Guo, A.C., Mandal, R., Bouatra, S., et al. (2011) The human serum metabolome. PLoS One 6 (2), e16957.
[4] Bouatra, S., Aziat, F., Mandal, R., Guo, A.C., Wilson, M.R., Knox, C., et al. (2013) The human urine metabolome. PLoS One 8 (9), e73076.
[5] Ottar, R., Giuseppe, P., Manuela, M., Bernhard, O.P. and Ines, T. (2013) Inferring the metabolism of human orphan metabolites from their metabolic network context affirms human gluconokinase activity. Biochem. J. 449 (2), 427–435.
[6] Salvemini, F., Franzé, A., Iervolino, A., Filosa, S., Salzano, S. and Ursini, M.V. (1999) Enhanced glutathione levels and oxidoresistance mediated by increased glucose-6-phosphate dehydrogenase expression. J. Biol. Chem. 274 (5), 2750–2757.
[7] Riganti, C., Gazzano, E., Polimeni, M., Aldieri, E. and Ghigo, D. (2012) The pentose phosphate pathway: an antioxidant defense and a crossroad in tumor cell fate. Free Radical Biol. Med. 53 (3), 421–436.
[8] Rohatgi, N., Nielsen, T.K., Bjørn, S.P., Axelsson, I., Paglia, G., Voldborg, B.G., et al. (2014) Biochemical characterization of human gluconokinase and the proposed metabolic impact of gluconic acid as determined by constraint based metabolic network analysis. PLoS One.
[9] Stetten, M.R. and Topper, Y.J. (1953) Pathways from gluconic acid to glucose in vivo. J. Biol. Chem. 203 (2), 653–664.
[10] Peekhaus, N. and Conway, T. (1998) What's for dinner?: Entner–Doudoroff metabolism in *Escherichia coli*. J. Bacteriol. 180 (14), 3495–3502.
[11] Zhang, Y., Zagnitko, O., Rodionova, I., Osterman, A. and Godzik, A. (2011) The FGGY carbohydrate kinase family: insights into the evolution of functional specificities. PLoS Comput. Biol..
[12] Tong, S., Porco, A., Isturiz, T. and Conway, T. (1996) Cloning and molecular genetic characterization of the Escherichia coli gntR, gntK, and gntU genes of GntI, the main system for gluconate metabolism. J. Bacteriol. 178 (11), 3260–3269.
[13] Kraft, L., Sprenger, G.A. and Lindqvist, Y. (2001) Crystallization and preliminary X-ray crystallographic studies of recombinant thermoresistant gluconate kinase GntK from *Escherichia coli*. Acta Crystallogr. D Biol. Crystallogr. 57 (8), 1159–1161.
[14] Kraft, L., Sprenger, G.A. and Lindqvist, Y. (2002) Conformational changes during the catalytic cycle of gluconate kinase as revealed by X-ray crystallography. J. Mol. Biol. 318 (4), 1057–1069.
[15] Chakrabarti, A., Miskovic, L., Soh, K.C. and Hatzimanikatis, V. (2013) Towards kinetic modeling of genome-scale metabolic networks without sacrificing stoichiometric, thermodynamic and physiological constraints. Biotechnol. J. 8 (9), 1043–1057.
[16] Pace, C.N. et al. (1995) How to measure and predict the molar absorption-coefficient of a protein. Protein Sci. 4 (11), 2411–2423.
[17] Wiseman, T., Williston, S., Brandts, J.F. and Lin, L.N. (1989) Rapid measurement of binding constants and heats of binding using a new titration calorimeter. Anal. Biochem. 179 (1), 131–137.
[18] I. Haq, B. Hill, Calorimetry in the fast lane: the use of ITC for obtaining enzyme kinetic constants, Microcal, LLC application note, 2002
[19] Bianconi, M.L. (2007) Calorimetry of enzyme-catalyzed reactions. Biophys. Chem. 126 (1), 59–64.
[20] Todd, M.J. and Gomez, J. (2001) Enzyme kinetics determined using calorimetry: a general assay for enzyme activity? Anal. Biochem. 296 (2), 179–187.
[21] Freyer, M.W. and Lewis, E.A. (2008) Isothermal titration calorimetry: experimental design, data analysis, and probing macromolecule/ligand binding and kinetic interactions. Methods Cell Biol. 84, 79–113.
[22] Cornish-Bowden, A. (1995) Briefly noted. Fundamentals of enzyme kinetics, revised edition. Anal. Biochem. 231 (1), 275.
[23] Bianconi, M.L. (2003) Calorimetric determination of thermodynamic parameters of reaction reveals different enthalpic compensations of the yeast hexokinase isozymes. J. Biol. Chem. 278 (21), 18709–18713.
[24] Coffee, C.J. and Hu, A.S.L. (1972) The kinetic characterization of gluconokinase from a pseudomonad. Arch. Biochem. Biophys. 149 (2), 549–559.
[25] Tsai, C.S., Shi, J.L. and Ye, H.G. (1995) Kinetic studies of gluconate pathway enzymes from *Schizosaccharomyces pombe*. Arch. Biochem. Biophys. 316 (1), 163–168.
[26] Heavner, B.D. and Price, N.D. (2015) Transparency in metabolic network reconstruction enables scalable biological discovery. Curr. Opin. Biotechnol. 34, 105–109.
[27] Shlomi, T. (2009) Metabolic network-based interpretation of gene expression data elucidates human cellular metabolism. Biotechnol. Genet. Eng. Rev. 26 (1), 281–296.
[28] Ruppin, E., Papin, J.A., De Figueiredo, L.F. and Schuster, S. (2010) Metabolic reconstruction, constraint-based analysis and game theory to probe genome-scale metabolic networks. Curr. Opin. Biotechnol. 21 (4), 502–510.
[29] Campoy, A.V. and Freire, E. (2005) ITC in the post-genomic era...? Priceless. Biophys. Chem. 115 (2), 115–124.
[30] Bertalanffy, L.V. (1968) General System Theory: Foundations, Development, Applications, Braziller, New York, p. XV, Braziller, New York.
[31] Fleming, R.M. and Thiele, I. (2011) Von Bertalanffy 1.0: a COBRA toolbox extension to thermodynamically constrain metabolic models. Bioinformatics 27 (1), 142–143.